DEVELOPMENT OF A PLANE STRAIN COMPRESSION TEST TO SIMULATE THE HOT ROLLING OF CARBON MANGANESE PLATE STEELS

BY

KEVIN MARK BANKS

FEBRUARY 1990

A dissertation submitted to the Faculty of Engineering, University of the Witwatersrand, Johannesburg, in fulfilment of the requirements for the degree of Master of Science in Engineering.

Department of Metallurgy and Materials Engineering
University of the Witwatersrand
Johannesburg, 1990.

DECLARATION

I declare that this dissertation is my own, unaided work except where due acknowledgement is made to others. It is being submitted for the degree of Masters of Science in Engineering at the University of the Witwatersrand, Johannesburg. It has not been submitted before for any degree or examination to any other university.

Kevin Mark Banks

1 day of MARCH 1990

ABSTACT

An instrumented hot deformation simulator was designed, constructed and commissioned at Iscor's Pilot Plant. A modified servohydraulic machine, using plane strain compression, simulated industrial plate rolling schedules. The simulation test included induction heating, multiple pass plane strain compression and either air cooling or quenching. The movement of the specimen between the different test stages was computer controlled. Accurate control of specimen temperature, strain strain rate and interpass hold times was achieved by means of sophisticated data acquisition equipment. A computer programme was written to simulate the hot rolling of plate in terms of roll separating forces, metallurgical changes during deformation as well as the final microstructure and mechanical properties of SC8 carbon manganese steel. Multiple linear regression was performed on the results obtained from multi-pass plane strain compression tests. It was found that chemical composition, finish temperature and finish strain were the most important process parameters affecting yield strength and impact energy of air cooled plate. A computer model was developed to simulate the temperature distribution in the deformation zone of a plane strain compression specimen at any point during or after a multi-pass test.

ACKNOWLEDGEMENTS

I would like to express my sincere thanks to Dr. A.Koursaris for his guidance and help throughout this research.

Thanks are also gratefully due to my collegues and technical staff for their part in the completion of this work.

In particular I would like to thank Mr.H.Ortner for financial assistance, Mr. H.S.Jordaan for his technical help, Mr.H.Michau for operation of the hot deformation simulator, Mr.T.Smit for programming assistance and all members of the Iscor Pilot Plant for their help in the machining of specimens.

Finally, I thank "Peaches" for her patience and moral support.

CONTENTS

TABLE OF SYMBOLS

Roman Symbols

A_{rad}	Radiation area, mm
A_{in}	Instantaneous area, mm²
A_o	Initial area, mm²
A_{c1}	Transformation end temperature, °C
A_{c3}	Transformation start temperature, °C
b	Platen width, mm
CVN	Charpy V notch value, J
c	Specific heat capacity, kW/m²K
CR	Cooling rate, °C/s
C	Heat transfer constant, kW/m²
%C	Carbon content, weight %
d	Grain size, μm
d_α	Ferrite grain Size (μm)
d_γ	Measured Austenite grain size, μm
d_γ'	Effective austenite grain size, μm
d_{gg}	Grain size after grain growth, μm
d_{rex}	Recrystallised austenite grain size, μm
d_o	Initial austenite grain size, μm
D	Thermal diffusivity
e%	percentage elongation
E	Emmissivity
f	Spread coefficient
F	Platen force or roll force, kN
FATT	Fracture appearance transition temperature, °C (50%)
h	Specimen or plate thickness, mm
h_o	Initial specimen or plate thickness, mm
h_f	Final specimen or plate thickness, mm
h_m	Mean specimen or plate thickness, mm
HV	Vickers hardness
HTC	Boundary condition factor
k	Thermal conductivity of steel, W/m°C
K_i	Temperature correction factor in pass i

l	Specimen or plate length, mm
L	Length of roll contact, mm
$\%Mn$	Manganese content, weight %
n	Strain hardening exponent
N	Nitrogen content, ppm
P_{ear}	Pearlite volume fraction, %
Q	Roll geometry function
Q_{gg}	Grain growth activation energy, J/mol
r	Reduction, %
rpm	Revolutions per minute
R	Roll radius, unflattened, mm
R_e	Yield stremgth, MPa
R_m	Ultimate tensile strength, MPa
s	Specific heat capacity, J/kg°C
S_v	Interface area per unit volume, mm^2/mm^3
$\%Si$	Silicon content, weight %
t	Time, s
t_c	Deformation contact time, s
t_{hold}	Hold time, s
t_{50}	Time for 50% recrystallisation
t_{99}	Time for 99% recrystallisation
T	Instantaneous Temperature °C or K
T_{amb}	Ambient temperature, °C
T_{centre}	Plate centre temperature, °C
T_d	Deform temperature, °C
T_f	Cooling end temperature, °C
T_{finish}	Finsh roll/deformation temperature, °C
T_i	Temperature in pass i, °C
T_m	Mean plate temperature, °C
T_R	Work roll temperature °C
$T_{surface}$	Plate surface temperature, °C
T_s	Cooling start temperature, °C
T_0	Initial temperature °C or K
v	Platen velocity, mms^{-1}
w	Slab, plate or specimen width, mm
W_p	Austenite fraction in interval δt

$V_{p,50}$	50% austenite fraction
X	Fraction of austenite recrystallised
X_{aa}	Fraction of austenite recrystallised during anisothermal conditions
X_r	Strengthening index
X_a	Anisothermal softening index
Z	Zener-Holloman parameter

Greek Symbols

α	Ferrite grain size, μm
α_{gg}	Grain growth parameter
α_{HCF}	Roll heat generation factor
$\delta\epsilon'$	Strain increment
δh	Decrease in thickness, mm
δt	Time increment, s
δt_{ac}	Time increment during air cooling °C
δT	Change in temperature, °C
δT_{ac}	Temperature drop due to air cooling, °C
δT_{con}	Temperature drop due to conduction, °C
δT_{wd}	Temperature rise due to deformation, °C
θ_o	Angle of bite, radians
θ	Roll angle, radians
ϵ'	Plane strain
ϵ_i	Strain in pass i
ϵ	Equivalent tensile strain
$\epsilon_x, \epsilon_y, \epsilon_z$	Strain in the x,y,z directions
ϵ_c	ϵ at which dynamic recrystallisation starts
ϵ_p	Strain to the peak flow stress
ϵ_{final}	Strain in the last pass
$\dot{\epsilon}$	Strain rate, s^{-1}
$\dot{\epsilon}_i$	Strain rate in pass i, s^{-1}
$\bar{\dot{\epsilon}}'_m$	Mean strain rate during rolling, s^{-1}

$W_{\gamma,50}$	50% austenite fraction
X	Fraction of austenite recrystallised
X_{aa}	Fraction of austenite recrystallised during anisothermal conditions
X_r	Strengthening index
X_s	Anisothermal softening index
Z	Zener-Holloman parameter

Greek Symbols

α	Ferrite grain size, μm
α_{GG}	Grain growth parameter
α_{RCF}	Roll heat generation factor
$\delta\epsilon'$	Strain increment
δh	Decrease in thickness, mm
δt	Time increment, s
δt_{ac}	Time increment during air cooling °C
δT	Change in temperature, °C
δT_{ac}	Temperature drop due to air cooling, °C
δT_{con}	Temperature drop due to conduction, °C
δT_{wd}	Temperature rise due to deformation, °C
θ_b	Angle of bite, radians
θ	Roll angle, radians
ϵ'	Plane strain
ϵ_i	Strain in pass i
ϵ	Equivalent tensile strain
$\epsilon_x, \epsilon_y, \epsilon_z$	Strain in the x,y,z directions
ϵ_c	ϵ at which dynamic recrystallisation starts
ϵ_p	Strain to the peak flow stress
ϵ_{final}	Strain in the last pass
$\dot{\epsilon}$	Strain rate, s^{-1}
$\dot{\epsilon}_i$	Strain rate in pass i, s^{-1}
$\bar{\dot{\epsilon}}'_R$	Mean strain rate during rolling, s^{-1}

$\dot{\epsilon}'_{psc}$	Strain rate during plane strain, s^{-1}
μ	Coefficient of friction
ρ	Steel density, kg/mm^3
σ	Equivalent tensile stress, MPa
σ_0	Onset of flow stress in pass 1, MPa.
σ_1	Maximum flow stress in pass 1, MPa.
σ_2	Onset of flow stress in pass 2, MPa.
σ'	Plane strain flow stress, MPa
$\bar{\sigma}'$	Mean Plane Strain flow stress, MPa
σ_w	Deformation resistance, MPa
σ_{disl}	Dislocation stress, MPa
$\sigma_{un.i}$	Undeformed flow stress in pass i, MPa
ρ'	Dislocation density, cm^{-2}

CHAPTER 1

INTRODUCTION

1.1 Statement of the problem

Iscor's steel development programme includes finding new ways of improving the quality of their flat-rolled products. Strip and plate products are sometimes rejected because of their failure to meet specification. Inconsistencies in the final machanical properties of steel processed from the same heat have also been found. These and related problems can invariably be attributed to inadequate alloying or inadequate control of the rolling process.

Traditionally, optimisation of hot rolling schedules was developed by trial and error on the plant itself. This was an expensive and time consuming method since experimental rolling schedules seriously hinder production. It was recognised that reliable data obtained from laboratory tests on the hot working characteristics of the material concerned contributed greatly in improving its mechanical properties in the as-rolled condition. Laboratory simulation of the hot rolling process has the added advantage of determining quantitatively the influence of important parameters on the final quality of the steel. Furthermore, quantitative knowledge of the material's response to hot working variables has been used in controlling the working process.

1.2 Background

Understanding the mechanisms controlling microstructural changes in austenite during conventional hot rolling (a high temperature thermomechanical treatment, HTMT) is essential if optimisation of rolling schedules is to be carried out effectively. During the last 15 years a great deal of work has been devoted to the controlled rolling of high strength low alloy (HSLA) steels. The interpretation of the influence of deformation parameters (temperature, strain, strain rate and hold time) on grain structure and grain size has advanced to the extent that mathematical relationships have been formulated to predict the evolution of microstructure during and after hot rolling.

In hot rolling, the behaviour of the material in any pass depends on the deformation variables (strain, strain rate, hold time and temperature) and on the microstructural features of the material entering the pass. This includes austenite grain size, extent of recrystallisation, grain growth and nature and degree of any precipitation [1]. These microstructural features depend critically on the conditions experienced in previous passes as well as on the chemical composition and initial microstructure of the material. The final microstructure depends on the state of the austenite before transformation and the cooling rate. It is well known that if one refines the final ferrite grain size through careful control of the deformation parameters, improved strength and toughness may be achieved.

In assessing the characteristics of rolling, all these factors must be taken into account. This may be done in two different but complimentary ways [2]:

a) Physical simulation of variables in industrial hot rolling using a hot deformation simulator.

b) Computation of microstructure, property and thermal changes in multi-pass hot rolling from basic relationships obtained from the results of laboratory simulation tests.

1.3 Objectives

The main objectives of this work were:

1. To design and construct a laboratory scale hot deformation simulator capable of achieving the temperatures, strains, roll separating forces, strain rates, delay periods and cooling rates commonly found in industrial hot plate rolling.

2. To develop and implement laboratory test procedures in order to simulate the mechanical and metallurgical changes occurring during and after the hot plate rolling of a carbon manganese steel (SC8).

3. To compare the final microstructure and mechanical properties of SC8 C-Mn steel processed in the plant with those of material processed

in the laboratory in order to assess the reliability of the results obtained from the laboratory simulator.

4 To incorporate the relevant structure - property relationships into a computer programme to predict and optimise important mechanical and metallurgical changes occurring during and after the hot plate rolling of SC8 steel plate.

CHAPTER 2

LITERATURE SURVEY

2.1 Introduction

A review of the literature concerning the hot rolling of carbon manganese steel plate and its simulation is presented in this chapter. A summary of the various thermomechanical treatments used to process steel is presented. Common hot workability tests are briefly assessed. Comparison is made between the hot deformation parameters encountered in plate rolling and plane strain compression tests. The quantification of microstructural changes as well as the influence of rolling parameters upon the changes occurring in the hot rolling of carbon manganese steels is discussed.

2.2 Classification of thermomechanical treatments

Thermomechanical treatment (TMT) or thermomechanical processing (TMP) involves a combination of thermal treatment and plastic deformation within a single heat treatment cycle to control the structure, morphology and grain size of the parent phase (e.g austenite) and subsequent subgrain structure in the transformation product phases (e.g ferrite) and/or interactions between dislocations and fine precipitates (e.g alloy carbides and carbonitrides) [3]. Its main objective is to achieve high strength, ductility and toughness in a wide variety of finished or semi-finished steels. Thermomechanical treatments can be classified into three broad categories, shown schematically in Figure 2.1 depending on the deformation process before, during or after the phase transformation.

Class I - Deformation is completed prior to the transformation of austenite. Examples are high temperature thermomechanical treatment and conventional hot rolling (HTMT), controlled rolling and low temperature thermomechanical treatment (LTMT), also called ausforming. HTMT and LTMT are applied to martensitic steels i.e for for high and low alloy steels with increased hardenability. Controlled rolling has been developed for pearlite-reduced steels (with low carbon content and little or no

pearlite structure), microalloyed steels and acicular ferrite (i.e low carbon bainitic) steels which are quenched and tempered. Prominent among these are microalloyed (low-carbon low-alloy C-Mn) steels which are extensively used as hot-rolled plate and strip.

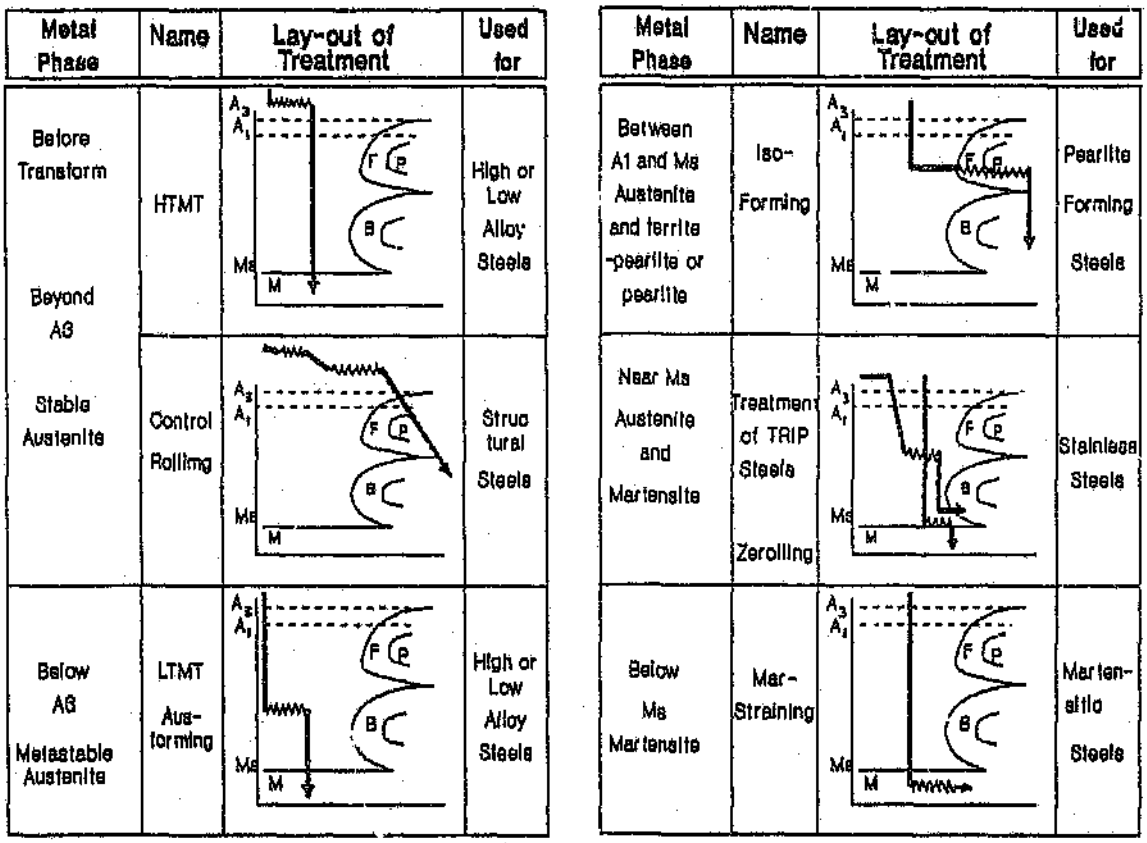

Figure 2.1 Classification of thermomechanical treatments

Class II - Deformation occurs during the transformation of austenite. Examples are the isoforming process where spheroidal carbides within a ferrite matrix form during deformation deformation of metastable austenite; treatment of TRIP steels where metastable austenite is initially deformed above Md temperatures and finally cold worked (i.e

Zerolled) at room temperatures to produce (strain-induced) martensite. Isoforming is applied to low alloy or pearlite forming steels while treatment of TRIP steels is confined to stainless or semi-stainless steels.

Class III - Deformation occurs after the transformation of austenite. Examples are marstraining, marforming and strain tempering or warm working. In marforming the martensite is cold worked prior to tempering to induce a dislocated substructure which improves the distribution of temper carbides.

2.3 Requirements of a hot deformation simulator

In simulating hot rolling a process comparable to hot rolling is necessary to allow for the variation of the deformation parameters within the wide limits found in practice. To carry out this simulation, a high performance, compact, computer-controlled installation including heating up and cooling facilities is required.

It is of prime importance that the specimen dimensions are sufficient to allow for the machining of tensile and charpy specimens in order to determine mechanical properties after deformation. In the simulation of any industrial process using laboratory methods it is important to use test pieces of representative initial structure i.e. the reheated specimen must have the same initial austenite grain size typically found in industrial reheating. A constant true strain rate must be achieved so that the stress required to deform the test material under known conditions of temperature, strain and strain rate can be determined. The problem with having a varying strain rate is that it is difficult to know how much of the flow stress variation is due to increasing strain and how much is due to the varying strain rate. It should be possible to determine the rolling force on the basis of deformation forces recorded in the simulation test [4]. One should also have the option of interrupting the deformation sequence at any point in order to examine the microstructure of intermediate stages.

2.4 Hot workability tests - a brief assessment

2.4.1 Laboratory scale hot rolling

The advantage of hot rolling on laboratory scale is that the mode of deformation in the test method and the practical working operation for which the data is required is essentially the same as industrial rolling.

The biggest limitation of this test method however, is that if one needs to simulate strip rolling, a high speed, multi-stand laboratory mill is required. The amount of space required together with the cost of such equipment make it an unattractive proposition.

2.4.2 Torsion testing

Torsion testing has been used by a number of workers [5-7] for the simulation of hot rolling since it is particularly amenable to the simulation of intermittent deformations. It has the advantage over compression testing that there are no problems with friction. Hot torsion can be used to give strain rates between 10^{-3} and 10^{3} s^{-1} and strains up to 20 without plastic instability [8]. The mode of deformation is shear so that theoretically there should be no change in the dimensions of the sample. However, in practice specimens undergo a change in the gauge length and a corresponding change in diameter during twisting [9]. This complication can be avoided by axially constraining the specimen, though this leads to the development of axial stresses.

The biggest problem with torsion tests is that of a stress, strain and strain rate gradient along the specimen radius. This makes it difficult to relate structural observations to the deformation parameters. This problem may be overcome by twisting thin walled tubes across which the strain and strain rate can be considered constant [10]. Unfortunately tubes tend to buckle at low strains and the main advantage of the test is lost.

2.4.3 Axisymmetric compression

In this test a cylindrical sample is compressed between flat platens whose cross-section is much larger than the initial cross-section of the samples. If a constant ram velocity is used [11] the true strain rate increases with deformation. However constant strain rates in the range 0.1 - 300 s^{-1} have been obtained by using a cam to increase the cross-head velocity as the test proceeds.

The main problem with axisymmetric compression is that above about 50% reduction (0.7 true strain) in height, barreling of the specimen occurs because of friction between the platens and the ends of the specimen and this causes problems in analysing the stress - strain data. This limits the usefulness of the test since simulation of rolling schedules involving total strains greater than 0.7 is not possible.

2.4.4 Plane strain compression

The plane strain compression test was developed to simulate hot rolling partly because of the difficulties found in the other testing methods already described. Plane strain compression also provides the nearest approximation to the conditions of stress that occur in rolling. Furthermore the area under compression remains almost constant so that true strains of more than 2.5 can easily be achieved.

A plane strain hot deformation simulator, "Wumsi", was developed at the Max-Planck Institut fur Eisenforschung, Dusseldorf [12-17]. The "Wumsi" is a computer-controlled, servohydraulic testing machine capable of performing multi-stage plane strain compression tests, in which a specimen is compressed between a lower working die and a fixed upper die. The servohydraulic unit was designed to simulate fast platen displacement - time schedules, which are characteristic of modern hot forming processes. The layout of the experimental equipment and the data acquisition facilities are shown in Figure 2.2 and Figure 2.3 respectively.

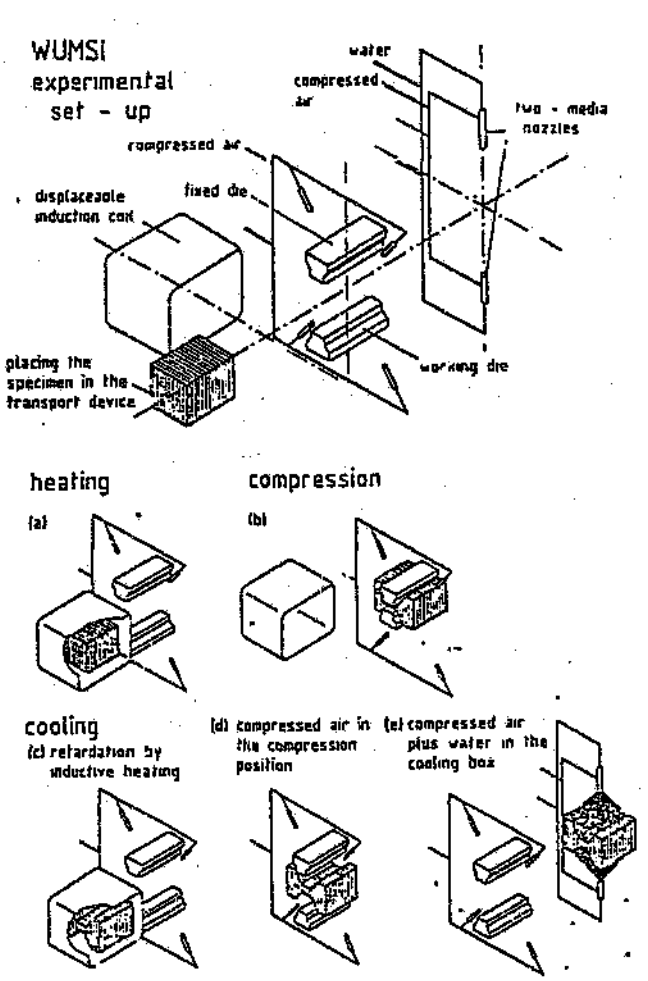

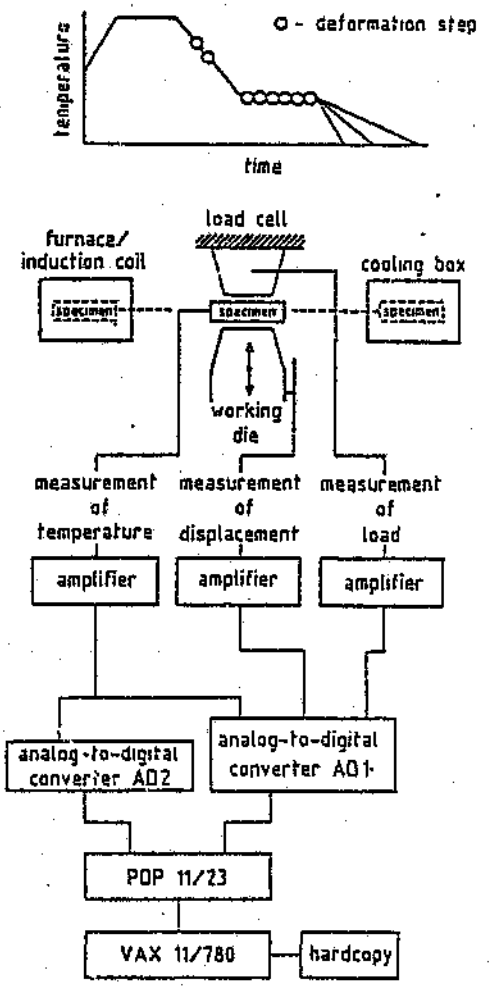

Figure 2.2

Figure 2.3

Experimental layout and data acquisition facilities of the "Wumsi" hot deformation simulator [12]

A sheathed thermocouple is embedded in the large, rectangular specimen to record the temperature during the deformation schedule and during cooling. The specimen is transported pneumatically into the induction furnace where it is either heated up, held at a predetermined temperature or cooled down at a controlled rate. These operations are performed automatically by applying a programmable set point unit. This facilitates

the simulation of temperature of slabs or forgings which are of much greater thickness.

After heating, the specimen is positioned between the two dies. The computer takes control and executes a previously entered deformation schedule, consisting of the following parameters: number of passes, strain and strain rate of each pass, delay times between passes as well as the delay time between the end of deformation and the start of the subsequent controlled cooling. If the actual parameters of the mill train are to be simulated, parameters such as roll radius, velocity of the billet etc. can be entered and processed.

Compressed air nozzles allow accelerated cooling during the deformation schedule. Two-media nozzles also enable the mixing of water and air to simulate water-jet descaling. After deformation, the specimen is pneumatically transferred into a cooling box where a wide range of cooling rates can be applied.

During an experiment, the displacement of the moving die, the load required and the specimen temperature are continuously logged. This data is amplified, digitized and stored on a computer for later analysis. The "Wumsi" has been successfully used in the following research fields: strain-hardening, softening by recovery and recrystallisation, precipitation, transformation, dual-phase structure, optimisation of rolling schedules and deformation resistance.

2.3 Comparison Of The Conditions Existing In Rolling And Plane Strain Compression

2.3.1 Mode of deformation

The typical flat rolling of plates, sheet or strip is essentially a plane-strain operation, since little widening of the workpiece results. This can be explained by examining the shape of the deformed zone in Figure 2.4. The length of contact, L, between the rolls and workpiece is usually much smaller than the width of the strip or plate, w. As the rolls induce a compressive stress, the plastic zone is thinned and is

free to expand in the rolling-direction, but lateral expansion in the y-direction is effectively restrained by the undeformed material on both sides of the roll gap. The net effect is a condition of plane strain, where ϵ_y , the strain in the y-direction, is zero and $\epsilon_x = -\epsilon_z$, except at the edges of the workpiece [18].

The plane strain compression test specimen, shown in Figure 2.5, is in the form of a thin plate or sheet that is compressed across its width, w, by narrow platens whose width, b, are wider than the initial specimen thickness, h_o. The elastic constraints of the platens prevent extension in the specimen width dimension (y), hence the name plane strain. There is deformation in the direction of platen motion (x) and in the specimen length direction (z). To ensure that lateral spread is negligible, the width of the strip should be 6-10 times the width of the platens [18].

For essentially homogeneous deformation, the ratio of platen width to strip thickness, b/h, should be between 2 and 4 at any instant.

2.5.2 Strain

In industrial flat rolling and plane strain compression, it is usual to define the instantaneous plane strain, ϵ', in terms of the initial and final workpiece thickness as:

$$\epsilon' = \ln (h_o/h) \qquad 2.1$$

This is then related to the equivalent true strain, ϵ, by means of the von Mises criterion as:

$$\epsilon' = 2/\sqrt{3}\ \epsilon \qquad 2.2$$

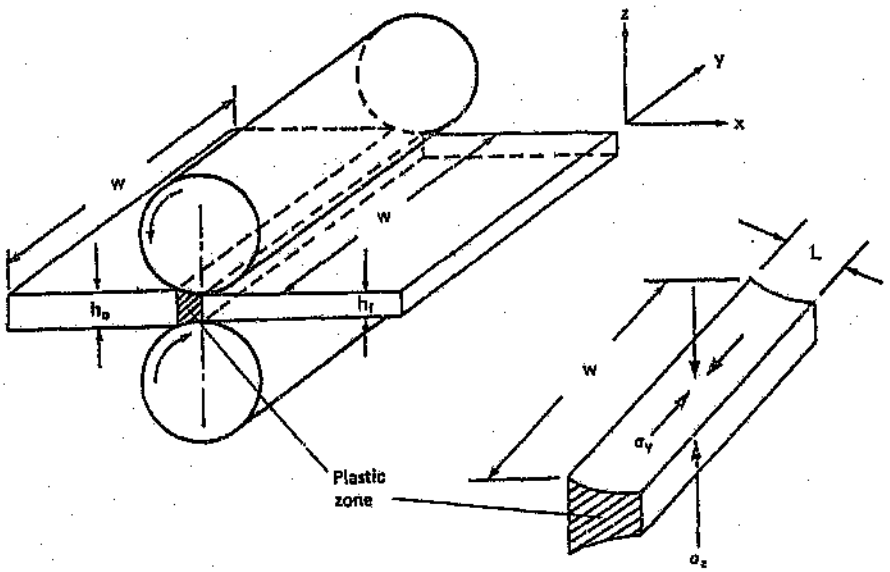

Figure 2.4 Schematic diagram of deformation in rolling

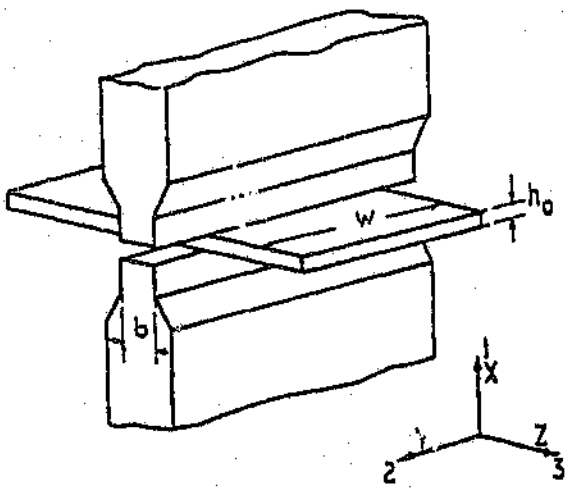

Figure 2.5 Geometry of the plane strain compression test

Similar to other hot deformation tests (e.g torsion, tension) the plane strain compression test yields an inhomogeneous distribution of strain in the deformation zone which is more severe if the platens are unlubricated and unheated. At the specimen/platen contact area there are zones of dead (nearly unstrained) material, and at both sides of the plastic zone the material is kept rigid. The strain distribution evaluated in the plane of symmetry (y = 0) [14] is illustrated in Figure 2.6. Nearly all the strain is applied on the centreline of the specimen.

Since the stress system during plane strain compression is not uniaxial the stress, strain and strain rate data are usually converted to equivalent tensile values using the von Mises criterion, so that they can be compared with data obtained from tensile or axisymmetric compression tests. However, the von Mises criterion ($2/\sqrt{3}$) is strictly applicable to pure plane strain conditions. A spread factor, f, takes into account the departure from plane strain compression observed in practice. Foster [19] found that the spread coefficient can be related to initial specimen width, w, and platen breadth, b as:

$$f = (1.155(b - w) + w)/b \qquad 2.3$$

$= 2/\sqrt{3}$ if conditions are purely plane strain.

Kapellner et al [13] found a correlation between the spread factor and initial width for 10mm thick specimens:

$$f = 0.0388 + 0.3402/b + 401.1/b^2 \qquad 2.4$$

2.5.3 Strain rate

At hot working temperatures, the strain rate is important in determining flow stress. The mean plane strain rate in hot rolling, $\bar{\dot{\epsilon}}_R'$, is defined as [2]:

$$\bar{\dot{\epsilon}}_R' = \frac{2\pi R\, rpm}{60\sqrt{R\,\delta h}} \ln[h_o / h_f] \qquad 2.5$$

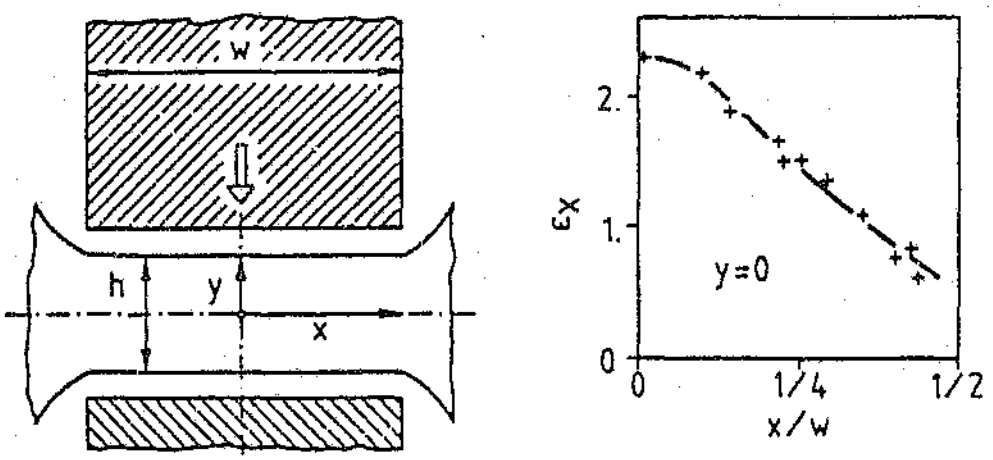

Figure 2.6 Strain distribution in the plane strain compression test [14]

In laboratory tests, it is usual to keep the strain rate constant at a value equivalent to the mean strain rate in a roll pass. Decreasing the platen velocity, v, in proportion to instantaneous specimen thickness, h, gives a constant strain rate. The strain rate may also be measured by determining the proportion of incremental strain to incremental time:

$$\dot{\epsilon}_{psc}' = -v/h = -\delta\epsilon'/\delta t \qquad 2.6$$

2.5.4 Deformation force and flow stress

Sims [20] derived equations for the distribution of pressure over the contact surface between workpiece and rolls. The roll separating force, F, obtained from these equations is given by:

$$F = w\,\bar{\sigma}'\sqrt{R\,\delta h}\,Q \qquad 2.7$$

where

$$Q = (\pi + L / h_m)/4 \qquad 2.8$$

$$L = (h_o - h_f)R \qquad 2.9$$

$$h_m = (h_o + 2h_f)/3 \qquad 2.10$$

The mean flow stress in rolling, $\bar{\sigma}'$, is found by numerically integrating the plot of flow stress in plane strain, σ', against changing roll angle, θ, between 0 radians and the angle of bite, θ_o, [21]. The roll angle is shown in Figure 2.7.

$$\bar{\sigma}' = \frac{1}{\theta_o}\int_0^{\theta_o} \sigma'\delta\theta \qquad 2.11$$

In plane strain compression θ_o in equation 2.11 is replaced by the total strain in the pass, ϵ_t.

Barager et al [22] developed a formula that predicts the flow stress of C-Mn steels in terms of strain for a given temperature range:

$$\sigma = A + B\epsilon^{0.4} + C\epsilon^{0.8} + D\epsilon^{1.2} \qquad 2.12$$

The constants A,B,C and D are determined by multiple linear regression of stress and strain data.

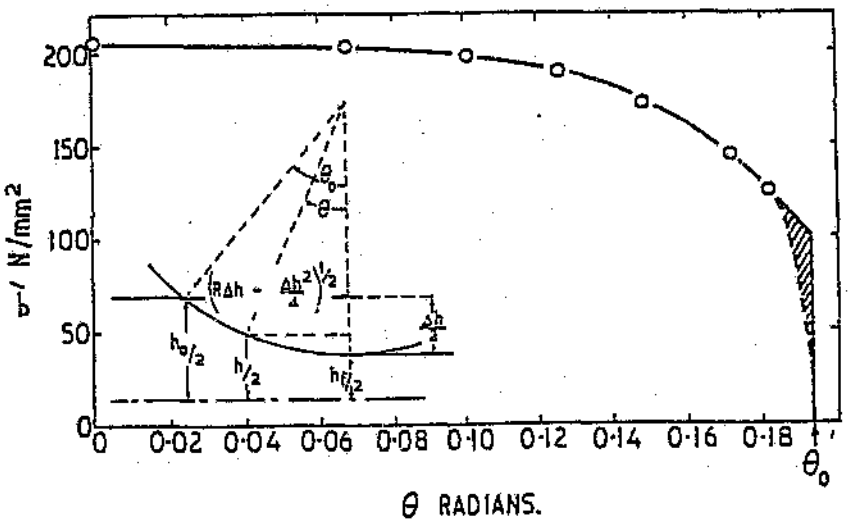

Figure 2.7 Plane strain stress versus roll angle [21]

The major disadvantage of plane strain compression testing is that the frictional force between the sample and the platens varies with the amount of deformation. In order to calculate the deformation stresses from the measured loads, allowances have to be made for the frictional forces.

Rowe [23] found the force, F, between two parallel dies and a flat workpiece to be:

$$F = w\, b\, \bar{\sigma}'\, f\, [1 + w/4\, h] \qquad 2.13$$

for sticking friction and

$$F = w\, b\, \bar{\sigma}'\, f\, [1 + 0.5\, \mu./\, h] \qquad 2.14$$

for sliding friction. These relationships are only applicable when

$$\mu w/h > \ln(1/2\mu) \qquad 2.15$$

To determine the plane strain flow stress, σ', from the deformation resistance, σ_w, in plane strain compression tesing, a formula derived from elementary plastomechanics [13] may be used:

$$\sigma' = \sigma_w/((\exp(\mu b/h) - 1)h/\mu b + h/4b) \qquad 2.16$$

Basically this formula applies only to sliding friction. The results of theoretical investigations of the flow of materials in plane strain deformation as well as slide marks on the contact surface of the specimen after the plane strain deformation test, however, show that in most cases a combination of static and sliding friction prevails. Nevertheless, the simplicity of the formula makes it a convenient one as long as $\mu l/h$ is kept to below about 1.5.

The deformation resistance, σ_w, is given by the instantaneous platen force divided by the instantantaneous area, A_{in}, beneath the platens:

$$\sigma_w = F / A_{in} \qquad 2.17$$

The instantaneous area increases due to the spread of material in the specimen width and is calculated using the following formula:

$$A_{in} = A_o(f\varepsilon + 1) \qquad 2.18$$

The term h/4b in equation 2.16 describes the amount of shear attributable to the platen penetrating into tue specimen, which is also known as "edge correction". Except for the coefficient of friction, μ, all variables in equation 2.16 can be either directly measured or calculated.

The coefficient of friction, μ, may be determined by performing two or more tests to about 90% deformation, at the same strain rate and temperature using specimens of different thickness [13]. The stress-strain curves obtained from these tests should be identical since the flow stress is independent of specimen geometry. The optimum value of μ

for use in equation 2.16 is that which gives identical flow curves for the different specimen thicknessses. By determining μ i. this way, any irregularities in the stress-strain curves can be allowed for.

2.5.5 Temperature

One of the most important factors in hot rolling is the temperature of the slab. The uncertainty of plate temperature tends to lead to an unavoidable increase in safety margin that must be allowed: the permissible rolling loads are unexploited, resulting in poor utilisation of the plant. Also, the finish temperature greatly influences the final microstructure which in turn affects the mechanical properties of the steel. The principle factors affecting the temperature in both hot rolling and plane strain compression testing are:

- Conduction within the plate/specimen during air cooling and during deformation
- Radiation losses during air cooling
- Convection losses during air cooling
- Heat loss due to water descale sprays (rolling only)
- Heat transfer between the plate/specimen and the work rolls/platens
- Heat gained by the plate/specimen due to deformation and friction

2.5.5.1 Numerical method for determining the temperature in plate rolling

Fourier's Law for heat conduction in an isotropic solid with constant thermal conductivity is given by:

$$\delta T/\delta t = k/s \quad (\delta^2 T/\delta x^2 + \delta^2 T/\delta y^2 + \delta^2 T/\delta z^2) \qquad 2.13$$

The temperature drop or rise of the plate is a function of heat losses or gains which in turn depend on the factors mentioned above. Since the length and the width of the plate are very large compared to the thickness, it can be assumed that the heat flow takes place between the flat surfaces only. In circumstances where unidirectional flow takes place the conduction within the plate can be expressed by the following equation:

$$\delta^2T/\delta^2t = 1/D\ \delta T/\delta t \qquad 2.20$$

At the surfaces of the plate the heat radiation follows the Stefan-Boltzmann equation:

$$k\ \delta T/\delta x = -\ E\ s\ (T^4 - T^4_{amb}) \qquad 2.21$$

The solution of equation 2.20 is achieved by using a numerical method. Harding [24] developed a finite difference computer model to simulate the temperature distribution in the plate at any stage during the rolling process. The numerical solution of heat flow as applied in predicting the temperature drop of the plate during rolling is rather involved, although it is useful when the temperature gradient inside the plate has to be known. For thin plates, a simpler and faster method, described below, is preferable [25].

2.5.5.2 Approximate method for determining the temperature in plate rolling

In rolling flat products such as plates, the top and bottom surfaces only of the workpiece are considered as heat radiating areas, the heat emitting from the surface of the edges being neglected. The solution of the Stefan - Bolzmann equation pertaining to plate cooling given in equation 2.21 may be rewritten in a simplified form as:

$$\delta T/\delta t = 2\ A_{rad}E\ s(T^4 - T^4_{amb}) \qquad 2.22$$

This may be done subject to three conditions:

i) $T >> T_{amb}$ (ambient temperature neglected)
ii) $w >> h$ and $l >> h$
iii) $\delta t < 20s$ (short time intervals)

The emissivity, E, is a strong function of temperature and is given by

$$E = T/1000\ (0.125\ T/1000 - 0.38) + 1.1 \qquad 2.23$$

where T is in °C.

Substituting a finite difference approximation into $\delta T/\delta t$ into equation 2.22 gives

$$\delta T_{ac} = - 2 s E T^4 \delta t / \rho c h \qquad 2.24$$

where T is in Kelvin.

If the initial temperature is T_o, the new temperature T can be calculated from

$$T = T_o + \delta T_{ac} \qquad 2.25$$

The values of E, c and used in equation 2.24 should be appropriate to the temperature.

Alternatively, to simplify equation 2.22 further, the values of E, c and .. are considered constant, independant of the temperature. Solving equation 2.22 analytically, gives:

$$\int it = - \frac{\rho c h}{2 s E} \int \frac{\delta T}{T^4} \qquad 2.26$$

which gives

$$t_{ac} = \rho c h T^{-3} / 6 s E + C_o \qquad 2.27$$

where C_o is a constant.

At $t_{ac} = 0$, $T = T_o$ [initial conditions]

$$t_{ac} = \rho c h / 6 s E(1/T^3 - 1/T^3_o) \qquad 2.28$$

thus,

$$T = T_o / \{T_o^3 \sqrt{1+6 s E T^3_o t_{ac} / \rho ch}\} \text{ degrees K} \qquad 2.29$$

Equation 2.29 is very convenient to use and it yields accurate prediction of the temperature drop during the air cooling of rolled plate.

In plate rolling, the temperature drop due to conduction to the work rolls, δT_{con}, can be easily derived from the heat balance equation. Heat

supplied to the rolls is proportional to the contact area and temperature difference between the plate and the rolls, and also to the time of contact. The proportionality factor is the roll heat-conduction coefficient. The heat supplied is assumed equal to the heat given up by the plate (This assumption is not strictly true since the conduction to the roller table is ignored).

The heat balance equation is

$$2(R\delta h)^{\frac{1}{2}} w (T-T_R)\alpha_{HGF} \frac{(1+r)60}{2\pi R\ rpm} = \delta T_{con}\ w\ h\ c \qquad 2.30$$

Hence

$$\delta T_{con} = \frac{60\alpha_{HGF}}{(1-r)\pi c\ rpm} \frac{r}{(R\delta h)^{\frac{1}{2}}} (T - T_R) \qquad 2.31$$

where α_{HGF} is the roll heat generation factor. From equation 2.31 it is seen that the temperature drop is proportional to the draft taken and inversely proportional to the rolling speed and rolled thickness. Equation 2.31 assumes constant temperature across the plate and the rolls temperature is uniform and constant along the length of the barrel.The effect of heat coduction losses typical of rolling passes is shown in Figure 2.8.

The temperature gained due to mechanical deformation is a function of mean flow stress and strain of the material rolled. The estimated temperature rise due to work done on the plate during deformation is given by:

$$\delta T_{wd} = \bar{\sigma}' \ln(h_o/h_s)/\rho c \qquad 2.32$$

Typical increases in temperature during the plate rolling of steel are shown in Figure 2.9

The descaling water sprays are used during certain rolling passes to ensure removal of the loose scale which would otherwise damage the

surface of the plate. The jets are operated at high pressure to generate high kinetic energy. The resulting water flow impinges on the plate and reduces its temperature. The heat transfer to the boiling water at the surface of the moving plate is very complex and cannot be sufficiently defined analytically [25].

The overall mean temperature of the plate at any time may then be approximated by:

$$T_m = T_o + \delta T_{ac} + \delta T_{con} + \delta T_{wd} \qquad 2.33$$

2.5.5.2 Numerical method for the detrmination of the temperature in plane strain compression testing

Foster [19] developed a finite difference computer model to simulate the temperature distribution in plane strain compression specimens and deformation platens during air cooling, furnace cooling and compression stages. The model is capable of predicting the specimen temperature at any point within 10 °C. This model is discussed in more detail in Appendix 1.

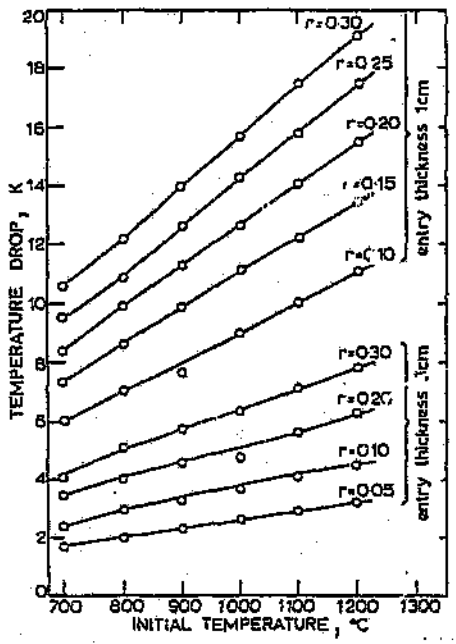

Figure 2.8 Temperature drop due to conduction during rolling[25]

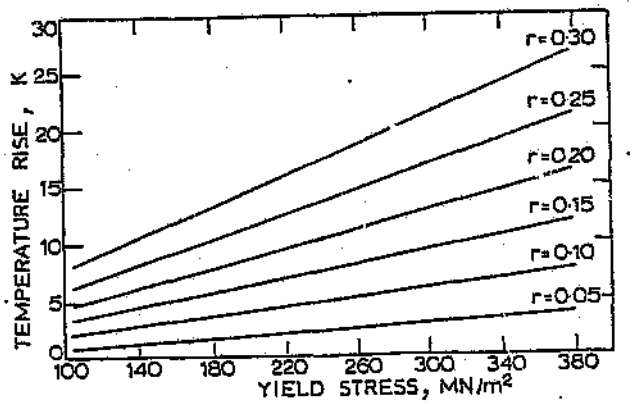

Figure 2.9 Temperature rise due to work done during rolling[25]

2.5.6 Cooling rate after deformation

The cooling rate after plate rolling may be predicted by means of the equivalent diameter method [26]. The "equivalent diameter" refers to that size of round bar in which the axial temperature falls through a specified range in the same time as the temperature in the slowest cooling position in an irregular shaped body. Table 2.1 shows the equivalent diameter for various rectangular plate dimensions. This value is then used in Table 2.2 to calculate the plate temperature at any time from the initial cooling temperature. For example, from Table 2.1, a plate 20 mm thick and 60 mm wide has an equivalent diameter of 30 mm. Referring to Table 2.2 it is seen that the time taken to cool a 30 mm round bar from 1000 °C to 700 °C is 37.2 seconds.

As a prerequisite for the evaluation of cooling curves the transformation behaviour of the steel has to be examined under equilibrium conditions. For this purpose, A_{c3} and A_{c1} transformation temperatures have to be determined in a preliminary test by performing a slow heating (0.01K/s)[17]. Afterwards, the recorded cooling curves are processed in

such a way that zero time is taken as the moment of crossing the A_{c3} temperature. Figure 2.10 shows a number of cooling curves processed in such a way as well as the previously measured A_{c3} temperature.

The transformations of austenite into the various kinds of microstructures such as ferrite, pearlite, bainite or martensite are heat generating i.e. exothermic processes, which result in characteristic deviations from the exponential course of the cooling curve. However, by the analysis of the cooling curve itself transformation temperatures can hardly be established. Any quantitative information on transformation ranges can only be gained by the computation of the differentiated form, $\delta T/\delta t$ of the cooling curve.

Table 2.1

Equivalent diameters for rectangular sections, air cooled

Width (mm)	Thickness (mm)										
	10	12	16	20	25	30	40	50	60	80	100
	mm	mm	mm	mm	mm	mm	mm	mm	mm	mm	mm
10	10										
12	11	12									
16	12	14	16								
20	13	15	18	20							
25	14	16	19	22	25						
30	15	17	21	24	27	30					
40	16	18	23	27	31	34	40				
50	17	19	24	29	33	38	45	50			
60		20	26	30	36	41	48	55	60		
80	18	21	27	33	38	44	54	62	69	80	
100	18	22	28	34	41	47	58	67	76	90	100
120	19	22	28	35	42	49	61	72	83	98	110
160	19	23	29	36	44	52	65	78	89	110	125
200	19	23	30	37	45	53	69	82	95	115	135
250	19	23	30	37	46	54	71	86	100	125	145
300	19	23	30	38	46	55	72	89	105	130	155
400	19	23	31	38	47	56	73	91	105	140	170
500	20	23	31	39	48	57	74	92	110	145	175
600	20	23	31	39	48	57	75	93	110	145	180
∞	20	23	31	39	49	59	78	97	115	155	190

Table 2.2

Axial cooling time for fractional intervals during air cooling of round steel bars of 0.01 - 2500mm diameter

Bar dia mm	Time to cool Fractional Temperature Intervals — seconds														
	0.95–0.90	0.90–0.85	0.85–0.80	0.80–0.75	0.75–0.70	0.70–0.65	0.65–0.60	0.60–0.55	0.55–0.50	0.50–0.45	0.45–0.40	0.40–0.35	0.35–0.30	0.30–0.25	0.25–0.20
0.01	0.0022	0.0029	0.0038	0.0048	0.0060	0.0075	0.0090	0.0108	0.0126	0.0145	0.017	0.0195	0.0223	0.0250	0.028
0.02	0.0050	0.0064	0.0080	0.0101	0.013	0.016	0.019	0.023	0.026	0.030	0.035	0.041	0.047	0.053	0.062
0.03	0.0080	0.0100	0.0125	0.0155	0.020	0.024	0.0295	0.035	0.041	0.048	0.055	0.064	0.074	0.084	0.097
0.04	0.0110	0.014	0.0175	0.022	0.0275	0.033	0.040	0.048	0.055	0.066	0.076	0.090	0.101	0.115	0.135
0.05	0.014	0.0175	0.022	0.028	0.0355	0.044	0.051	0.061	0.071	0.083	0.097	0.112	0.130	0.150	0.175
0.075	0.023	0.028	0.035	0.043	0.055	0.067	0.081	0.097	0.113	0.132	0.155	0.180	0.21	0.237	0.277
0.10	0.032	0.038	0.0475	0.060	0.076	0.094	0.112	0.132	0.155	0.182	0.214	0.250	0.29	0.335	0.385
0.20	0.073	0.084	0.105	0.130	0.160	0.200	0.24	0.285	0.33	0.39	0.46	0.54	0.63	0.72	0.84
0.30	0.115	0.132	0.165	0.205	0.250	0.300	0.36	0.43	0.51	0.60	0.71	0.84	0.99	1.12	1.32
0.40	0.16	0.185	0.23	0.28	0.345	0.425	0.50	0.60	0.71	0.84	0.98	1.15	1.33	1.55	1.80
0.50	0.21	0.24	0.29	0.36	0.44	0.54	0.64	0.77	0.91	1.06	1.26	1.50	1.75	2.00	2.35
0.75	0.33	0.39	0.48	0.56	0.69	0.83	0.98	1.17	1.40	1.67	1.95	2.32	2.72	3.17	3.72
1.00	0.45	0.53	0.64	0.77	0.94	1.13	1.34	1.60	1.90	2.25	2.7	3.15	3.7	4.37	5.1
2.0	1.01	1.20	1.40	1.65	2.00	2.40	2.8	3.4	4.05	4.85	5.8	6.8	8.1	9.5	11.5
3.0	1.60	1.87	2.20	2.60	3.10	3.70	4.3	5.3	6.2	7.5	9.1	10.5	13.0	15.5	19.0
4.0	2.2	2.55	3.00	3.60	4.3	5.1	5.9	7.2	8.4	10.0	12.1	14.5	17.5	21	25.5
5.0	2.85	3.25	3.85	4.6	5.5	6.5	7.5	9.2	11.0	13.0	15.7	18.5	22.5	27.5	33
7.5	4.5	5.15	6.0	7.1	8.4	9.9	11.7	14.0	16.7	20.2	24.5	29	35.5	43	52
10.0	6.3	7.2	8.2	9.9	11.4	13.5	16.0	19.0	23	27.5	33.5	40	48.5	59	73
20.0	14.0	16.0	18.2	21	24	28	33.5	40	48.5	59	71	86	105	128	163
30.0	22.3	25	28.2	32.5	37.2	42.5	51.5	62	75	91	113	136	166	203	255
40.0	31.5	34.5	39	44.5	51	59	71	85	103	125	154	188	228	280	360
50.0	40	44	49	57	65	76	89	108	132	160	198	237	295	360	460
75	63.5	70	77	87	99	119	139	168	203	245	305	370	455	570	730
100	88	95	106	120	135	160	190	220	270	335	410	505	620	780	1000
200	194	208	226	250	280	328	385	465	570	710	870	1090	1330	1700	2170
300	305	328	355	390	435	500	595	715	870	1100	1350	1700	2100	2650	3450
400	425	455	492	535	595	680	810	980	1190	1500	1870	2310	2900	3650	4750
500	545	580	625	675	750	845	1010	1220	1500	1900	2330	2950	3640	4650	6100
750	855	900	971	1030	1130	1290	1520	1870	2280	2900	3550	4500	5900	7150	9600
1000	1161	1215	1300	1380	1530	1730	2050	2500	3100	3900	4900	6200	8000	10200	13500
1500	1801	1900	2030	2150	2350	2700	3150	3750	4750	6000	7600	9600	12200	16000	21000
2000	2501	2600	2750	2950	3200	3500	4150	5100	6400	8200	10200	13200	17000	22000	29000
2500	3251	3420	3580	3750	4000	4450	5250	6500	8000	10500	13100	17000	21800	28500	37500

ure 2.11 illustrates the determination of the start and end of the transformation range on the cooling curve T(log t). Additionally, two numerically differentiated forms of the cooling curve are displayed, which enable the interactive evaluation of the transformation points. Firstly, the differentiated temperature values or cooling rate, CR, are displayed as a function of time, CR(log t). Secondly, a time-independent display, CR(T) is drawn, which refers the cooling rate directly to the temperature values. Distinct local peaks can be seen on both cooling rate (CR) curves. The points of deviation from the smooth parts of the curves correspond to the start and end of trasformation. The transformation start, T_s, and end temperatures, T_e, for various cooling rates can then be joined to generate a complete CCT diagram.

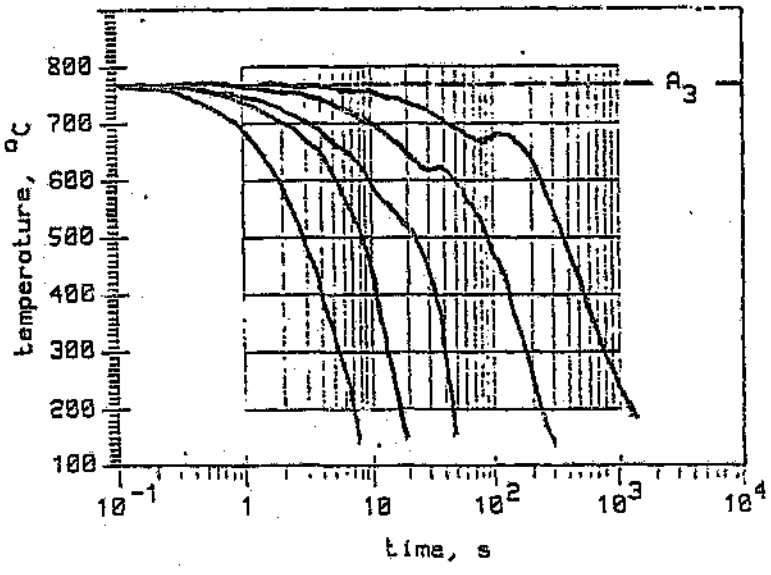

Figure 2.10 Cooling curves with zero time taken as moment of crossing the A_3 temperature[17]

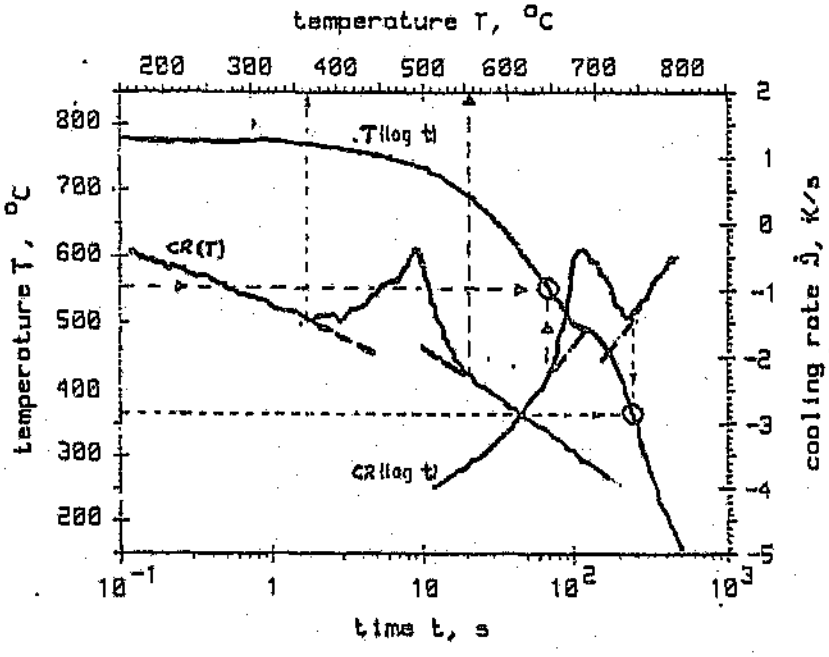

Figure 2.11 Determination of specimen cooling rate and transformation start and transformation end temperatures[17]

2.6 Microstructural changes in the hot working of C-Mn steels

Microstructural changes that take place during deformation are referred to as 'dynamic' changes and those that take place in the time intervals between passes as 'static' changes.

In the simulation of multi-pass deformation the microstructure resulting from recrystallisation and grain growth in the first pass is assumed to become the starting structure for the second pass, etc if deformation takes place in the fully recrystallised region ($T > 1050°C$) [1,2,27]. However, if recrystallisation is incomplete (predominant in the intermediate temperature range ($950°C < T < 1050°C$), the grain size in the recrystallised fraction and the grain size and in the unrecrystallised fraction must be taken into account [2,27]. The amount of retained strain present in the unrecrystallised fraction determines the subsequent recrystallisation kinetics.

2.6.1 Dynamic structural changes

These are structural changes arising from the competing effects of work hardening and of softening by dynamic recovery and dynamic recrystallisation. The occurrence of dynamic recrystallisation depends primarily on the rate of dynamic recovery.

2.6.1.1 Dynamic recovery

This is a thermally activated process and is favoured at low strain rate and/or deformation at high temperature [27].

The characteristic form of the stress-strain curve for dynamic recovery is shown in Figure 2.12a. Initially work hardening is rapid, leading to an increase in dislocation density and a rise in flow stress. As the dislocation density increases, dynamic recovery occurs more rapidly and leads to softening by annihilation of some of the dislocations and rearrangement of others to form subgrain boundaries.

At point S in the figure, the hardening and softening processes balance, leading to a steady state flow stress and a well developed, approximately equiaxed, dislocation subgrain structure at higher strains.

2.6.1.2 Dynamic recrystallisation

With steel in the austenitic condition, dynamic recovery is relatively slow, leading to a more rapid increase in dislocation density with increasing strain and to the development of subgrains with boundaries that are not well formed [27]. The disorder in the subgrain boundaries increases with increasing dislocation density which increases with increasing strain until a critical total dislocation density is reached at which nucleation of new grains takes place. The nucleation and growth of these grains is called dynamic recrystallisation.

Dynamic recrystallisation results in the characteristic form of stress-strain curve illustrated in Figure 2.12 [27]. Work hardening and slow dynamic recovery lead to the rapid increase in flow stress initially and this would continue if dynamic recovery were the only softening process. The flow stress falls as recrystallisation proceeds leading to a maximum in stress at strain ϵ_p. At a critical strain, ϵ_c, dynamic recrystallisation occurs and provides an additional softening mechanism as the new grains form.

Under normal hot working conditions dynamic recrystallisation is a very potent mechanism of grain refinement. Dynamic recrystallisation does not occur in plate rolling in the austenite region since high strains cannot be obtained [27]. In later passes however, when there is considerable retained strain, this form of recrystallisation may well occur.

Lebon et al [28] have shown by optical microscopy that ϵ_p and the critical strain for dynamic recrystallisation, ϵ_c, may be approximately related by:

$$\epsilon_c = 0.8\epsilon_p \qquad 2.34$$

$$\epsilon_p = 4.9\times10^{-4}\, d_o^{1/2}\, Z^{0.15} \qquad 2.35$$

For C-Mn steels, Z is given by [27]:

$$Z = \dot{\epsilon} \exp \frac{312\,000}{8.314\,T} \qquad 2.36$$

where T is in Kelvin.

Two experimental techniques may be used to determine the onset of dynamic recrystallisation:

1) Sekine [29] plotted log Z versus reciprocal of recrystallised austenite grain size ($1/d_{\gamma}$) for a C-Mn steel shown in Figure 2.13. The onset of dynamic recrystallisation occured where the plot started to follow a linear relationship.

2. Kaspar et al [13] plotted strain hardening exponent, n, against strain (Figure 2.14). The onset of dynamic recrystallisation occured when the n-value passed through n=0. The strain hardening exponent was calculated from equation 2.37

$$n = \delta \ln(\sigma)/\delta \ln(\varepsilon) \qquad 2.37$$

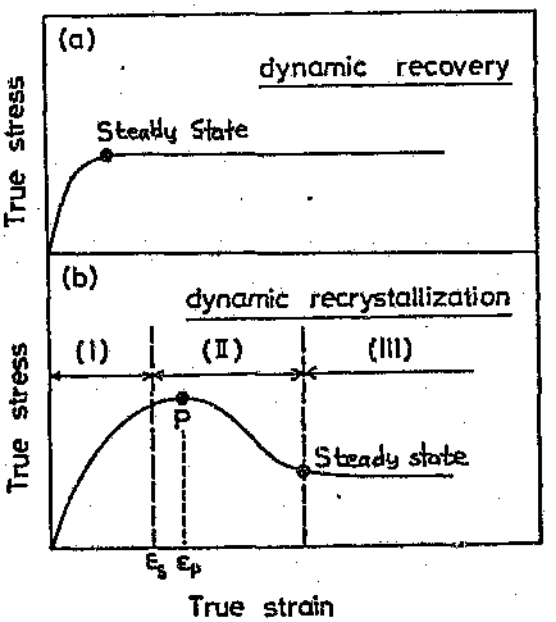

Figure 2.12 **Characteristic stress-strain curve for dynamic recovery and recrystallisation [27]**

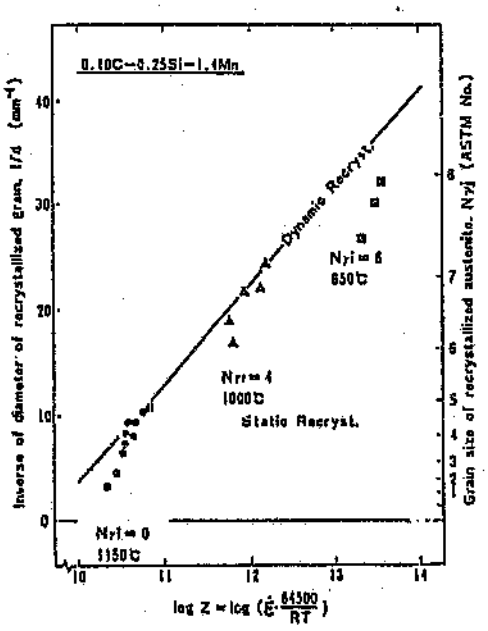

Figure 2.13 Plot of log[Z] against reciprocal grain size to determine the beginning of dynamic recrystallisation [29]

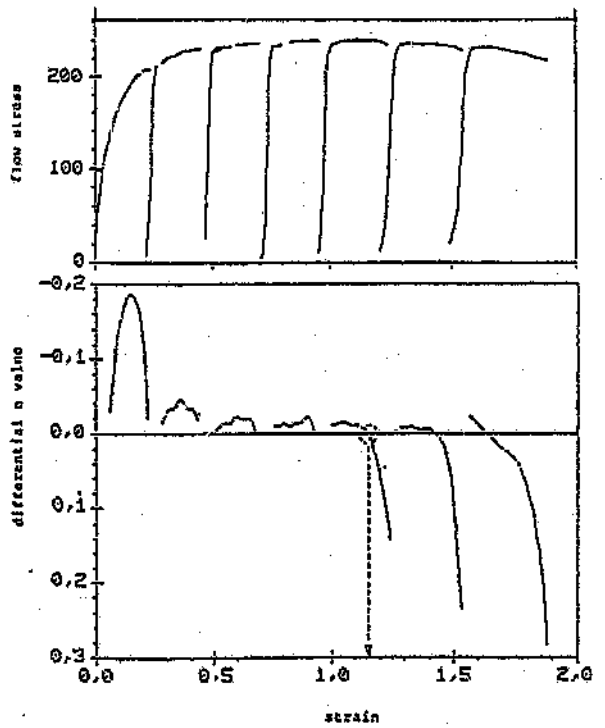

Figure 2.14 Plot of strain hardening exponent against strain to determine onset of dynamic recrystallisation [13]

2.6.2 Static structural changes

The dislocation structures introduced by deformation make them thermodynamically unstable so that on holding at high temperature after deformation further structural changes occur by the process of static recovery and static recrystallisation [27].

2.6.2.1 Static recovery

For strains less than the critical strain for static recrystallisation, the only restoration process that occurs is static recovery. Static recovery occurs immediately after deformation and involves the annihilation of dislocations. The rate of recovery decreases with time since the driving force is the dislocation density [30]. If the applied strain is greater than the critical strain for static recrystallisation, static recovery takes place in the incubation period before recrystallisation.

Solute additions e.g Nb, decrease the rate of static recovery since they increase the incubation time for static recrystallisation [31].

2.6.2.2 Static recrystallisation

If the applied strain is less than that necessary for the onset for dynamic recrystallisation, ϵ_s, then statically recrystallised austenite grains form preferentially at the original austenite grain boundaries. Figure 2.15 [32] shows that the rate of recrystallisation slowly increases as nuclei are produced and then accelerates to a maximum, but ultimately decreases due to impingement of the growing grains. The fraction of recrystallised austenite as a function of hold time can be described by the Avrami equation 2.38:

$$X = 1 - \exp(-0.693(t_{hold}/t_{50})^2 \qquad 2.38$$

Whittaker [33] defined a temperature-compensated time equation for recrystallisation kinetics which takes into account the continually

changing temperature of the steel over discrete time intervals (Figure 2.16).

$$X_{dc} = 1 - \exp(-0.693(W_p/W_{p.50})^2 \qquad 2.39$$

where

$$W_p = \Sigma\, Z\delta t \qquad 2.40$$

$$W_{p.50} = Z\, t_{50} \qquad 2.41$$

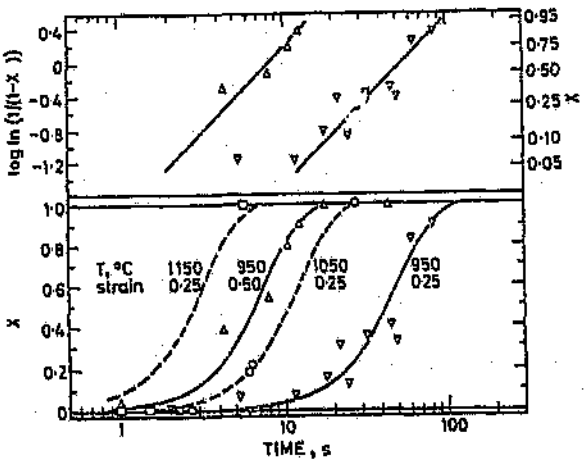

Figure 2.15 Recrystallisation curves for low-alloy steel[AISI 5160] of initial grain size 100 μm deformed at $1s^{-1}$ [32].

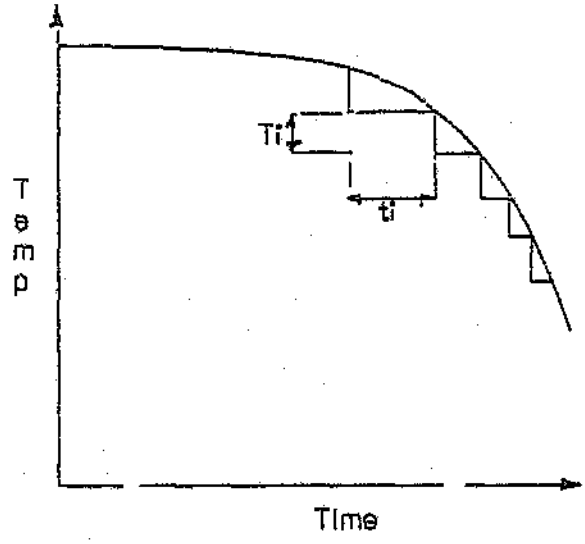

Figure 2.16 Time-temperature compensation curve for determining the fraction of austenite that has recrystallised under anisothermal conditions [33].

The rate of recrystallisation in a given material is determined by the stored energy, the density of favourable nucleation sites and the temperature. Sellars and Whiteman [34] derived the following relationships to describe the kinetics of static recrystallisation for C-Mn steels:(see Figure 2.17).

$$t_{s0} = 2.5\times10^{-19} d_0^{2} \epsilon^{-4} \exp(300000/8.314T)$$

$$\text{for } \epsilon < 0.8\epsilon_p \qquad 2.42$$

$$t_{s0} = 1.1\times10^{-5}\, Z^{-0.6} \exp(300000/8.314T)$$

$$\text{for } \epsilon > 0.8\epsilon_p \qquad 2.43$$

The time for full recrystallisation to take place, t_{95}, may be approximated [19] by

$$t_{95} = 2 \times t_{s0} \qquad 2.44$$

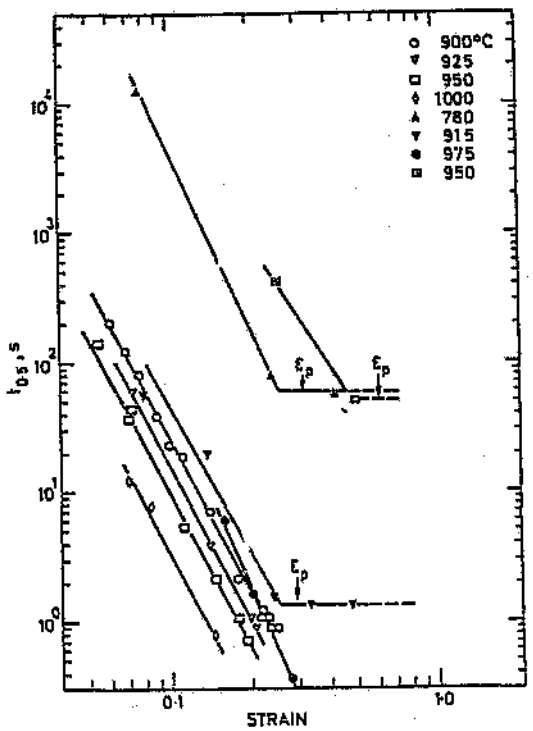

Figure 2.17 Dependance of time for 50% recrystallisation on strain for C-Mn and low-alloy steel [34]

For strains less than ϵ_s, the stored energy, i.e. the driving force for recrystallisation, increases as the strain increases. The strong dependence of t_{s0} on ϵ^{-4}, as given in equation 2.42, has been observed by several authors [35,36,37,38]. The rate of recrystallisation is also determined by the original austenite grain size since grain boundaries act as preferred sites for nucleation [36,39]. Decreasing the original grain size therefore increases the density of favourable nucleation sites and the rate of recrystallisation [36,40]. The abrupt change from strain and grain size dependence to independence at $\epsilon = \epsilon_s$ arises because pre-existing recrystallisation nuclei are always present in the deformed structure at $\epsilon > \epsilon_s$, and the driving force remains constant. Recrystallisation rate is also particularly sensitive to temperature. In

general, a decrease in the holding temperature decreases the rate of recrystallisation. Apart from the holding temperature, the variables which increase recrystallisation rate also decrease the recrystallised grain size. Sellars and Whiteman [34] derived the following equations to define the statically recrystallised grain size for C-Mn steels after a particular pass (Figure 2.18):

$$d_{rex} = 0.5 \frac{d_o^{0.67}}{\epsilon} \qquad \epsilon > \epsilon^* \qquad 2.45$$

$$d_{rex} = D^* Z^{-u} \qquad \epsilon < \epsilon^* \qquad 2.46$$

where

$$D^* = 1.8 \times 10^3 \, Z^{-0.15} \qquad 2.47$$

$$\epsilon^* = 0.57 d_o^{0.17} \epsilon_p \qquad 2.48$$

and u is a constant.

If recrystallisation does not take place, the effect of accumulated strain must be taken into account when calculating the effective austenite grain size for the following pass. In plate rolling, equation 2.45 should be used to calculate the recrystallised grain size since the applied strain is almost never greater than ϵ^* [34].

Ouchi [41] determined the statically recrystallised austenite grain size in hot rolled C-Mn steels in terms of interfacial grain boundary area, flow stress, strain and roll geometry factor:

$$d_{rex} = 0.17/(S_v \, \bar{\sigma} \, \epsilon \, Q)^{1/3} \qquad 2.49$$

where

$$S_v = \{1.67(\epsilon - 0.1) + 1\}(2/d_o) + 63(\epsilon - 0.3) \qquad 2.50$$

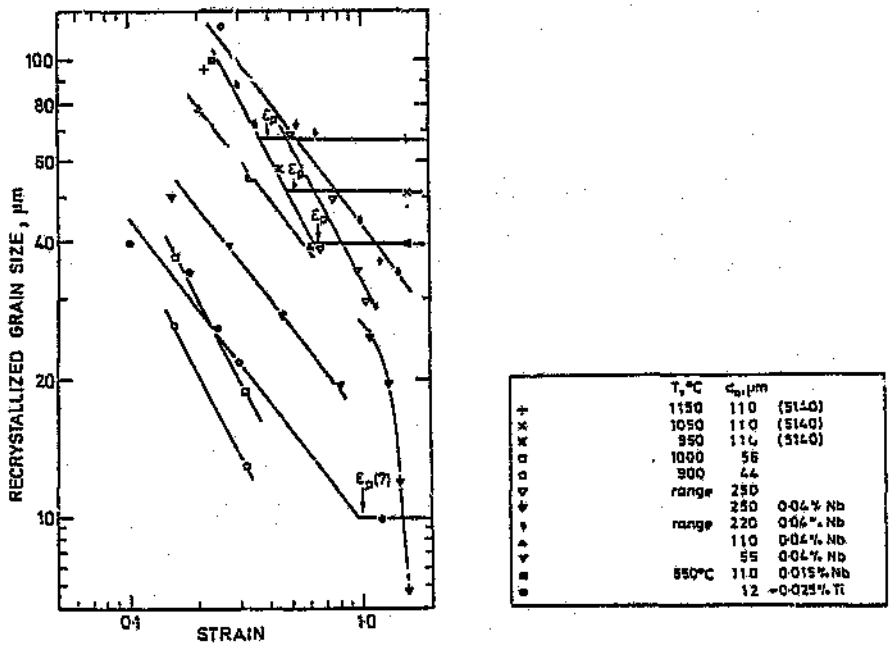

Figure 2.18 Effect of strain on static recrystallised grain size [34]

A modified double-stroke test was developed by Striesselberger et al [14] to evaluate the anisothermal softening ratio (fraction recrystallised), X_a, occurring in austenite during interpass hold times or anisothermal strengthening, X_σ, during deformation (Figure 2.19). Both the rise in temperature due to deformation heating and the temperature drop due to radiation during the hold period are taken into account. By employing this method for multi-pass hot deformation schedules, the state of austenite strengthening/softening can be evaluated at any intermediate stage of working. The anisothermal sorftening ratio is given by:

$$X_a = (K_1\sigma_1 - K_2\sigma_2) / (K_1\sigma_1 - \sigma_e) \qquad 2.51$$

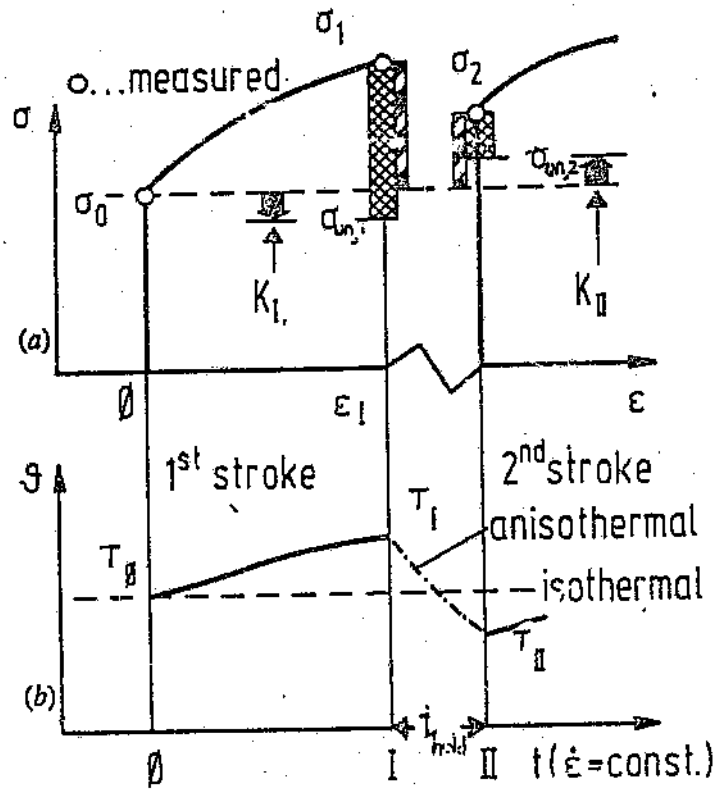

Figure 2.19 Principle of the double stroke technique for evaluating mechanical softening during deformation [14]

Figure 2.20 shows how to determine the temperature conversion factors, K_1 and K_2. The symbols $\sigma_{um,1}$ and $\sigma_{um,2}$ are the yield stresses of the material with no prior deformation at the temperature, strain rate and strain of the end of the first pass and beginning of the second pass respectively.

If $X_n = 1$, the structure is fully recrystallised. If $X_n = 0$, the structure is unrecrystallised.

By determining the strengthening ratio, X_r, the strengthened state of the material at the beginning and end of each deformation can be measured. For the first pass,

$$X_r = (\sigma_1 - \sigma_0)/\sigma_0 \qquad 2.52$$

2.6.2.3 Grain growth

The grain size due to isothermal grain growth, d_{gg}, at time t is related to the recrystallised grain size, d_{rex}, by the equation [42]:

$$d_{gg}(t) = d_{rex}(1 + \alpha_{gg} \ln (t/t_{99})) \qquad 2.53$$

Choquet et al [42] found that $\alpha_{gg} = 0.195$ for C-Mn steels.

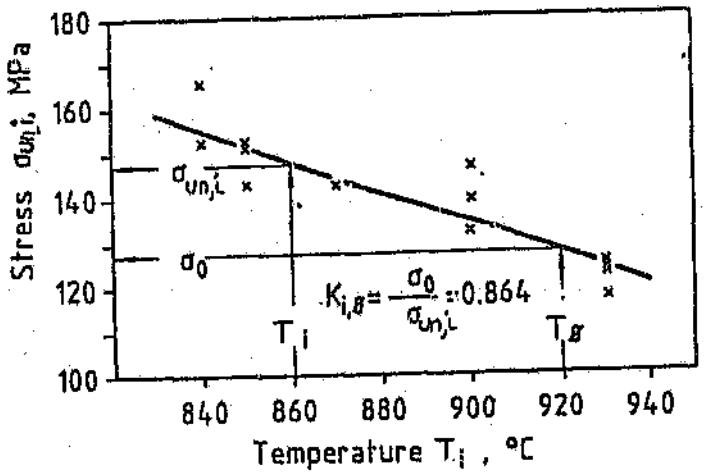

Figure 2.20 **Yield stress of undeformed S32 C-Mn steel as a function of temperature: shows method to determine temperature conversion factor for T = 920°C and T = 860°C [14].**

Grain growth under continuous cooling conditions may be calculated [42] using equation 2.53, assuming that the activation energy (300 000 J/mol) remains constant during cooling.

$$d_{gg}(t) = d_{rex}(1+\alpha_{gg}\ln(t/t_{99})) - 300000(1/T-1/T_d)/8.314 \qquad 2.54$$

Foster [19] studied the kinetics of grain growth of C-Mn steels at various temperatures. From Figure 2.21 it is seen that grain growth is favoured at high temperatures and long holding times. The following equation was found to describe grain growth kinetics in C-Mn steels at 950°C:

$$d_{gg}^2 = d_{rex}^2 + 26.2\, t_{hold} + 2000(1 - \exp(t_{hold}/7) \qquad 2.55$$

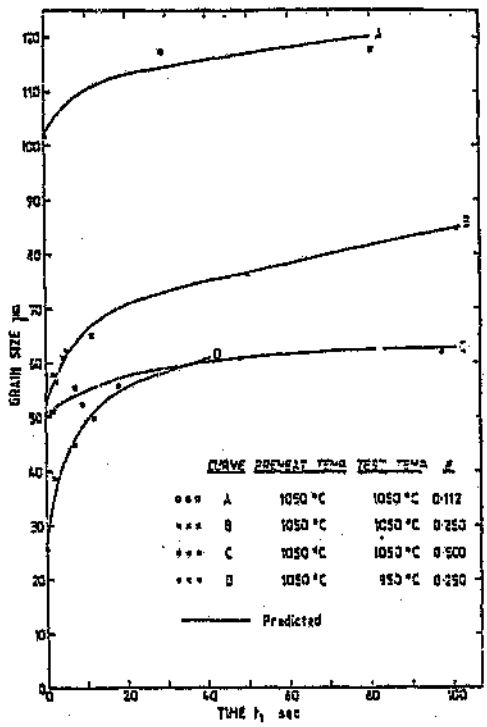

Figure 2.21 Grain growth after static recrystallisation in plain carbon steels [19]

2.6.3 Effect of deformation parameters on statically recrystallised grain size

2.6.3.1 Strain

In C-Mn steels, strain is a most important parameter affecting recrystallised austenite grain size. Figure 2.18 shows that the larger the strain the finer the recrystallised grain size [34]. Since dynamic recrystallisation results in finer grain size than static

recrystallisation, very high reductions at high temperatures and low strain rates should be aimed for. However, in industrial hot rolling, these conditions cannot be met and schedules have to be designed using small to medium reductions. Typical conditions (high rolling temperatures, low to medium strains) on the Vanderbijlpark plate mill result in a fully recrystalllised austenite microstructure.

Austenite microstructure may be divided into three different morphologies: fully recrystallised by static or dynamic recrystallisation , partially recrystallised and elongated or unrecrystallised microstructures [43]. Micrographs showing various austenite microstructures [44] are given in Figure 2.22.

Figure 2.23 shows a schematically represents the expected austenite microstructure as a function of deformation temperature and strain for a given initial austenite grain size. At high rolling temperatures, full recrystallisation occurs at fairly small to medium strains resulting in a refined, equiaxed austenite structure. However, grain growth is also favoured at high temperatures and thus the optimum condition between ease of recrystallisation and recrystallised grain size must be found [45]. If small amounts of strain (typically 8-14%) are applied at high temperature the resulting austenite is partially recrystallised consisting of a combination of large and small grains. If rolling takes place repeatedly in the partially recrystallised region at high temperatures, full recrystallisation will eventually result [46]. Very low strains (< 8%) in the high temperature region produce abnormally large austenite grains, larger than the initial grain size, and persist throughout subsequent passes. This is to be avoided since large austenite grains are difficult to recrystallise and are detrimental to toughness [7].

It is also seen that when medium to large strains are applied to the austenite structure in the no - recrystallisation region at low temperatures (A_{r3} - 950 °C), the grains become elongated or "pancaked". This introduces deformation bands and substructures into the grains. Deformation bands and pancaked grains are advantageous for grain refinement since they respectively, act as nucleation sites for ferrite

formation and as structural boundaries that inhibit the subsequent grain growth of ferrite [43].

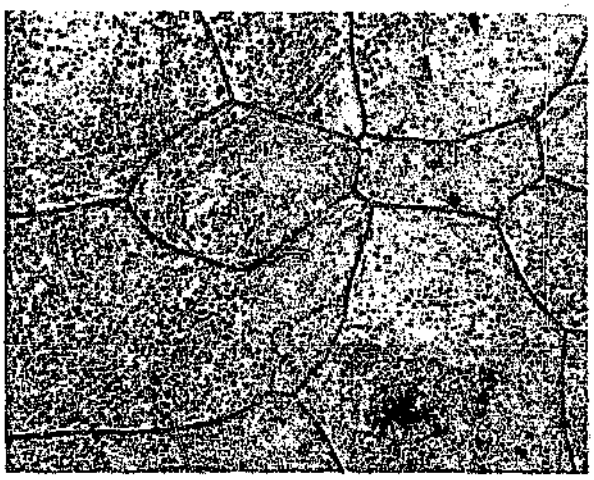

a) Undeformed austenite

b) Partially recrystallised

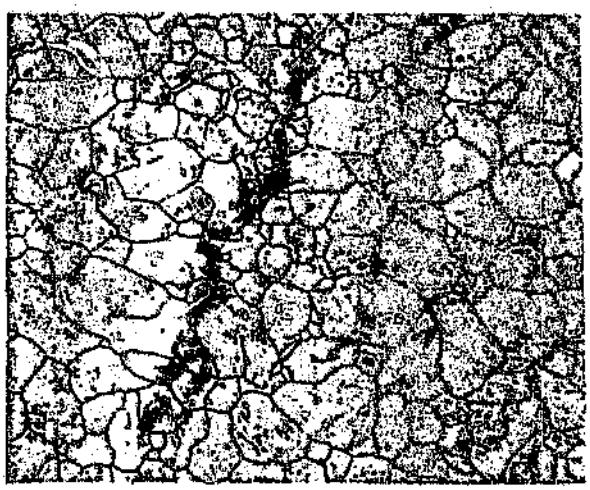

c) Fully recrystallised

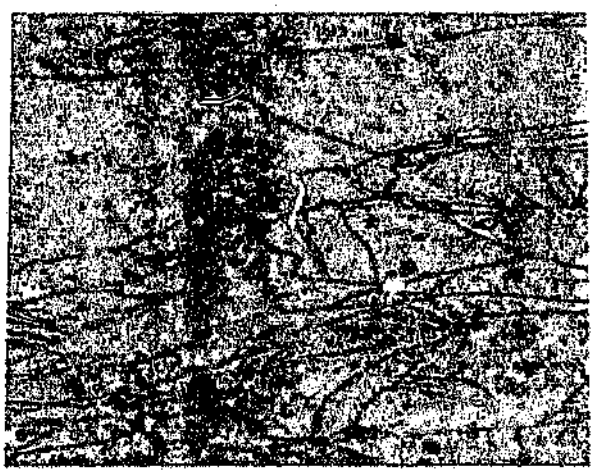

d) Elongated (no recrystallisation)

Figure 2.22. Different austenite microstructures

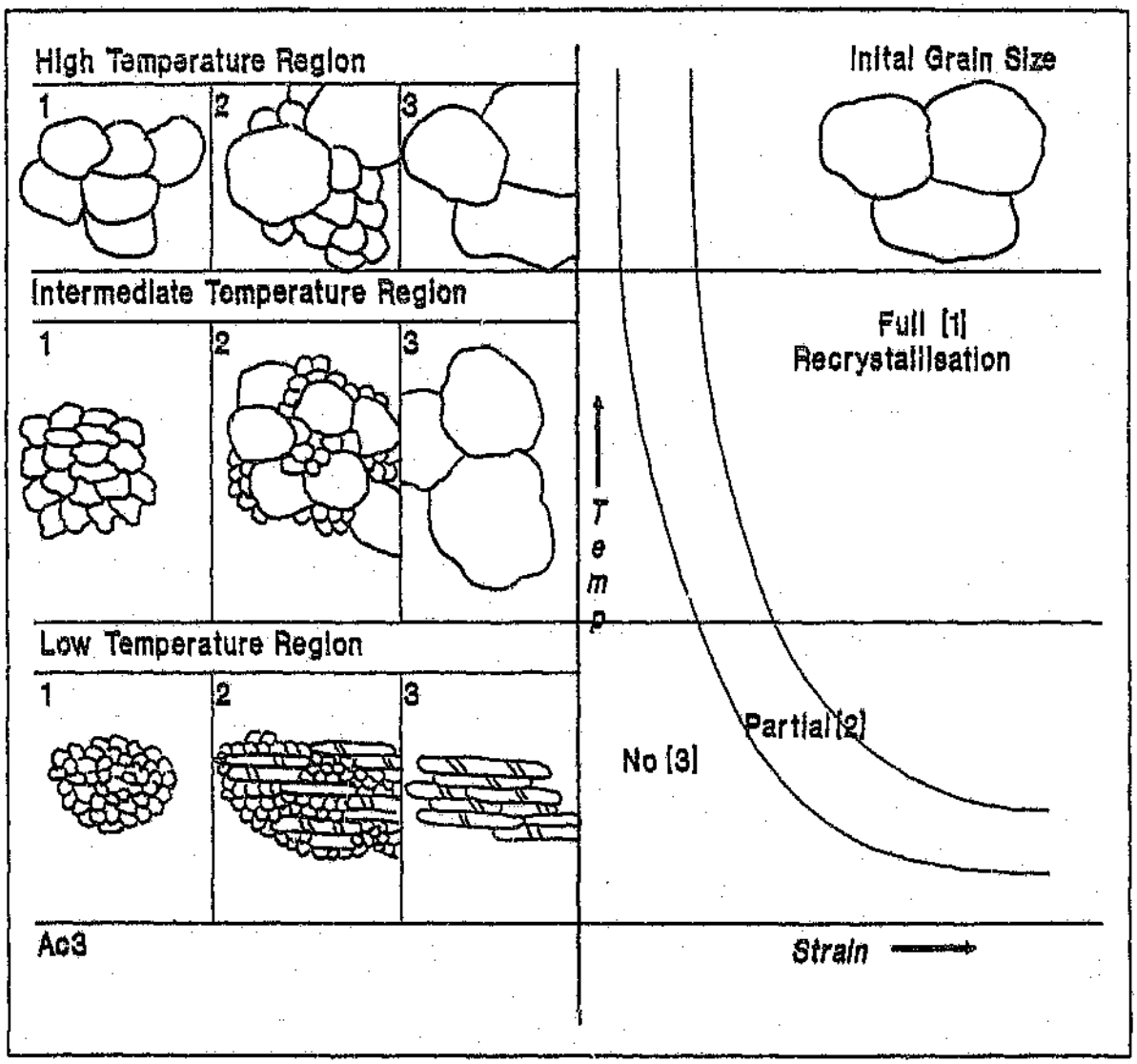

Figure 2.23 Microstructural changes occurring in the hot working of steel

2.6.3.2 Temperature

Low reheat temperatures promote finer recrystallised grain size [43,48] which increases toughness and strength. Small initial grain sizes reduce the critical reduction for dynamic and/or static recrystallisation [28].

There is no general agreement in the literature concerning the effect of rolling temperature on recrystallised austenite grain size. According to Sellars [34] and Tanaka [43], rolling temperature does not have a significant effect on grain size for C-Mn steels. Speich [49] and Gohda [48] however, maintain that the lower the rolling temperature in the austenite region, the finer the grain size.

2.6.3.3 Strain rate

From equation 2.5 it was seen that large roll radii, high roll speeds and large strains result in large strain rates. Although some authors [4,15] found that strain rate has no influence on microstructure in C-Mn steels within one or even two orders of magnitude, Ouchi et al [46] found that an increase in strain rate reduces the grain size during hot rolling.

2.6.3.4 Hold time

It is seen fom Figure 2.17 that at medium to high temperatures (T > 950 °C) the recrystallisation times are very rapid in C-Mn steels. In hot rolling, the time for full recrystallisation to take place is usually well within interpass delay times provided the initial grain size is small enough and sufficient strain is applied (equation 2.45). At lower temperatures , recrystallisation is more sluggish and there may be insufficient time after rolling for recrystallisation to be completed which leads to a mixed grain structure and poor toughness. Too long a holding period however, leads to undesirable grain growth. Recrystallisation times are much longer in microalloyed steels due to carbonitride precipitation retarding the nucleation of new grains.

2.6.4 Transformation to ferrite

The most important microstructural feature that improves the final mechanical properties of C-Mn steels is the ferrite grain size which

strongly influences both strength and toughness. There are various ways of refining ferrite [50]:

- Recrystallisation of austenite by repeated deformation in the high temperature region
- Deformation in the no - recrystallisation region to form subgrains in the austenite which act as nucleation sites
- Increasing the austenite to ferrite volume ratio by accelerated cooling through the transformation region
- Recrystallisation of strain - induced ferrite by deforming in the two-phase (intercritical) region
- Use of precipitates and inclusions as nuclei for ferrite during transformation (generally not applicable in C-Mn steels)

Suehiro [51] found that the transformed ferrite grain size may be expressed in terms of the ferrite transformation start temperature, A_{r3}, and the prior austenite grain size, d_γ.

$$d_\alpha = (5.51 \times 10^{10}\, d_\gamma^{1.75} \exp -(1072/A_{r3}))^{1/3} \qquad 2.5$$

The effect of stored strain in hot deformation on the transformation kinetics may be accounted for by using the effective austenite grain size expressed in equation 2.56 as a function of residual dislocation density, ρ'.

$$d_\gamma' = d_\gamma / (1 + 10^{-11}\, \rho'^{1.154}) \qquad 2.57$$

Umemoto [52] found that the ferrite grain size, formed from continuously cooled, fully recrystallised austenite, may be expressed in terms of austenite grain size prior to transformation and cooling rate.

$$d_\alpha = 5.7\, CR^{-0.26}\, d_\gamma^{0.46} \qquad 2.58$$

An effective way of refining the ferrite is by increasing the amount of ferrite nulclei by increasing the cooling rate [53-59] through the transformation range (A_{r3} - A_{r1}) instead of conventional air cooling. A

dramatic increase of yield and tensile strength can be obtained without deteriorating toughness. The effect of the cooling start and end temperatures as well as the cooling rate on the tensile strength and toughness of steel are shown schematically in Figure 2.24.

It is generally considered that a cooling rate of about 20 $°Cs^{-1}$ results in adequate microstructure and properties in C-Mn steel [54]. The optimum cooling rate, however, for a particular steel depends on the chemical composition.

Accelerated cooling from above the A_{r3} effectively shifts the A_{r3} to a lower value and produces ferrite grain refinement by a mechanism similar to that by alloying. However, too fast a cooling rate always results in undesirably coarse bainite. This arises from the fact that only preferential sites on austenitic grain boundaries are able to nucleate ferrite. Finish accelerated cooling below about 450 °C usually gives rise to a large strengthening effect accompanied by noticeable deterioration in FATT due to the presence of large amounts of various low temperature transformation products. Finish accelerated cooling above 500 °C is preferred in practice [55].

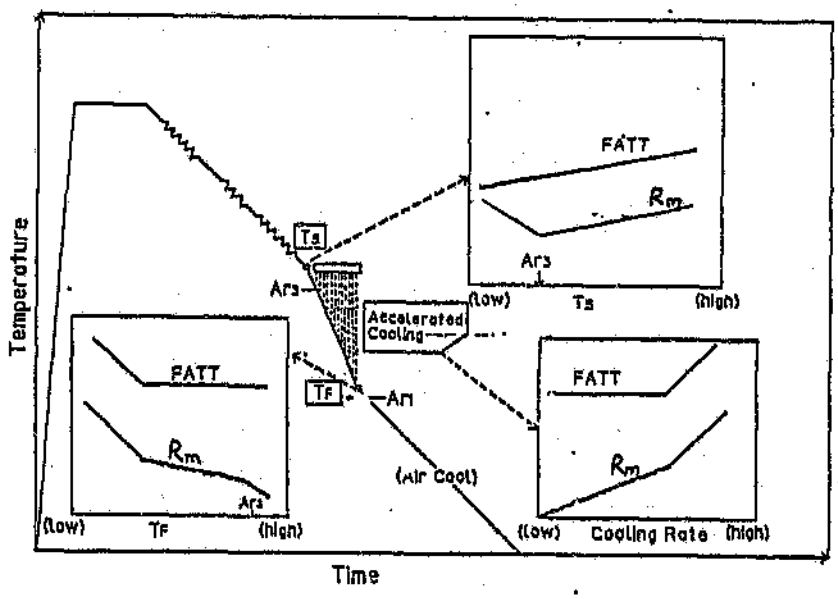

Figure 2.24 Effect of cooling start and end temperatures and the cooling rate on the tensile strength and toughness of steel [54]

2.7 Correlation between microstructure and mechanical properties

The unique feature of ferrite grain refinement is that it improves both strength and toughness. However, the strength and toughness of ferritic-pearlitic steels depend not only on the final ferrite grain size but also on the volume proportion and distribution of the pearlite (or bainite).

2.7.1 Yield strength

The effects of chemical composition and ferrite grain size on the yield stress of ferritic-pearlitic steels are usually represented in the form of empirical equations examples of which are given below. Strengthening contributions due to solid solution strengthening is accounted for by the chemical composition terms.

$$R_e = 105 + 83[Si] + 43[Mn] + 18.4d_\alpha^{-1/2} + 1540[N] \quad [60] \quad 2.60$$

$$R_e = 105 + 84[Si] + 33[Mn] + 17.5d_\alpha^{-1/2} \quad [61] \quad 2.61$$

Speich [49] found that low deformation temperatures in the ferrite/pearlite region also produced a strengthening contribution from the dislocation substructure generated in the ferrite.

$$R_e = 8 + 10[Si] + 5[Mn] + 2.6d_\alpha^{-1/2} + \sigma_{disl} \quad 2.62$$

The effect of finishing temperature on the R_e-ferrite grain size relationship is shown in Figure 2.25. The usual $d_\alpha^{-1/2}$ dependence of yield strength is obeyed until low finish temperatures (677°C) where a sharp departure from this trend is observed and the yield stress increases rapidly with little further decrease in grain size. Speich [49] found that pearlite only contributes about 7 MPa to the strength of low carbon steels.

2.7.2 Tensile strength

Whilst pearlite in low carbon steels does not affect the yield stress, it has an effect on tensile strength. Small ferrite grain size and high volume fractions of pearlite increase the tensile strength [62].

$$R_{ss} = 15.4(19.1+1.8[Mn]+5.4[Si]+0.3[pear]+0.5\ d_{\alpha}^{-1/2}) \qquad 2.63$$

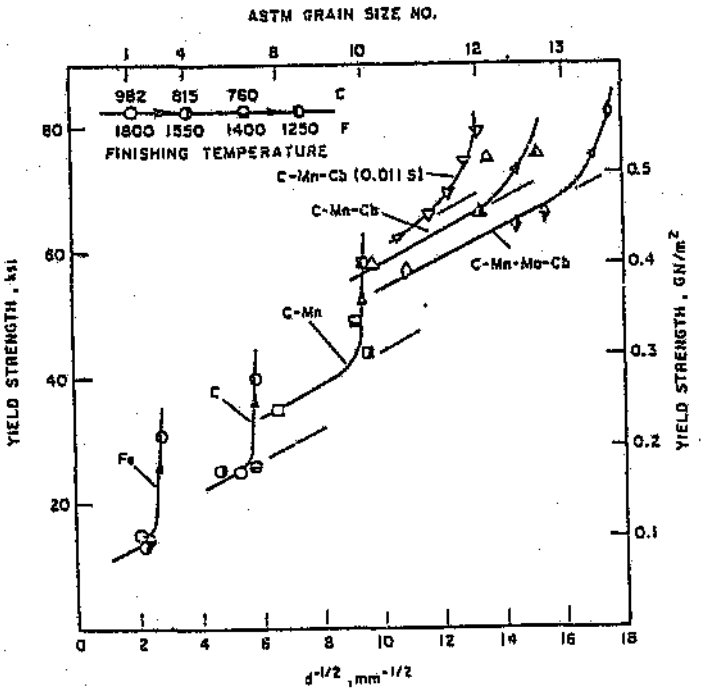

Figure 2.25 Effect of finishing temperature on the yield stress - grain size relationship [48]

2.7.3 Toughness

The major toughness parameters which have been correlated with grain size are the impact - transition - temperature , ITT, and the fracture - appearance - transition - temperature, FATT. The general equation developed [61] to relate the ITT with ferrite grain size is:

$$A.ITT = \ln(A) - \ln(B) - \ln(d_{\alpha}^{-1/2}) \qquad 2.64$$

where A and B are constants, ITT is in °C and d_{α} is in mm.

Many relationships have been formulated to show the effect of grain size and composition on FATT. A typical relationship is as follows [62].

$$FATT = -19 + 44[Si] + 700[N] + 2.2[Pear] - 11.5.d_{\alpha} \qquad 2.65$$

where FATT is in °C.

Small pearlite colonies are beneficial to the FATT because cleavage cracks are often observed to stop and change direction at pearlite colony boundaries [64].

The effect of finishing temperature and composition on the FATT of C- Mn steels [49] is given in Figure 2.26. The transition temperature of all steels decreases with decreasing finishing temperature according to a $d^{-1/2}$ relationship if all the deformation is in the austenite region. When deformation is extended to the austenite/ferrite zone the FATT increases with little change in grain size.

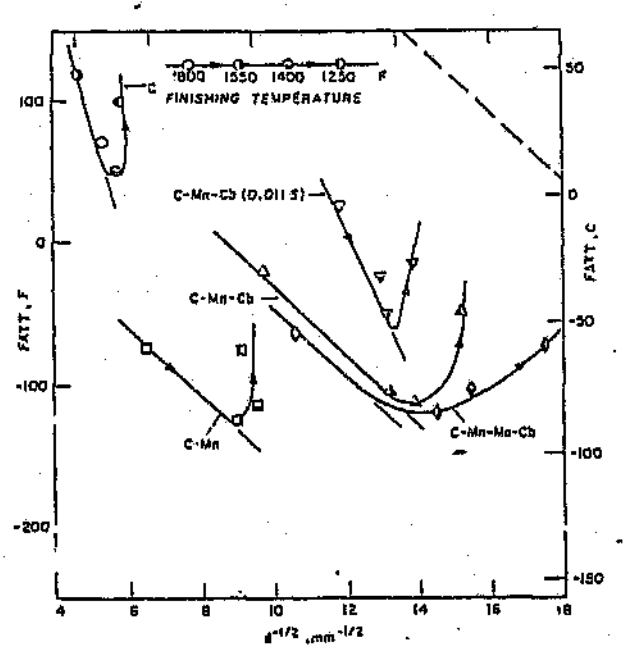

Figure 2.26 Effect of finishing temperature and composition on the FATT of C-Mn steels [49].

2.8 Computer simulation of multi-pass rolling

If the basic relationships between the deformation variables and microstructural changes discussed above are verified or established from single and multi-pass laboratory tests, the sequential changes during multi-pass rolling can be computed [1,34]. By combining these microstructural changes with a finite difference computation of temperature changes in plane strain compression testing, rolling conditions can be closely simulated, as illustrated in Table 2.3.

Equations for flow stress as a function of rolling variables and microstructure can be incorporated into the computer program to enable the prediction of rolling loads (and torques).

Table 2.3

Simulation results for rolling with 20% reductions per pass and 15s hold time between passes [1].

	ROLLING		PLANE STRAIN COMPRESSION		COMPUTATION	
	Temp °C	d μm	Temp °C	d μm	Temp °C	d μm
0.12%C, 1.46%Mn, 0.032%Nb steel						
Reheat	1160	110	1160	110	1160	110
Pass 1	1140		1139	60	1142	58
Pass 2	1060		1058	39	1061	38
Pass 3	900		900	40	899	38
				(53 x 31)		(47 x 30)
Pass 4	850	37	850	39	848	38
		(57 x 23)		(61 x 25)		(59 x 24)
Ferrite		8.3		7.5		9.5
0.12%C, 1.46%Mn steel						
Reheat			1127	115	1127	115
Pass 1			1092	55	1083	61
Pass 2			1027	44	1025	48
Pass 3			904	32	900	35
Pass 4			850	32	850	32
				(70% Rex.)		(43% Rex.)
Ferrite				9		12-15

The advantage of this form of simulation is that there are no limitations to the deformation conditions that can be simulated. The disadvantage is that it requires a considerable body of reliable basic data to establish the complex quantitative structure-property relationships required for a particular material.

3 EXPERIMENTAL PROCEDURES

3.1 Introduction

This chapter discusses the equipment and experimental methods used during plane strain compression tests. Techniques used for retrieving and analysing data are presented. The formulation of a computer programme to predict the temperature distribution in a rectangular specimen during plane strain compression is briefly presented with a more detailed discussion given in Appendix 1. A computer programme written to simulate important thermal, mechanical and kinetic changes occurring during hot plate rolling is discussed.

3.2 Materials

Three samples of as-rolled SC8 C-Mn plate steel of slightly different chemical composition were supplied by Iscor Vanderbijlpark Works. The samples were cut from the tail end of each plate. The chemical compositions of each sample are given in Table 3.1.

Table 3.1

Chemical Composition of SC8 C-Mn Steel

	C	Mn	Si	S	Al	P	N
Grade A:	0.11	1.21	0.27	0.003	0.004	0.004	0.002
Grade B:	0.18	1.05	0.27	0.003	0.004	0.004	0.002
Grade C:	0.11	0.65	0.27	0.003	0.004	0.004	0.002

3.3 Experimental techniques used in plane strain compression testing

3.3.1 The servo-hydraulic machine and ancillary equipment

Plane strain compression tests were performed on a modified, 1500 kN capacity servo - hydraulic machine. The test arrangement is shown in Figure 3.1a. Photographs showing the plane strain compression specimen during the reheating and deformation stages of the plane strain compression test are given in

Figures 3.1b and Figure 3.1c respectively. The testing machine comprises essentially of:

1. A 100mm stroke servo actuator.

2. Electronic control unit comprising of three mode controls (displacement, strain and load) and additional modules viz. computer control interface, IBM micro computer, monitor, dual disk system, Epson printer and plotter.

3. Hydraulic power pack supplying 180 litres/min at 280 bar via high pressure hoses.

The servo-actuator is capable of applying 50 mm of stroke to the ram in tension and compression . Four accumulators were added to the machine to increase the hydraulic capacity for faster strokes in order to achieve similar strain rates (1 - 100 s^{-1}) to those found in rolling.

Compression platens, whose dimensions are shown in Figure 3.2, were machined from H13 high temperature die steel. The platen breadth was 30mm. This gave a b/h ratio of 1.2 (see section 2.5.1) for 25 mm thick specimens. After machining, the tools were hardened by austenitising at 1050°C for 12 hours, followed by air cooling. Special fixtures were made to mount the upper and lower platens to the ram and base respectively of the servo-hydraulic machine.

The specimen transport trolley, shown in Figure 3.3, conveyed the specimen between the three (induction heating, deformation and air/water cooling) regions of the plane strain compression test. The trolley was mounted on four wheels which moved along angle iron rails by means of two pneumatic cylinders operating at 5 bar air pressure. The trolley was open at one end to facilitate specimen movement into the induction coil during a heating period.

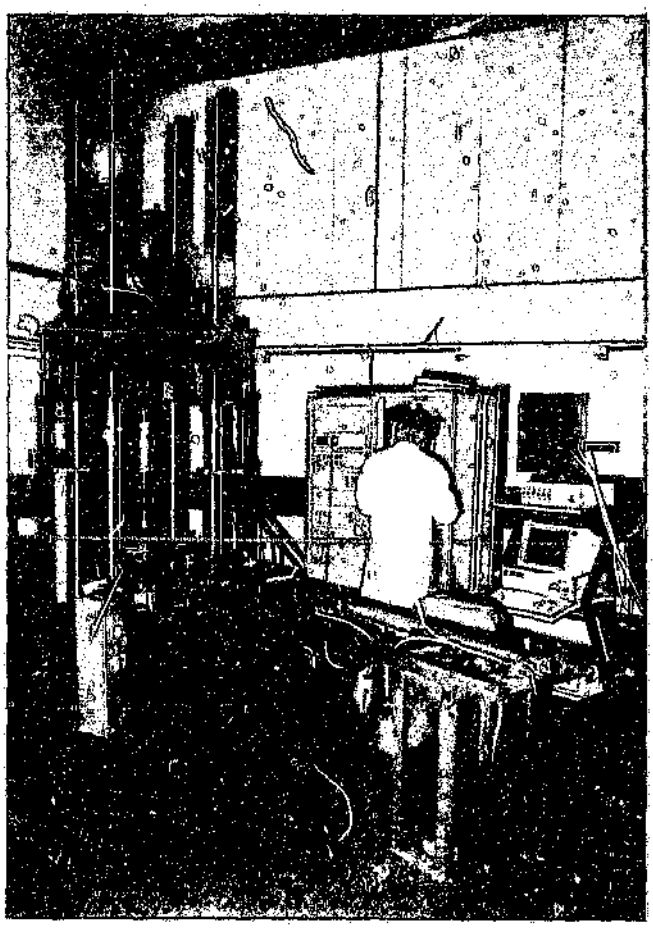

Figure 3.1a Plane strain compression test layout

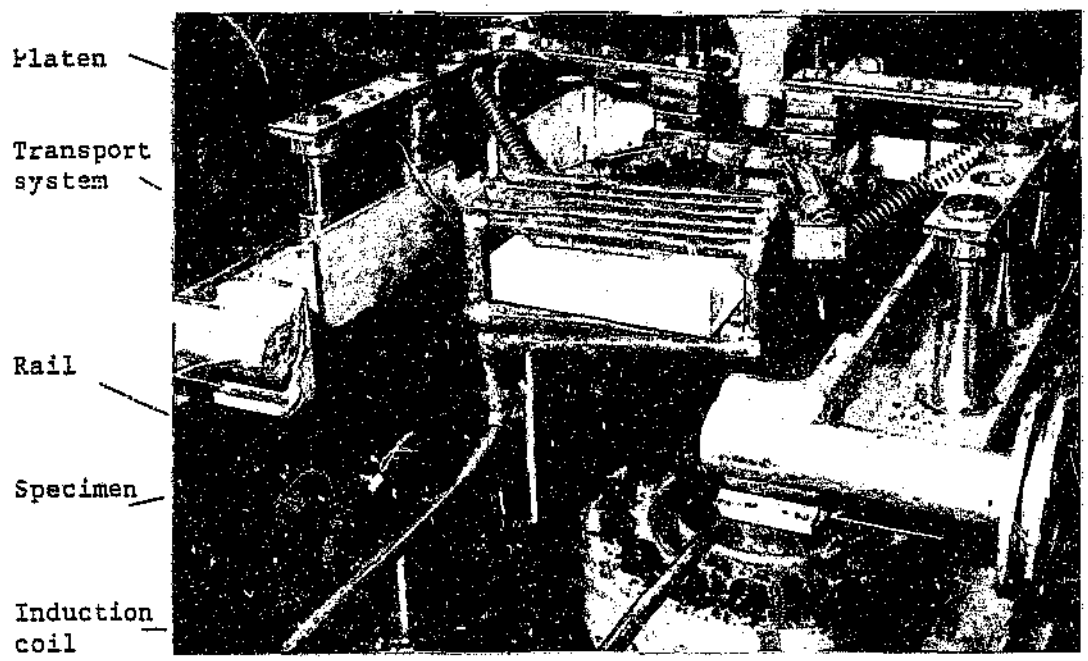

Figure 3.1b Reheating the specimen by induction

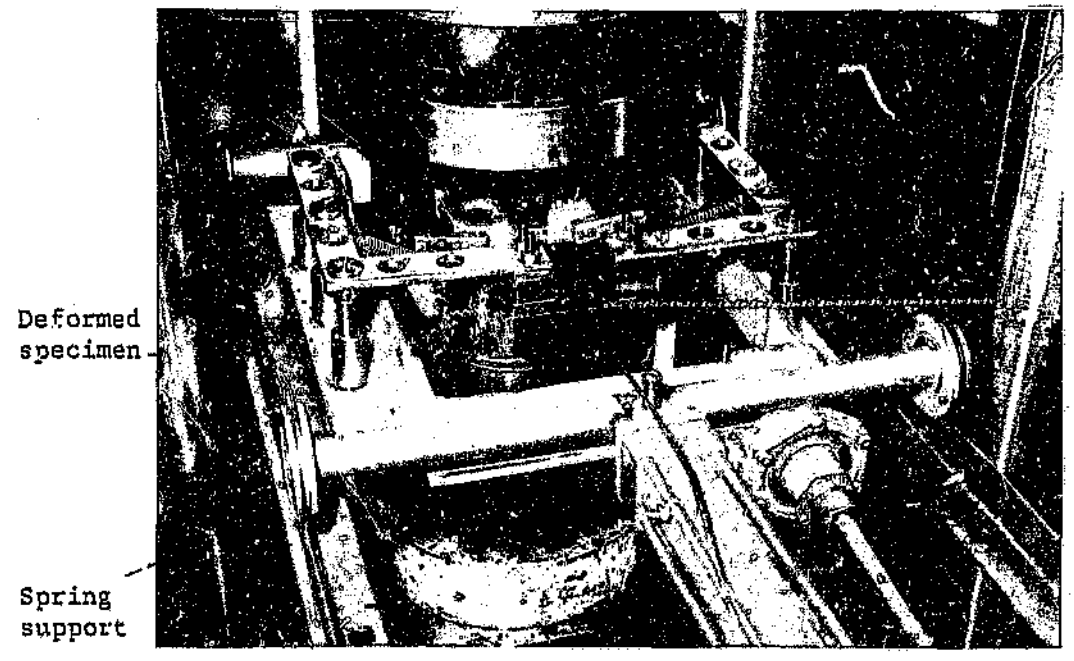

Figure 3.1c Deforming the specimen

Both cylinders were operated manually through on/off switches. The specimen was supported in the centre of the trolley by means of two stainless steel arms attached to each end of one side of the specimen. The arms were attached to a cross support resting on three springs fixed on either side of the trolley. The arms were free to open symmetrically as the specimen extended lengthwise during deformation and ensured that the specimen remained central between the platens. The arms were spring loaded to allow the specimen to be pushed by the upper platen onto the lower platen during deformation whilst supporting it freely between deformations . This first of all allows the specimen to be moved easily to and from the deformation region and secondly reduces the heat transfer between the specimen and platen to a minimum.

The first cylinder (400 mm full stroke) was attached to the rear of the trolley and to the front of the second cylinder and enables specimen transportation to and from the heating and deformation regions. The second cylinder (1100 mm full stroke) was fixed to the end of the rail support structure and facilitated the movement of the specimen to and from the deformation and cooling regions. The air pressure was adjusted to provide a specimen travelling time between each region of less than 1 second.

A 50 kW capacity induction furnace was used to reheat the specimen to the required austenitising temperature. The furnace has a PID (potential integral differential) controller which enables the user to vary and control the specimen heating cycle. Due to the shape of the specimen, a rectangular induction coil had to be made to provide a uniform heating rate to the specimen. The coil was manufactured out of 10 mm diameter copper tubing.

A second computer, complete with PC-Labcard®, a multi - function control card, has recently been installed which enables the specimen heating cycle to be controlled from a remote set point. The computer also controls the pneumatic cylinders thereby allowing simultaneous, automatic control of the specimen temperature and specimen transportation.

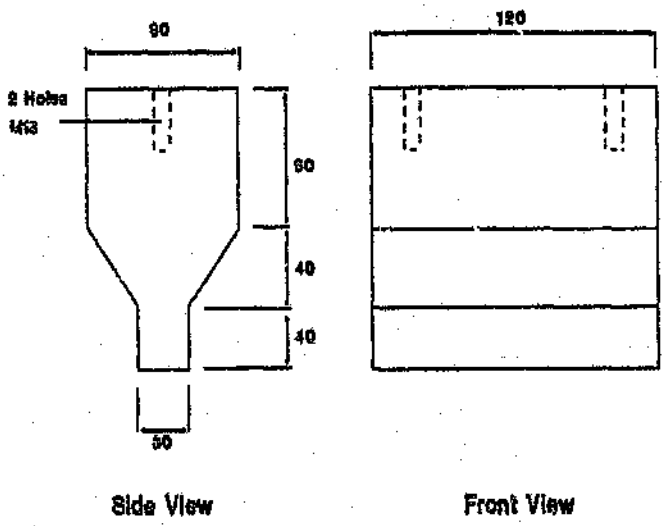

Figure 3.2 Platen Dimensions

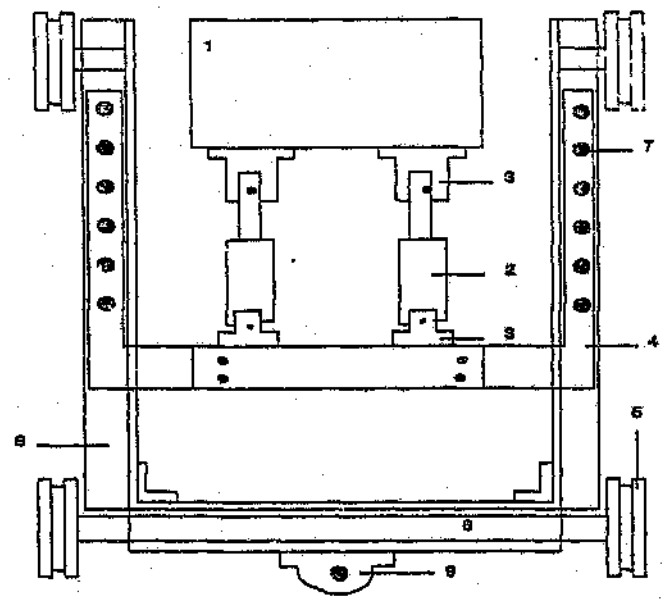

Legend:
1. Specimen
2. Piston
3. Piston attachment
4. Cross support
5. Trolley wheel
6. Wheel axle
7. Spring
8. Angle iron frame
9. Attachment to pneumatic cylinder

Figure 3.3 Specimen Transport Trolley

The quench unit consisted of adjustable brass nozzles fixed to aluminium blocks situated above and beneath the fully retracted specimen position (Figure 3.4). The distance from the nozzle ends to the specimen surface was 120 mm. Water channels , drilled into the interior of the blocks, supplied water to the specimen top and bottom surfaces. The nozzle apertures were adjusted to vary the water velocity and hence specimen cooling rate according to the requirements of each test.

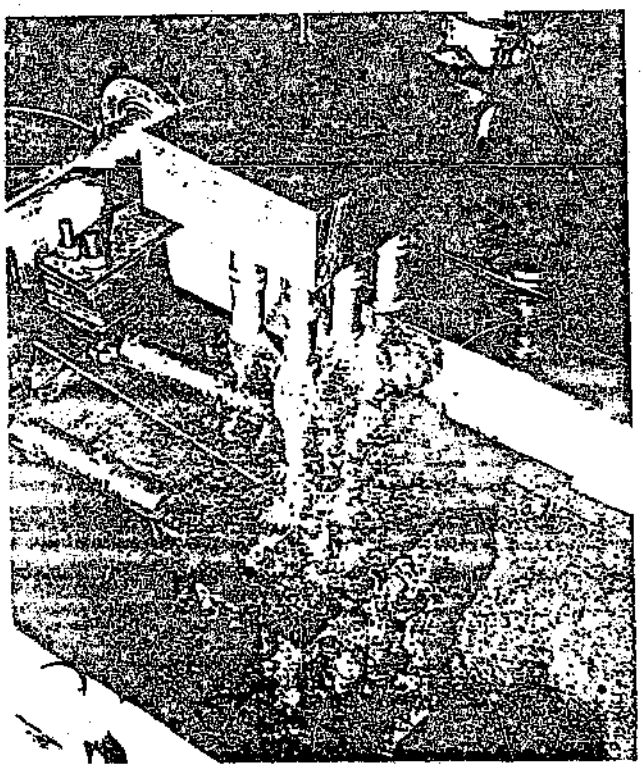

Figure 3.4 Water cooling apparatus used in plane strain compression tests

3.3.2 Specimen preparation

The dimensions of the specimen were 25x90x120mm³ and were chosen so that:

a) The maximum load capacity of the machine (1500 kN): should not be exceeded during deformation. Wide specimens have a large deformation area and result in large force requirements.

b) The deformed material should be sufficiently thick to allow the preparation of tensile and Charpy impact specimens.

c) Plane strain conditions should be obtained or approximated as closely as possible: thin, wide specimens are necessary for this. (see section 2.5.1).

Holes were drilled to position thermocouples in the centre of the specimen. K-type, mineral insulated, inconel sheathed thermocouples of 2.5mm diameter were implanted into the holes to continuously measure the temperature of the specimen in the deformation zone.

To overcome oxidation to a certain degree, the specimens were sand blasted and given two coats of Rockgrip heat recistant aluminium paint.

3.3.3 Plane strain compression test sequence

A multi-section ramp program, MULTR2, was written by MAND (Pty) Ltd. to control the servo-hydraulic machine.

At the start of a test the test number and machine control mode i.e. load, strain or position were entered followed by the load, strain and position limits. The time into the test, in seconds, followed by the actuator position required at that point were entered. The programme was capable of controlling fourteen continuous time-position sequences. A graphic display of the time-position sequence during a typical four pass plane strain compression schedule is given in Figure 3.5).

Load , time and platen position data were logged (the fastest data acquisition rate was $0.005s^{-1}$) and stored in binary format on hard disk. Sample output data are given in Figure 3.6. A programme was written in TurboBasic in order to convert this data to ASCII text format. The data represented in this format could then be further analysed using standard computer packages. Listings of the computer programmes converting load, position and time to ASCII code are given in Appendix 2.

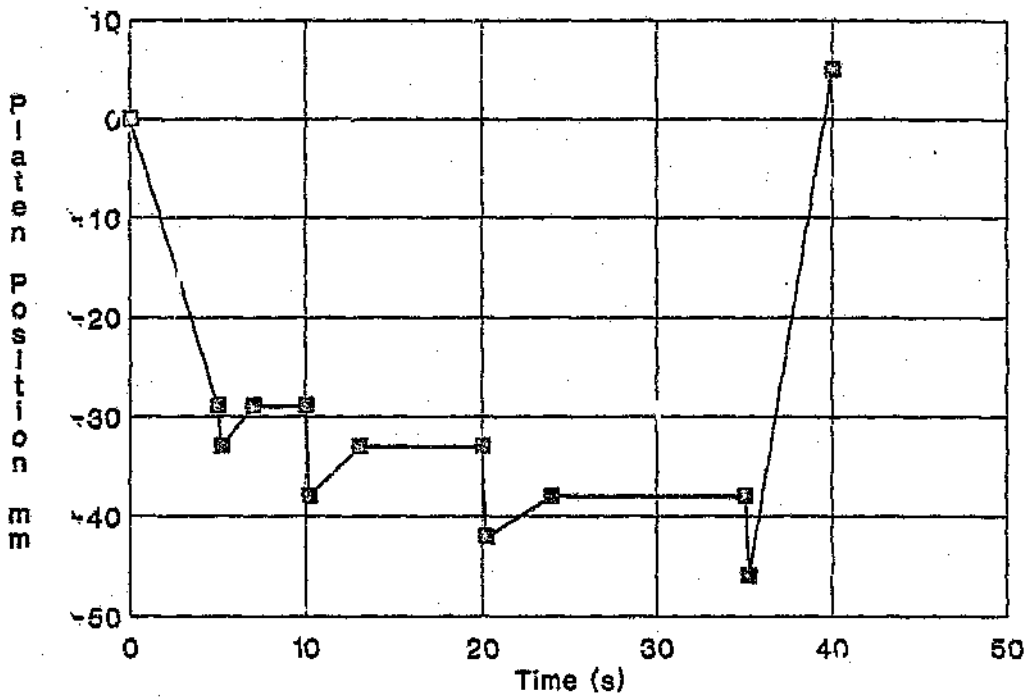

Figure 3.5 Graphic display of time-position sequence during a four pass plane strain compression test

FEEDBACK DATA

TIME (Seconds.)	LOAD (kN)	STRAIN (%)	POSITION (mm)
0.000	1.421	-0.005	-5.029
0.900	1.431	-0.005	-6.384
1.800	1.450	-0.005	-7.739
2.700	1.445	-0.005	-9.094
3.600	1.440	-0.005	-10.449
4.500	1.455	-0.005	-11.792
5.400	1.504	0.000	-13.147
6.300	1.538	-0.005	-14.502
7.200	1.533	-0.005	-15.869
8.100	1.528	-0.005	-17.212
9.000	1.539	-0.005	-18.579
9.900	1.528	-0.005	-19.922
10.780	1.489	-0.005	-20.068
11.680	1.450	-0.005	-20.081
12.580	1.426	-0.005	-20.068
13.480	1.440	-0.005	-20.068
14.380	1.455	-0.010	-20.068
15.280	1.455	-0.010	-20.068
16.180	1.465	-0.005	-20.068
17.080	1.484	-0.005	-20.068
17.980	1.533	-0.005	-20.081
18.880	1.563	-0.005	-20.068
19.780	1.543	-0.005	-20.068
20.660	1.504	-0.005	-18.762
21.560	1.489	-0.005	-16.980
22.460	1.494	-0.005	-15.149

Figure 3.6 Sample of test output data

Before the start of a test, the exact position of the upper platen at the start of the first deformation was determined. This was done by slowly lowering the platen until a small increase in the initial load was recorded. This increase in load indicated that both platens were flush against the upper and lower specimen surfaces. At the beginning of the test, the upper platen took 30 seconds to reach the upper surface of the specimen from its initial position (0 mm). The initial ramp period of 30 seconds was too long for certain tests. When it was required to deform the specimen shortly after reheating, a shorter time interval was included at the beginning of the program inputs.

After the specimen was reheated to the required austenitising temperature and soaked for 30 minutes, the first cylinder (400mm stroke) was activated and transported the specimen to a fixed point directly between the upper and lower deformation platens. Temperature data acquisition commenced immediately after the specimen was retracted from the furnace.

After the specimen was positioned between the two platens, the machine control programme, MULTR2, was initiated and the programmed upper platen time-position sequence was carried out.

After the deformation sequence was complete, the second pneumatic cylinder (1100 mm stroke) was activated and transported the specimen to the cooling unit where the specimen was cooled according to test requirements. Most specimens were air cooled to simulate cooling rates found during run-out table cooling after plate rolling. Some specimens were subjected to varying cooling rate ($1°Cs^{-1}$ - $50°Cs^{-1}$) in order to determine the effect of cooling rate on final microstructure.

3.3.4 Measurement and calculation of deformation parameters

3.3.4.1 Calculation of temperature

The specimen centre temperature was continuously monitored. Thermocouple voltage readings were recorded using a six channel IF85 data acquisition unit. The strong inconel sheathing ensured that the thermocouple remained functional throughout each test. Software for communications between the data

acquisition unit and a computer was written by the author and is given in Appendix 3. The data acquisition unit has the capability of recording at a sampling rate of less than 1us. The sampling rate was chosen to allow sufficient recording time for the entire duration of the test (e.g. 50ms = 14 min. of recording time). Voltages recorded during a test were converted to temperature, °C and time, s, using programme CONVERT, given in Appendix 3.

3.3.4.2 Calculation of strain

The equivalent strain, ϵ, was calculated from the platen position data using equation 2.1 and equation 2.2. The initial specimen thickness, h_o, corresponded to the initial upper platen position before the first deformation. The position of the lower platen remained constant throughout a test.

The strain origin for each pass ($\epsilon = 0$) during multi-pass tests was taken at the point of total relaxation of stress in the previous pass.

Table 3.2 showed excellent agreement between recorded and measured final total specimen strain, the maximum difference between the two being not more than 4%. The recorded strain did not quite achieve the programmed strain due to the momentum offset of the machine. To compensate for this error, slightly larger strain values than required were programmed into the computer programme.

3.3.4.3 Calculation of strain rate

The instantaneous strain rate throughout a test was found by calculating the ratio of the incremental change in strain with respect to incremental change in time from equation 2.6.

Figure 3.7 shows the effect of strain rate on deformation time for 25mm thick specimens. Strain rate increased hyperbolically with decrease in deformation time and reached a maximum of 2.5 s^{-1}. This corresponded to a total deformation time of 0.1 second. Strain rates faster than 2.5 s^{-1} could not be achieved due to the actuator speed limitations. The machine cannot respond

effectively to shorter deformation times than 0.1 second. Higher strain rates may be obtained on thinner specimens (< 25mm).

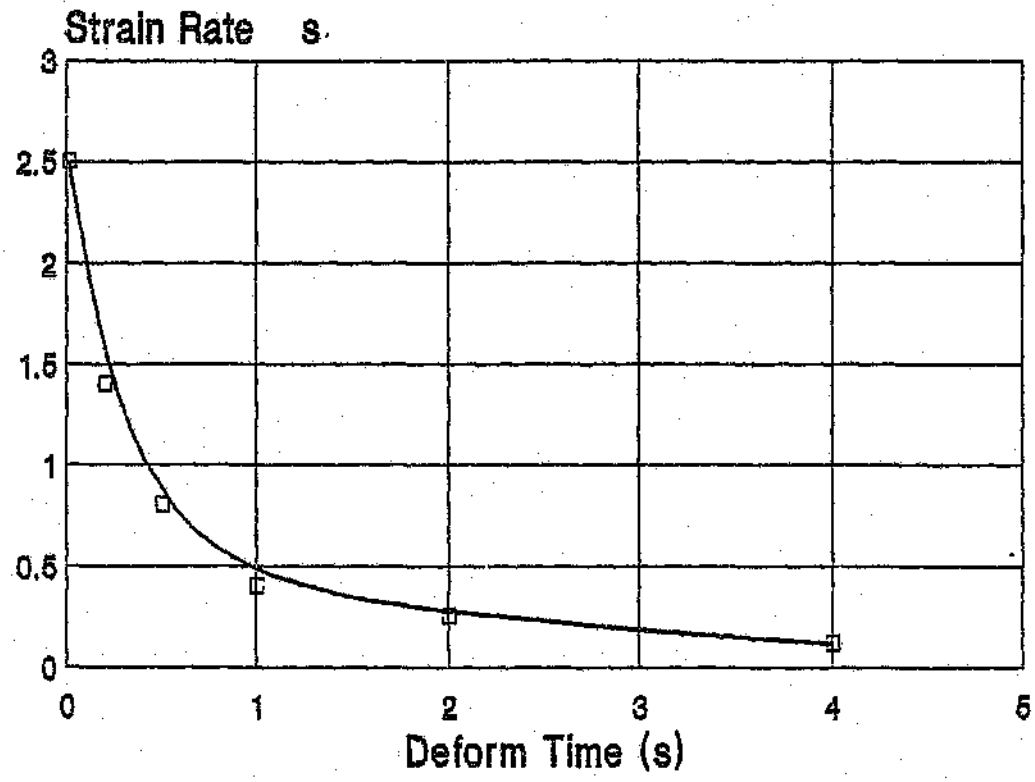

Figure 3.7 Influence of deformation time on strain rate q(25mm thick specimens, deformed 1125°C)

Table 3.2

Comparison of recorded and measured specimen total strains for selected tests

No:	Measured	Recorded	% Error
S2	0.26	0.27	4
S7	0.51	0.52	2
S13	0.97	0.95	2
S14	0.98	0.99	1
S15	0.76	0.76	0
S16	0.86	0.85	1
S21	0.79	0.81	3
S23	0.88	0.88	0

From Figure 3.8 it is seen that the strain rate in S16 had a fairly flat region at the beginning of each deformation then decreased rapidly towards the end of deformation as the velocity of the ram approached zero. The strain rate behaviour encountered in plane strain compression tests was similar to the strain rate response found in plate rolling [21]. The strain rate during rolling is at a maximum at the plane of entry and steadily decreased to zero at the plane of exit.

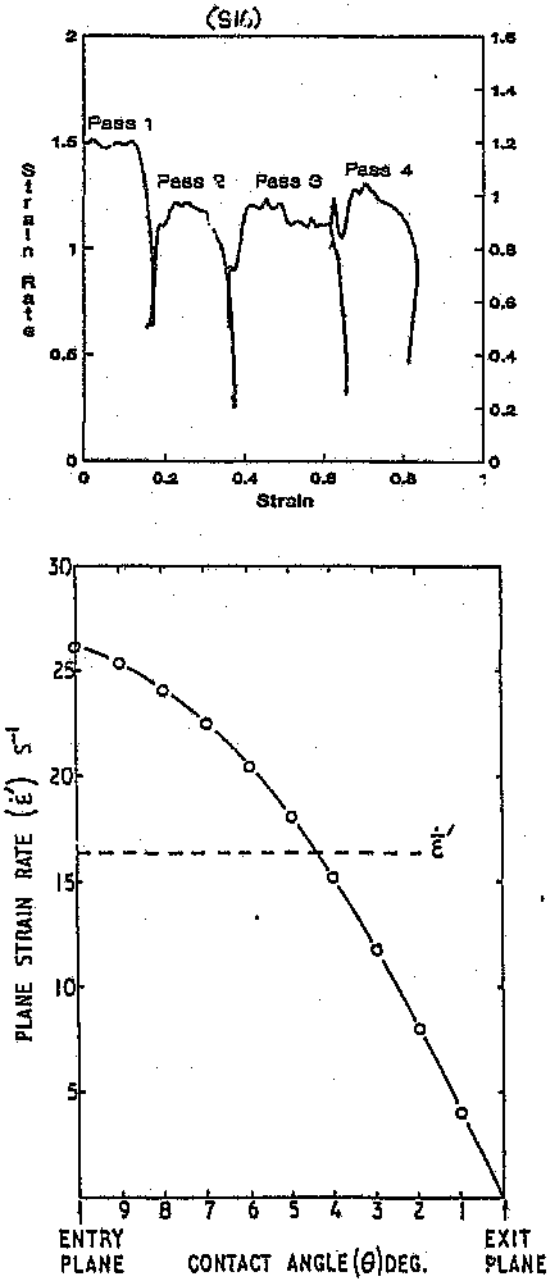

Figure 3.8 Comparison between strain rate response during plane strain compression and hot rolling

3.3.4.4 Calculation of flow stress

The flow stress during plane strain compression tests was calculated from the platen force-position data using the procedure outlined in section 2.4.4. A mean coefficient of friction of 0.42 was used in all flow stress calculations since this value was found by Kapellner et al [13] to be applicable for a wide range of C-Mn steels in unlubricated plane strain compression specimens. This value is applicable for specimen thicknesses between 18 and 40 mm. The onset of flow stress was taken at a strain of 0.015. This value was chosen since the stress is very sensitive at values lower than 0.015 and could result in large errors.

The mean stress during each pass was determined using equation 2.11 by numerically integrating the area under each flow curve, the lower limit of integration being the strain at the start of each pass ($\epsilon = 0$) and the upper limit of integration taken as the total strain in the pass, ϵ_1.

A modified version of Barager's formula (see equation 2.12) [22] was used to predict the hot flow stress of C-Mn steel in terms of temperature, strain and strain rate:

$$\sigma' = \dot{\epsilon}^{0.13}_{psc}(B\epsilon^{0.4} + C\epsilon^{0.8} + D\epsilon^{1.2}) \qquad 3.7$$

The constants B,C and D were determined by multiple linear regression for various temperature ranges in the practical plate rolling region (1250°C > T > 1000°C) and are given in the following chapter (Table 4.3 in section 4.1.6.1).

3.3.4.5 Measurement of cooling rate

Figure 3.9 shows a plot of water flow rate (litres/min) as a linear function of the setting of the spray nozzle situated above and below the specimen during the cooling stage. The flow rate was determined by measuring the time taken for the water to fill a 10 litre container. Figure 3.10 shows a plot of cooling rate at A_{cs} (866°C) as a function of water flow rate. The fastest cooling rate recorded using the existing apparatus was 35°Cs^{-1} for a 25 mm thick specimen and the slowest rate was 2°Cs^{-1} during air cooling. By consulting these graphs it was possible to set the water nozzles to apply the

required cool rate to the specimen. Direct quenching to room temperature or accelerated cooling at different rates was possible.

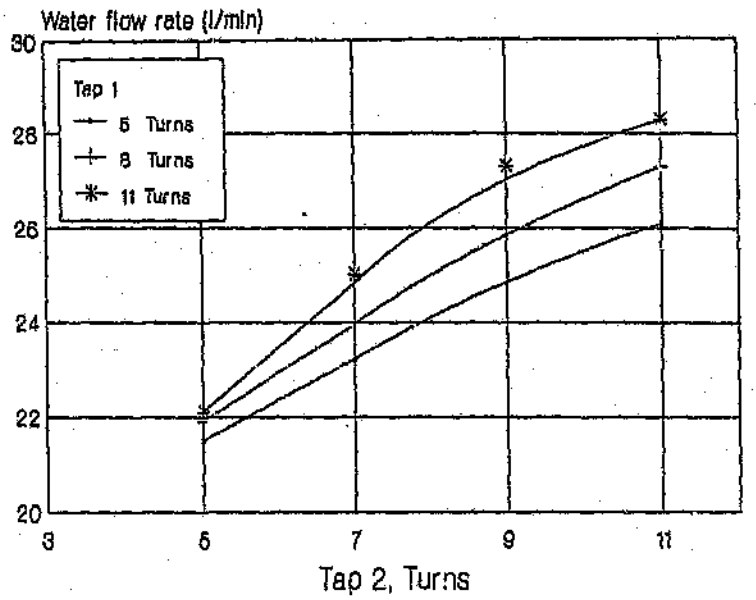

Figure 3.9 Water flow rate as a function of nozzle opening

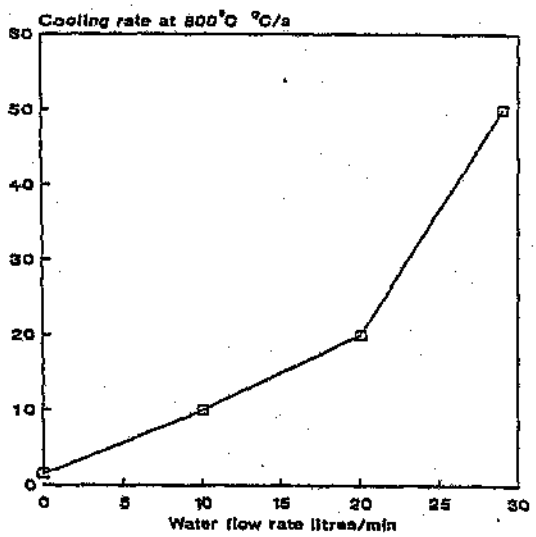

Figure 3.10 Cooling rate as a function of water flow rate (25mm specimen)

3.3.4.6 Calculation of strain hardening exponent

The strain hardening exponent, n, was calculated from the $\ln(\sigma)$-$\ln(\varepsilon)$ data found from the respective flow curve using equation 2.37. A Turbo Pascal numerical differentiation program, DERIV.PAS, was used to perform the calculations.

3.4 Initial grain size tests

Simple tests were conducted to determine the effect of austenitising temperature on austenite grain size. Specimens (30 x 30 x 30 mm^3) were heated in a rapid heating furnace and soaked for one hour at temperatures between 900°C and 1250 °C before quenching in cold water. The prior austenite grain size was then determined and quantitatively related to the corresponding reheat temperature using an exponential curve fit.

3.5 Metallography

Considerable spread of material occurred at the specimen edge during large deformations. Metallographic sections were therefore taken at a minimum distance of 15mm from the specimen edge in the deformation zone. Grain size determinations were always taken in the mid-thickness position of the deformation zone. The air cooled ferrite pearlite microstructure of specimens was studied rather than prior austenite structures since mechanical properties in the as-deformed condition were required. Ferrite grain sizes as well as ferrite and pearlite volume percentages were determined by means of image analysis. A two percent Nital solution was used to etch the ferrite - pearlite structure in air cooled specimens. A warm (70 °C) saturated aqueous picric acid solution was used to etch prior austenite grains in quenched specimens obtained from initial grain size tests. All micrographs were taken at 400X magnification.

3.6 Mechanical tests

Standard ASTM tensiles tests were conducted on specimens machined from the deformation zone of each plane strain compression specimen. Due to size limitations, only two specimens could be machined per plane strain compression specimen. Three sub standard (7.5x10mm) Charpy specimens were also machined

from each plane strain compression specimen. The V-notch was taken along the centre of the deformation zone shown in Figure 3.11

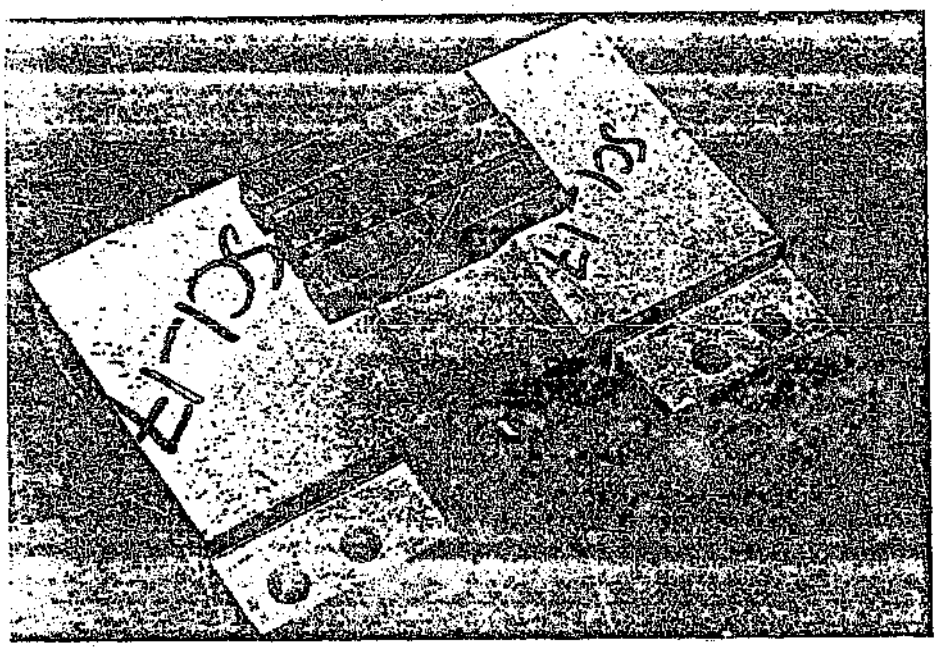

Figure 3.11 Deformed plane strain compression specimen showing the positions from where tensile and Charpy specimens were machined.

3.7 Model to simulate the temperature distribution in plane strain compression specimens

A finite difference computer model, PSC_TEMP, was written in Turbo Pascal to simulate the temperature distribution in a rectangular steel specimen before, during and after plane strain compression. The model is discussed in detail in Appendix 1. The programme takes into account heat transfer within the specimen as well as heat losses due to heat conduction to the platen, convection to the surroundings and radiation. The temperature rise in the specimen due to work done during deformation is also accounted for. A flow chart showing the logical stages of PSC_TEMP is shown in Figure 3.12. Sample input data are shown in Figure 3.13. The programme predicts the temperature at any point in the specimen deformation zone as well as the platens during

simple air cooling or multi-pass plane strain compression tests. Sample output data are shown in Figure 3.14.

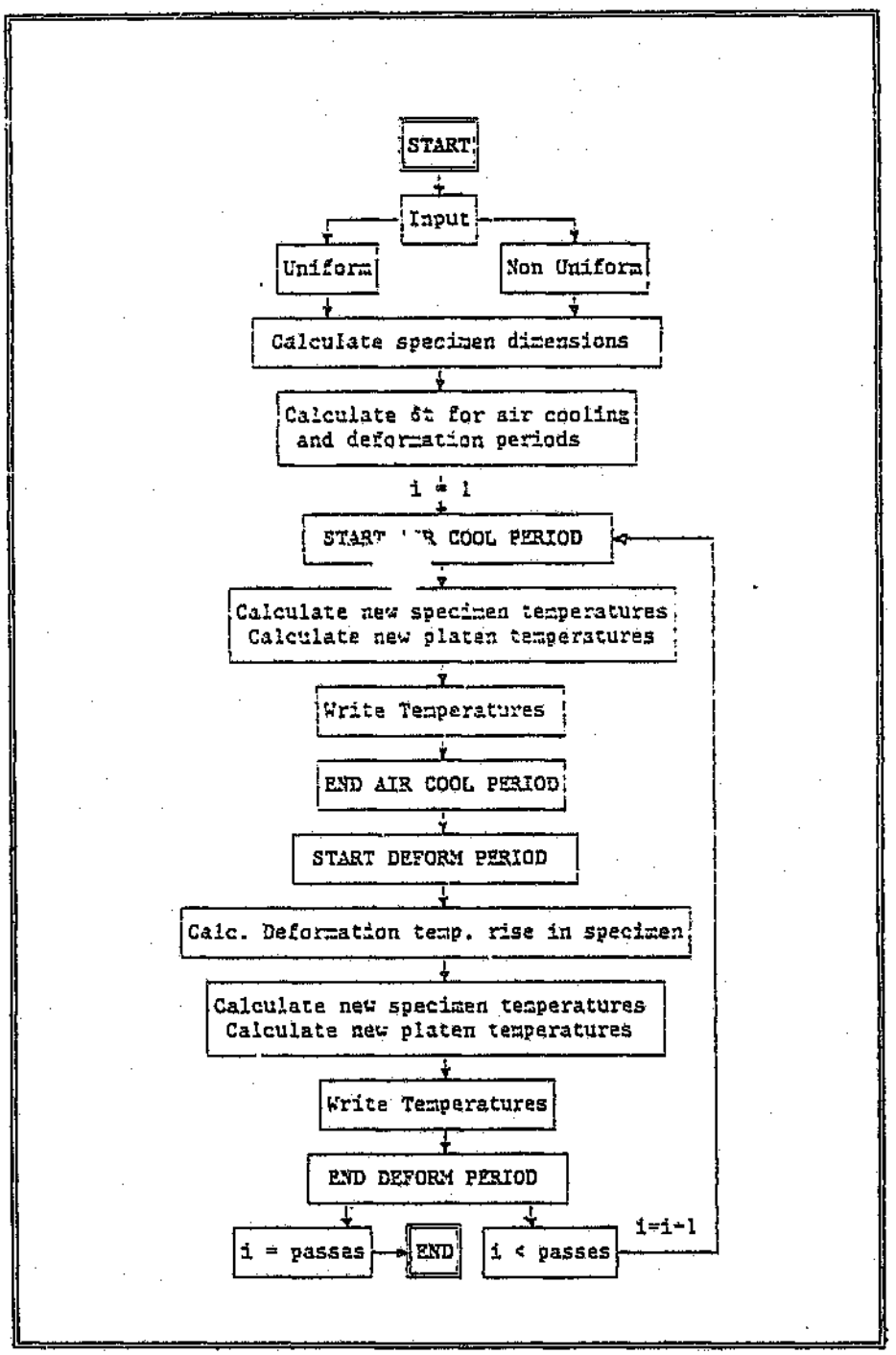

Figure 3.12 Flow chart showing the stages of programme PSC_TEMP

```
Schedule Number : 2          File Name for Output Data File : Temp_F4

Number of Passes: 3          Temperatures

Element width :0.003         Initial Specimen :1250
Element height:0.0025        Initial Platen   :25
                             Ambient          :25

HTC for deformation :18      Uniform / Non-Uniform [U/NU] :U

Boundary condition factor :0.9

Pass:    Strain:    Stra.. Rate:    Mean Stress:    Delay Time:
   1      0.13         1                80              6
   2      0.14         1                97              5
   3      0.2          1                113             4
```

Figure 3.13 Sample input data for programme PSC_TEMP

```
                                        Platen
 ------------------------------------------------
  25    25    25    25    25
  25    25    25    25    25
  25    25    25    25    25
  43    43    43    42    43
 217   217   216   208   216
 ------------------------------------------------

                                              Specimen
 ------------------------------------------------------------
 918   914   916   931   935  1193  1205
1194  1172  1173  1178  1196  1216  1220
1229  1226  1226  1227  1229  1230  1231
1237  1236  1236  1236  1237  1237  1237
1240  1240  1240  1240  1241  1241  1240
 ------------------------------------------------------------

Deformation:  Pass   1   Time:  6.26
```

Figure 3.14 Sample output data for programme PSC_TEMP

3.8 Model to simulate the mechanical and metallurgical changes during hot plate rolling

A computer programme, **PLATESIM**, was written in Turbo Pascal 5.0 to predict the roll separating forces, evolution of austenite, plate temperature, ferrite grain size and mechanical properties of SC8 C-Mn steel plate during and after hot rolling. The programme was run on an IBM compatible AT personal computer. A flow chart showing the logical stages of **PLATESIM** is given in Figure 3.15. A listing of the programme is given in Appendix 4. The aim of writing the programme was to supply the Vanderbijlpark plate mill with an accurate and quick method for optimising their plate rolling schedules.

The inputs necessary to run the programme were entered either directly from the keyboard or from a data file. TSteel SC8 rolling schedules consisting of up to 17 passes may be simulated. A sample of input data is shown in Figure 3.16. For ease of use, a schematic diagram showing the current position of the slab/plate during the rolling schedule was included in the input stage of the programme.

The nominal strain and mean strain rate during each pass were calculated from equation 2.1 and equation 2.5 respectively. The flow stress of the slab was calculated using equation 3.7 for a specific temperature range. The mean stress was found by analytically integrating equation 3.7 over the strain range using equation 3.8:

$$\bar{\sigma}' = \frac{\dot{\epsilon}^{0.3}_{PSC}}{\epsilon_1} \int_0^{\epsilon_1} (B\epsilon^{0.4} + C\epsilon^{0.8} + D\epsilon^{1.2})\, \delta\epsilon \qquad 3.8$$

The roll separating forces were calculated from Sim's theory using equation 2.7. The roll geometry factor, Q, was calculated using equations 2.8-2.10. Initially the roll force was overestimated in the early passes. This was attributed to the assumption that the slab width remained constant throughout the schedule. Subsequently, a linear increase in billet/plate width with pass reduction was incorporated into programme **PLATESIM**. This provided a much better estimation of the roll force in the early passes.

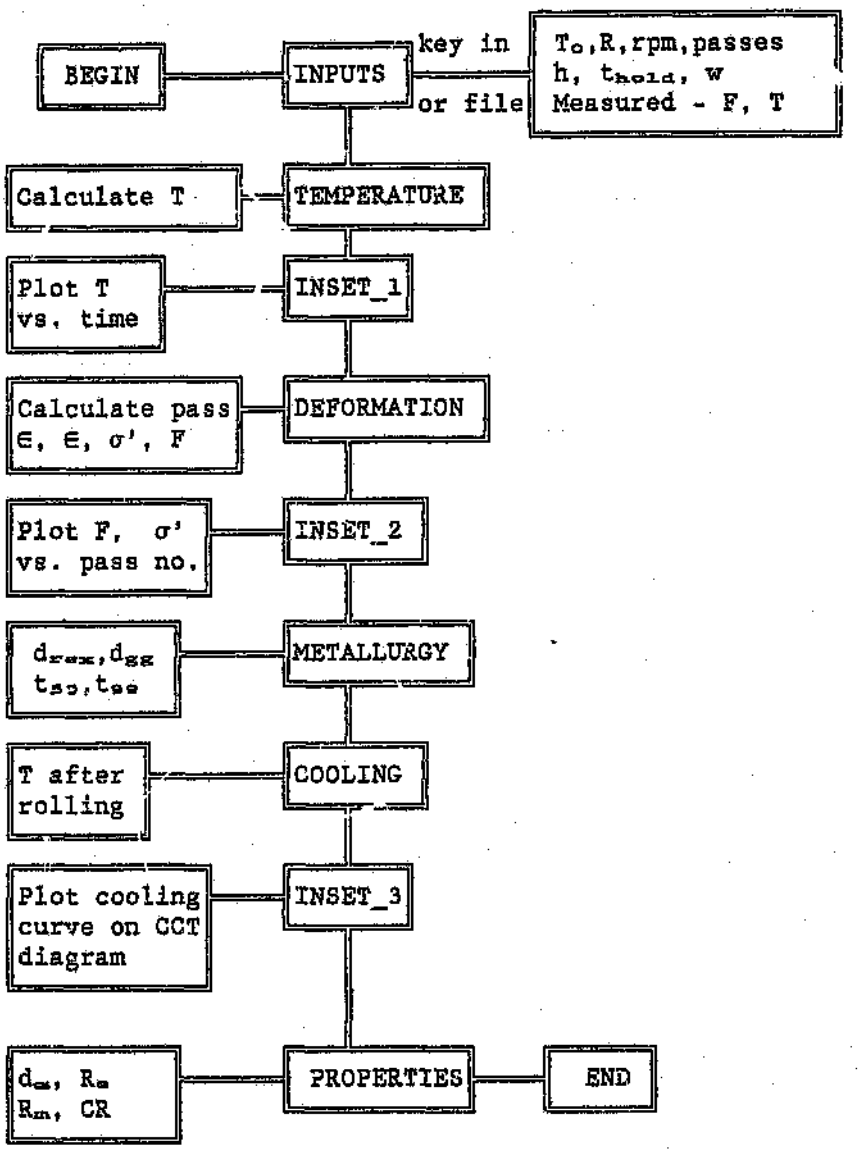

Figure 3.15 Flow chart showing the stages of programme PLATESIM

Since plate rolling was always conducted at high temperatures on the Vanderbijlpark mill (T > 1050°C), it was assumed that full recrystallisation took place after each pass. The recrystallised austenite grain size and the time required for recrystallisation to be completed were found from equation 2.45 and 2.44 respectively. The grain growth kinetics after recrystallisation was simulated using equation 2.55.

Since only plate surface temperatures can be measured on the plant, it was essential that programme PLATESIM provided an estimate of the surface temperature for comparitive purposes. Linear regression was performed on the surface temperature and mean temperature data obtained by Rauderski [63]. The temperature profile in steel plates is given in Figure 3.17. The mean plate temperature with respect to rolling time, found from equation 2.33, was substituted into equation 3.9 to calculate the plate surface temperature.

$$T_{surface} = 0.6T_m + 381 \qquad (3.9)$$

Equation 3.9 was an oversimplification since the temperature gradient is not linear. Nevertheless, the predicted plate surface temperatures were in fairly good agreement with the corresponding measured values.

Inputs from (k)eyboard or fi(l)e : l

Reheat: 1220	°C	Pass	h(mm)	°C	t(s)	Force	Finish Temp
Thick : 210	mm	1	180	1180	6	1300	1071
W (i) : 1250	mm	2	160	1175	10	1300	
W (f) : 2540	mm	3	140	1170	6	2200	
Radius: 490	mm	4	120	1160	5	2600	
r.p.m : 60		5	100	1150	5	2800	
Passes: 13		6	84	1147	5	2400	
To : 227	µm	7	75	1134	5	800	
t(ruf): 6	s	8	62	1127	5	2200	
Rotation : 2		9	50	1116	6	2600	
		10	39	1103	5	2600	
		11	30	1095	5	2600	
		12	24	1084	5	2200	
		13	20	1073	5	1600	

Figure 3.16 Sample input data for programme PLATESIM

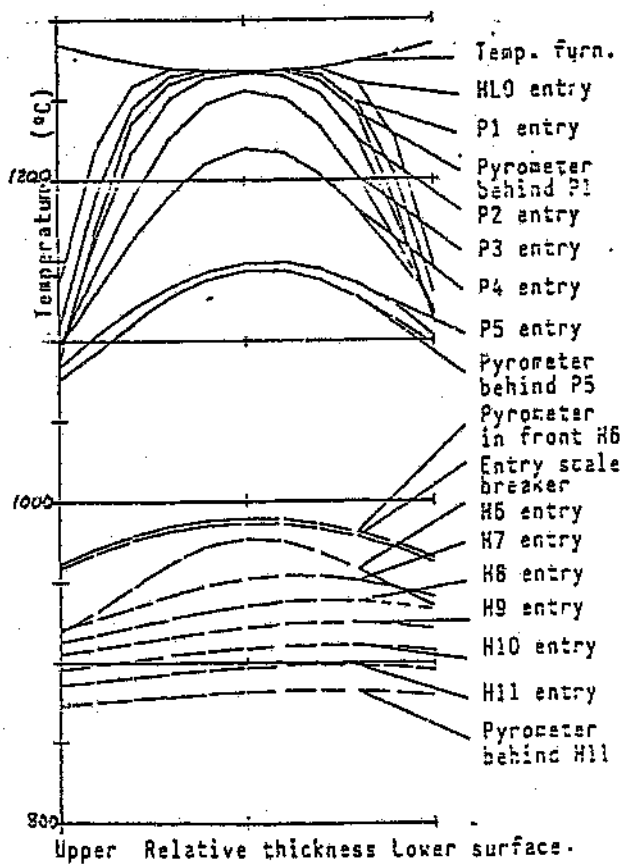

Figure 3.17 Temperature profile across slab during plate rolling [63]

The air cooling rate of the plate was simulated using the equivalent diameter method described in section 2.5.6. The equivalent air cooling rate of a round steel bar for various plate dimensions was determined. These values were used to formulate an equation which determined the cooling rate, CR, for any final plate thickness:

$$CR = 1.1 + (h - 0.25)/10 \qquad 3.10$$

A conventional CCT diagram of an 0.19C-1.2Mn-0.42Si steel (similar in chemical composition to SC8) was incorporated into PLATESIM to enable the user to get a fair idea of what microstructure to expect after subjecting the plate to a particular cooling rate. It should be mentioned that conventional CCT diagrams should only be used when the starting microstructure before transformation is fully recrystallised i.e. when no accumulated strain, due to deformation in the no recrystallication region, is present in the material. The use of this

diagram was justified in the present work since all C-Mn plate rolling schedules on the Vanderbijlpark plate mill are finished at high temperatures (T > 1050°C) and result in fully recrystallised austenite being formed prior to transformation.

The ferrite grain size resulting from air cooling the specimen down to room temperature was calculated from equation 2.58.

Multiple linear regression was used on data obtained from all three SC8 steel grades to generate equations describing the yield strength and Charpy impact energy at 0°C in terms of chemical composition and important process parameters. The relevant formulae are given in the following chapter (see Equation 4.7 and Table 4.5).

It was not possible to determine the fracture - appearance - transition-temperature, FATT, from a single plane strain compression experiment because only three Charpy specimens could be machined from the deformation zone ~~. was estimated that at least 20 Charpy tests are required for a reliable FATT determination. However, the influence of ferrite grain size on toughness was studied on a semi-quantitative basis by means of Charpy impact energy tests, conducted at 0°C.

Output data, corresponding to the input data in Figure 3.16, are given in Figure 3.18. The printout includes for each pass, the total strain, the mean flow stress, simulated and measured roll separating forces, measured and simulated deformation temperatures, hold times, strain rates, recrystallised austenite grain size, and austenite grain size after grain growth. Also included in the printout are the austenite grain size just prior to transformation, the ferrite grain size, the yield and tensile strengths as well as the impact energy at 0°C.

Pass	$\Sigma\epsilon$	σm	P(m)	T(s)	T(m)	drex	dgg	Hold	P(s)	$\dot{\epsilon}$rate
1	0.15	68	979	1214	1180	123	181	6	1300	3.9
2	0.27	65	749	1202	1175	138	173	10	1300	3.7
3	0.41	68	1638	1198	1170	118	157	6	2200	4.2
4	0.56	73	1792	1195	1160	96	143	5	2600	4.8
5	0.74	79	2009	1192	1150	76	129	5	2800	5.7
6	0.92	79	1847	1189	1147	74	123	5	2400	6.1
7	1.03	72	1211	1183	1134	111	126	5	800	5.3
8	1.22	85	1883	1175	1127	67	114	5	2200	7.3
9	1.44	92	2042	1160	1116	55	101	6	2600	8.6
10	1.69	125	2844	1148	1103	44	87	5	2600	10.4
11	1.95	133	2893	1132	1095	38	75	5	2600	12.2
12	2.18	130	2337	1111	1084	40	70	5	2200	12.7
13	2.36	125	1832	1086	1073	47	66	5	1600	12.7

Cool rate (°C/s)	τ(μm)	α(μm)	σy(MPa)	σUTS(MPa)	CVN 0°C
1.22	66	22.2	292	447	39

Figure 3.18. Sample output data for programme PLATESIM

Key to Figure 3.18

Symbol	Meaning
$\Sigma\epsilon$	Total strain
T(s)	Simulated temperature, °C
T(m)	Measured temperature, °C
P(s)	Simulated roll separating force, tons
P(m)	Measured roll separating force, tons
drex	Recrystallised austenite grain size, μm
dgg	Austenite grain size after grain growth, μm
hold	Interpass delay time, s
$\dot{\epsilon}$rate	Strain rate s^{-1}
σm	Mean flow streess, MPa
σy	Yield strength, MPa
σUTS	Tensile strength, MPa
CVN	Impact energy at 0°C, Joules

4 EXPERIMENTAL RESULTS

This chapter presents the results of multi-pass plane strain compression tests conducted on steel SC8. The effect of the important process parameters on strength and toughness are given. Equations, determined by multiple linear regression, were formulated which quantitatively predict the yield strength and impact energy in terms of process parameters. Results obtained from computer model, PLATESIM, are presented and compared with parameter measurements taken on the Vanderbijlpark plate mill.

4.1 Results of plane strain compression tests

The results of single and multi - pass plane strain compression tests on SC8 C-Mn plate steel are presented in Table 4.1. The specimens were marked with an S prescript followed by the test number. This notation was used to identify a specific test or specimen throughout this chapter. Specimens S1,S3,S5,S6,S8 and S28 were rejected because of noise problems encountered in the thermocouple readings. The platen load and platen position, specimen temperature and test times were analysed on an IBM compatible personal computer using software programmes written in Turbo Pascal and Quickbasic. Borland's Quatrro Spreadsheet and Harvard Graphics were used to analyse the raw data and present it for output.

4.1.1 Performance of specimens and test equipment

Figure 4.1 shows the geometry of specimen S18 after a total strain of 0.62 over four passes. The measured reduction in thickness was constant across the specimen width The specimen size (25x90x120 mm³) was ideally suited for the equipment used e maximum platen load recorded was 1130 kN at 680°C. This value was well within the maximum load limit of 1500 kN for the servohydraulic machine and confirms that, for the specimen size used, virtually any plate rolling condition can be simulated for C-Mn steels. Total strains of 0.98 were achieved without any sticking of the specimen to the non lubricated platens. However, when one specimen was deformed to a total strain of 1.6 at a strain rate of 0.2, bending at the specimen ends and sticking of the specimen to the platens occurred.

Table 4.1
Plane strain compression test results

Test	C	Mn	Pass	T_e °C	T_s °C	ε	thold s	$\dot{\varepsilon}$ s-1	d_m µm	Pear %	CVN J	R_m MPa	R_m MPa	e% %
S2	.18	1.04	1	1240	1195	.09	13	2.5						
			2		1150	.17	6	2.5	24	23	39	282	474	34
S15	.18	1.04	1	1225	1125	.31	30	1.7						
			2		1010	.45	40	1.7	14	23	57	311	522	31
S14	.18	1.04	1	1240	1135	.38	30	0.4						
			2		1010	.60	40	0.4	17	23	-	-	-	-
S12	.18	1.04	1	1200	1140	.38	30	0.9						
			2		985	.48	40	0.9	-	-	-	-	-	-
S10	.18	1.04	1	1220	1133	.29	30	2.5						
			2		937	.28	70	2.5	20	19	48	296	489	37
S4	.11	1.20	1	1220	1075	.23	45	2.5						
			2		1051	.17	5	2.5	24	14	65	266	454	38
S7	.11	1.20	1	1245	1095	.28	35	2.5						
			2		1047	.23	10	2.5	24	17	67	275	467	38
S9	.11	1.20	1	1200	1120	.26	30	2.5						
			2		990	.32	40	2.5	19	17	69	293	469	37
S13	.11	1.20	1	1230	1144	.36	30	0.1						
			2		947	.60	40	0.1	8	15	105	323	473	30
S11	.12	0.86	1	1210	1140	.38	30	0.2						
			2		980	.62	40	0.2	17	10	112	285	443	36
S16	.11	1.20	1	1200	1139	.18	30	2.5						
			2		1076	.19	15	2.5						
			3		1072	.27	1	2.5						
			4		1066	.22	1	2.5	19	15	95	281	463	34
S27	.11	1.20	1	1100	1083	.20	8	2.5						
			2		1058	.20	2	2.5						
			3		1019	.25	2	2.5						
			4		965	.26	2	2.5	27	27	92	265	466	35
S21	.11	1.20	1	1230	1135	.18	30	2.5						
			2		852	.20	100	2.5						
			3		844	.26	1	2.5						
			4		836	.15	1	2.5	15	15	110	306	475	31
S18	.11	1.20	1	1218	1143	.12	30	2.5						
			2		812	.15	140	2.5						
			3		809	.25	1	2.5						
			4		807	.10	1	2.5	9	15	92	305	479	32
S25	.18	1.04	1	1230	1225	.17	10	2.5						
			2		1185	.07	5	2.5						
			3		1166	.10	5	2.5						
			4		1130	.37	5	2.5	19	26	37	301	384	6.4
S17	.18	1.04	1	1240	1144	.18	30	2.5						
			2		887	.19	100	2.5						
			3		882	.27	1	2.5						
			4		876	.14	1	2.5	16	24	67	321	520	29
S22	.18	1.04	1	1175	1100	.15	30	2.5						
			2		840	.26	140	2.5						
			3		837	.25	1	2.5						
			4		832	.15	1	2.5	16	24	70	317	489	32
S19	.18	1.04	1	1240	1142	.18	30	2.5						
			2		792	.19	160	2.5						
			3		789	.25	1	2.5						
			4		782	.10	1	2.5	10	23	72	299	495	26
S20	.18	1.04	1	1200	1130	.19	30	2.5						
			2		730	.16	200	2.5						
			3		700	.25	1	2.5						
			4		680	.11	1	2.5	8	18	60	333	491	30
S23	.11	.65	1	1230	1142	.17	30	2.5						
			2		820	.19	200	2.5						
			3		750	.26	1	2.5						
			4		748	.26	1	2.5	8	15	110	305	445	31
S24	.11	.65	1	1240	1140	.21	20	2.5						
			2		1074	.21	20	2.5						
			3		1005	.22	20	2.5						
			4		943	.19	20	2.5	21	12	101	270	441	28
S29	.18	1.04	1	953	937	.19	12	2.5	5.8	25	39	353	541	29
S30	.18	1.04	1	1001	986	.19	7	2.5	-	23	22	389	556	22

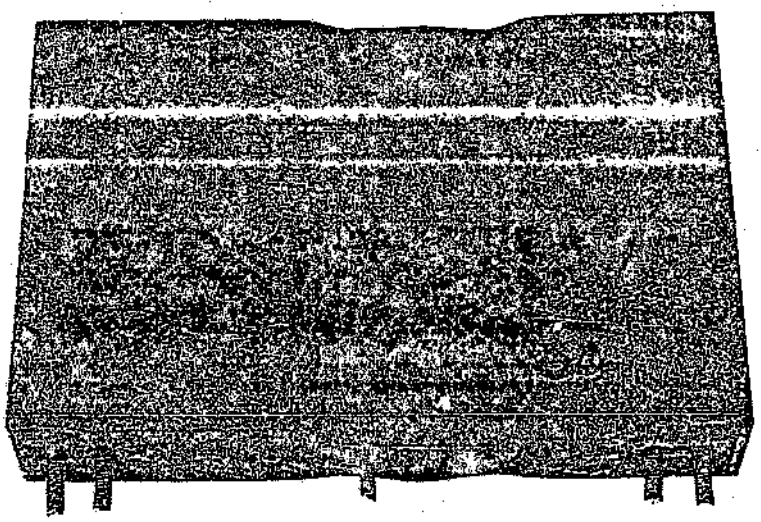

Figure 4.1 Photograph of deformed specimen S18

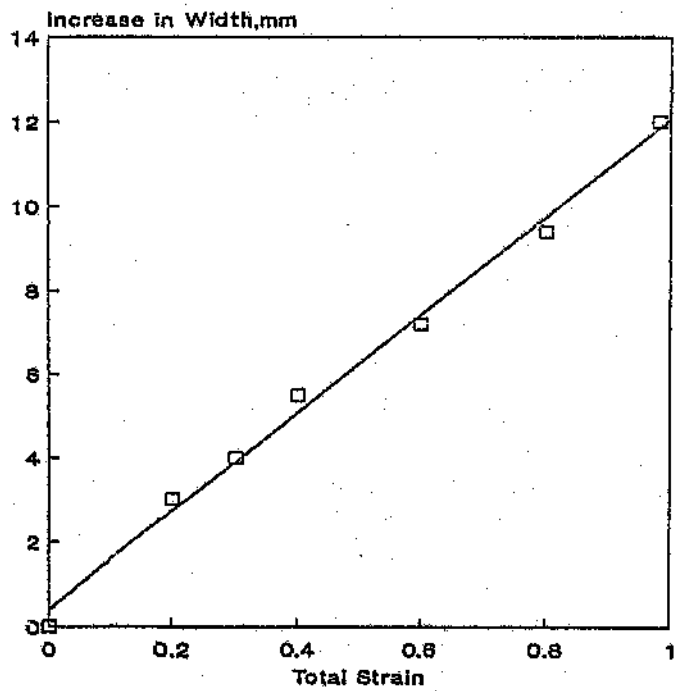

Figure 4.2 Increase in deformation zone width as a function of total strain

The average increase in spread in the deformation zone as a function of nominal strain is given in Figure 4.2. It was found that the mean width of the specimen in the deformation zone increased linearly with the amount of total strain applied to the specimen. The maximum recorded increase in specimen width was 12 mm at a strain of 0.98.

The deformation platens (b = 30mm) were suitable for deforming 25x90x120mm³ rectangular specimens in single and multi-pass schedules. The non lubricated platens were used for 40 high temperature multi-pass tests without blunting their sharp edges. This confirmed that the H13 steel, used to manufacture the platens, was suitable for high temperature compression tests.

The stainless steel arms and spring system (Figure 3.1) used to support the specimen during induction heating and multi-pass deformation were successful in preventing bending or buckling of any ancillary equipment during deformation. A disadvantage of using this specimen support system was that it caused an uneven temperature distribution on one side of the specimen during the test.

The semi-automatic specimen transport system proved to be efficient in transporting the specimen to and from the heating, deformation and cooling stages of the test. The travel time for full contraction of the 1100 mm pneumatic cylinder was 1.5 seconds. The travel time for full contraction for the 400 mm pneumatic cylinder was 0.7 second. These small delay times were satisfactory for the present work although much faster cylinder speeds can be achieved by adjusting the air pressure gauge. Computer hardware and software has recently been commissioned to simultaneously control the specimen movement and the specimen heating cycle.

The 50 kW induction furnace was capable of heating the specimen to 1250°C within 3 minutes. Thermocouple readings were not affected due to the induction since the furnace was switched off immediately after soaking the specimen at the austenitizing temperature. Some noise was encountered whilst the specimen was cooling down. This can be attributed to specimen contraction and dirt in the thermocouple holes.

4.1.2 Specimen Temperature

4.1.2.1 Comparison between measured and simulated specimen temperature during air cooling

Undeformed specimens (h=25 mm) were air cooled from 1220°C and 1000°C respectively. Figure 4.3 shows the measured time-temperature history and simulated time-temperature history, calculated using programme, PSC_TEMP, for each specimen.

The effect of oxidation acting as an insulator at the specimen surface was clearly seen in Figure 4.3. The simulated and measured cooling curves agreed more closely when the specimen was reheated to intermediate temperatures (1000°C) where significant oxidation did not occur. The difference between the measured and simulated temperatures in the centre of the specimen during cooling from 1000°C was 10 to 15°C. At higher reheat temperatures (1220°C), oxidation acted as a thermal insulator and caused the simulated temperature to differ somewhat from the measured temperature. The difference between measured and simulated centre temperatures during cooling from 1200°C was 15 to 25°C.

The close agreement between measured and simulated specimen cooling curves showed that the heat transfer coefficient, calculated using equation A1.15, gave fairly accurate predictions of the temperature at the surface of the specimen. Also, the number of finite elements chosen were sufficient to simulate the heat flow within the specimen.

4.1.2.2 Comparison between measured and simulated specimen temperature during plane strain compression

The temperature distribution in the specimen during multi-pass plane strain compression tests was simulated using computer programme, PSC_TEMP. Figure 4.4 shows the measured and simulated temperature - time plots for multi-pass, anisothermal, plane strain compression tests, S25 and S27. Specimens S25 and S27 were reheated to 1230°C and 1100°C respectively. The initial (marked 2) and final (marked 1) thermocouple positions are also shown. It was seen that large and rapidly changing temperature gradients between the surface and centre of the specimen were formed during and immediately after each deformation. At the start of each deformation, the centre of the specimen

experienced a temperature rise due to deformation heating. At the same time, positions close to the surface of the deformation zone dropped in temperature because of conduction of heat to the

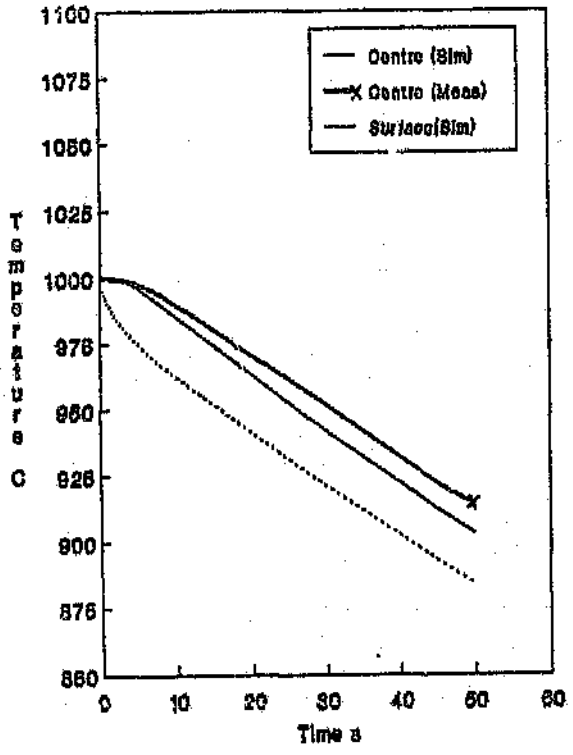

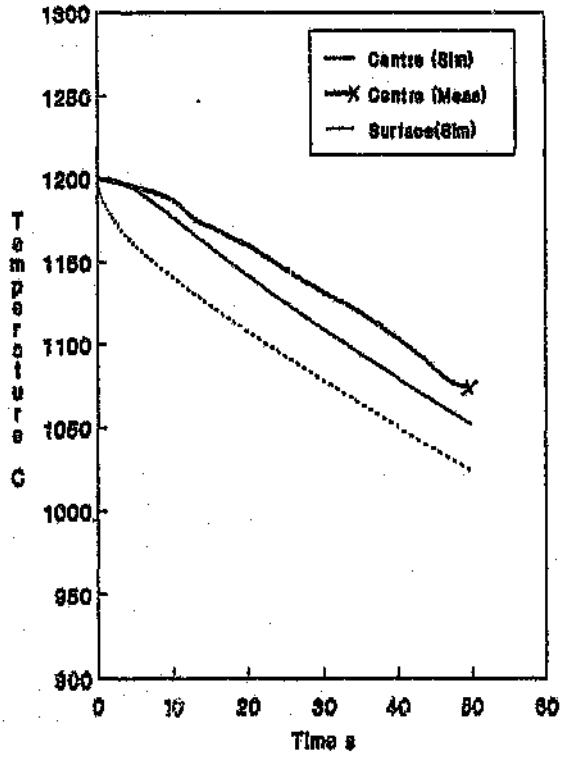

Figure 4.3 Temperature during air cooling of undeformed plane strain compression specimens, (simulated versus measured)

colder platens. Immediately following deformation, there was thus a steep temperature gradient through the specimen thickness in the deformation zone and heat flowed rapidly from the specimen centre to the surface. This was observed by a sharp decrease in temperature at the specimen centre. This net heat loss in the deformed zone of the specimen led to a steep longitudinal temperature gradient in the specimen and heat flowed rapidly from the neighbouring, undeformed material into the deformation zone. Once the steep temperature gradient had dissipated, the simulated temperature at the two

corresponding thermocouple positions approached equilibrium during the intermediate air cooling period until the next deformation took place. This suggested that heat flowed continuously towards the deformation zone equilibrating the cooling rates in the sections of different

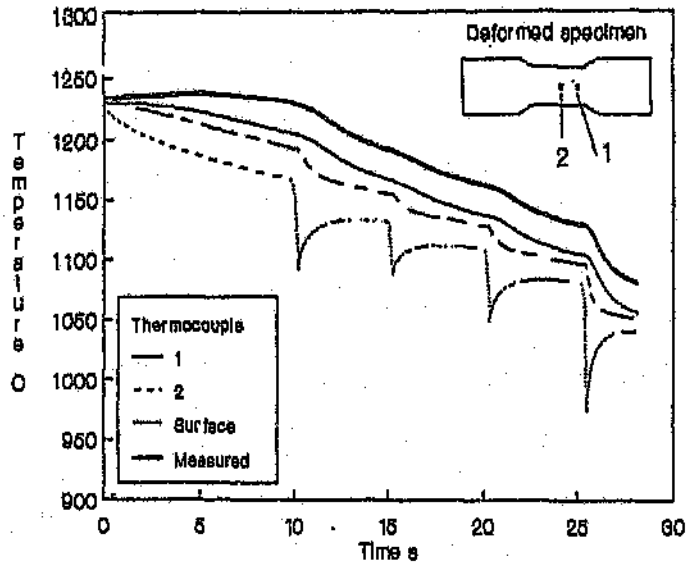

S25: Four pass schedule

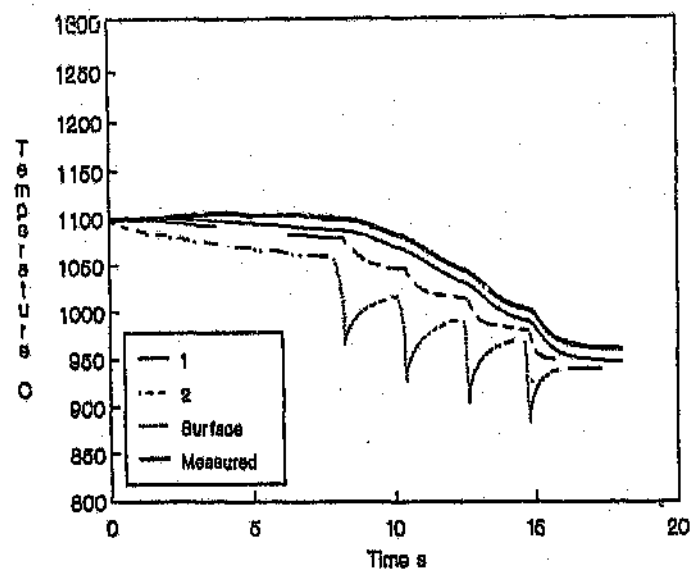

S27: Four pass schedule

Figure 4.4 Specimen temperature during multi-pass plane strain compression tests S25 and S27 (simulated versus measured)

thickness. As the volume of material in the deformation zone decreased with consecutive passes, the temperature drop in the deformation zone increased.

It was seen that the simulated temperature furthest from the specimen centre (marked 1) was in best agreement to the measured specimen temperature. This was understandable since the thermocouple was displaced from its central position during deformation. It was seen that the simulated temperature at the specimen centre was always lower than the temperature at the final thermocouple position. The simulated and measured temperatures were in very good agreement in the early stages of the test but differed increasingly in the last stages. This error could be due to a programming error by allowing too much heat transfer from the specimen surface to the platen. A further explanation is the insulating effect of scale on the specimen surface. The simulated temperature did not however, deviate from the measured value at any time by more than 25°C. During deformation, the simulated surface temperature dropped and rose again very rapidly. This can be explained by the rapid exchange of heat between the hot specimen surface and the much colder platens during a deformation. The surface temperature however, approached equilibrium conditions few seconds after the deformation.

Platen surface temperatures rose to between 200°C and 400°C during deformation, depending on contact time and deformation temperature. After deformation, the platen surface temperature dropped rapidly due to heat conduction to their colder interiors. The platen temperature could not be measured due to difficulties in attaching thermocouples to the platens.

Two constants, C and HTC, had to be determined for use in programme PSC_TEMP. The time-temperature histories of the specimen centre element, simulated using different heat transfer constants, C, (see Appendix 1, equations A1.43 and A1.44) are given in Figure 4.5. The optimum value had be determined by trial and error. It was found that large heat transfer constants caused the simulated surface temperature to drop too low. The optimum heat transfer constant for the given test configuration was found to be 10 kW/m^2K. A value of 0.9 chosen for the boundary condition factor, HTC, (Appendix 1, equation A1.9) was suitable for simulating the heat transfer between the deformed and undeformed zone of the specimen. Very short stable time intervals (equation A1.23) were necessary after the first pass due to the reduction in element

height. The optimum specimen element width and initial height to ensure stable heat transfer within and from the specimen was found to be 2.5mm.

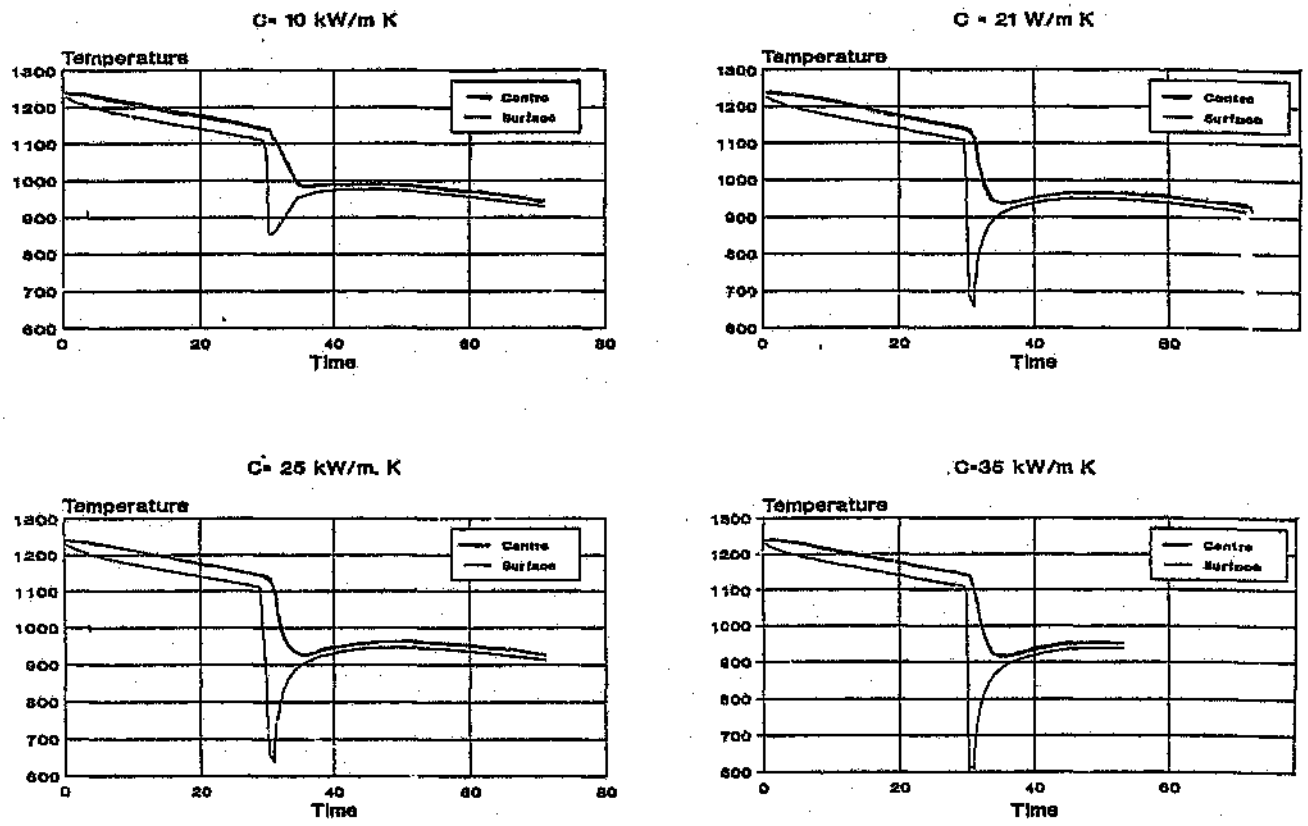

Figure 4.5 Effect of using different heat transfer constants , C, in programme PSC_TEMP, on the simulated specimen temperature.

4.1.2.3 Influence of reheat temperature on initial austenite grain size

Micrographs showing the austenite grain size at reheat temperatures of 1150°C and 1250°C are given in Figure 4.6. All specimens were held for 1 hour at temperature. The austenite grain sizes at 1150 and 1250°C were 200μm and 270μm respectively.

A plot of reheat temperature against initial austenite grain size is given in Figure 4.7. It was seen that the austenite grain size increased exponentially with increase in temperature. The results were in agreement with values obtained for C-Mn steels of similar chemical composition by various authors [3,29,64].

It was assumed that the grain size expressed as a function of temperature could be given by

$$d_\gamma = A \exp (Q_{aa}/8.314\ T) \qquad 4.1$$

where A is a constant, T is in Kelvin and the soaking time is kept constant at one hour.

Taking the logarithm of both sides gives

$$\ln(d_\gamma) = \ln(A) + Q_{aa}/(8.314\ T) \qquad 4.2$$

Linear regression for data obtained from initial grain size tests resulted in the following constants:

$$\ln(d_\gamma) = 9.847 - 6601\ T^{-1} \qquad R^2 = 0.9748 \qquad 4.3$$

4.1.2.4 Effect of reheat temperature on ferrite grain size

The small influence of reheat temperature on ferrite grain size is shown in Figure 4.8. Four pass schedules S24 and S27 were reheated to 1240°C (d_γ = 250μm) and 1100°C (d_γ = 150μm) respectively. Both specimens were deformed at approximately the same temperature, strain and strain rate per pass. The ferrite grain size in both specimens was between 21 and 22μm. A similar effect was also found in two pass schedules, S4 and S7.

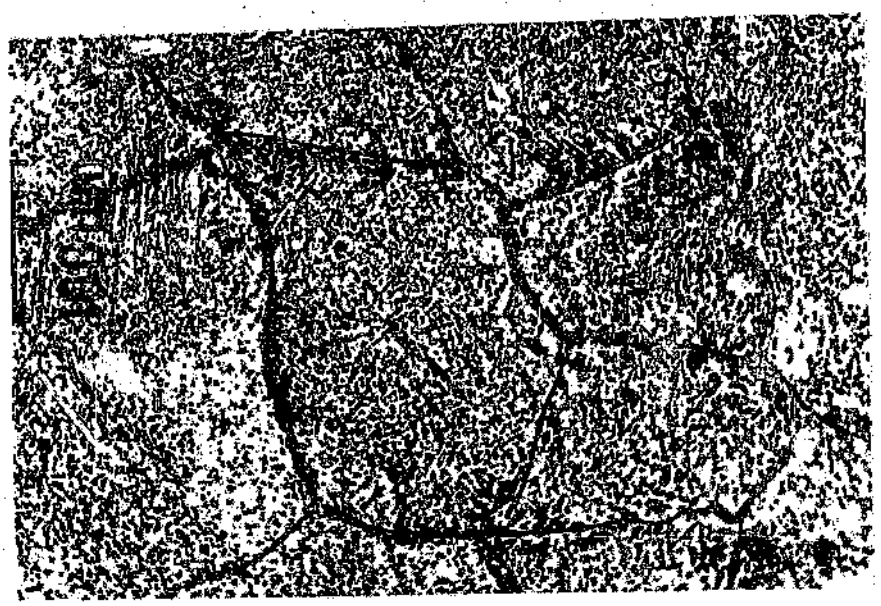

Reheat 1150°C (X400)

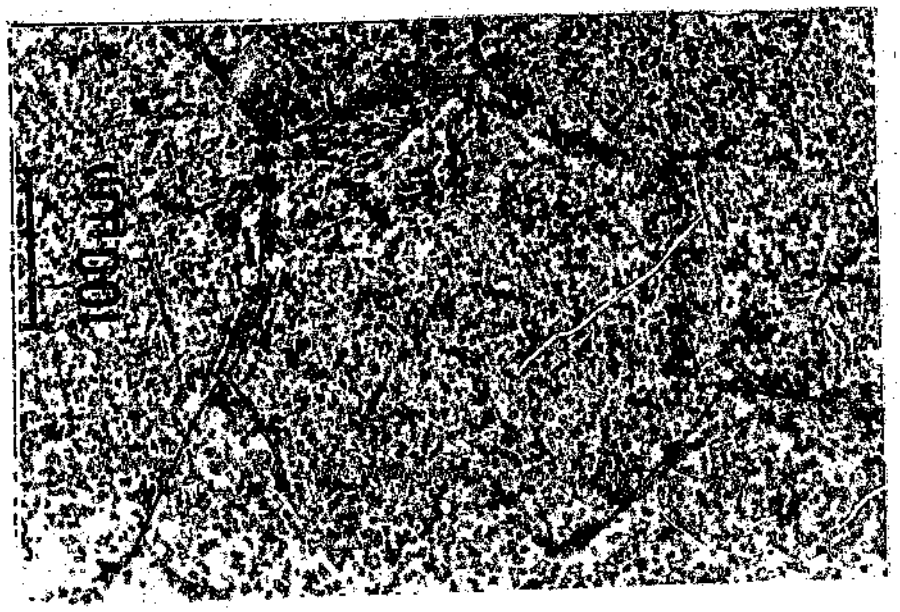

Reheat 1250°C (X400)

Figure 4.6 Micrographs showing austenite grain size at 1150°C and 1250°C

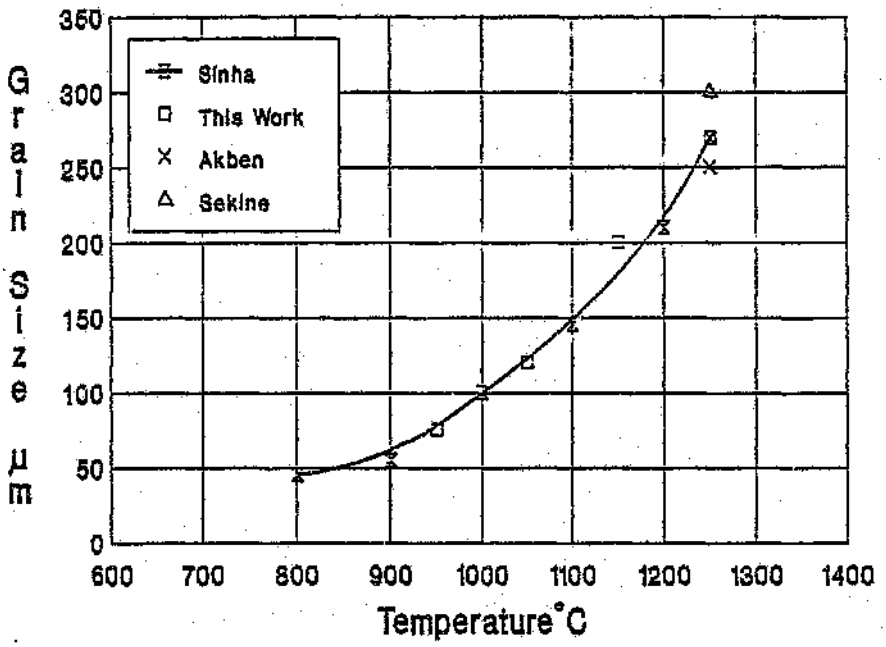

Figure 4.7 Austenite grain size as a function of reheat temperature

S24: Reheat 1240°C

Pass	T	∈
1	1140	.21
2	1074	.21
3	1005	.22
4	943	.19

d_α = 21µm

S27: Reheat 1100°C

Pass	T	∈
1	1083	.20
2	1058	.20
3	1019	.25
4	965	.26

d_α = 22µm

Figure 4.8 Effect of reheat temperature on final microstructure X400

4.1.2.5 Effect of finish temperature on ferrite grain size

Lowering the temperature in the final pass during multi-pass plane strain compression tests significantly refined the as-deformed ferrite grain size. Figure 4.9 shows the microstructure of specimens, S25 and S20, finished after four passes at 1130°C and 680°C respectively. The microstructure of specimen S25 was coarse but equiaxed and had a ferrite grain size of 19μm. The microstructure of specimen S20 showed alternating regions of fine and coarse ferrite (mean d_α = 8μm).

Figure 4.10 shows the relationship between finishing temperature and mean ferrite grain size in all multi-pass tests. It was seen that, for all SC8 grades, lower finish temperatures resulted in finer ferrite. These grain sizes were in close agreement with DeAardo's [58] results obtained from 0.12C-1.3Mn-0.3Si steel. Ferrite grain sizes found in this work were larger than those found by Vodopivec [65] for an 0.13C-0.46Mn steel grade. Ferrite grain refinement was significant when the finsh temperature was lowered within the 1150°C-850°C temperature range but became increasingly difficult when the finish temperature was below 800°C.

Pearlite banding was more significant in specimens finished at low temperatures. This is clearly seen in Figure 4.11.

4.1.3 Effect of carbon content on microstructure

After deforming at high finishing temperatures, the air cooled microstructures consisted of ferrite and pearlite in all steels. The pearlite volume fraction decreased with decreasing carbon content. This is clearly seen in Figure 4.12 where S9 (0.11C) and S15 (0.18C) were given approximately the same amounts of strain and both finished at approximately 1000°C. Specimen S9 contained 17% pearlite and S15 contained 23% pearlite. Pearlite banding was present in both structures when viewed at lower magnification which was typical of air cooled manganese containing ferrite/pearlite plate steels.

a)S25 (X400)
Reheat 1250°C

Pass	T	∈
1	1225	.17
2	1185	.09
3	1160	.10
4	1130	.37

d_{α} = 19 μm

b)S20 (X400)
Reheat 1200°C

Pass	T	∈
1	1130	.19
2	730	.16
3	700	.25
4	680	.11

d_{α} = 8 μm

Figure 4.9 Micrographs showing the effect of finish temperature on microstructure X400

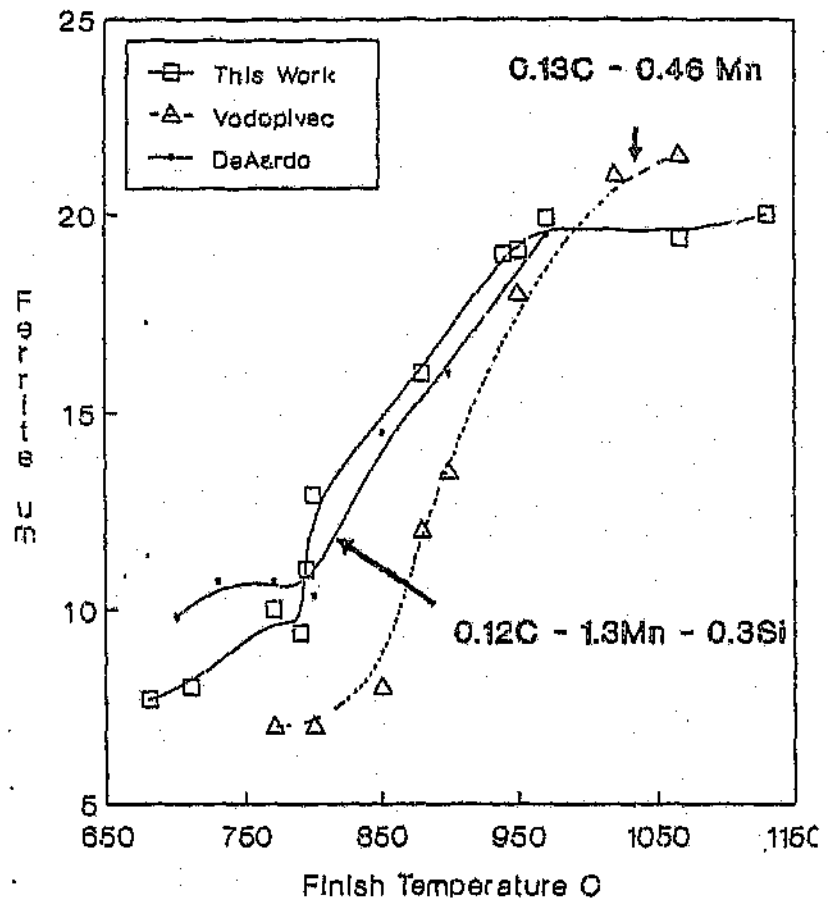

Figure 4.10 Effect of finishing temperature on ferrite grain size

S16 Finish temperature = 1066°C

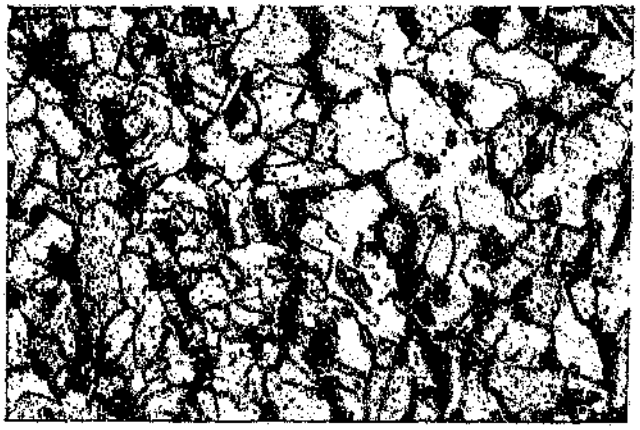

S21 Finish temperature = 836°C

Figure 4.11 Micrographs showing the effect of pearlite banding at progressively lower finishing temperatures. X400

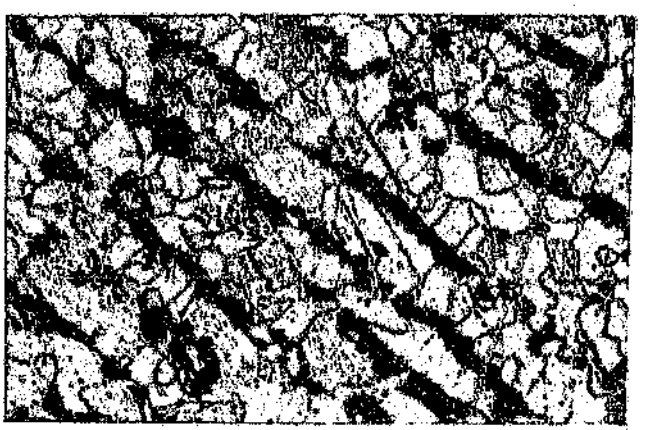

S18 Finish temperature = 807°C

Figure 4.11 (Cont) Micrographs showing the effect of pearlite banding at progressively lower finishing temperatures. X400

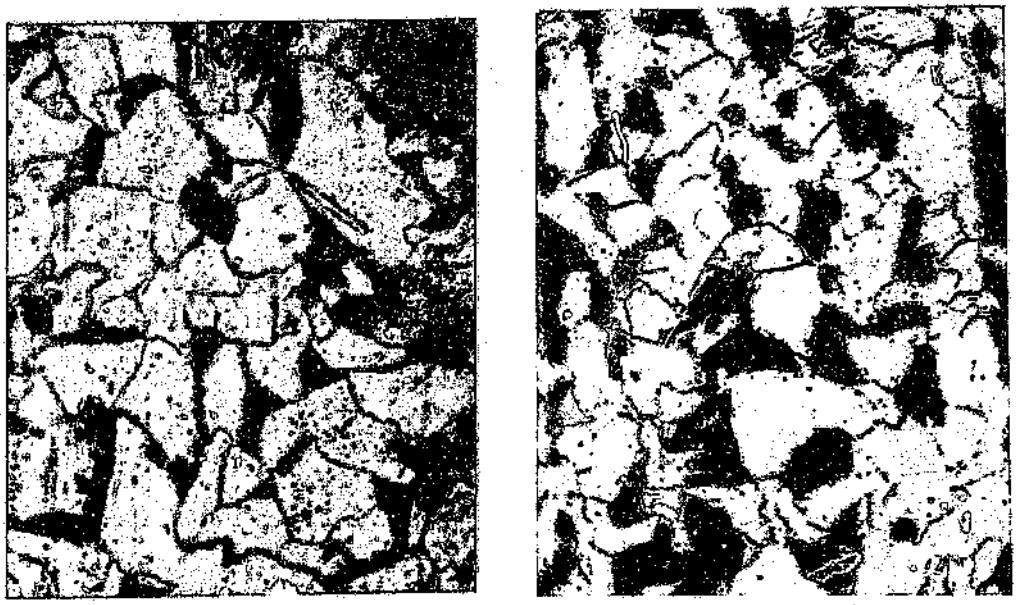

a)S9 (0.11C) X400
Reheat 1200°C

Pass	T	ε
1	1120	.26
2	990	.32

d = 19 μm

b)S15 (0.18C) X400
Reheat 1225°C

Pass	T	ε
1	1125	.31
2	1010	.45

d = 14 μm

Figure 4.12 Micrographs showing the effect of carbon content on pearlite volume fraction X400

4.1.4 Cooling rate

4.1.4.1 Effect of cooling rate on hardness

Figure 4.13 shows graphically the cooling rate at the A_{r3} temperature (866°C) for tests S2, S21, S29 and S30. These specimens experienced cooling rates of 2, 2.8, 15 and 35 $°Cs^{-1}$ respectively.

In order to determine the uniformity of cooling, hardness values were determined through the thickness of the deformation zone. Figure 4.14-4.16 shows the hardness maps in the deformation zones of specimens S2, S29 and S30. It was found that increasing the cooling rate increases the hardness gradients in both the width and thickness planes. For a cooling rate of $35°Cs^{-1}$, the

maximum difference in hardness between centre and surface was 60 HV30 whereas the maximum difference for a cooling rate of $2°Cs^{-1}$ was 3 HV30. Micrographs showing the final microstructures of specimens S2, S29 and S30 are given in Figure 4.17.

The top water nozzles were more efficient in cooling the specimen resulting in slightly higher hardness of the top specimen surface.

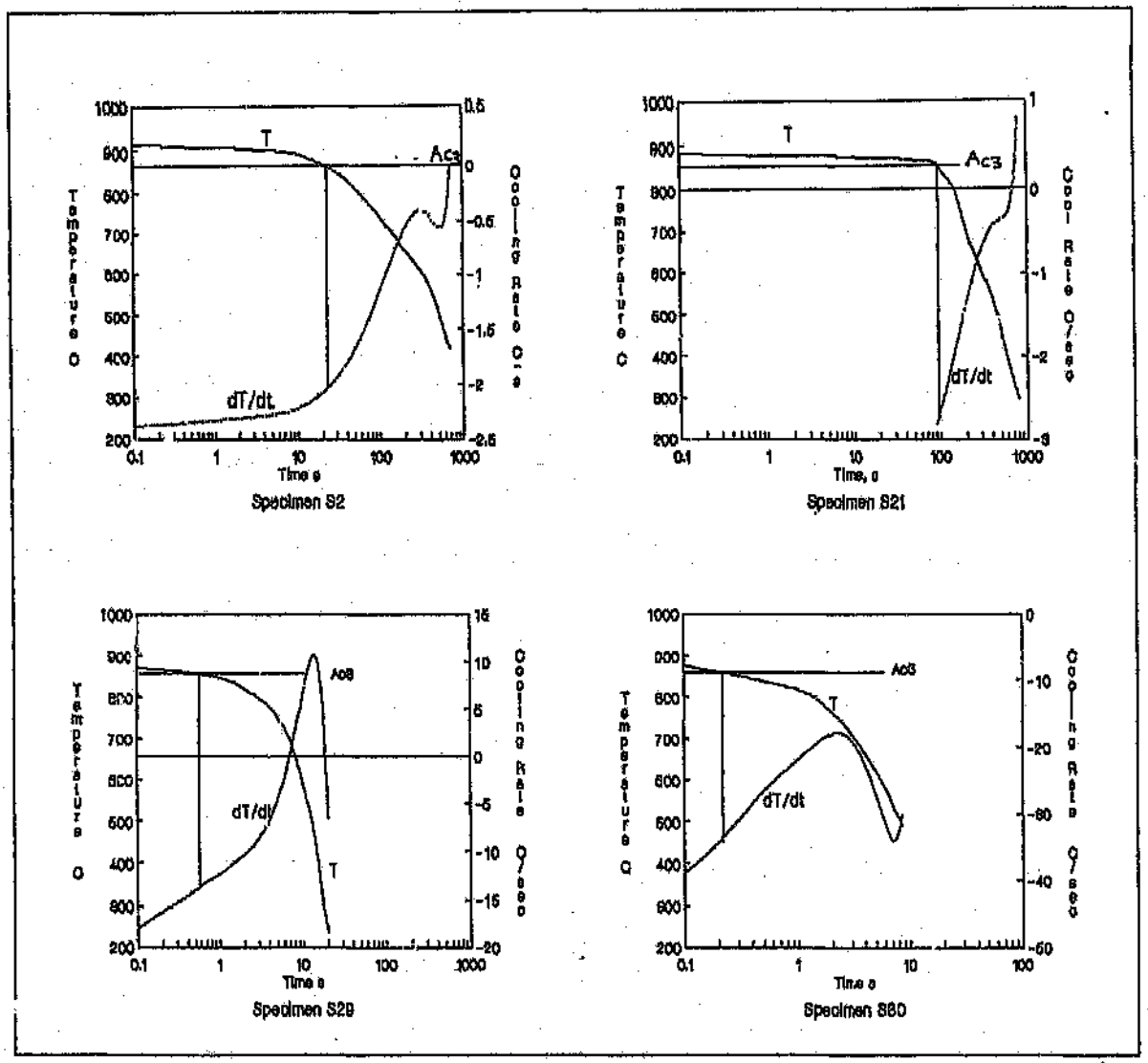

Figure 4.13 Determination of cooling rates for specimens S2, S21, S29 and S30

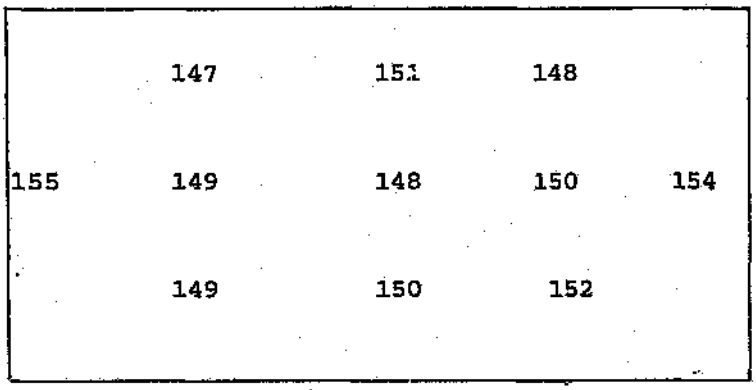

Figure 4.14 Hardness profile across deformation zone (spec. S2)

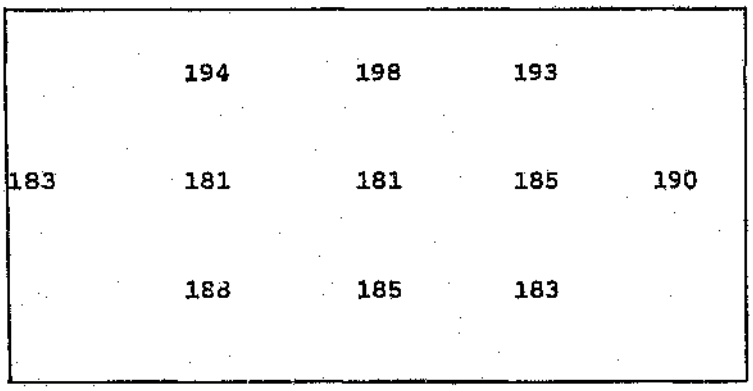

Figure 4.15 Hardness profile across deformation zone (spec.S29)

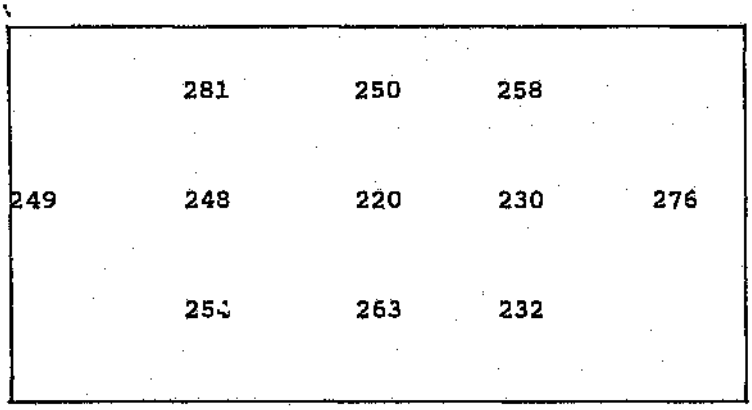

Figure 4.16 Hardness profile across deformation zone (spec. 30)

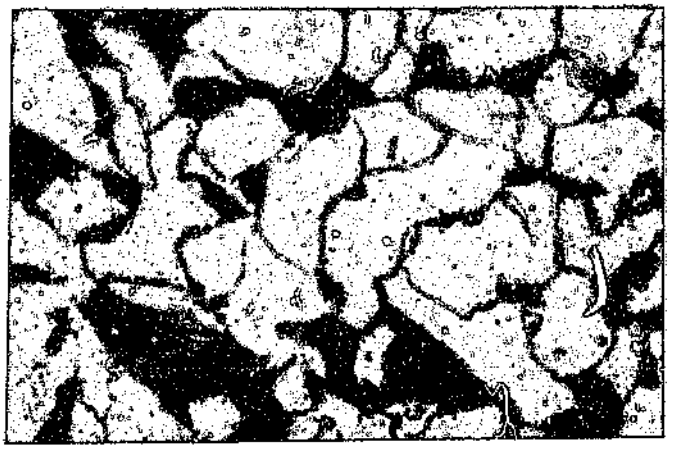

A) S2: Cooling Rate at 866°C = $2°Cs^{-1}$

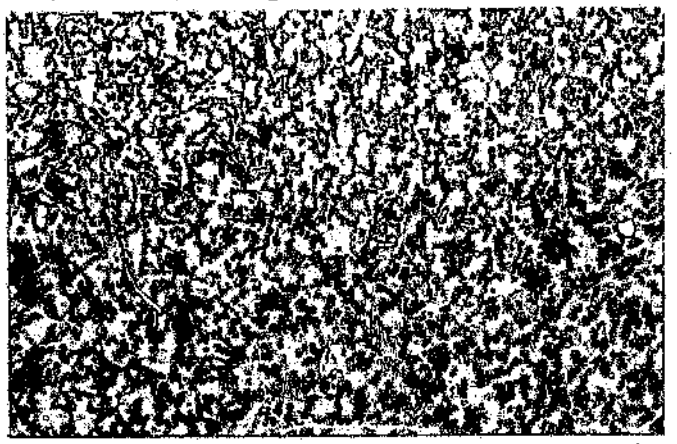

B) S29: Cooling Rate at 866°C = $15°Cs^{-1}$

C) S30: Cooling Rate at 866°C = $35°Cs^{-1}$

Figure 4.15 Microstructure showing the effect of cooling rate on ferrite grain size (Etched 2% Nital, 400X magnification)

4.1.4.2 Prediction of ferrite grain size for slow cooling rates

It was found from examining various ferrite grain size prediction models [51,52], that equation 2.58 (used in conjunction with equation 2.45 and equation 2.44), which simulates the ferrite grain size in terms of austenite grain size before transformation and cooling rate, was the most suitable for steel SC8. It must be noted that equation 2.58 is applicable to C-Mn steel continuous cooled from fully recrystallised austenite i.e the residual stress due to deformation was not taken into account. Calculated austenite grain sizes and cooling rate obtained from air-cooled (about $2°Cs^{-1}$) plane strain compression tests were fitted to equation 2.58 to quantitatively predict the final ferrite grain size. The measured ferrite grain size is plotted in Figure 4.18 against calculated ferrite grain size. It was seen that for large ferrite grain sizes ($d > 18\mu m$, obtained at high finishing temperatures and from fully recrystallised austenite) the predicted values obtained from equation 2.58 were in good agreement with measured values. However, for smaller ferrite grain sizes ($d < 18\mu m$), the predicted values were somewhat larger than the measured value by about $5\mu m$. This can be attributed to residual strains in the structure, generated by deforming the steel at low temperatures ($T < 850°C$), resulting in unrecrystallised austenite with elongated or "pancaked" grains. On transformation, this "pancaked structure" provides more potential sites for ferrite nucleation than a fully recrystallised austenite structure.

Due to limited tests, it was not possible to quantify the effect of faster cooling rates on the ferrite grain size.

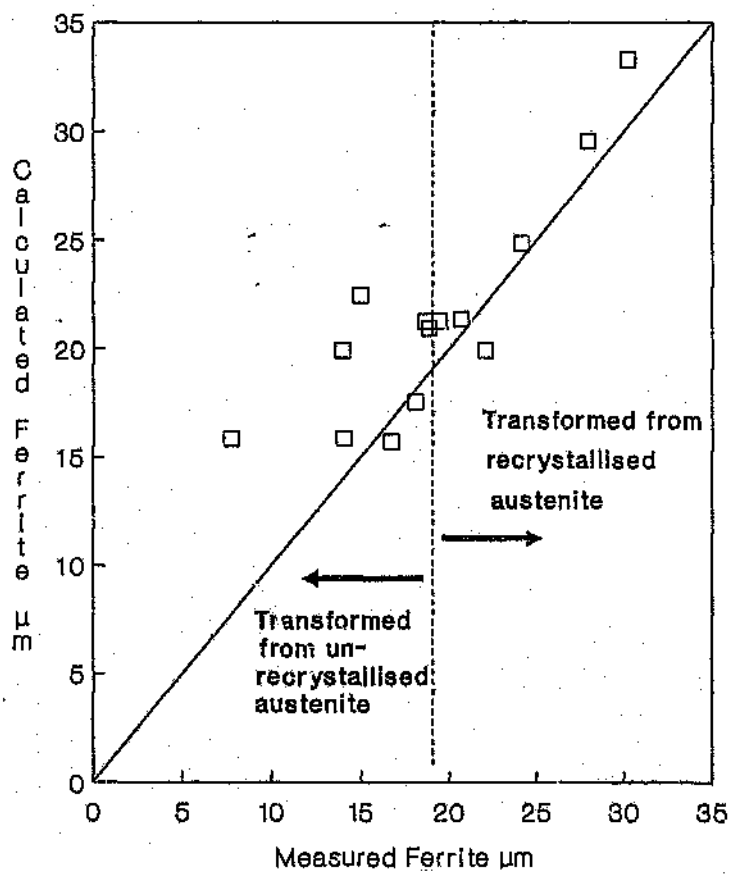

Figure 4.18 **Comparison between measured and calculated ferrite grain sizes**

4.1.5 Effect of strain on ferrite grain size

The effect of final strain on the ferrite grain size is shown in Figure 4.19. Both specimens S10 and S13 were reheated to 1200°C and 1250°C respectively and given similar strains of 0.29 and 0.36 in the first pass at temperatures of 1133°C and 1144°C. The amount of strain applied in the second pass, conducted at 940°C, was varied. S10 had a ferrite grain size of 20μm after 0.28 strain in the second pass. The ferrite grain size in S13 was 8μm after a final strain of 0.6.

The effect of finish strain and finish temperature on ferrite grain size for various two pass schedules is shown in Figure 4.20. Increased strain and decreased temperature in the last pass refined the ferrite grain size.

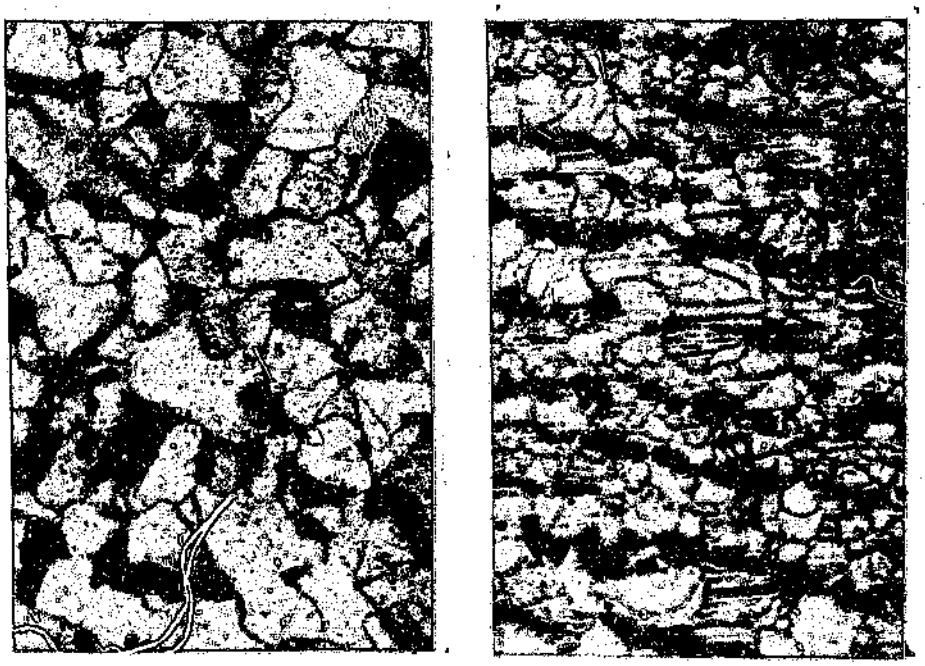

S10

Reheat 1200°C

Pass	T	∈
1	1133	.28
2	937	.28

d_α = 20 μm

S13

Reheat 1250°C

Pass	T	∈
1	1144	.37
2	947	.60

d_α = 8 μm

Figure 4.19 Micrographs showing the effect of finish strain on ferrite grain size X400

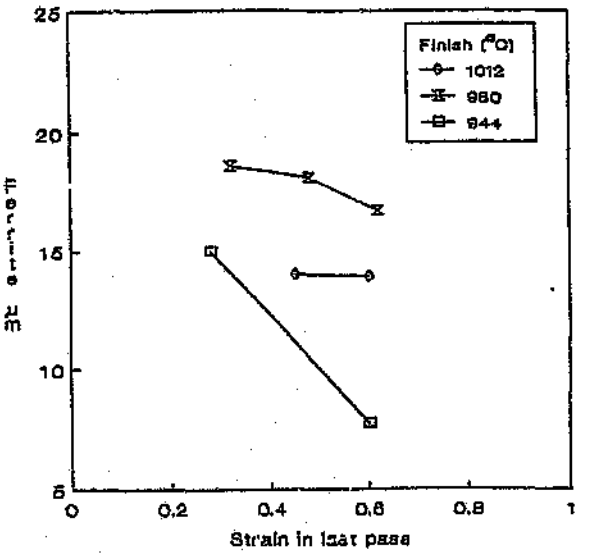

Figure 4.20 Effect of finish strain and finish temperature on ferrite grain size

4.1.6 Analysis of flow curves

4.1.6.1 Flow stress

The platen load , plotted against platen position for specimen S16 is given in Figure 4.21. It was seen that platen force increased in each subsequent pass due to continuous cooling conditions in the specimen after reheating was completed.

The equivalent flow stress, corrected using the Von Mises criterion, of four multi - pass plane strain compression tests conducted in the high temperature austenitic region (> 990°C) , was plotted against nominal strain in Figure 4.22. The numbers above each flow curve indicate the temperatures at which each pass commenced. The flow stress was simulated using a modified form of Barager's formula (equation 3.7). The constants for equation 3.7 were found from plane strain compression tests using multiple linear regression and are shown in Table 4.3 for various temperature ranges. Results of the simulated flow stress during multi-pass plane strain compression schedules are also given in Figure 4.22. There was close agreement between measured and simulated flow stresses for deformation at high temperatures (T > 990°C).

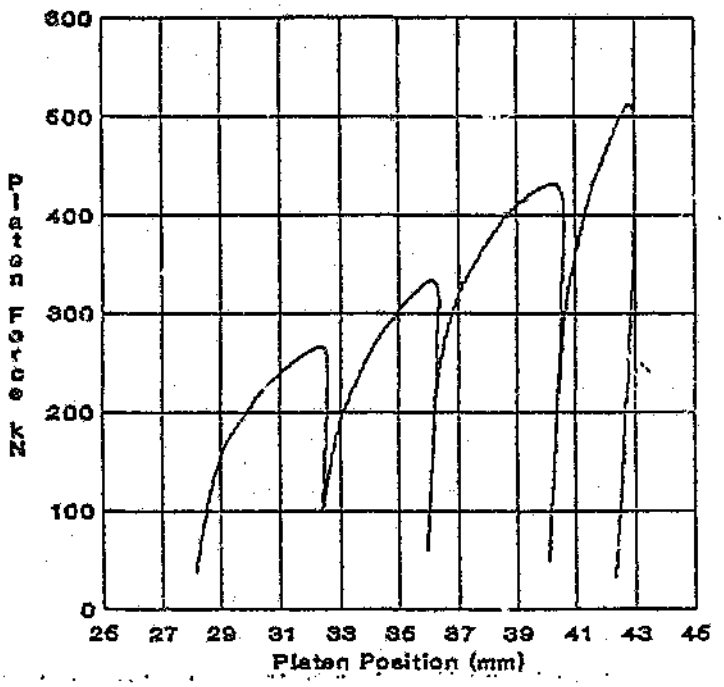

Figure 4.21 Platen load vs. platen position (specimen S16)

Table 4.3

Flow stress constants for Eqn. 3.7

Temperature Range	B	C	D
T > 1150°C	122	-39	-56
1150 > T > 1115°C	153	-49	-70
1115 > T > 1040°C	179	-79	-44
1040 > T > 950°C	204	-109	-18
950 > T > 825°C	206	157	-264
825 > T > 700°C	267	231	-371

It is seen in Table 4.4 that the mean flow stress for deformation conditions, compared favourably with results obtained by Akben et al [64] from torsion tests on 0.12C - 1.2Mn steels.

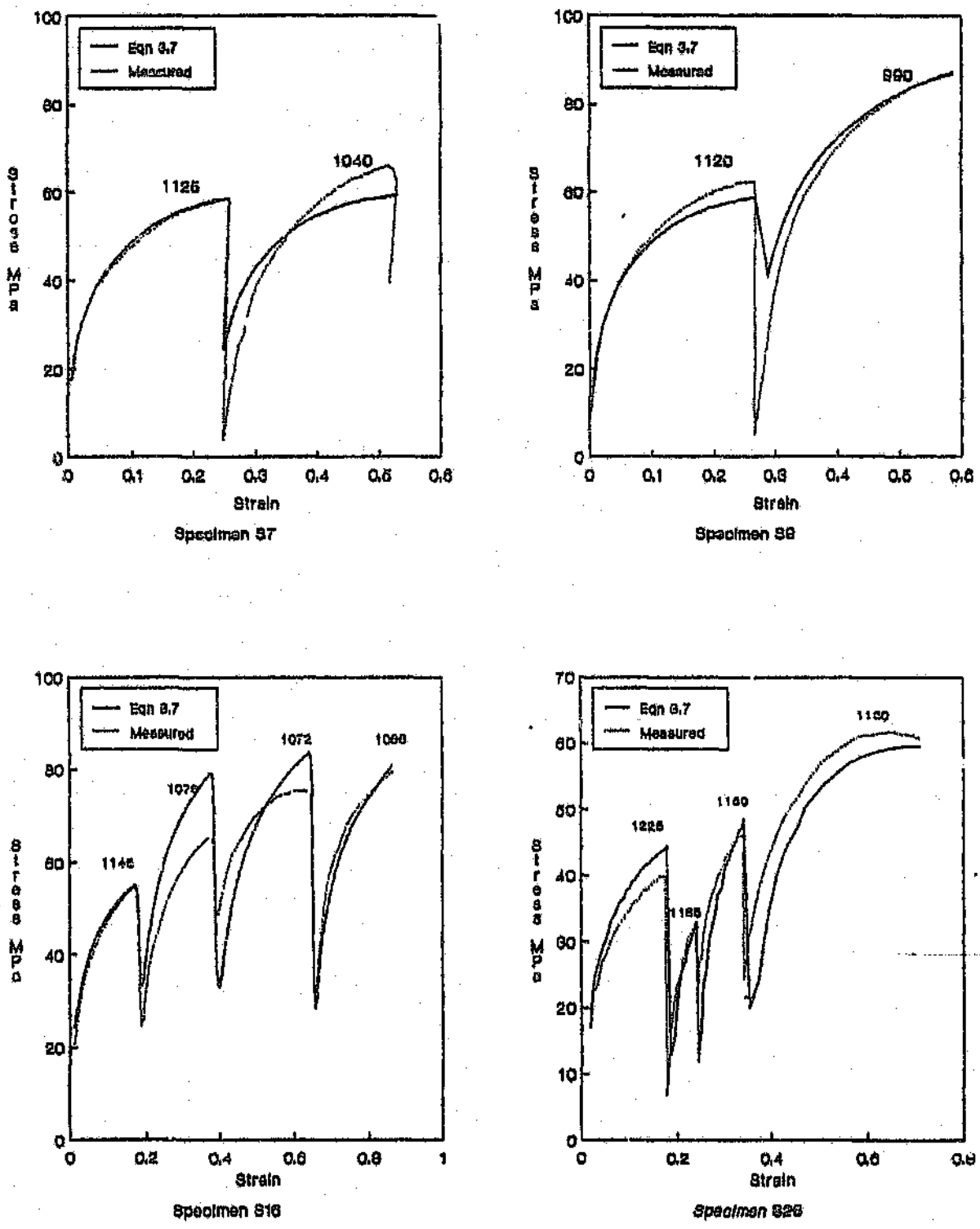

Figure 4.22 Hot flow curves for SC8 plate steel for multi - pass plane strain compression tests S7, S9, S16 and S25

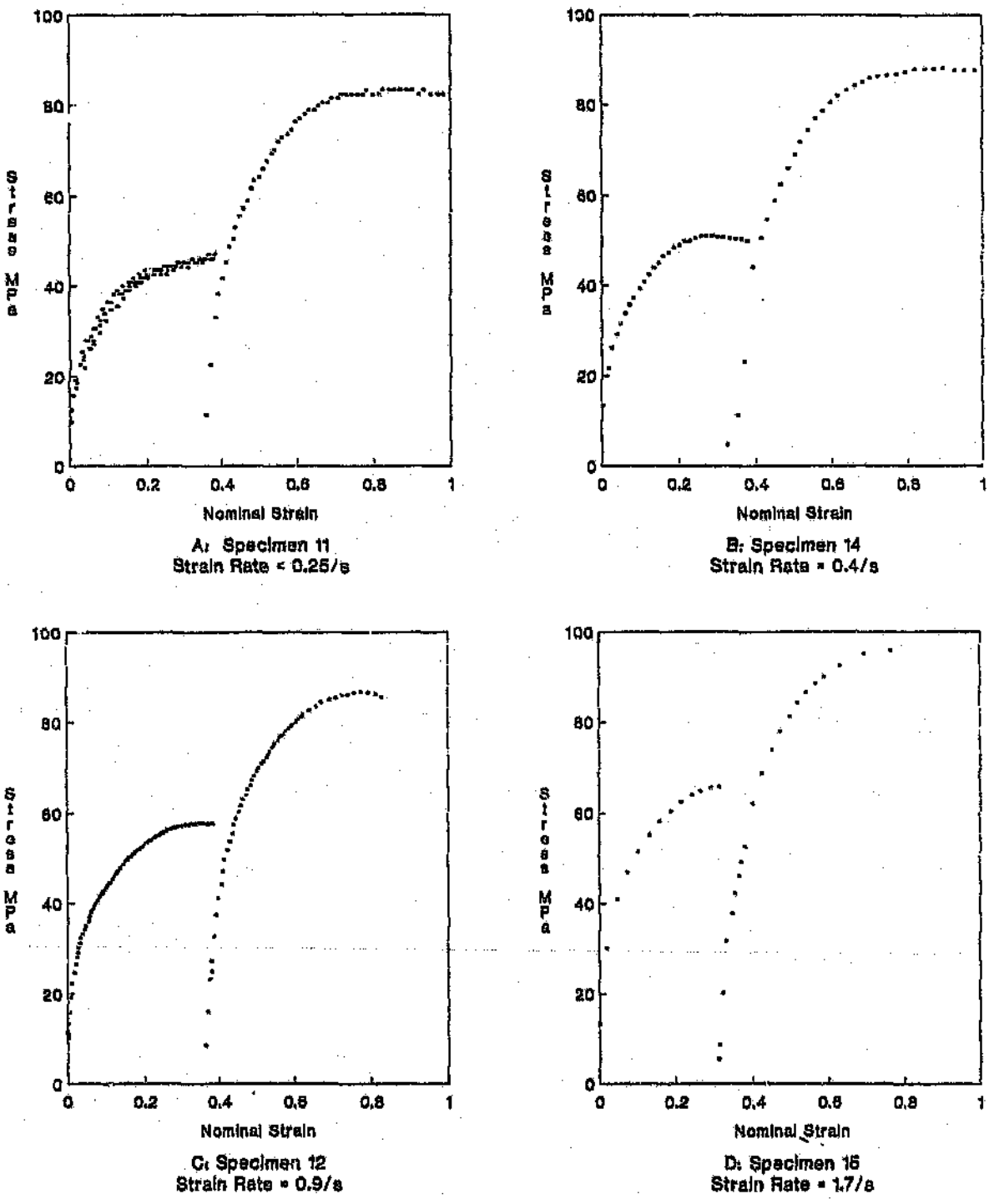

Figure 4.23 Hot flow stress versus strain rate during multi -pass plane strain compression tests S11, S12, S14 and S15

Table 4.4

Comparison between calculated mean flow stress in specimen S16 and flow stress values obtained by Akben [64] for similar test conditions

Pass Numbe.	$\dot{\epsilon}$ s^{-1}	T °C	ϵ	σ' Eqn 3.7	σ' Akben
1	2.5	1145	.18	49	47
2	2.5	1076	.19	61	55
3	2.5	1072	.27	71	68
4	2.5	1066	.22	77	74

Figure 4.23 shows the influence of strain rate on flow stress for specimens S11, S12, S14 and S15. The deformation parameters in all four tests were similar. The strain rate was varied between 0.25 and 1.7 s^{-1}. It was found that varying the strain rate between 0.25 and 0.9s^{-1} had almost no effect on the flow stress. However, when the strain rate was increased to 1.77 s^{-1} in S15, the flow stress in each pass was about 12 MPa higher than in the previous tests. This effect is expected to become more pronounced as the strain rate is increased further. Investigations into the influence of higher strain rates on various phenomena were prevented due to the velocity limit of the machine servo-actuator.

A comparison of measured and simulated flow stress at low temperatures is given in Figure 4.24 for specimen S20. At low temperatures (730-680°C) equation 3.7 was not accurate in predicting the flow stress. In the first pass of S20 at 1130°C, the simulated flow stress was in good agreement with the measured values. However, in the last two passes at 700°C and 680°C respectively, the simulated flow stress was significantly lower than the measured values.

4.1.6.2 Deformation induced transformation

Figure 4.25 shows the flow curve of specimen S23, in which the start of the austenite to ferrite transformation was induced by deformation. The first pass was conducted at 1142°C and the shape of the flow curve was typical of a specimen deformed in the fully recrystallised austenite range. Significant strengthening took place in pass two which was conducted in the no

and 748°C respectively show the typical shape of flow curves when strain induced transformation of austenite to ferrite occurs. A flattening out and eventual drop in the flow stress is recorded due to the softer ferrite phase. If deformation is continued in this region the flow stress starts to increase again due to strain hardening of the ferrite.

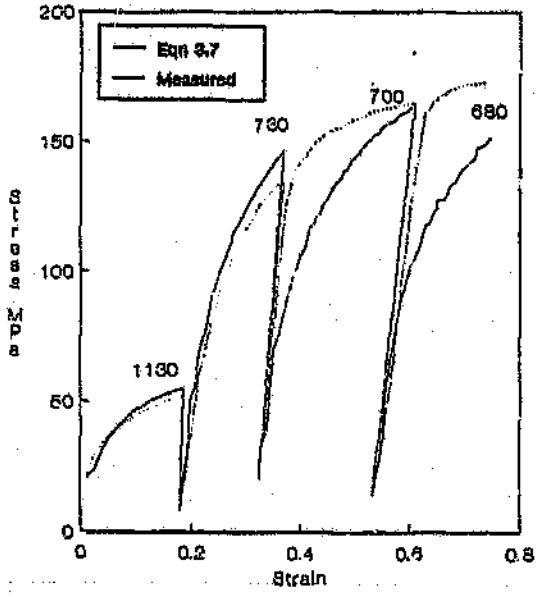

Figure 4.24 Flow stress at low temperatures (specimen S20)

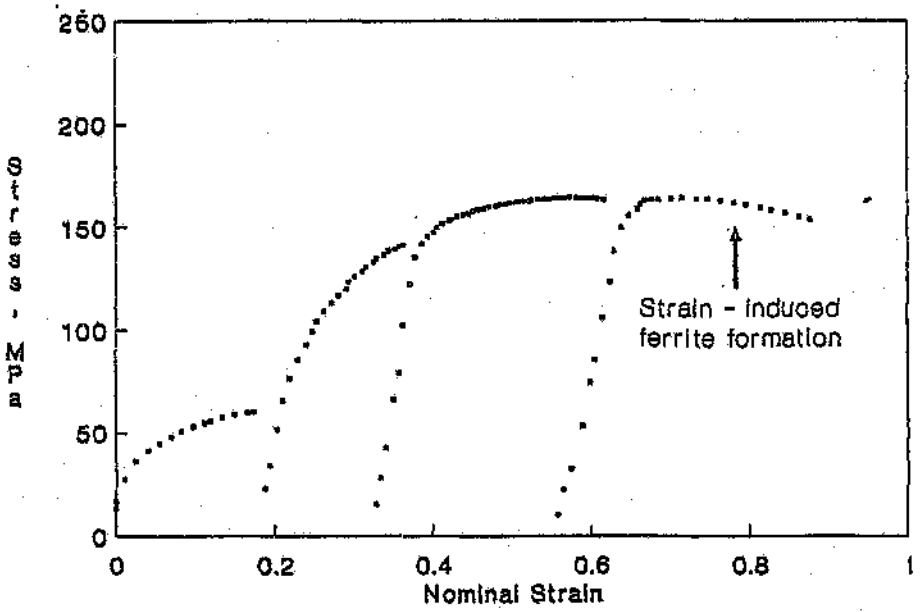

Figure 4.25. Effect of strain induced ferrite transformation on the shape of the flow curves in specimen S23

4.1.6.3 Anisothermal softening

Figure 4.26 shows the undeformed flow stress, $\sigma_{un,i}$, as a function of deformation temperature T_i for SC8 steel. Using linear regression, the undeformed flow stress at a strain rate of $2.5s^{-1}$ was represented as a function of temperature only, according to equation 4.4:

$$\sigma_{un,i} = 291.7 - 0.2234\ T°C \quad (MPa) \qquad 4.4$$

The results from the evaluation of the anisothermal softening ratio X_o are shown in Figure 4.27. S7 was reheated to 1245°C and deformed in two passes; the first at 1095°C and 0.28 strain and the second pass at 1047°C and 0.23 strain. The values of σ_o, σ_1 and σ_2 were 31, 59 and 36 MPa respectively. From Figure 4.26, K_1 and K_2 were found to be 0.81 and 0.66 respectively. The anisothermal restoration index was 1.04 which showed that the structure was fully recrystallised. S2 was reheated to 1240°C and deformed in two passes at 1195°C at 0.09 strain and 1150°C at 0.17 strain. The values of σ_o, σ_1 and σ_2 were 33, 44 and 40 MPa respectively. K_1 and K_2 were found to be 1.2 and 1.12

respectively. The restoration index was 0.404 showing that only 40% of the austenite recrystallised.

The anisothermal restoration indices for S2 and S7 are in agreement with the results obtained by Sekine [29] shown in Figure 4.28. As predicted, the austenite structure after the first pass of a 0.11C steel with an initial austenite grain size of 270μm (reheat 1220-1250°C) and deformed at 1095°C and 0.28 strain was fully recrystallised. The predicted austenite morphology after deformation at 1195°C and 0.09 strain was a partially recrystallised structure.

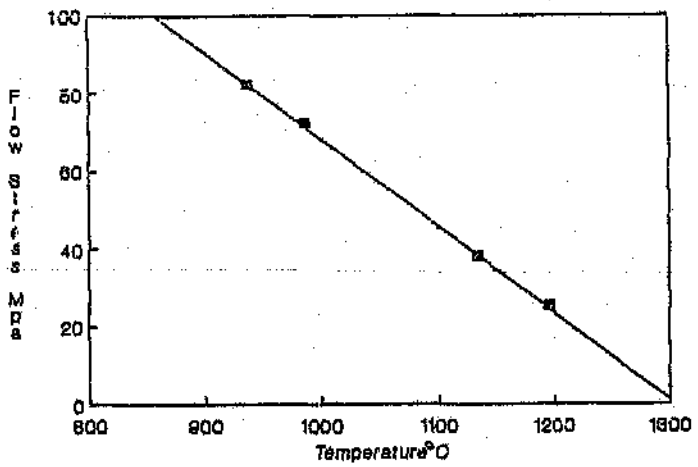

Figure 4.26 Undeformed flow stress of SC8 steel

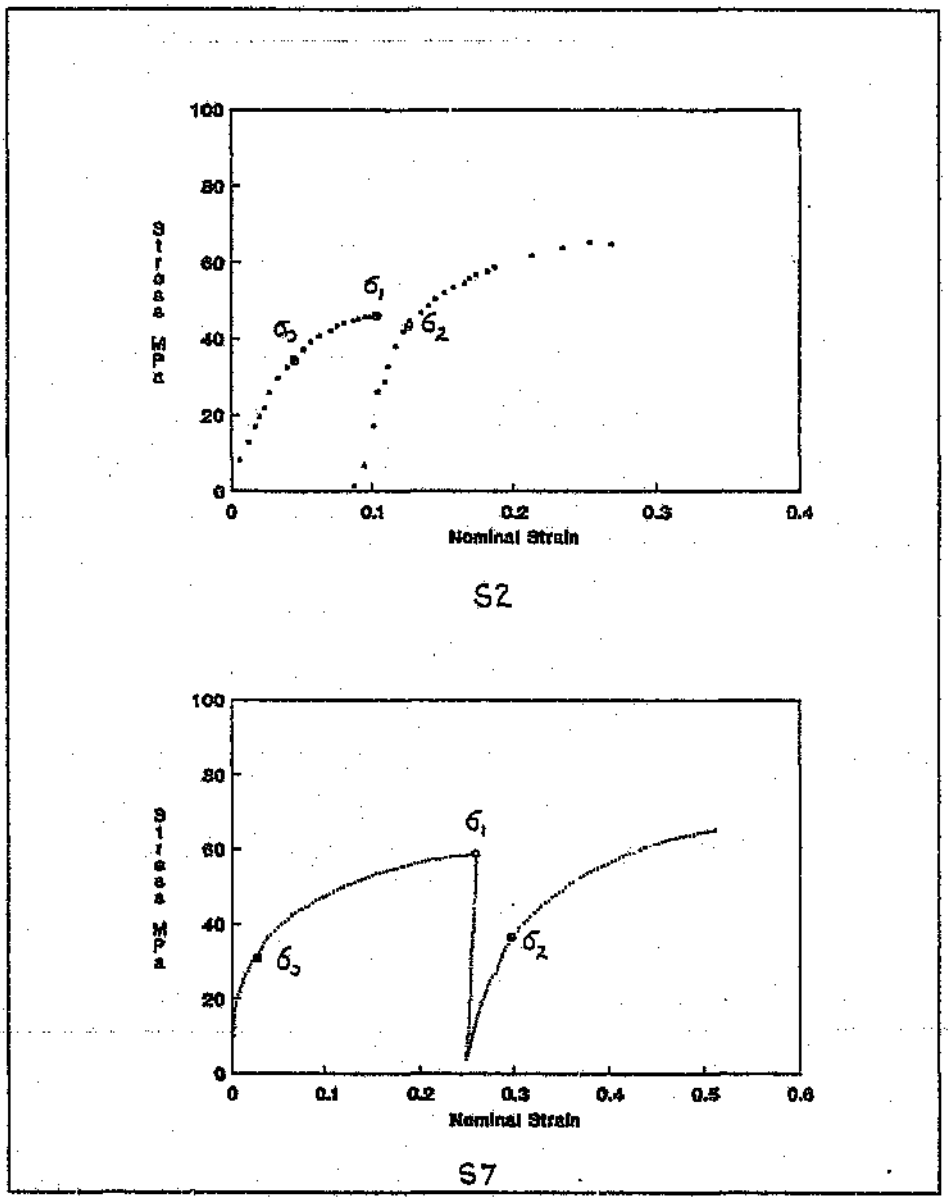

Figure 4.27 Double stroke results for specimens S2 and S7

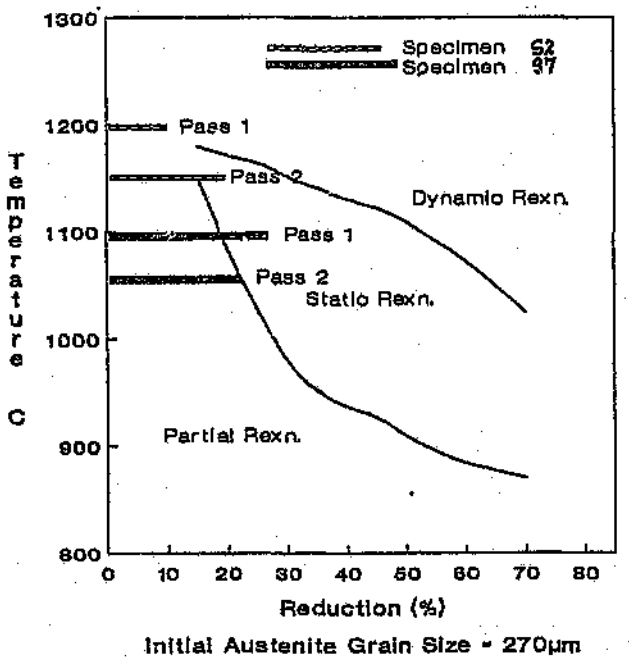

Figure 4.28 Predicted austenite structure for S2 and S7

4.1.6.4 Strain hardening exponent

The strain hardening exponent, n, was continuously monitored throughout two multi-pass plane strain compression tests, S16 and S20. The results are given in Figure 4.29. It can be seen that the value of n did not pass through zero at any stage during deformation of specimen S16 implying that dynamic recrystallisation did not take place. In S20 however, the strain hardening exponent passes through zero in the last pass indicating that dynamic recrystallisation occurred.

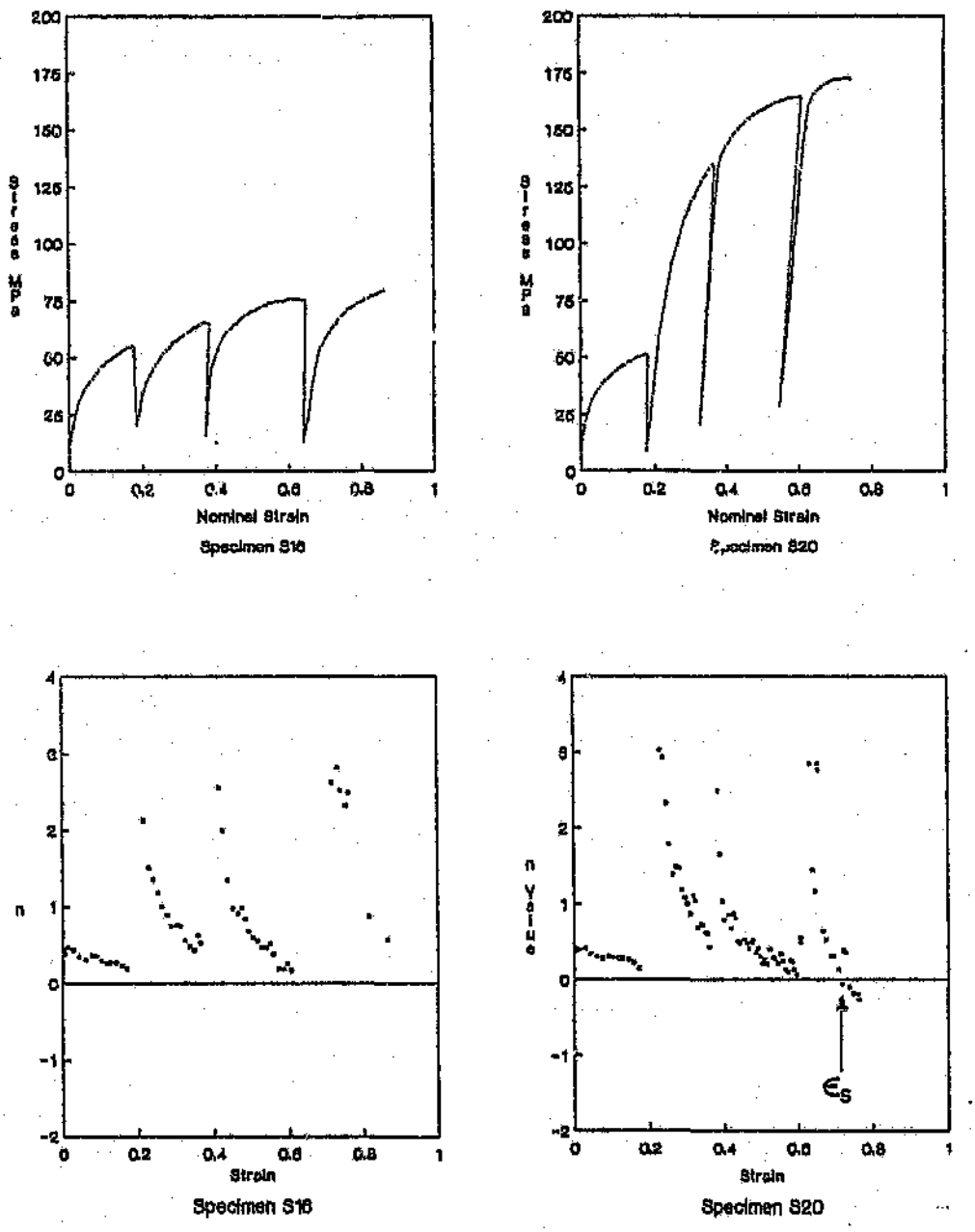

Figure 4.29 Strain hardening exponent versus strain(refer to Figure 4.9b for specimen S20 and Figure 4.11a for specimen S16)

4.1.7 Ferrite grain size

4.1.7.1 Effect of ferrite grain size on yield strength

The results of measured and simulated yield strength values (equation 2.61) for the three different grades of steel SC8, compressed in plane strain are given in Figure 4.30. It can be seen that simulated yield strength increased linearly with increasing $d_\alpha^{-1/2}$. This behaviour was also found for grain sizes in the 8 to 15 μm range. However, at d_α values greater than 16μm the measured proof strength values were somewhat lower than the simulated values. Nevertheless, there was generally good agreement between measured and simulated values. The yield stress of steel SC8 with 0.18% carbon was 330 MPa and 335 MPa for ferrite grain sizes of 8μm and 25 μm respectively.

The effect of chemical composition on yield strength is also shown in Figure 4.30 . The yield strength of the higher C steel (0.18C) was about 20 MPa higher than the 0.11C steel for any given ferrite grain size. Lower manganese content (0.65%) resulted in lower yield strength for a given carbon content and given ferrite grain size due to less solid solution strengthening.

Simple regression analysis was performed on the yield strengths and ferrite grain sizes of all air cooled specimens given in Table 4.1 and resulted in the following Hall-Petch type equations:

Grade A: $R_\alpha = 199 + 11.3\ d_\alpha^{-1/2}$ MPa $R^2 = 0.82$ 4.5

Grade B: $R_\alpha = 243 + 8.15\ d_\alpha^{-1/2}$ MPa $R^2 = 0.89$ 4.6

and d_α is in mm.

The correlation coefficients were rather low and led to the conclusion that an accurate prediction of yield strength in terms of ferrite grain size only could not be formulated for the entire range of deformation conditions used in this work. A more accurarte approach to quantifying yield strength is discussed in section 4.1.8.

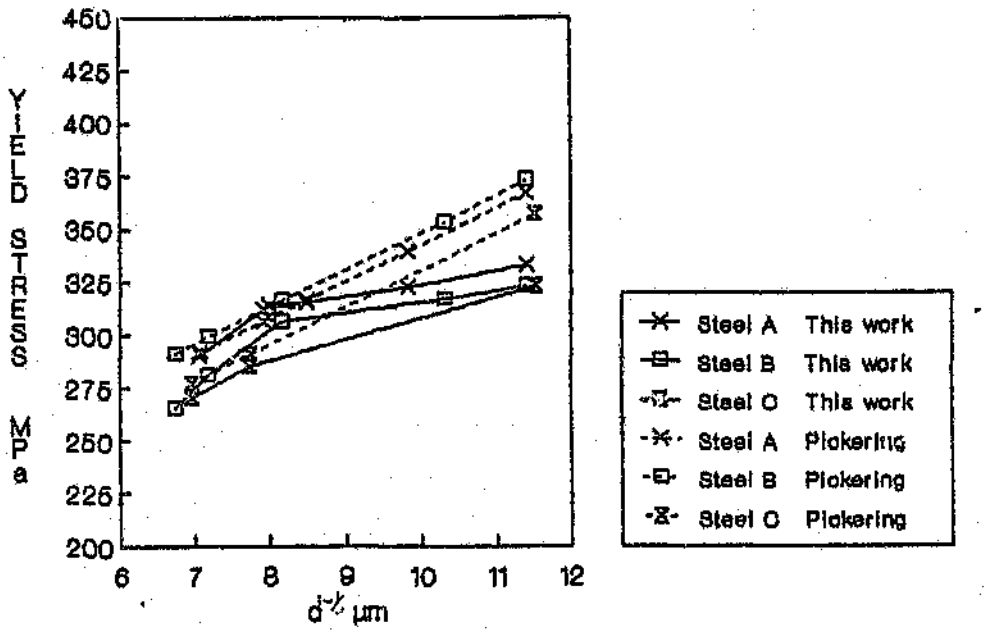

Figure 4.30 Influence of ferrite grain size and chemical composition on yield strength

4.1.7.2 Effect of ferrite grain size on tensile strength

The results of measured and simulated tensile strength for the three SC8 grades is given in Figure 4.31. It is seen that the tensile strength increased only slightly with decrease in ferrite grain size. Over the ferrite grain size

range of 8μm to 25μm the tensile strength of the 0.11C-0.63Mn varied between 420 MPa and 440 MPa. The tensile strength of the C.11C-1.2Mn grade varied between 460 and 475 MPa whilst the 0.18C-1.05Mn grade showed tensile strengths of between 475 and 500 MPa over the ferrite grain size range considered. The predicted tensile strength showed a slightly larger increase (30-50 MPa) between 8μm and 25μm.

For a given ferrite grain size, the tensile strength increased with increased carbon and manganese contents. For the 0.11C steel at 8μm, the tensile strength was 400 MPa compared to 410 for the 0.18C steel grade. There was good agreement between measured and simulated (equation 2.62) tensile strengths. Taking all air cooled tests into account, the measured and simulated tensile strengths did not differ by more than about 20 MPa.

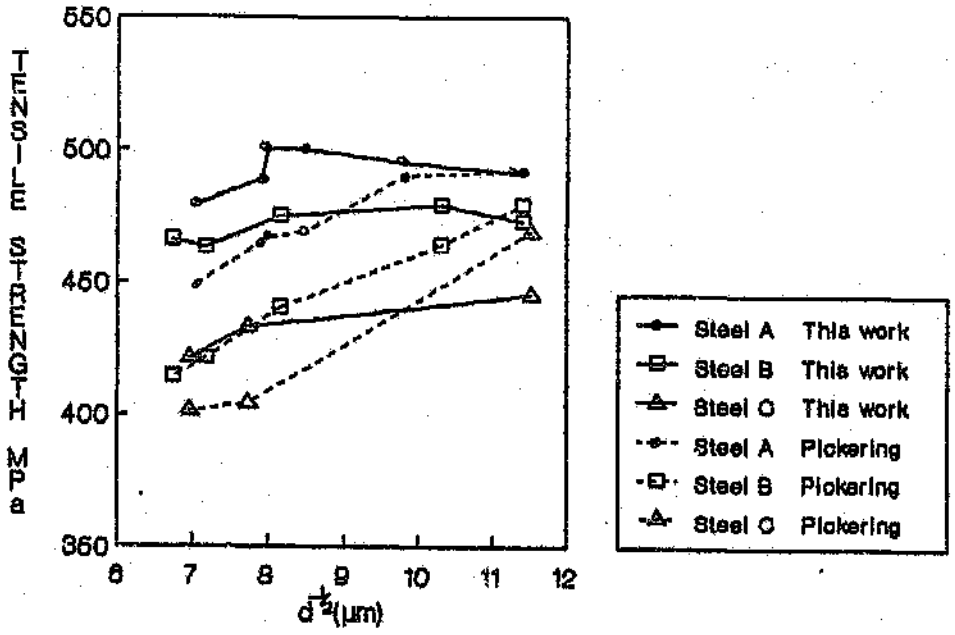

Figure 4.31 Influence of ferrite grain size and chemical composition on tensile strength

4.1.7.3 Effect of ferrite grain size on impact values

The effect of ferrite grain size and chemical composition on the average impact energy at 0° C is shown in Figure 4.32. The impact energy of all steels increases with decreasing ferrite grain size according to a $d_{\alpha}^{-1/2}$ until about 11 μm. At ferrite grain sizes below 11 μm the impact energy started to decrease. This observation was in good agreement with results obtained by Speich et al [49].

Chemical composition had a marked effect on impact value, independent of grain size. For a given ferrite grain size, the lower carbon steel(0.11C) had higher impact values than the higher carbon (0.18C) steel. It was found that a decrease in manganese content also improved the impact value slightly.

For the 0.11C steel, the elongation decreased from 36% at 25 μm to 30% at 8μm. This showed that refinement of ferrite grain size did not reduce ductility to a large extent. Elongation in the 0.18C steel was about 2% higher than the 0.11C steel for a given ferrite grain size.

4.1.8 Experimental simulation of plate rolling schedules

In simulating hot plate rolling it was assumed that the main metallurgical influences on the material must be found in the last passes. Hence the first pass of each schedule was performed between 1120 and 1150°C to induce a certain amount of recrystallisation associated with early roughing. The parameters in the remaining passes were chosen to simulate different conditions toward the end of plate rolling.

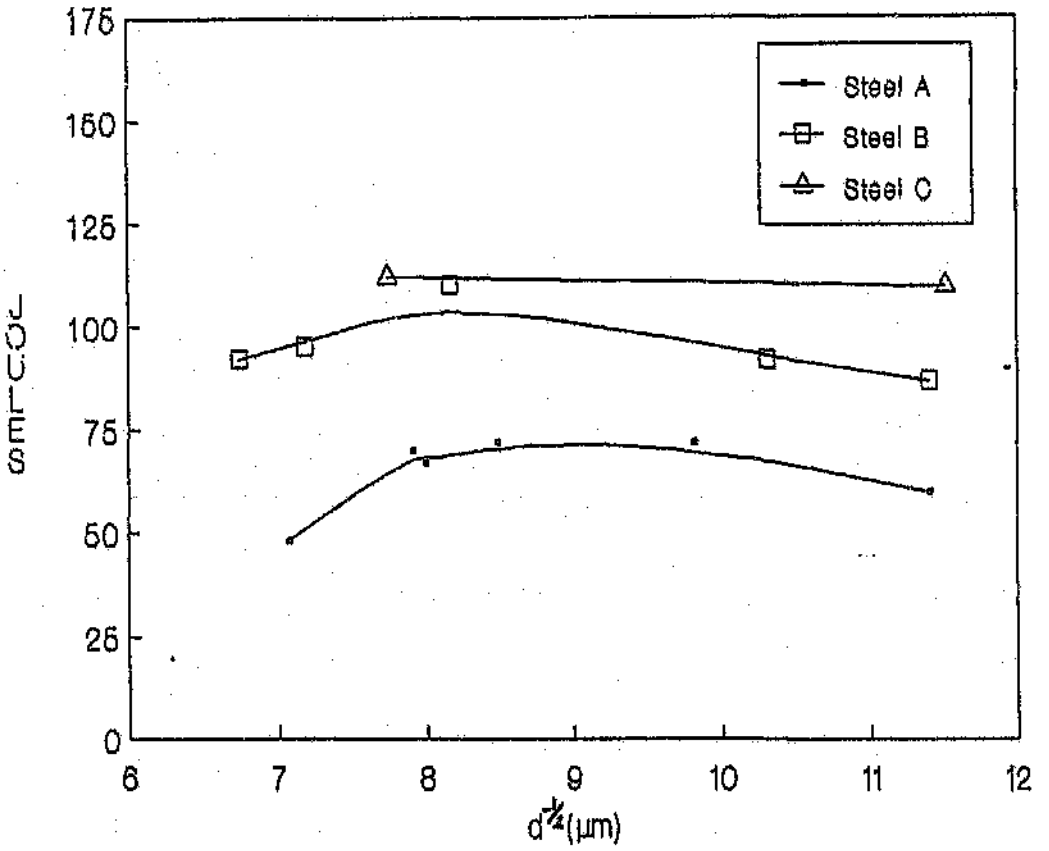

Figure 4.32 Influence of ferrite grain size and chemical composition on impact energy at 0°C

Multiple linear regression was performed on all the air cooled specimens in Table 4.1 to quantitatively determine the influence of the important rolling parameters on mechanical properties. The regression equation took the following form:

$$\text{Property} = A + B\ \%C + C\ \%Mn + D\ \epsilon_f + E\ T_{finish} \qquad 4.7$$

where A-E are constants. The properties of interest included the yield strength and the impact value at 0°C. The constants determined for the yield strength and impact energy are given in Table 4.5.

Table 4.5
Constants for equation 4.7

Property	A	B	C	D	E	Correlation
R_e, MPa	321	255.3	32.4	76.3	-0.119	0.9598
CVN, 0°C, J	227	-514.7	-	37.8	-0.095	0.9251

It is seen from Table 4.5 that carbon content, finish strain and finish temperature had the most influence over both yield strength and impact energy. An increase in carbon content improved yield strength but decreased impact values. An increase in manganese content also improved yield strength. The high correlation coefficients implied that this regression equation was representative of the overall behaviour of steel SC8 when subjected to range of deformation conditions given in Table 4.1. Equation 4.7 was incorporated into programme PLATESIM to predict the yield strength and impact values of steel SC8 using actual mill data. Results are given in the following section.

4.1.9 Summary of plane strain compression tests

Multi-pass plane strain compression tests were conducted successfully on a modified servo-hydraulic machine. The control programme, MULTR2, was capable of performing up to six consecutive deformations on 25mm thick steel specimens well within the 1500kN load capacity of the machine. The maximum strain rate that could be achieved on these specimens was $2.5s^{-1}$. Strains of up to 0.96 were possible without any sticking to the non lubricated platens. The specimen transport system was able to transport the plane strain compression specimen rapidly to and from the heating, deformation and cooling stages of the test. The data acquisition systems used were able to record test data well within the required limit. The specimen temperature, strain, strain rate and cooling rate were accurately controlled. The specimen temperature at any point in the

deformation zone was predicted to within a maximum error of 25°C of the measured values using a finite difference computer programme, PSC_TEMP.

The flow stress of SC8 plate steel was accurately predicted at any strain and strain rate in the practical rolling temperature range using equation 3.7. The ferrite grain size obtained from continuously cooling fully recrystallised austenite may be adequately described by Umemoto's equation. Low finishing temperatures, large finish strains and medium cooling rates were all found to play a significant role in refining the ferrite grain size.

Yield and tensile strength increased with decreasing ferrite grain size. The optimum Charpy value at 0°C was found at a ferrite grain size of about 13-15 μm. Impact values decreased at smaller ferrite grain sizes. The reheat temperature did not have a direct influence on final ferrite grain size. Impact energy values increased with decreasing carbon and manganese contents. The optimum cooling rate for SC8 steel lies between 15 and 35Cs^{-1}.

Multiple linear regression equations were formulated to predict the yield strength and impact energy at 0°C in terms of chemical composition, finish strain and finish temperature. The high correlation coefficients implied that the above mentioned parameters governed the final quality of air cooled steel SC8.

4.2 Plate rolling results

This section presents a comparison between measured results of deformation parameters found in industrial hot plate rolling and the corresponding predicted values obtained from the computer programme, PLATESIM.

Results of the rolling parameters measured and simulated during rolling of SC8 C-Mn steel plate at the Iscor Plate Mill, South Works, Vanderbijlpark are shown in Tables 4.6 -4.9. Final microstructure and mechanical properties were determined from samples cut from the tail end of each plate after the rolling process.

A computer programme, PLATESIM, based on the results obtained from plane strain compression tests (section 4.1) and models discussed in Chapter 2, was written to simulate the mechanical and metallurgical changes occurring during

and after hot plate rolling. The formulation of the programme was discussed in Chapter 3.

Key to Symbols used in Tables 4.6 to 4.9:

ϵ	: Nominal strain
$\dot{\epsilon}$	: Strain rate (s^{-1})
d_{recx}	: Recrystallised Grain Size(μm)
d_{gg}	: Grain Size after grain growth(μm)
F(m)	: Measured Roll Force(tons)
F(s)	: Simulated Roll Force(tons)
T(m)	: Measured Surface T (°C)
T(s)	: Simulated Surface T(°C)
Time	: Interpass time(s)

Table 4.6
Measured and simulated deformation parameters - SCHEDULE 1

Initial Width: 1250mm Reheat Temp: 1206°C C : 0.18
Final Width : 2540mm Average RPM:60 Mn: 1.05

Pass	Height	ϵ	$\dot{\epsilon}$	T(m)	T(s)	time	F(m)	F(s)	drex	dgg
Heat	210	0	0			8	0	0	220	*
1	180	.15	3.9	1141	1139	10	1300	1224	120	126
2	160	.27	3.7	1136	1128	5	1300	936	108	116
3	140	.41	4.2	1120	1124	6	2200	2047	91	98
4	120	.56	4.8	1110	1121	5	2600	2240	70	78
5	100	.74	5.7	1105	1117	5	2800	2511	51	61
6	84	.92	6.1	1100	1113	7	2400	2309	45	56
7	..	1.03	5.3	1100	1108	6	800	1513	56	66
8	62	1.22	7.3	1095	1102	10	2200	2353	43	55
9	50	1.44	8.6	1090	1091	6	2600	2552	34	50
10	39	1.69	10.4	1088	1082	6	2600	2844	28	44
11	30	1.95	12.2	1075	1071	6	2600	2893	24	42
12	24	2.18	12.7	1074	1058	6	2200	2337	27	44
13	20	2.36	12.7	1065	1052	10	1600	1832	34	66
Out				1071						

Property / Parameter		Measured	Simulated
Ferrite Grain Size	(μm)	25	22.9
Cooling Rate	($°Cs^{-1}$)	0.98	1.22
Yield Strength	(MPa)	330	295
Tensile Strength	(MPa)	444	429
Elongation	(%)	14.4	-
Impact Energy 0°C	(Joules)	35	39

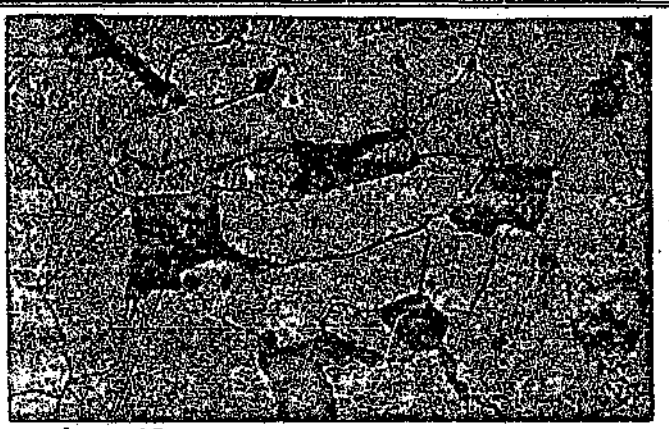

d_{α} = 25μm X 400

Table 4.7
Measured and simulated deformation parameters - SCHEDULE 2

Initial Width: 1250mm Reheat: 1206°C C : 0.18
Final Width : 2540mm Ave. RPM: 60 Mn: 1.05

Pass	Height	ϵ	$\dot{\epsilon}$	T(m)	T(s)	time	F(m)	F(s)	drex	dgg
Heat	210	0	0				0	0	220	*
1	180	.15	3.9	1140	1140	5	1300	1224	131	135
2	170	.21	2.5	1120	1130	10	800	532	135	142
3	150	.34	3.9	1105	1126	5	2200	1970	110	116
4	130	.48	4.5	1110	1123	5	2800	2137	84	91
5	110	.65	5.2	1105	1118	5	2800	2363	61	71
6	90	.85	6.2	1100	1114	6	3000	2692	43	55
7	80	.97	5.2	1100	1111	5	900	1590	55	65
8	65	1.18	7.5	1100	1104	7	2400	2595	39	52
9	50	1.44	9.4	1100	1094	10	2600	3155	27	45
10	38	1.72	11.0	1095	1085	6	3000	3161	23	41
11	30	1.95	11.6	1076	1076	7	2800	2577	26	42
12	24	2.18	12.7	1074	1061	6	2200	2337	28	44
13	20	2.36	12.7	1065	1054	10	1600	1832	34	67
Out				1060						

Property / Parameter		Measured	Simulated
Ferrite Grain Size	(μm)	22	20.1
Cooling Rate	($°Cs^{-1}$)	0.96	1.22
Yield Strength	(MPa)	330	297
Tensile Strength	(MPa)	455	435
Elongation	(%)	14	-
Impact Energy 0°C	(Joules)	37	37

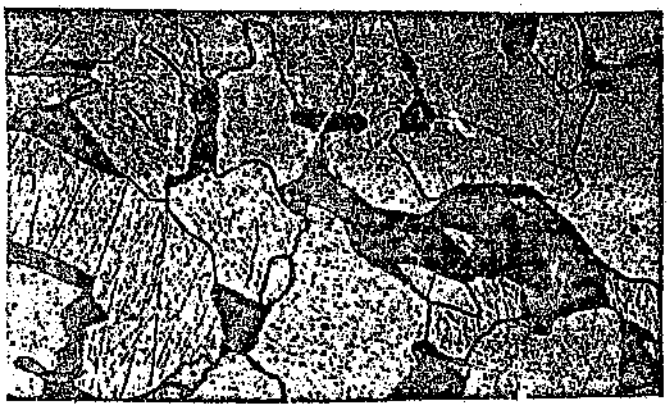

d_α = 22μm X 400

Table 4.8
Measured and simulated deformation parameters - SCHEDULE 3

Initial Width: 1250mm Reheat Temp: 1206°C C: 0.18
Final Width : 2540mm Average RPM: 60 Mn: 1.04

Pass	Height	ϵ	$\dot{\epsilon}$	T(m)	T(s)	time	F(m)	F(s)	drex	dgg
Heat	210	0	0	1150	1137		0	0	250	*
1	200	.05	2.1	1120	1127	7	750	496	250	252
2	180	.15	3.3	1105	1124	10	2100	1787	193	198
3	160	.27	3.7	1100	1121	5	2400	1902	147	150
4	140	.41	4.2	1100	1118	5	2400	2047	108	113
5	120	.56	4.8	1100	1115	5	2500	2240	77	84
6	104	.71	5.0	1095	1112	5	2200	2020	68	76
7	96	.79	3.9	1095	1105	5	800	1201	76	83
8	80	.97	6.3	1092	1099	5	2000	1908	53	63
9	64	1.19	7.8	1083	1093	5	2400	2785	36	49
10	50	1.44	9.2	1075	1090	5	2700	2953	28	44
11	40	1.56	9.8	1070	1085	5	2900	2544	28	44
12	31	1.92	11.8	1067	1074	8	2500	2816	25	42
13	24	2.18	13.5	1060	1067	10	2300	2722	24	42
14	20	2.36	12.7	1065	1060	10	1900	1832	33	66
Out				1065						

Property / Parameter		Measured	Simulated
Ferrite Grain Size	(μm)	22	20.4
Cooling Rate	($°Cs^{-1}$)	0.98	1.22
Yield Strength	(MPa)	333	295
Tensile Strength	(MPa)	444	420
Elongation	(%)	15	-
Impact Energy 0°C	(Joules)	40	39

$d_{\alpha} = 22\mu m$ X 400

Table 4.9
Measured and simulated deformation parameters - SCHEDULE 4

Initial Width: 1250mm Reheat : 1206°C C : 0.18
Final Width : 2540mm Average RPM: 60 Mn: 1.04

Pass	Height	ϵ	$\dot{\epsilon}$	T(m)	T(s)	time	F(m)	F(s)	drex	dgg
Heat	240	0	0			8	0	0	250	*
1	220	.09	2.7	1155	1140	10	1600	688	232	235
2	200	.18	3.0	1144	1138	5	1600	901	203	206
3	170	.35	4.1	1134	1127	6	1300	1367	109	117
4	158	.42	2.9	1122	1124	5	1300	682	117	123
5	130	.62	5.1	1108	1094	5	2600	2968	64	79
6	110	.78	5.2	1102	1092	7	2900	2456	56	66
7	90	.99	6.2	1098	1098	6	2700	2798	41	55
8	77	1.14	6.0	1095	1092	10	2400	2116	47	59
9	68	1.27	5.8	1090	1087	6	2600	1668	59	69
10	55	1.48	8.2	1085	1086	6	2600	2665	40	54
11	43	1.73	9.[illegible]	1088	1078	6	2800	2976	29	47
12	33	1.99	11.6	1070	1074	6	2800	3083	25	42
13	25	2.27	13.7	1060	1065	5	2400	122	22	40
14	20	2.49	13.9	1050	1060	10	2200	2366	27	43
15	16	2.72	15.5	1050	1052	10	1800	2297	28	68
Out				1060						

Property / Parameter		Measured	Simulated
Ferrite Grain Size	(μm)	22	20.3
Cooling Rate	($°Cs^{-1}$)	0.98	1.31
Yield Strength	(MPa)	333	296
Tensile Strength	(MPa)	441	425
Elongation	(%)	14	-
Impact Energy 0°C	(Joules)	35	37

d_{α} = 22μm X 400

4.2.1 Plate mill reheating temperature

The reheating furnace temperature of all SC8 schedules was between 1206°C and 1220°C. It was assumed that the ingots attained the furnace temperature at the end of soaking. The ingot soaking times were between 1 and 2 hours. The initial austenite grain size corresponding to this temperature range was found from equation 4.1 to be between 220μm and 250μm.

4.2.2 Strain during rolling

All SC8 ingots had a starting thickness of between 210mm and 240mm and were reduced in 12-14 passes to a final thickness of between 16 and 20 mm. The total nominal strain, calculated from equation 2.1, was between 2.36 and 2.47.

4.2.3 Strain rate during rolling

Work rolls of 492mm radius were used in all schedules and operated at an average roll speed of 50 rpm. The strain rate in each pass was calculated, using these values, from equation 2.5. The mean strain rate was between $2.1s^{-1}$ in the initial pass and about $15s^{-1}$ in the final pass.

4.2.4 Plate temperature

The plate surface temperature was measured using a radiation pyrometer situated at the plane of entry to the mill. The finishing temperature was measured using a radiation pyrometer situated about 5m from the plane of exit of the mill. The measured and simulated slab centre temperatures for Schedule 1 are shown in Figure 4.33. Clearly seen is the drop in simulated temperature due to air cooling and the temperature rise due to deformation heat input. It was found that a significant difference existed between the simulated centre and surface temperature of the plate which gradually decreased with time. After 10 seconds into the schedule the simulated centre temperature was about 1220°C and the simulated surface temperature was 1120°C. Immediately after the last pass the centre temperature was 1130°C whilst the surface temperature was 1075°C. There was very good agreement between measured and simulated surface temperatures although the simulated temperature was consistently lower than

the measured values by about 20°C. The maximum difference throughout the schedule was about 25°C. It was also found that the temperature rise due to deformation and the temperature drop due to conduction to the work rolls was more pronounced in the last passes where the temperature was lower. The faster temperature drop experienced between the last passes was due to a more rapid heat loss from thinner plates.

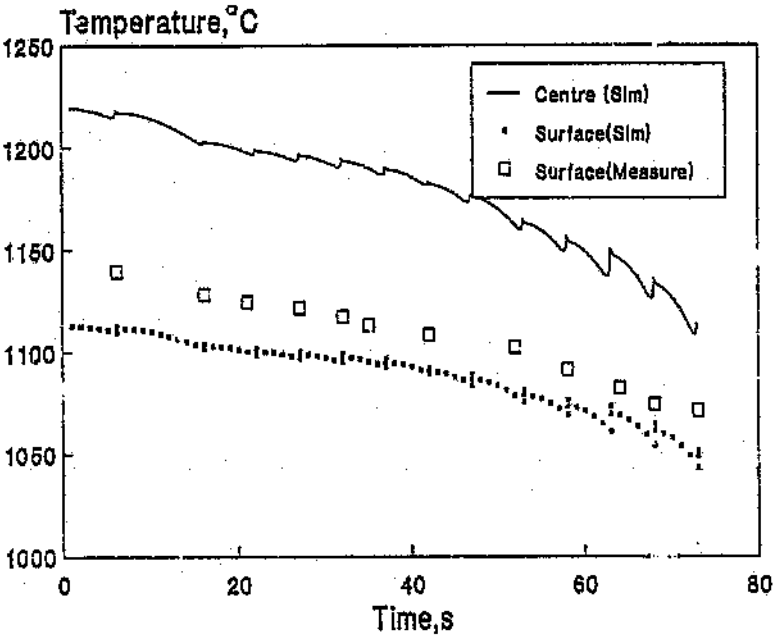

Figure 4.33 Measured and simulated plate temperature in Schedule 1

4.2.5 Roll separating force

A comparison between predicted and measured roll separating forces for plate rolling schedules is shown in the Mechanical Response graphs in Figures 4.34 - 4.37. There was very good agreement overall. Measured and predicted roll separating forces were fairly low (600-1600 tons) in all the initial passes due to the relatively narrow width (1250-1500 mm) of the plates as well as the high ingot temperature in the early stage of rolling (1150-1100°C). As soon as slab rotation took place to achieve the desired plate width, the roll force increased considerably to between 2200 and 3200 tons. A significant drop in roll force in the middle of the schedule was recorded because of plate profile

correction. Decrease in the roll force in the final few passes was due to small reductions in order to achieve the required final thickness.

4.2.6 Evolution of austenite

Equation 2.45 and equation 2.53 were incorporated in the computer program PLATESIM and used to simulate the kinetics of static recrystallisation and grain growth of the austenite during plate rolling schedules 1,2,3 and 4.

The simulated evolution of austenite during schedules 1,2,3 and 4 are shown in the Metallurgical Response graphs of Figures 4.34-4.37. In the early stages it was seen that the simulated austenite was reduced to between 50 and 60 μm after the fifth pass. In the middle passes however (1100-1070°C) there was little difference in the predicted grain size. This was because, at high rolling temperatures (1120-1040°C) and medium strains (0.15-0.25), the austenite reaches a limiting recrystallised grain size after which further refinement using conventional hot rolling practice becomes increasingly difficult. Towards the end of the schedule, small strains result in fairly large recrystallised austenite grain sizes. The predicted final austenite grain size was between 66μm and 68μm for all SC8 rolling schedules.

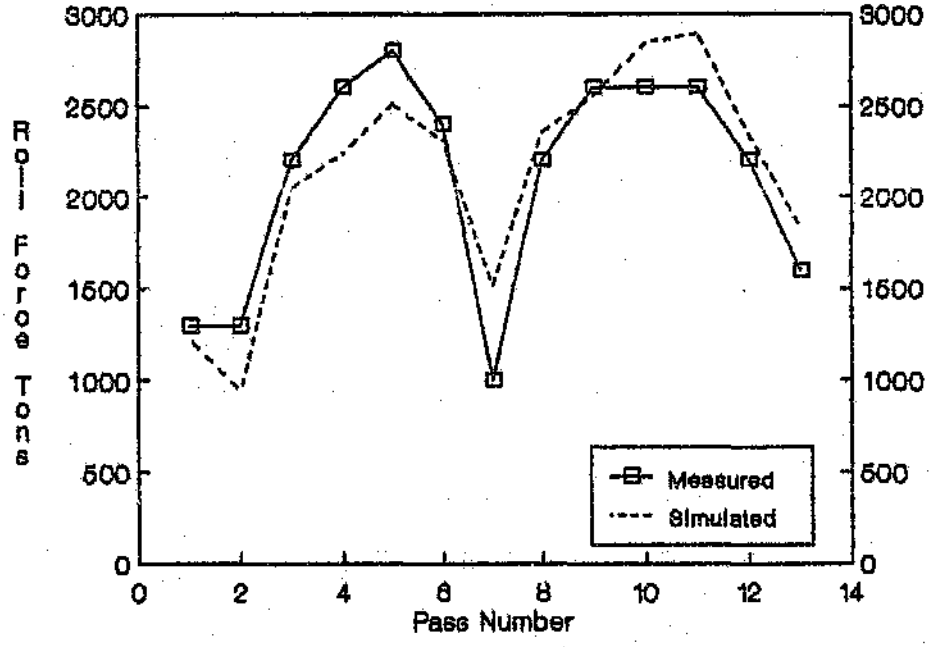

Mechanical Response - Schedule 1

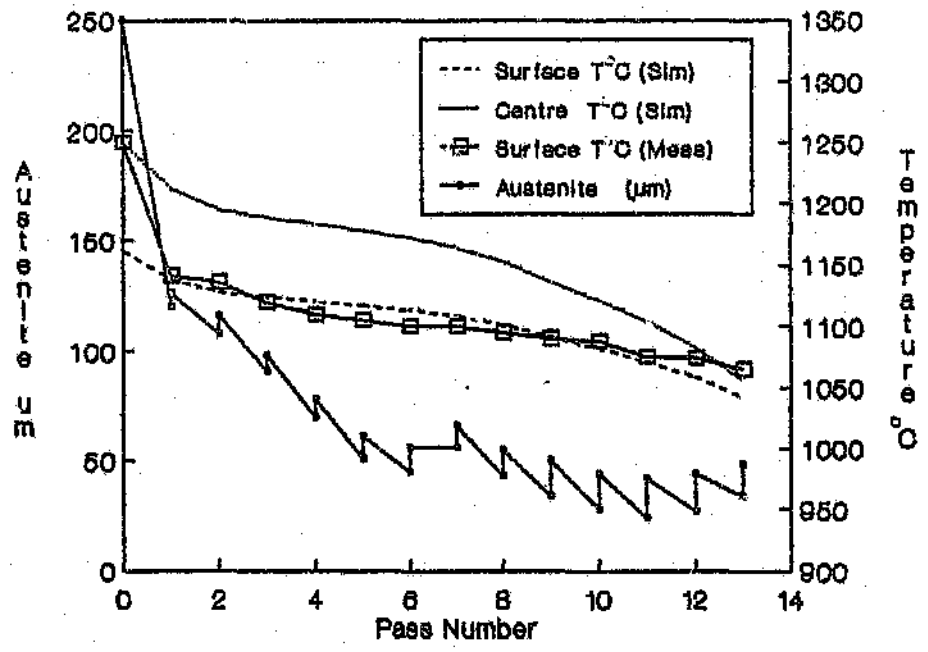

Metallurgical Response - Schedule 1

Figure 4.34 Measured and simulated deformation parameters versus pass number - Schedule 1

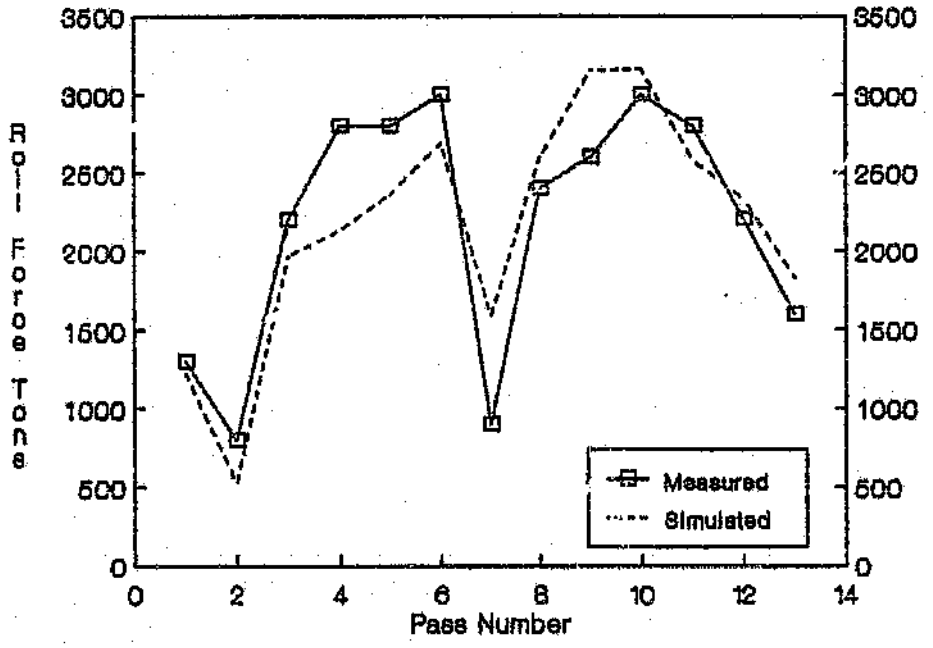

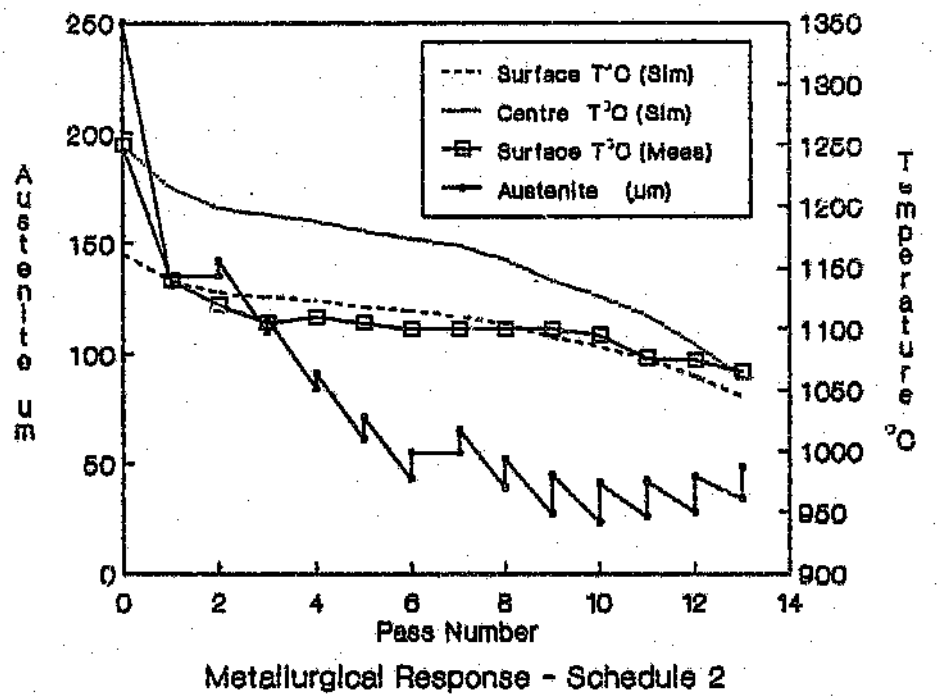

Figure 4.35 Measured and simulated deformation parameters versus pass number - Schedule 2

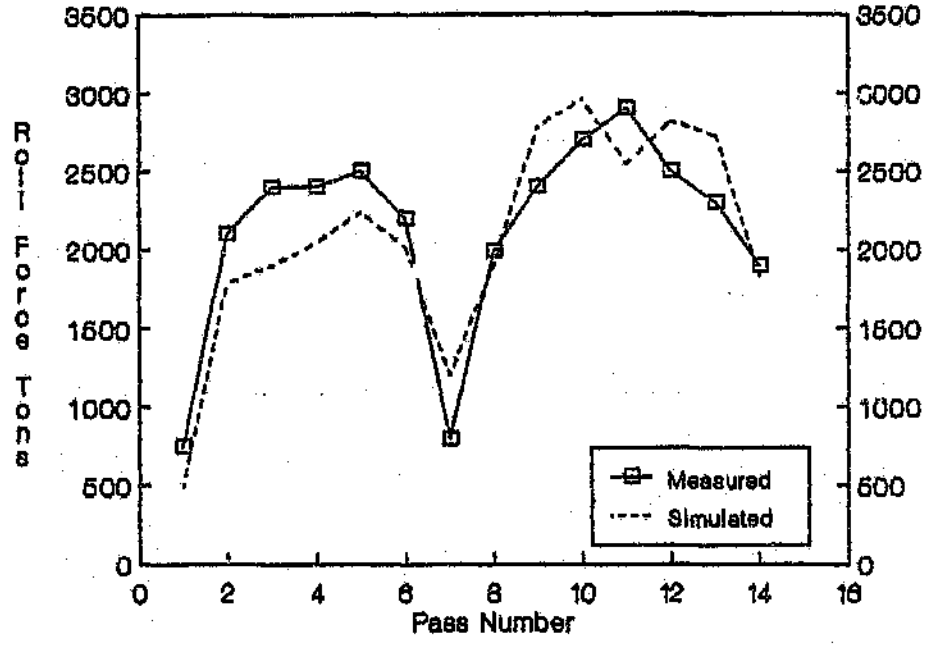

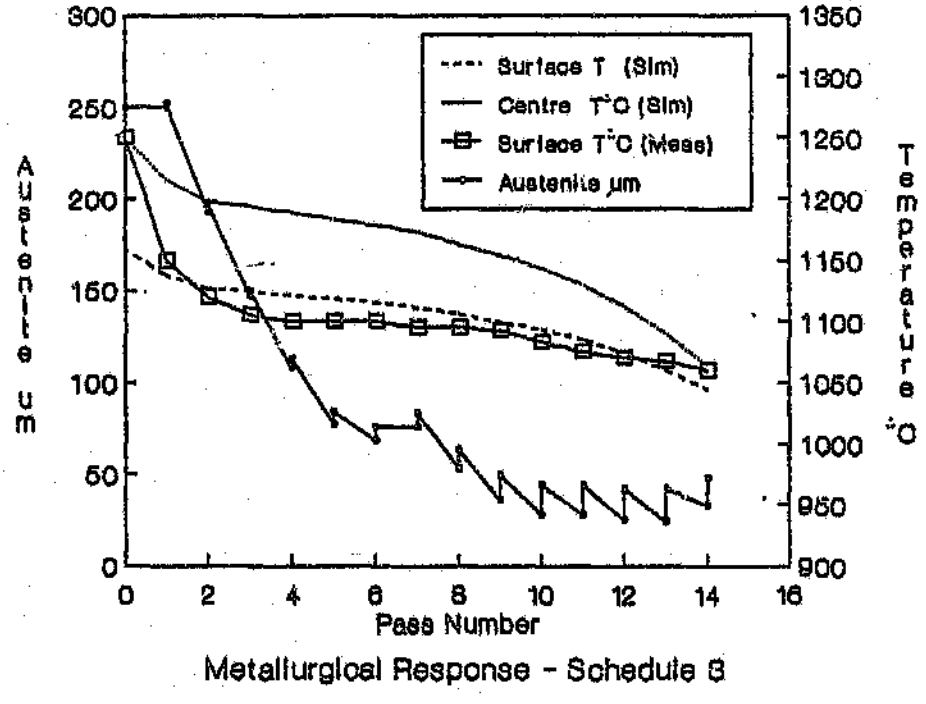

Figure 4.36 Measured and simulated deformation parameters versus pass number - Schedule 3

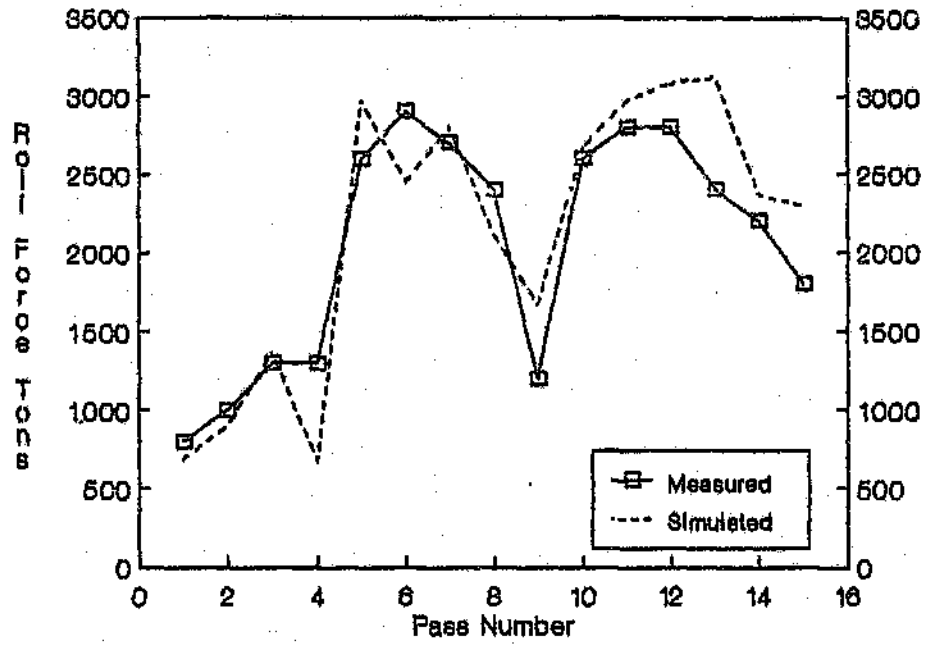

Mechanical Response - Schedule 4

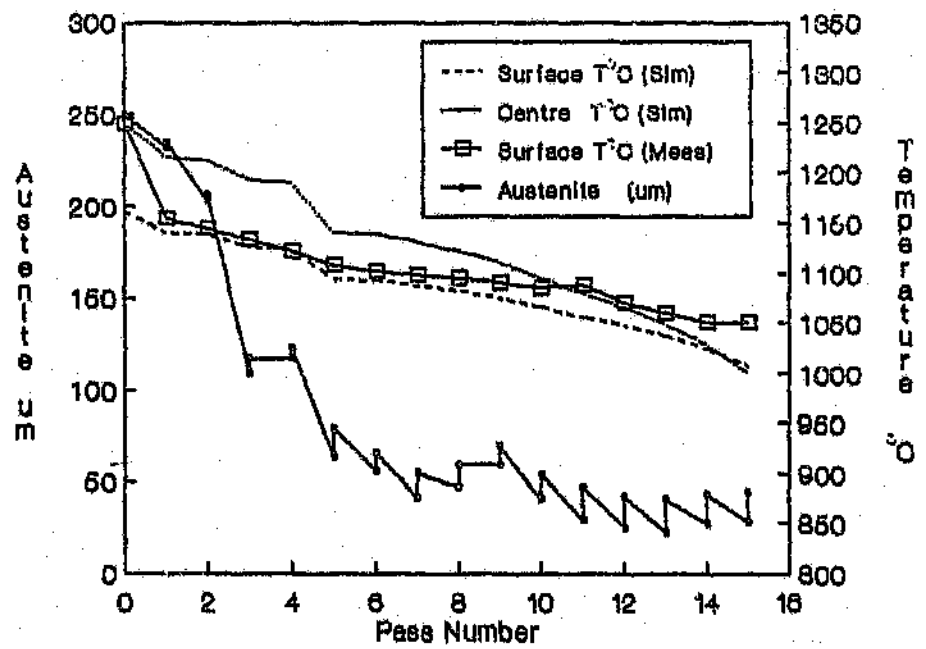

Metallurgical Response - Schedule 4

Figure 4.37 Measured and simulated deformation parameters versus pass number - Schedule 4

4.2.7 Plate cooling rate

After the last pass the SC8 plates were air cooled from about 1050°C-1070°C down to room temperature. At about 950°C, a light water cool was applied to the plate as it passed through a cooling spray bank and were subjected to water cooling for about 3 seconds. The cooling rate during the brief water cooling period was determined by extrapolating temperature - time measurements at points of entry and exit of the cooling sprays. The average cooling rate for all plates was found to be 1.22 $°Cs^{-1}$ during air cooling periods and 15$°Cs^{-1}$ during the water cooling period. It was found that the water cooling applied to the plate was insufficient to have a significant effect on the cooling rate since the temperature only dropped from 950°C to 900°C during this period.

4.2.8 As-rolled ferrite grain size

All microstructures obtained from as-rolled samples consisted of uniform coarse ferrite and pearlite (see Tables 4.6-4.9). Ferrite grain sizes varied between 22 and 25 μm.

Predicted ferrite grain sizes calculated from equation 2.58 for the four plate schedules compared reasonably well with the measured values. The measured grain size for schedules 1,2,3 and 4 were 25,22,22 and 22 μm respectively. The predicted values for schedules 1,2,3 and 4 were 22.9, 20.1, 20.4 and 20.3 μm respectively.

4.2.9 Mechanical properties

The simulated yield stress (equation 4.7) values were consistently lower than the measured yield strengths obtained for the SC8 grade A steel in schedules 1,2,3 and 4. For the four schedules considered, the average simulated yield stress was 296 MPa and the average measured value was 331 MPa. The simulated tensile stress (equation 2.62) was also consistently lower than the measured value although the mean error of 3.6% was somewhat less than in the yield stress. The average simulated tensile strength was 427 MPa and the measured mean yield strength was 443 MPa.

The measured Charpy values at 0°C were all low to the very high finishing temperatures on the mill (T > 1050°C). The measured impact energy of all four schedules was between 35 and 40 Joules. The simulated impact values, using equation 4.7, compared well with the measured values. For example, in schedule 1, the simulated impact energy was 39 J at 0°C, compared with the measured value of 35 J.

4.2.10 Improvement of rolling schedules - SCHEDULE 1

The hot deformation parameters encountered during the hot rolling of schedule 1 were varied using the simulation programme, PLATESIM. The mechanical properties obtained by varying certain rolling parameters are given in Table 4.10. The resulting roll separating forces are given in Figure 4.38.

Decreasing the reheat temperature in schedule 1A from 1250°C to 1150°C resulted in a reduction in ferrite grain size from 22.9 μm to 20.6μm due to the lowering of the simulated finish temperature from 1052°C to 1041°C. The lower reheat temperature resulted in an increase of approximately 15 MPa in the yield strength.

Increasing the predicted cooling rate in schedule 1B from 1.2°Cs^{-1} to 15°s^{-1} resulted in a reduction in predicted final ferrite grain size from 22.9μm down to 14.3μm. The yield strength and impact energy for these conditions were not determined because the model only takes air cooling into account. However, an increase in yield strength without a deterioration in impact energy were expected due to the significant grain refinement.

Doubling the work rolls speed to 120 rpm in schedule 1C resulted in very little change in microstructure and mechanical properties. Although the roll separating forces were higher in all passes in schedule 1C, they did not exceed the mill capacity of 4000 tons.

An increase in strain in the final pass was simulated in schedule 1D. The roll separating force in the last pass was well above the mill capacity of 4000 tons.

Table 4.10

Optimisation of Schedule 1 using Programme PLATESIM

Sched.	Reheat	rpm	CR	d_γ	d_{ϵ_1}	R_e	R_m	CVN
1	1206	60	1.2	66	22.9	295	447	39
1A	1150	60	1.2	52	20.6	310	451	39
1B	1206	60	15	67	14.3	-	-	-
1C	1206	120	1.2	68	22.5	287	447	39
1D	1206	60	1.2	46	19.5	314	454	48

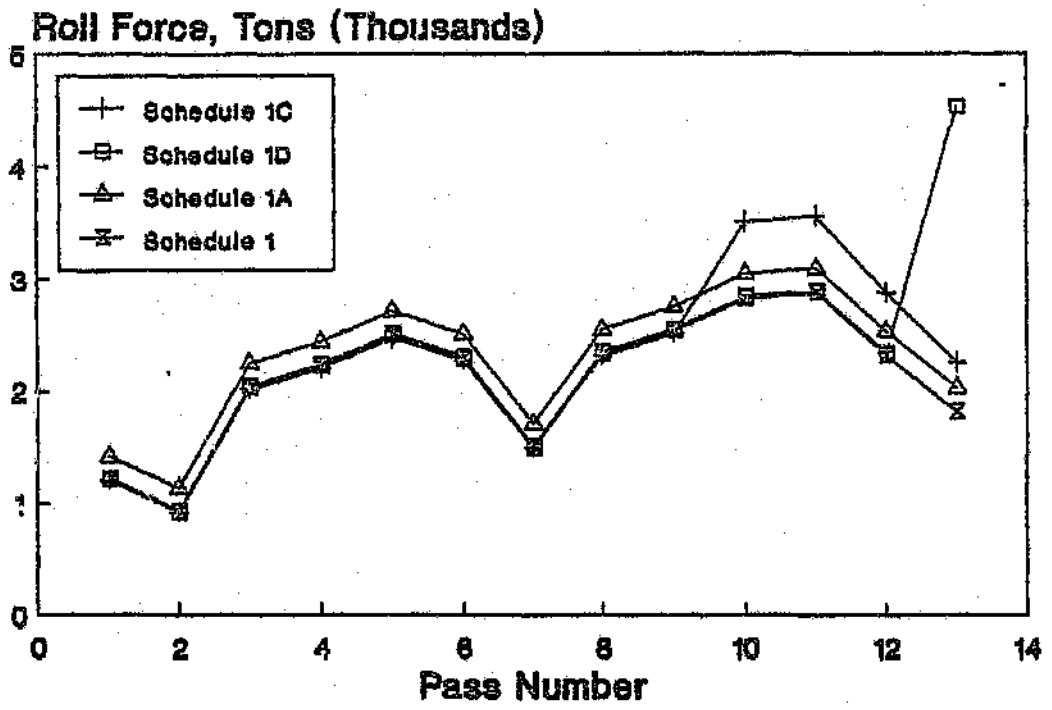

Figure 4.38 Roll separating forces resulting from Schedules 1, 1A, 1C and 1D

CHAPTER 5 DISCUSSION

5.1 General discussion

The hot deformation simulator has performed exceptionally well in the short period of its use, both in respect of the basic simulation concept and in respect of its technical design. The incorporation of computer equipment to control the induction furnace, the deformation sequence and the movement of the specimen between each process region as well as the rapid data acquisition has improved the efficiency of the test significantly. The results obtained for C-Mn steel SG8 were in fairly good agreement with values obtained in the literature for steels of similar composition. This has pointed out a new way of analysing the complex processes occurring in the material during industrial deformation, particularly hot rolling, more scientifically and with greater detail than ever before. The plane strain compression test not only allows the shaping conditions of existing production plants to be simulated in the laboratory, as well as the investigation of schedules using extreme parameters which may only be practically implemented at a later stage. This makes the hot deformation simulator capable not only of scientifically explaining phenomena which are already known empirically, but of providing the opportunity of advancing into uncharted territory ahead of technology in the field of material development.

The simulation of hot rolling of microalloyed steels is a distinct possibility in the future, although the higher flow stresses of these steels will require the use of smaller rectangular specimens.

In the simulation of thermomechanical processes, the shape and final thickness of the specimen should allow sampling of various secondary specimens for metallographic, hardness and mechanical tests. However, small specimens are advantageous for thermal analysis as temperature variations within the specimen are less serious. Therefore, plane strain compression on large rectangular bulk specimens will in the future be supported by tests on small, cylindrical specimens. Iscor Research and Development has recently purchased a GLEEBLE 1500 testing machine to accomplish this.

Most laboratory tests do not simulate the temperature conditions of a rolling pass closely due to the differences existing between the laboratory and the

rolling mill. However, the use of relevant mean strain rates and temperatures lead to useful flow calculations. The proof of this is that, when the correct microstructure is present, the rolling loads predicted by using the flow stresses in a rolling theory such as that of Sims are in very good agreement with measured values. The key to this is to ensure that the appropriate initial microstructure for the pass of interest is present in the specimens.

A number of factors prevent a complete industrial rolling schedule (typically 13 passes, total strain = 2.5) to be simulated in one plane strain compression test. These include very high friction between the platens and specimen at high strains, machine load limitations, machine programming limitations (only 5 or 6 passes can be simulated in a single test), as well as rapid heat losses from the specimen. However, if the initial austenite morphology and grain size are known before a particular pass in the complete rolling schedule, then the resulting microstructure after that pass/passes can be determined. Adding to this the assumption that the most important metallurgical changes occur in the last passes, the final microstructure and mechanical properties can be simulated. The results in this work showed that if plane strain compression tests are concentrated in the final plate rolling passes for C-Mn steels, the final microstructure and mechanical properties may be predicted fairly accurately.

5.2 Measurement of temperature

From the examination of individual temperature measurements recorded during rolling it was evident that despite the efforts to obtain accurate readings, there were some inconsistencies. The temperature measurement errors were attributed to scale on the surface of the plate, water vapour or smoke obscuring pyrometer readings. In hot rolling, the material moves through the entire roll gap during each pass. In plane strain compression, the geometry is such that only the centre region of the specimen is deformed. Also temperature losses from the side of the specimen have more of an influence in plane strain compression tests than in rolling in which b >> h. In spite of unavoidable errors in temperature readings, a large number of readings made it possible to evaluate the simulation model used for predicting plate temperature. However, if the first pass temperature is incorrectly predicted, all the subsequent

readings will be in error. It is possible that the predicted temperatures were more accurate than the measured temperatures because of the difficulties encountered during measuring.

5.3 Effect of temperature on microstructure and mechanical properties

Reheat temperature

Because of the large dependence of the recrystallised austenite grain size on the austenite grain size before deformation, the initial difference in simulated austenite grain size with reheat temperature disappeared fairly rapidly with successive deformations. Lowering the reheat temperature however, had an indirect effect on the state of the austenite prior to transformation to ferrite. By lowering the reheat temperature the deformation temperature during each subsequent pass as well as the finish temperature were reduced. The reheating temperatures in plate rolling were very high (1220°C) resulting in large initial austenite grain sizes. This large initial grain size is hardly likely to affect the final ferrite grain size significantly because the large strains experienced in reducing the plate from 210mm down to 20mm tends to reduce the affect. Lowering the reheat temperature effectively reduces the deformation temperature of all successive passes. The traditional slab reheating temperature of 1250°C which has, in the past, softened the slabs for easy rolling in plate mills can be lowered for high speed production. Low temperature reheating gives the rolled products a definite improvement in yield and toughness. Moreover, the energy saving may be easily combined with efforts to save alloying elements and reduce heat treatment by the use of controlled rolling and controlled cooling. Finishing at too low a temperature may result in excessive mill loads.

Finish temperature

The finish rolling temperature and the final strain are - besides the slab reheating temperature - the most important process parameters in the thermomechanical processing of plates and play a decisive role in the metallurgical process of recrystallisation, precipitation and transformation. High finishing temperatures (> 1050°C) result in the steel being in the recrystallisation region and will produce coarse ferrite-pearlite microstructures and low yield strengths and toughness values. Finishing in the

no-recrystallisation region (1000°C > T > A_{r3}) will result in elongated prior austenite and a refinement in the ferrite grain size leading to increased strength. Although grain refinement has a favourable influence on toughness, heavy elongation of grains during deformation in this region can result in a drop in toughness due to increasing dislocation strengthening and unfavourable crystallographic orientation. By means of a lower finish temperature in the two phase region, the increased effect of precipitation hardening and dislocation density produces substantially higher strength values. The finish temperature is determined by the desired strength and toughness properties, whereby the load limits of the rolling stands must also be taken into account.

5.4 Simulation of specimen temperature

The number of finite elements chosen in the deformation zone in PSC_TEMP (5 elements in the thickness direction and 7 elements in the length direction) was sufficient to simulate the temperature distribution in plane strain compression specimens during air cooling and deformation. When less than 35 elements were used, the heat transfer within and from the specimen was not stable and the temperature dropped too rapidly. Although greater accuracy would have been achieved if multiple columns of rhomboidal elements were used, the choice of one column of rhomboidal elements at the edge of the deformation zone provided a simple and fairly accurate means of predicting the rate of heat transfer between deformed and undeformed regions of the specimen.

The heat transfer coefficient, H (Appendix 1, equation A1.15) was found to be suitable in accounting for radiation and convection losses from the specimen surface to the surroundings. The optimum heat transfer constant, C, in (Appendix 1, equations A1.43 and A1.44) was found to be about 10 kW/m²K. These values were in good agreement with the values of 4 - 21 kW/m²K found by Foster [19] for plane strain compression specimens. The constants in equation A1.15 and C would have to be re-formulated if specimens and platens of other geometries are used in the future.

Equation 3.7 (see section 4.1.6.1), which predicts the flow stress of steel SC8 in terms of process parameters was used to calculate the temperature rise due to work done on the specimen. Relevant constants in this equation however,

will have to be determined for each steel that is simulated using programme PSC_TEMP.

5.5 Effect of strain on microstructure and mechanical properties

The strain in the last passes of a multi-pass deformation schedule refined the final microstructure of steel SC8 significantly. This was most effective when specimens were finished in the low temperature region. This is due to little if any recrystallisation taking place at low temperatures and results in an elongated austenite structure in which deformation bands and other substructures are formed. These substructures provide more nucleation sites for ferrite than fully recrystallised austenite and result in a finer ferrite grain size. The degree of strain in the last pass and the finish temperature must be optimised to produce a fine final structure to improve strength and toughness.

It is not always a simple matter to apply large strains in practice for fear of exceeding the rolling mill capacity. A small increase in finish strain increases the roll separating forces significantly. This is because the rolling force is a strong function of flow stress which in turn is increased by an increase in strain.

5.6 Effect of strain rate on microstructure and flow stress

The strain rate increased with increasing plate reduction. However, no significant changes in microstructure were found by increasing the rolling speed from 60 rpm to 120 rpm. This observation is in agreement with Kaspar et al [12] who found that an increase in strain rate of up to 1 order of magnitude did not influence the microstructure in C-Mn steels. Ouchi[46] however, found that an increase in strain rate refines the recrystallised austenite grain size and hence the transformed ferrite grain size. Faster strain rates increased the flow stress at high temperatures because of the rapid build up of dislocations in the material. This effect becomes more pronounced at lower rolling temperatures where it is more difficult for recrystallisation to take place.

On the basis of results obtained from this work the only advantage of increasing the strain rate is to increase production rates. The rolling mill

capacity must always be taken into consideration when strain rates are increased on the mill since rolling force is a strong function of the rolling speed.

5.7 Performance of cooling apparatus

Fairly uniform hardness values were obtained for slow and intermediate cooling rates. This implied that, for the water flow rates used during these tests, the water nozzle spacings allowed an even distribution of water over the upper and lower surfaces of the specimen. More careful control must be exercised when the specimen is cooled at very fast rates since the hardness gradient becomes more severe.

One drawback of the cooling unit on the hot deformation simulator is the cooling rate limit. The maximum cooling rate that can be simulated on 25 mm thick specimens is $35°Cs^{-1}$. Fully martensitic structures are not obtained for C-Mn steels when 25 mm thick plane strain compression specimens are subjected to this cooling rate. Either the cooling rate needs to be increased or the initial specimen thickness reduced if a fully martensitic structure is to be obtained for examining prior austenite structures at intermediate stages of a deformation schedule.

5.8 Flow curves and roll separating force

No corrections for geometry or friction effects on the flow stress were included in this work. In plane strain compression tests, thicker specimens have the effect of increasing the flow stress for a given set of deformation conditions. In contrast to this, frictional effects give higher flow stresses in thinner specimens. The opposing effects of specimen geometry and friction on flow stress tend to cancel one another out [19].

Deviation of the simulated flow stress from the measured stress at lower deformation temperatures can be explained in terms of the metallurgical changes taking place in the steel. Above 950°C ,the amount of applied strain

required for full recrystallisation to take place is less than at temperatures below 950°C. Deformation in the intermediate temperature range (1050-950°C) resulted in partially recrystallised austenite and a certain amount of residual strain was generated in the unrecrystallised structure. Deformation in the low temperature regions resulted in unrecrystallised austenite and a certain amount of residual strain was present in the specimen when it entered the following pass. Retained strain generated in the partially recrystallised and non recrystallised structures must be taken into account separately in the flow stress simulation model using the following equation [22]:

$$\sigma'(\varepsilon_i, T_i, \dot{\varepsilon}_i) = X\sigma'(\varepsilon_i, T_i, \dot{\varepsilon}_i) + (1-X)\sigma'(\varepsilon_i+\varepsilon_{i-1}, T_{i-1}, \dot{\varepsilon}_{i-1}) \quad 4.8$$

It should be noted that successful application of equation 4.8 requires accurate quantitative knowledge of the metallurgical changes occurring in the steel during and after deformation.

In the plane strain compression test, part of the shaping energy is consumed in heating the specimen. When the deformation is large the temperature of the specimen increases significantly. This leads to a reduction in flow stress and should be taken into account. Acting in opposition to this is the fact that a large amount of heat is lost to the platens through thermal conduction which tends to neutralise the heating up effect. When the shape of the flow stress curves are interpreted metallurgically, it is important to distinguish accurately between the causes of flow stress drops, which may, apart from the temperature increase of the specimen, include dynamic recovery, recrystallisation and precipitation processes.

Deformation induced transformation is attributed to differences in the number of slip systems in austenite and ferrite which makes it possible to identify the formation of ferrite from the flow curve. If continuous deformation is conducted over the entire rolling temperature range (1200°- 700°C) the flow stress increases steadily due to the drop in temperature as well as dislocation build-up in the no recrystallisation region. However, low temperatures it is possible to detect the start of ferrite transformation under mill conditions, A_{r3} , by a drop in the flow stress. This has been achieved by other workers [66,67,68].

A quick check on the state of the austenite at any stage of a multipass deformation schedule using the anisothermal softening index obtained from multiple pass hot rolling simulations or on line measurements can reduce the number of microstructural investigations normally required.

Although the simulated roll separating forces were generally very close to the measured values errors in the predicted values were attributed to a number of factors. Firstly the mean flow stress obtained for a specific strain and strain rate over a determined temperature range might not be applied accurately to the mill because of uncertainties regarding the plate temperature. Secondly, the instantaneous plate width was not known and can result in errors when calculating the actual deformation area during rolling. Finally, frictional effects were accounted for in rolling by including the roll geometry factor, Q, in roll force calculations. No correction for the effect of friction on mean flow stress was made in plane strain compression.

The underestimation of roll force in the early passes may be explained in terms of the plate width. The computer programme **PLATESIM** underestimated the width in the early passes. The exact increase in slab width during each pass was not measured. The computer model assumed that after the required final width was attained in the early passes, no further increase in width occurred due to the prevailing plane strain conditions. The large roll forces in the middle passes can be explained in terms of strain and austenite grain size. Large strains in the middle passes result in larger mean flow stresses and hence larger roll forces. Also, the medium strains found in the middle passes were sufficient in fully recrystallising the austenite resulting in smaller austenite grain sizes during deformation. It is well known that smaller austenite grain size increases roll separating forces for a given set of deformation conditions.

5.9 Evolution of austenite during hot rolling

The structural refinement of austenite during the hot rolling of steels is produced by successive recrystallisation events during or after repeated rolling reductions at high temperatures. In the low-temperature range, a heavily deformed, unrecrystallised austenite is desirable, as this increases the number of nucleation sites for ferrite formation. This contributes to the improvement of the mechanical properties of the steel.

Static recrystallisation takes place very rapidly in C-Mn steels at high temperatures (less than 1 second) if medium strains (15-25%) are applied. Actual mill delay times were used in the simulation and provided ample time for full recrystallisation and grain growth to take place during the middle passes where medium strains were applied. Very low strains however, were applied to the slab during the early passes which might have been insufficient for recrystallisation to have taken place. Accumulated strain energy in the material led to the eventual recrystallisation of the austenite in the middle passes.

When recrystallisation times are much shorter than interpass times, or much longer than interpass times, then small errors are of little consequence. However, when recrystallisation times are similar to interpass times, small errors can result in large differences between the predicted and observed microstructures. The rolling of SC8 plate steel took place between 1250°C and 1050°C and recrystallisation times at these temperatures are very short. This implied that only small errors occurred in the calculation of the evolution of austenite during these rolling schedules.

5.10 Mechanical properties

Equation 4.5 and equation 4.6, which correlated the yield strengths of steel A and steel B in terms of ferrite grain size only, were not accurate enough in predicting the yield strengths of steel SC8 under most deformation conditions during multi-pass plane strain compression tests. This was due to the presence of residual strain in some specimens deformed at very low temperatures resulting in an additional increase in strength. The non-linear dependence of ferrite grain size with finishing temperature also affected the accuracy of the correlation. It was found that the finish strain and finish temperature, as well as chemical composition, had to be taken into account to accurately predict the yield strength for any rolling schedule. The use of equation 4.7 produced more accurate results than equation 4.5 or equation 4.6. Although equation 4.7 was only formulated to predict yield strength and impact energy, the same procedure may be used to formulate similar equations that predict other mechanical properties, such as elongation and tensile strength, in terms of process parameters.

The small variation in tensile strength in all air cooled tests implied that little, if any, strain hardening occurs in steel SC8 under hot rolling conditions. This small variation in tensile strength was expected since SC8 is a C-Mn steel and no dynamic carbonitride precipitation occurs during deformation which results in no strain hardening taking place.

The decrease in impact energy at ferrite grain sizes larger than 16μm (high temperatures, air cooling) was attributed to the slow cooling rate resulting in coarse interlamellar pearlite spacings which are detrimental to toughness.

At relatively low finishing temperatures, a marked downward trend in the impact energy was found, and the Charpy value decreased with decreasing ferrite grain size. This downward deviation in impact energy probably resulted due to deformation of the steel in the two-phase region (austenite-ferrite). The drop in Charpy values can be attributed to an increased dislocation density in the ferrite which causes a deterioration in toughness [49].

The ferrite grain size to achieve the maximum impact energy at 0°C in SC8 steel lies between 12.3μm and 15.6μm.

CHAPTER 6 CONCLUSIONS

1 Plane strain compression tests gave reliable, quantitative predictions of the roll separating forces and microstructural changes in industrial rolling processes. Limitations to the precision of the simulations were imposed by the test and by the complex variations in deformation conditions in the rolled plate.

2 The conditions of plane strain compression testing are suitable for the simulation of hot plate rolling. With computer control the strain and strain rate history in each pass can be closely simulated to give the required stress conditions

3 Problems with oxidation were partly overcome by applying two coats of aluminium paint to the test pieces. This coat is effective in preventing oxidation up to 1180°C although at temperature above this the effect is lost.

4 A finite difference computer model, PSC_TEMP, can be used to predict the temperature distribution in plane strain compression specimens during air cooling and deformation. The simulated and measured temperatures did not differ by more than 25°C for any deformation schedule.

5 The model developed by Seredynski to simulate the temperature during plate rolling is accurate to within 30°C of the measured values. Differences between measured and computed temperature values can be attributed to a non-linear temperature gradient existing across the plate.

6 Good agreement was obtained between the measured and simulated hot flow stresses using equation 3.7. The equation gave excellent results at temperatures above 1000°C. However, at temperatures below 1000°C, the simulated flow stress differed markedly from the measured values. This was due to equation 3.7 not taking into account the effect of increased strengthening due to dislocation build-up when the specimen is deformed in the no-recrystallisation and two-phase regions.

7 The double stroke technique is useful for determining the amount of recrystallisation taking place between passes during multi-pass deformation. This technique may be used as a quick method to monitor the evolution of austenite during rolling simulations thereby avoiding time consuming metallographic examinations.

8 Sims model for predicting the roll separating force was successful in providing good agreement with measured forces.

9 Lower finish roll temperatures and large strains in the last pass refined the ferrite grain size significantly leading to superior mechanical properties

10 The cooling rate during plane strain compression may be accurately determined by differentiating the cooling curve using a numerical method. The differentiated form of the cooling curve may also be used to determine the start and end of transformation in steels and further processed to generate deformation CCT diagrams.

11 The influence of industrial rolling parameters on yield strength and impact energy of steel SC8 may be determined by performing simple multiple linear regression on data obtained during plane strain compression tests.

12 Computer programme, **PLATESIM**, is a quick and efficient method for designing plate rolling schedules for steel SC8. The programme may be used for other C-Mn steels but the constants in the equations used to describe the various mechanical and metallurgical phenomena during rolling must be determined in the laboratory.

REFERENCES

1 Sellars C.M. Computer modelling of hot-working processes. Mat.Sci and Tech. 1. April 1985. pp325-332.

2 Sellars C.M. Private communication. University of Sheffield. 1989.

3 Sinha F. Optimisation of hot rolling schedules. Trans ISIJ. 25. 1987. pp126-134.

4 Sellars C.M, Sah J.P, Beynon J.H and Foster S.R. Plane strain compression testing at elevated temperatures. Internal Report. University of Sheffield. 1976.

5 Whittaker H.J. Ph.D Thesis. University of Sheffield. 1973.

6 Barraclough D.R. Ph.D Thesis. University of Sheffield. 1974.

7 Cole A.T. Ph.D Thesis. University of Sheffield. 1976.

8 McQueen H.J. Deformation mechanisms in hot working. J.of Metals. 20. 1968. pp31-38.

9 Bailey J.A, Haas S, Sah M.K. Int.J. of Mech.Sci. 14. 1972, p735.

10 Hodierne F.A. J.Inst.Met. 91. 1963. p267.

11 Sims R.B and Loijou N. J. Mech. Phys. Solids. 1. 1953. p234.

12 Kaspar R and Pawelski O. Grain refinement of microalloyed austenite by static recrystallisation after hot deformation. Metal Working. Steel Research. 9. 1985. pp477-481.

13 Kapellner W and Kaspar R. Determination of flow curves by the plane strain hot compression test. Steel Research, 57(6). 1986, pp 256-261.

14 Striesselberger A, Kaspar R and Pawelski O. Measurement and evaluation of the anisotherm l softening of austenite after hot deformation. Metallurgical Transactions.16A. Jan 1985. pp 67-72.

15 Kaspar K and Pawelski O. Austenite grain in the process of thermomechanical treatment. Mat Tch. Steel Research. 5. 1986. pp 199-206.

16 Kaspar R, Kapellner W and Pawelski O. Effect of austenite deformation on the continuous cooling transformation of medium carbon steels. Z. Metallkunde, H.8. 1987. pp569-575.

17 Kaspar R, Kapellner W and Pawelski O. Determination of CCT diagrams by thermal analysis after simulated hot deformation processes. Metal Working. Steel Research. 57(11). 1986. pp557-562.

18 Boer C.R. Rebelo N, Rydstad H and Schroder R. Eds. Process Modelling of Metal Forming And Thermomechanical Treatment. MRE. BBC Brown, Boveny and Co. Switzerland. 1983.

19 Foster S.R. Simulation of hot rolling of low carbon steels. Ph.D Thesis. Sheffield University. 1981.

20 Sims S. Proc. Inst. Mech. Eng. 168. 1954. p191.

21 Sellars C.M, Richardson G.J and Hawkins D.H. Eds. Worked Examples In Metalworking. The Institute of Metals. London. 1985. p84.

22 Barager D.C and Ruddle G.E. The prediction of rolling force during controlled rolling. Fourth international rolling conference. The science and technology of flat rolling. 1,2. Deauville, France. June 1-3, 1987. ppB.1-B1.11.

23 Rowe S.W. Principles Of Metalworking. Pub. Arnold E. London. 1965.

24 Harding W. Temperature and structural changes in hot rolling. Ph.D Thesis. Sheffield University. 1977.

25 Seredynski F. Prediction of plate cooling during rolling - mill operation. JISI. March 1973. pp197-203.

26 Atkins M. Ed. Atlas Of Continuous Cooling Transformation Diagrams For Engineering Steels. British Steel Corp. Sheffield Labs. Rotherham.

27 Sellars C.M. Course notes presented at International Symposium on Materials Engineering. University of the Witwatersrand. Nov 1985.

28 Le Bon A, Rofes-Vernis J and McGTegart W.J. JISI. 211, 1973. p703.

29 Sekine H, Maruyama T and Kageyama H. Grain refinement through hot rolling and cooling after rolling. Thermomechanical Processing Of Microalloyed Austenite. Proc. of Int Conf. on Thermomechanical Processing of Microalloyed Austenite. Pittsburgh. USA. Aug 17-19. 1981. DeAardo A.J, Katz G, Wray P. Eds. The Metal Soc. of AIME. pp141-162.

30 Jonas J.J. Proc. 4th Int. Conf. on Strength of Metals and Alloys. 3. Nancy, France. 1976. pp976-1002.

31 McQueen H.J., Wong W.A and Jonas J.J. Can.J.Phys. 45, 1967. p1225.

32 Sellars C.M. The physical metallurgy of hot working. Proc.Int Conf. on Hot Working and Forming Processes. Sheffield Univ. July 1979. pp3-15.

33 Whittaker H.J. Ph.D Thesis. University of Sheffield. 1973.

34 Sellars C.M and Whiteman J.A. Recrystallisation and grain growth in hot rolling. Metals Science. March-April 1979, pp 187-194.

35 Djaic R.A.F and Jonas J.J. Recrystallisation of high C steel between intervals of high temperature deformation. Metal. Trans. 4. 1973. pp 621-625.

36 Kozasu I, Ouchi C, Sampei T and Okita T. Hot rolling as a high temperature thermomechanical process. Microalloying 75. Ed. Korchynsky M. 1. pp120-133. 1976.

37 Crosbie G.A and Baker A.J. Controlled rolling simulation in micro - alloyed steels. Thermomechanical Processing Of Microalloyed Austenite. Proc. of Int Conf. on Thermomechanical Processing of Microalloyed Austenite. Pittsburgh. USA. Aug 17-19. 1981. DeAardo A.J, Katz G, Wray P. Eds. The Metal Soc. of AIME. pp 433-454.

38 Glover G and Sellars C.M. Static recrystallisation after hot deformation of iron.Met. Trans. 3. 1972, pp2271-2280.

39 Jonas J.J, Sellars C.M and McGTegart W.J. Strength and structure under hot working conditions. Met. Review 130(14) 1969, pp1-24.

40 Barraclough D.R and Sellars C.M. Static recrystallisation and restoration after hot deformation of Type 304 stainless steel. Met.Science. 13. 1979. pp257-267.

41 Ouchi C and Okita T. Austenitic grain refinement through static recrystallisation immediately after hot rolling. Transactions ISIJ. 24. 1984. pp726-733.

42 Choquet P, de Lamberterie B, Perdrix C, Biausser H. FAST:A new model for accurate prediction of rolling force application on the Solmer hot strip mill. Fourth International Rolling Conference. The Science And Technology Of Flat Rolling. 1,2. Deauville,France. June 1-3, 1987. pp B5.1-B5.8.

43 Tanaka T,Tabata N and Hatamura T. Three stages of the controlled rolling process. Microalloying '75. Balance J.B. Ed. AIME, 1977. pp107-118.

44 Banks K.M and Mostert R.J. The design of a system for designing Quatough controlled rolling schedules in order to obtain a fine austenite grain structure without exceeding rolling mill load limitations. Int. report, Iscor Research and Development. 1986, Pretoria, South Africa.

45 Tanaka T, Enami T, Kimura M, Saito Y and Hatamuro H. Formation mechanism mechanism of mixed austenite grain structure. Thermomechanical Processing Of Microalloyed Austenite. Proc. of Int Conf. on Thermomechanical Processing of Microalloyed Austenite. Pittsburgh. USA. Aug 17-19. 1981. DeAardo A.J, Katz G, Wray P. Eds. The Metal Soc. of AIME. pp 195-216.

46 Ouchi C, Sampei T and Okita T. Microstructural changes of austenite during hot rolling and their effect on transformation kinetics. Hot Deformation of Austenite Ballance J.B. Ed. AIME. 1977. pp316-340.

47 Yoshi C, Morikawa H, Onoe Y and Hoh K. Formulation of static recrystallisation of austenite in hot rolling process of steel plate. Trans ISIJ. 27. 1987. pp425-431.

48 Gohda S, Watanabe K and Hashimoto Y. Effects of the inter- critical rolling on structure of low carbon steel. Transactions ISIJ. 21, 1981. pp6-15.

49 Speich G.R, Dabkowski D.S. Effect of deformation in the austenite and austenite-ferrite regions on the strength and fracture behaviour of C, C-Mn, C-Mn-Nb, and C-Mn-Nb-Mo steels. Hot Deformation of Austenite Ballance J.B. Ed. AIME. 1977. pp 557-587.

50 Esaka K, Matsumura Y, Koyama K and Tashoro M. Hot rolled plain carbon steel sheets with a good combination of high strength and formability. HSLA Steels, Metallurgy and Applications. Conf. proc. Gray J.M, Ko.T, Shouhua.Z, Baorong.W, Xishan.X Eds. ASM Int. 1985. pp 959-968.

51 Suehiro M, Sato K, Tsukano Y, Yada H, Senuma T and Matsumura Y. Computer modelling of low carbon steel in hot strip rolling. Trans. ISIJ. 27. 1987. pp439-445.

52 Umemoto I and Tamura I. Ferrite grain refinement by work-hardening of austenite and accelerated cooling. Trans.ISIJ. 27. 1987. pp373-382.

53 Tacke G, Litzke H and Raquet E. Investigations into the efficiency of cooling systems for wide-strip hot -rolling mills and computer-aided control of strip cooling. Accelerated Cooling Of Steel. Southwick.P.D. Ed. Met. Soc. 1985. pp35-55.

54 Kozasu I. Overview of accelerated cooling of plate. Accelerated Cooling Of Steel. Southwick.P.D. Ed. Met. Soc. 1985. pp15-30.

55 Le Bon A and Perdrix.Ch. Optimum cooling conditions for the accelerated cooling of plates. Accelerated Cooling Of Steel. Southwick.P.D. Ed. Met. Soc. 1985. pp123-132.

56 Morikawa H and Hasegawa T. Microstructures and strengthening factors of accelerated cooled plate. Accelerated Cooling Of Steel. Southwick.P.D. Ed. Met. Soc. 1985. pp83-96.

57 Takeda T, Hosokawa Y, Suzuki T and Hashimoto T. Development of dynamic accelerated cooling process. Accelerated Cooling Of Steel. Southwick.P.D. Ed. Met. Soc. 1985. pp 133-149.

58 DeAardo A.J. The influence of thermomechanical processing and accelerated cooling on ferrite grain refinement in micro -alloyed steels. Accelerated Cooling Of Steel. Southwick.P.D. Ed. Met. Soc. 1985. pp97-119.

59 Tamura I. Some fundamental steps in thermomechanical processing of steels. Trans. ISIJ. 27. 1987. pp763-775.

60 Bucher J.H, Grozier J.D and Enrietto J.F. Strength and toughness of hot rolled ferritic-pearlitic steels. Fracture - an Advanced Treatise. Fracture of Metals. 6. Academic Press, New York, 1967. p247.

61 Pickering F.B and Gladman T. Metallurgical Development In Carbon Steels.The Iron and Steel Institute. 10. London. 1963. pp113-121.

62 Pickering F.B. Physical Metallurgy And The Design Of Steels. Materials Science Series. London. 1978. p155.

63 Raudensky F. Simulation of thermal processes in the billet in hot rolling. Hutnicke Listy. 43(9). 1988. pp623-628.

64 Akben T and Cheng X. Effect of different plate rolling schedules on hot strength and structure of Ti-microalloyed steels. Fourth international rolling conference. The science and technology of flat rolling. 1,2. Deauville, France June 1-3, 1987. pp121-133.

65 Vodopivec H. The effect of finish roll temperature and carbon content on the microstructure and mechanical anisotropy of 0.04-0.13%C steels. Trans. ISIJ. 28. 1988. pp117-124.

66 Yue S, Boratto F and Jonas.J.J. Designing an industrial controlled rolling schedule using simple statistical process analysis and laboratory modelling. Prepared for Conf. on Hot And Cold Rolling, Cincinnati, Ohio. 1987.(not yet submitted).

67 Boratto F, Barbosa R, Yue S and Jonas.J.J. Effect of chemical composition on the critical temperatures of microalloyed steels. Prepared for Int.Conf. on Phys.Metall. of Thermomechanical Processing of Steels and Other Metals (Thermec-88). Tokyo, Japan. June 1988. (not yet submitted).

68 Samuel F.H, Yue S and Jonas J.J. Effect of dynamic recrystallisation on microstructural evolution during strip rolling. Prepared for Int.Conf. on Phys.Metall. of Thermomechanical Processing of Steels and Other Metals (Thermec-88). Tokyo, Japan. June 1988. (not yet submitted).

APPENDIX 1

SIMULATION OF THE TEMPERATURE DISTRIBUTION IN SPECIMENS AND PLATENS DURING PLANE STRAIN COMPRESSION (LISTING OF PROGRAMME PSC_TEMP INCLUDED)

SYMBOLS

A	Area, mm^2
C	Heat transfer constant
D_∞	Distance penetrated by temperature gradient into specimen, mm
ext[i]	Elongation of specimen during pass i, mm
H	Heat transfer coefficient for radiation & convection during air cooling
H_o	H at start of deformation, t = 0
H_1	H at end of interval, t = δt
$\bar{H}$	Average H during compression
HTC	Boundary condition factor
J1-J5	Heat flow through platen element, kW/m^2
k	Thermal conductivity of specimen steel
k'	Thermal conductivity of platen steel
Q1-Q5	Heat flow through specimen element, kW/m^2
Q2*	Heat flow along x direction from notional column, kW/m^2
s	Specific heat capacity of specimen steel
s'	Specific heat capacity of platen steel
$T^{sp}_{N.M}$	Specimen element temperature, t = 0
$T^{sp}_{N.M}{}^*$	Specimen element temperature, t = δt
$T^{pl}_{N.M}$	Platen element temperature, t = 0
$T^{pl}_{N.M}{}^*$	Platen element temperature, t = δt
$T^{sp}_{w.M}$	Specimen surface element temperature, t=0
$T^{pl}_{w.M}$	Platen surface element temperature, t=0
$T^{sp}_{w.M}{}^*$	Specimen surface element temperature, t=δt
$T^{pl}_{w.M}{}^*$	Platen surface element temperature, t=δt
T^{sp}_{sur}	Specimen surface temperature, t=0
T^{pl}_{sur}	Platen surface temperature, t=0
$T^{sp}_{sur}{}^*$	Specimen surface temperature t=δt
$T^{pl}_{sur}{}^*$	Platen surface temperature t=δt
T^{sp}	Initial temperature of specimen, °C
T1,T2	Temperatures of rectangular elements adjacent to rhomboidal elements
V	Element columns

VV	Element columns in deformation zone
Vol	Specimen Element volume, mm^3
Vol'	Platen element volume, mm^3
W	Number of element rows
x_{flow}	Distance between the discrete elements, mm
ΣJ	Net platen element heat flow , kW/m^2
ΣQ	Net specimen element heatflow, kW/m^2
$\delta Q/\delta t$	Rate of heat flow, kW/m^2
δt	Time interval, s
δx	Element width, mm
$\delta y[i]$	Element thickness in pass i, mm
$\delta y[0]$	Initial element height, mm
δz	Element breadth,mm
δt_{max}	Stable calculation time , seconds
δT^{sp}_{def}	Temperature rise in specimen due to plastic deformation,°C
δT^{pl}_{cond}	Temperature gain in platen elements in deformation zone due to conduction to the specimen during deformation, °C.
δT^{sp}_{cond}	Temperature loss, °C, in specimen surface elements in the deformation zone due to conduction to the platens during deformation
δT^{sp}	Temperature drop in specimen elements due to conduction within the specimen, °C

A1.1 Introduction

The heat conduction inside the workpiece during hot rolling or plane strain compression testing depends on the initial temperature distribution and on the thermal properties of steel. The temperature gradient inside the workpiece is a function of time and may be calculated by solving equation A1.1 for an isotropic solid with constant thermal conductivity

$$\frac{\delta^2 T}{\delta x^2} + \frac{\delta^2 T}{\delta y^2} + \frac{\delta^2 T}{\delta z^2} = \frac{1}{D}\frac{\delta T}{\delta t} \qquad \text{A1.1}$$

If one assumes that there is no heat flow through the sides of the workpiece then equation A1.1 may be rewritten as:

$$\frac{\delta^2 T}{\delta x^2} = \frac{1}{D}\frac{\delta T}{\delta t} \qquad \text{A1.2}$$

The solution of this differential equation lies in numerical analysis based on the finite difference method which solves for the temperature change at discrete points in the workpiece over discrete time intervals. Using this method, Harding [24] and Foster [19] developed mathematical models that predict the temperature changes occurring during hot rolling and plane strain compression testing respectively.

A1.2 Heat flow during air cooling in an undeformed plane strain compression specimen. (Refer to Figure A1)

Two-dimensional heat conduction was considered between the elements of a longitudinal section of the specimen i.e. ignoring heat flow from the sides of the specimen.

It was also assumed that the top and bottom faces of the specimen were subjected to identical cooling conditions (radiation and convection). This assumption allows, by symmetry, the consideration of only one quarter of the longitudinal slice (see inset to Figure A1). The representative section of the specimen consists of W rows each of initial height $\delta y[0]$ and V columns each of constant width δx. This section does not represent the whole length of the

specimen since this would require a very large number of elements. Instead, a notional column of elements is considered at M = 0 which allows the length of the section under consideration to be reduced.

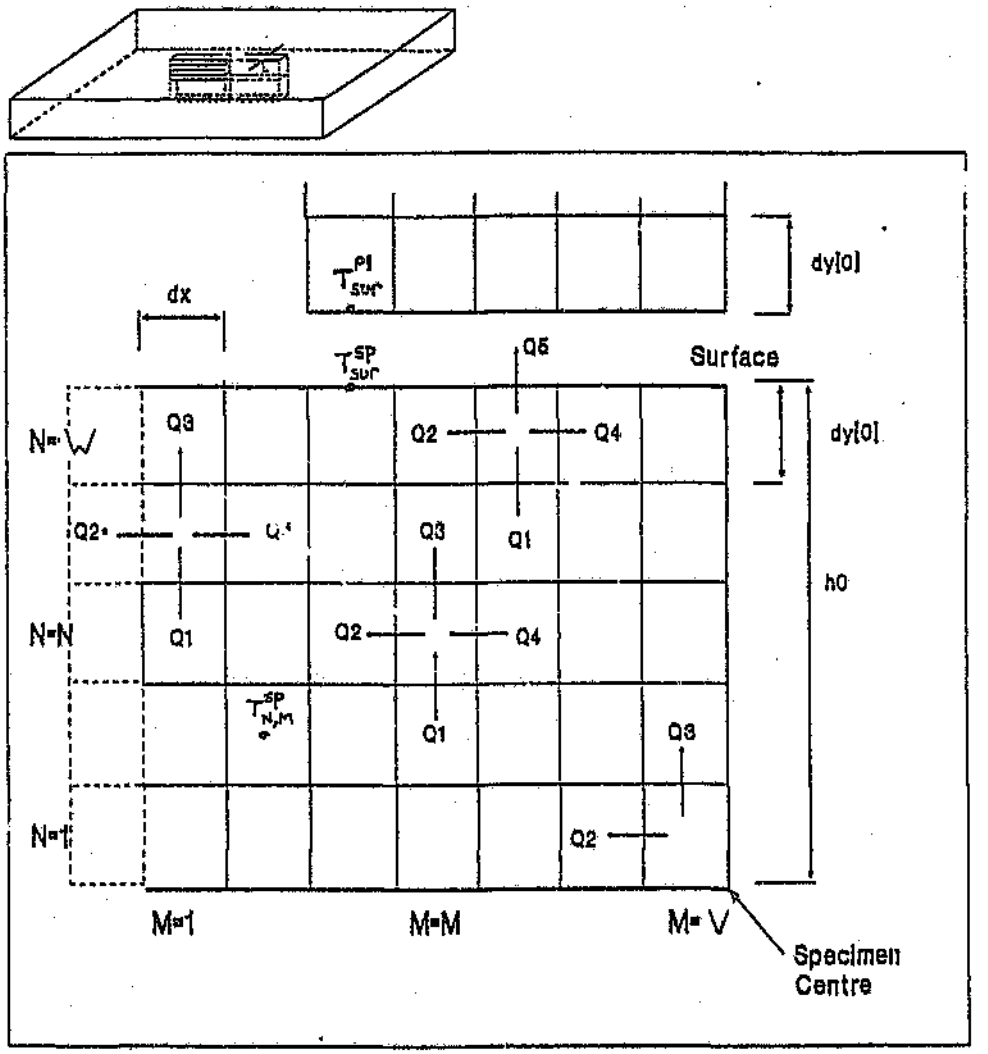

Figure A1 Element dimensions and heat flow in an undeformed plane strain compression specimen

Each element, of constant length, δz, in the section, is represented using matrix notation as N,M, where N is the row number and M the column number. The temperature at each node is represented by $T^{sp}_{N,M}$. The finite difference approximation then allows the representation of equation A1.2 by

$$Q = \frac{k\ A\ (T^{n}P_{N,M^{*}} - T^{n}P_{N,M})\ \delta t}{x_{flow}} \qquad \text{A1.3}$$

Considering the heat flow between the N,M element and its four surrounding elements , equation A1.3 gives the amount of heat flowing between adjacent nodes in a small time interval, δt, as

$$Q1 = (T^{n}P_{N,M} - T^{n}P_{N+1,M})\ k\ \delta x\ \delta z\ \delta t\ /\delta y[0] \qquad \text{A1.4}$$

$$Q2 = (T^{n}P_{N,M} - T^{n}P_{N,M-1})\ k\ \delta y[0]\ \delta z\ \delta t\ /\ \delta x \qquad \text{A1.5}$$

$$Q3 = (T^{n}P_{N-1,M} - T^{n}P_{N,M})\ k\ \delta x\ \delta z\ \delta t\ /\delta y[0] \qquad \text{A1.6}$$

$$Q4 = (T^{n}P_{N,M+1} - T^{n}P_{N,M})\ k\ \delta y[0]\ \delta z\ \delta t\ /\ \delta x \qquad \text{A1.7}$$

The convention used is that heat flow away from the centre element, (1,V) , is positive.

The net heat flow into the N,M element is given by

$$\Sigma Q = -Q1 - Q2 + Q3 + Q4 \qquad \text{A1.8}$$

Considering the situation where M = 1 , since the M = 0 column consists of notional elements that have no defined temperature, Q2 cannot be calculated using equation A1.3 as it was for M > 1. Instead, Q2 is estimated using a boundary condition factor, HTC:

$$Q2^{*} = HTC\ .\ Q4 \qquad \text{A1.9}$$

The use of the notional column of elements therefore allows firstly the number of elements in the section to be reduced and secondly the heat flow across the boundary XX' to be controlled.

The net amount of heat, Q, flowing into any non-surface element is given by one of the following combinations:

M = 1, N = 2 to (W- 1)	$\Sigma Q = Q4 - Q2^{*} + Q1 - Q3$	A1.10
N = 1, M = 2 to (V - 1)	$\Sigma Q = Q4 - Q2 - Q3$	A1.11
N = 1, M = V	$\Sigma Q = - Q2 - Q3$	A1.12
M = V, N = 2 to (W - 1)	$\Sigma Q = - Q3 - Q2 + Q1$	A1.13

$M = 1, N = 1 \qquad \Sigma Q = Q4 - Q3 - Q2^{*} \qquad A1.14$

In any hot working operation a certain amount of heat is lost at the surface during air cooling due to radiation and convection. The heat lost from the specimen surface is governed by the heat transfer coefficient, H , which is a function of the surface temperature, T^{sp}_{sur}. The relationship between T^{sp}_{sur} and H for plane strain compression specimens is given by Foster as

$$H = 0.032(T^{sp}_{sur}-T_{amb}) + 3.23\times10^{-11}(T^{sp}_{sur}{}^{4}-T_{amb}{}^{4}) \qquad A1.15$$

Equation A1.15 is also used for calculating the heat lost from the platen surface by replacing the specimen surface temperature, T^{sp}_{sur}, with the platen surface temperature, T^{pl}_{sur}.

Foster[19] found that the specimen surface temperature may be approximated by equation A1.14:

$$T^{sp}_{sur} = T^{sp}_{W,M} + \frac{H\,\delta y[i]}{2\,W\,k}\left[\frac{W^3 - (W-1)^3}{3} - W^2\right] \qquad A1.16$$

where $T^{sp}_{W,M}$ is the specimen surface element centre temperature.

The heat lost from the specimen surface to the surroundings, Q5, in a time interval, δt, is given by

$$Q5 = H\,\delta x\,\delta z\,\delta t \qquad A1.17$$

Thus, for the surface elements

$N = W, M = 2$ to $V-1$	$\Sigma Q = - Q5 - Q2 + Q1 + Q4$	A1.18
$N = W, M = 1$	$\Sigma Q = - Q5 - Q2^{*} + Q1 + Q4$	A1.19
$N = W, M = V$	$\Sigma Q = - Q5 - Q2 + Q1$	A1.20

Having found ΣQ for any element, the new temperature for that element at the end of the time interval may be calculated. The temperature change in an element due to conduction from its four neighbouring elements over a time interval, δt, is given by

$$\delta T^{n}P = \frac{\Sigma Q}{\delta x\ \delta z\ \delta y[i]\ \rho\ s} \qquad \text{A1.21}$$

where ΣQ is the net heat flow through an element and $\delta y[i]$ is the element height in the i^{th} pass.

The new temperature, $T^{n}P_{N,M}{}^{n}$, at the end of time interval δt is given by

$$T^{n}P_{N,M}{}^{n} = T^{n}P_{N,M} + \delta T^{n}P \qquad \text{A1.22}$$

Equations A1.4-A1.22 were also used in determining the conduction within the compression platens in both air cooling and deformation since the element dimensions remain constant during both periods. The only changes are:

a) The elemental height remains constant at dy[0]
b) The notional column at M = 1, is replaced with a column of surface elements.
c) The heat flow, Q, is replaced with J for notational purposes.

The successful solution of explicit finite difference equations is dependent on the correct choice of the computational time, δt. If δt is too large, spurious temperatures are obtained from the computations. Foster [19] found the maximum allowable stable time, δt_{max}, for finite difference calculations in plane strain compression testing to be

$$\delta t_{max} = \frac{\delta y[i]^{2}\ \rho\ s}{6\ k} \qquad \text{A1.23}$$

A1.3 Plane Strain Compression

A1.3.1 Dimension Changes During Plane Strain Compression(Refer to Figure A2)

During a period of deformation the elements in the specimen shoulder remain unchanged, while the geometries of the elements in the deformation zone are altered. As the deformation proceeds the elemental height in the deformation zone (initially dy[0]) is reduced to δy[i]. Several assumptions have been made concerning the changing geometry of the elements during deformation:

- The volume of material in the specimen remains constant throughout the deformation.
- True plane strain conditions exist so that the specimen does not spread in the breadth direction i.e δz of each element remains constant.
- All elements between the tools remain equal in shape and size, except thickness.
- Elements remain in vertical columns throughout the deformation.
- The line of symmetry UU'in Figure A2 remains stationary at the centre of the platen width throughout.
- The line of symmetry XX' in Figure A2 remains at the mid thickness of the specimen throughout the deformation.
- The elemental material that is effectively squeezed out from beneath the platens to form a column of rhomboidal elements of equal volume between the deformed and undeformed elements.

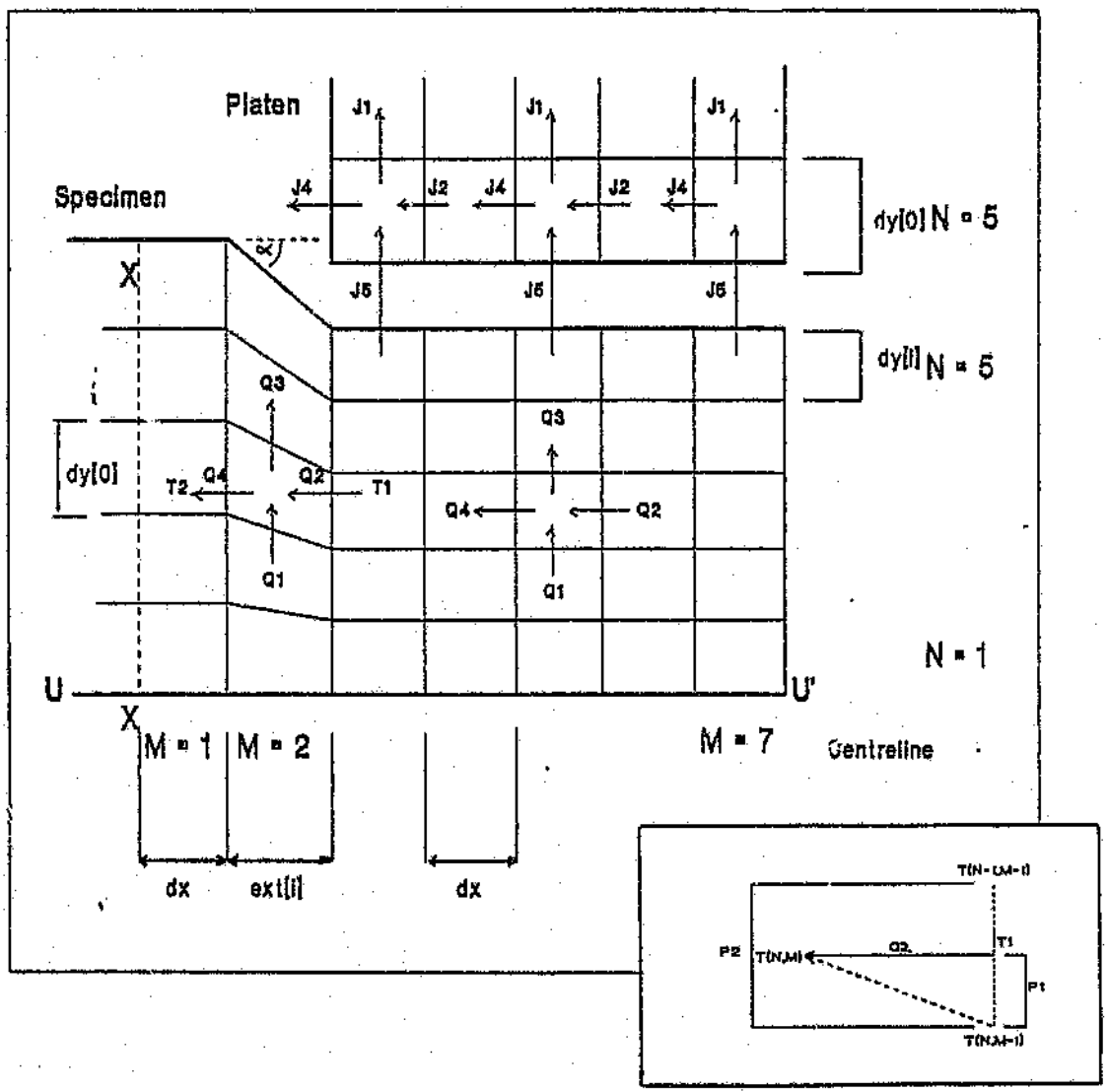

Figure A2 Element dimensions and heat flow in a deformed plane strain compression specimen

A1.3.1.1 Specimen element dimension changes in deformation zone

In plane strain deformation, the strain applied to the specimen during pass i is

$$\epsilon' = \ln(h_o / h_x) = \ln \frac{\delta y[0]}{\delta y[i]} \qquad \text{A1.24}$$

$$= \frac{\delta t}{\delta \epsilon} \qquad \text{A1.25}$$

Rearrangement of equations A1.24 and A1.25 gives

$$\delta y[i] = \frac{\delta y[0]}{\exp(\delta \epsilon)} \qquad \text{A1.26}$$

Equation A1.26 gives the height of the elements in the deformation zone for any period during a test.

A1.3.1.2 Specimen element dimensions just outside the deformation zone

During deformation the dimensions of the elements remaining between the platens are continually changing. Consequently the dimensions of elements at the platen edges are also continually changing and the relevant dimensions of these elements must therefore be calculated for each interval.

It was assumed that the elements in the column at the platen edges (M = 2) are rhomboidal in shape and increased in volume with successive deformations. However this assumption greatly simplifies the calculations of the specimen dimensions and heat transfer.

The width of the rhomboidal elements, ext[i], is obtained by manipulation of the equation defining the area of a rhombus:

$$ext[i] = \frac{\delta x \cdot \delta y[i]}{\delta y[i-1] + \delta y[i]} \qquad \text{A1.27}$$

The longer parallel side remains constant at the initial element height, $\delta y[0]$, whereas the shorter side equals the height of the elements under the platen, $\delta y[i]$, for that pass. During deformation the representative temperature of an element is assumed to remain at the centre of gravity of the element.

A1.3.2 Heat Transfer During Plane Strain Compression

During deformation, the rate of heat transfered between the specimen and platens is governed by the average heat transfer coefficient, H, and is a function of element thickness and the heat transfer coefficients at the beginning and end of the contact period. H is not simply related to time and must be estimated.

Before and after deformation, heat is considered to flow in the specimen thickness direction and along the specimen length (i.e. in the z and x directions) for all specimen elements, as in air cooling. The area of the heat conducting path is perpendicular to the direction of heat flow.

Considering the N,M element in Figure A2, the formulae for Q1 - Q4 remain basically the same as for air cooling (equations A1.4- A1.7) the only difference being that the deformed element dimensions are used in the calculations i.e.

$$Q1 = (T^{n}P_{N,M} - T^{n}P_{N+1,M})\, k\, \delta x\, \delta z\, \delta t / \delta y[i] \qquad A1.28$$

$$Q2 = (T^{n}P_{N,M} - T^{n}P_{N+1,M})\, k\, \delta y[i]\, \delta z\, \delta t / \delta x \qquad A1.29$$

$$Q3 = (T^{n}P_{N-1,M} - T^{n}P_{N,M})\, k\, \delta x\, \delta z\, \delta t / \delta y[i] \qquad A1.30$$

$$Q4 = (T^{n}P_{N-1,M} - T^{n}P_{N,M})\, k\, \delta y[i]\, \delta z\, \delta t / \delta x \qquad A1.31$$

For the rhomboidal column of elements, heat flow in the X direction is given by:

$$Q4 = (T1 - T^{n}P_{N,M})\, k\, \delta z\, \delta t / ext[i] \qquad A1.32$$

$$Q2 = (T2 - T^{n}P_{N,M-1})\, k\, \delta z\, \delta t / ext[i] \qquad A1.33$$

It was shown by Foster [19] that the value of T1 obtained by interpolation is

$$T1 = T^{sp}_{N,M+1} - \frac{(T^{sp}_{N,M+1} - T^{sp}_{N+1,M+1})\ P_1}{P_2} \qquad \text{A1.34}$$

where P_1, P_2 are defined in Figure A2. The value of T2 is obtained in a similar way.

A1.3.2.1 Specimen Surface Temperatures in deformation zone during deformation

Foster [18] found that the surface element temperature of the specimen in the deformation zone at the end of a time interval, δt, is given by equation A1.35:

$$T^{sp}_{sur} = T^{sp}_{w,M} - \frac{H_1\ \delta y[i]}{2\ W\ k}\left[2W - \frac{D_{sc}}{\delta y[i]}\right]\left[\frac{D_{sc}}{\delta y[i]}\right] \qquad \text{A1.35}$$

$$D_{sc} = \frac{6\ k\ \delta t}{\rho\ s} \qquad \text{A1.36}$$

The surface temperatures, T^{pl}_{sur}, of the platen at the end of time interval, δt, were also calculated using equation A1.35, except that the platen surface element temperatures, $T^{pl}_{w,M}$, were used and k is replaced with k'.

A1.3.2.2 Temperature drop due to conduction to the platens

The temperature drop at the surface of the specimen due to conduction during deformation is

$$\delta T^{sp}_{cond} = \frac{2\ \bar{H}}{\delta y[i]\ s\ \rho}\ \delta t \qquad \text{A1.37}$$

The temperature rise at the surface of the platens due to conduction during deformation is

$$\delta T^{pl}_{cond} = \frac{2\ \bar{H}}{\delta y[0]\ s'\ \rho'}\ \delta t \qquad \text{A1.38}$$

The temperature at the centre of the specimen surface elements at the end of the deformation time interval, δt, is given by

$$T^{sp}_{w,M''} = T^{sp}_{w,M} + \frac{\Sigma Q}{\text{Vol } s\ \rho} - \delta T^{sp}_{cond} \qquad \text{A1.39}$$

Similarly the surface temperature at the centre of the platen surface elements is given by

$$T^{pl}_{w,M''} = T^{pl}_{w,M} + \frac{\Sigma J}{\text{Vol}'\ s'\ \rho'} - \delta T^{pl}_{cond} \qquad \text{A1.40}$$

A suitable value of, δt, was calculated so that the distance penetrated by the temperature gradient into the specimen ,D_m, is just less than the specimen element thickness in the deformation zone, $\delta y[i]$. Ideally, the value of the stable calculation time increment, δt_{max}, giving $\delta y[i] = D_m$, is required. However, this cannot be obtained by equating the relationships for D_m and $\delta y[i]$ and an iteration method is therefore used to find a value of δt_{max} such that

$$(\delta y[i] - D_m) = 0.0001 \qquad \text{A1.41}$$

The value of D_m that satisfies equation A1.41 is used in equation A1.23 to calculate δt_{max}.

A1.3.2.3 Estimation of Heat Transfer Coefficient Between Specimen and Platen During Deformation

The heat transfer coefficient is a rapidly changing function with time and it is necessary to average its value for any particular time interval. Since it is not simply related to time it is impossible to obtain the true value of H and it was found by Foster [19] to be estimated using equations A1.42 - A1.50:

$$\bar{H} = \frac{H_o + 9H_1}{10} \qquad \text{A1.42}$$

where

$$H_o = C\ (T^{sp}_{sur} - T^{pl}_{sur}) \qquad \text{A1.43}$$

$$H_1 = C\ (T^{\circ}P_{sur}{}^{*} - T^{p1}{}_{sur}{}^{*}) \qquad \text{A1.44}$$

where

$$T^{\circ}P_{sur}{}^{*} - T^{p1}{}_{sur}{}^{*} = \frac{T^{\circ}P_{W.M} - T^{p1}{}_{W.M} + F1 - F2}{1 + F3 + F4} \qquad \text{A1.45}$$

and

$$F1 = \frac{\Sigma Q}{\delta x\ \delta y[i]\ \varphi\ s} - \frac{\Sigma J}{\delta y[0]\ \delta x\ \varphi\ 's'} \qquad \text{A1.46}$$

$$F2 = 0.1\ C\ \delta t(T^{\circ}P_{sur} - T^{p1}{}_{sur})\left[\frac{1}{\delta y[0]s'\ \varphi\ '} + \frac{1}{\delta y[i]s\ \varphi}\right] \qquad \text{A1.47}$$

$$F3 = 9\ F2 \qquad \text{A1.48}$$

$$F4 = C\left[\frac{\delta y[i]}{2\ W\ k}\left[2W - \frac{D_{\infty}}{2\ \delta y[0]}\right]\left[\frac{D_{\infty}}{2\ \delta y[0]}\right] + \frac{F10\ \delta y[0]}{2\ k'}\right] \qquad \text{A1.49}$$

where

$$F10 = (W + 1)^2 - 0.33\ \{(W+1)^3 - W^3)\} \qquad \text{A1.50}$$

A1.3.2.4 Temperature rise due to mechanical work

The temperature gained due to mechanical work in both rolling and plane strain compression is a function of the yield stress, R_{∞}, of the material deformed and of the thickness ratio [19].

$$\delta T^{\circ}P_{def} = \frac{R_{\infty}}{s} \ln \frac{h_o}{h_f} \qquad \text{A1.51}$$

$\delta T^{\circ}P_{def}$ is added to each element temperature after deformation.

```
uses
dos,crt;

Const

V  = 7;
VV = 5;
W  = 5;

Type

array1type  = array[1..5,1..7]of real;
array2type = array[1..5,1..7]of real;
array3type = array[0..15]of real;
array4type = array[1..15]of integer;

Var

JJ,II,HH,GG,dx,dyy,HT,k1,s1,rho1,H,k,s,rho   :real;
DD,FF,EE,Toolinit,Tamb,deltaT,add,add1       :real;
J1,J5,J2,J3,J4,Q1,Q2,Q3,Q4,Q5,Tinit,L        :real;
factor,delta,drop,rise,distance,dtdeftry     :real;
F1,F2,F3,F4,F10,C,D_x,Dxx,Hnew,Hold,Hmean    :real;
AA,CC,counter,test,i,passes,m,n              :integer;
plus1,plus2,nett,nett1,nett2                 :integer;
dtool,dspec,spec,tool,Q,J                    :array1type;
surface,toolsurface                          :array2type;
KK,LL,dy,deftime,timeair,dtair,dtdef         :array3type;
MM,NN,extension,strain,rate,stress           :array3type;
logger                                       :array4type;
BB,filestrain,filename                       :string[80];
strainfile,thefile                           :text;
key,A,U,NU                                   :char;


Procedure Initial;
begin
clrscr;
Textcolor(13);
writeln('                              **  INPUTS **');
writeln;
window(1,1,79,30);
textcolor(11);
writeln('Schedule Number :         File Name for Output Data File :');
writeln;
writeln('Number of Passes:         Temperatures ');
writeln;
writeln('Element width :           Initial Specimen :');
writeln('Element height:           Initial Platen   :');
writeln('                          Ambient          :');
writeln;
writeln('HTC for deformation :     Uniform / Non-Uniform [U/NU] : ');
writeln;
writeln('Boundary condition factor :');
```

```
writeln;
writeln('Pass:    Strain:    Strain Rate:     Mean Stress:   Delay Time:');

textcolor(white);
gotoxy(19,3);
readln(test);
gotoxy(60,3);
readln(filename);
gotoxy(19,5);
readln(passes);
gotoxy(45,7);
readln(tinit);
gotoxy(45,8);
readln(toolinit);
gotoxy(45,9);
readln(tamb);
gotoxy(16,7);
readln(dx);
gotoxy(16,8);
readln(dyy);
gotoxy(22,11);
readln(C);
gotoxy(57,11);
readln(key);
gotoxy(28,13);
readln(factor);

for i:=1 to passes do
begin
gotoxy(6,15+i);
writeln(i);
gotoxy(12,15+i);
readln(strain[i]);
gotoxy(25,15+i);
readln(rate[i]);
gotoxy(41,15+i);
readln(stress[i]);
gotoxy(56,15+i);
readln(timeair[i]);
end;

assign(thefile,filename);
rewrite(thefile);

if key = 'U' then
begin
for m:=1 to V do begin
for n:=1 to W do begin
Spec[n,m]:=Tinit;
end;
end;
end
else
begin
```

```
clrscr;
textcolor(13);
writeln('Non Uniform Temperature Input');
textcolor(11);
writeln;
writeln('_____Surface_____');
writeln;
textcolor(14);
writeln('[5,7]      [5,6]      [5,5]      [5,4]      [5,3]      [5,2]      [5,1]      ');
writeln;
writeln('[4,7]      [4,6]      [4,5]      [4,4]      [4,3]      [4,2]      [4,1]      ');
writeln;
writeln('[3,7]      [3,6]      [3,5]      [3,4]      [3,3]      [3,2]      [3,1]      ');
writeln;
writeln('[2,7]      [2,6]      [2,5]      [2,4]      [2,3]      [2,3]      [2,1]      ');
writeln;
writeln('[1,7]      [1,6]      [1,5]      [1,4]      [1,3]      [1,3]      [1,1]      ');
textcolor(11);
writeln('Centre_____Midthickness_____');
textcolor(15);
gotoxy(6,5);
readln(spec[5,7]);
gotoxy(18,5);
readln(spec[5,6]);
gotoxy(30,5);
readln(spec[5,5]);
gotoxy(41,5);
readln(spec[5,4]);
gotoxy(52,5);
readln(spec[5,3]);
gotoxy(63,5);
readln(spec[5,2]);
gotoxy(74,5);
readln(spec[5,1]);
gotoxy(6,7);
readln(spec[4,7]);
gotoxy(18,7);
readln(spec[4,6]);
gotoxy(30,7);
readln(spec[4,5]);
gotoxy(41,7);
readln(spec[4,4]);
gotoxy(52,7);
readln(spec[4,3]);
gotoxy(63,7);
readln(spec[4,2]);
gotoxy(74,7);
readln(spec[4,1]);
gotoxy(6,9);
readln(spec[3,7]);
gotoxy(18,9);
readln(spec[3,6]);
gotoxy(30,9);
readln(spec[3,5]);
```

```
gotoxy(41,9);
readln(spec[3,4]);
gotoxy(52,9);
readln(spec[3,3]);
gotoxy(63,9);
readln(spec[3,2]);
gotoxy(74,9);
readln(spec[3,1]);
gotoxy(6,11);
readln(spec[2,7]);
gotoxy(18,11);
readln(spec[2,6]);
  toxy(30,11);
readln(spec[2,5]);
gotoxy(41,11);
readln(spec[2,4]);
gotoxy(52,11);
readln(spec[2,3]);
gotoxy(63,11);
readln(spec[2,2]);
gotoxy(74,11);
readln(spec[2,1]);
gotoxy(6,13);
readln(spec[1,7]);
gotoxy(18,13);
readln(spec[1,6]);
gotoxy(30,13);
readln(spec[1,5]);
gotoxy(41,13);
readln(spec[1,4]);
gotoxy(52,13);
readln(spec[1,3]);
gotoxy(63,13);
readln(spec[1,2]);
gotoxy(74,13);
readln(spec[1,1]);
end;

for m:=3 to 7 do begin
for n:=1 to W do begin
Tool[n,m]:=Toolinit;
end;
end;
clrscr;
add:=0;
add1:=0;
dy[0]:=dyy;

for i:= 1 to passes do begin
dy[i]:=dy[i-1]/exp(strain[i]);
extension[i]:=2*dx*dy[i]/(dy[i-1]+dy[i]);
deftime[i]:=strain[i]/rate[i];
end;
```

```
(*for i:=1 to passes do begin
writeln(thefile,timeair[i]:10:4);
writeln(thefile,deftime[i]:10:4);
end;*)
rho:=7800;
s:=650;
k:=24;
rho1:=8215;
s1:=425;
k1:=26;
clrscr;
writeln;
textcolor(13);
writeln;
writeln('          Element Dimension Changes');
writeln('          ________________________________________');
textcolor(11);
writeln('            Pass          Height (mm)     Extension (mm)  ');
textcolor(white);
writeln;
for i:=1 to passes do begin
writeln(i:14,dy[i]*1000:17:2,extension[i]*1000:19:2);
end;
textcolor(13);
writeln('          ________________________________________');
readln;
end;

Procedure Air_Stable_Time;
begin
clrscr;
textcolor(13);
writeln('          Times (seconds)');
writeln('          ________________________________');
writeln;
textcolor(14);
writeln('          Air Cooling:');
textcolor(11);
writeln('          Pass     Hold Time        Stable Interval');
textcolor(white);
writeln;
for i:= 1 to passes do begin
dtair[i]:=sqr(dy[i-1])*rho*s/(6*k);
writeln(i:14,timeair[i]:10:0,dtair[i]:23:4);
end;
writeln;
writeln;
end;


{-----------------------------------------------}
{- Iteration for Stable Time During Deformation  -}
{-----------------------------------------------}
```

```
Procedure Deform_Stable_Time;
begin
textcolor(14);
writeln('          Deformation:');
textcolor(11);
writeln('          Pass     Contact Time     Stable Interval');
textcolor(white);
writeln;
for i:= 1 to passes do begin
dtdeftry:=1;
repeat
begin
dtdeftry:=dtdeftry-0.01;
distance:=sqrt(6*dtdeftry*k/(s*rho));
end;
until (distance - dy[i]/2) < 0.0001;
dtdef[i]:=dtdeftry;
writeln(i:14,deftime[i]:10:2,dtdef[i]:23:4);
end;
textcolor(13);
writeln('          ____________________________________');
readln;
end;


Procedure Print_Tool;
begin
clrscr;
writeln;
textcolor(13);
writeln('                                    Platen');
textcolor(11);
writeln('          ____________________________');
textcolor(white);
for n:= 1 to w do begin
writeln(tool[n,7]:15:0,tool[n,6]:7:0,tool[n,5]:7:0,
        tool[n,4]:7:0,tool[n,3]:7:0);
end;
(*writeln(toolsurface[5,7]:15:0,toolsurface[5,6]:7:0,toolsurface[5,5]:7:0,
                  toolsurface[5,4]:7:0,toolsurface[5,3]:7:0);*)
textcolor(11);
writeln('          ____________________________');
writeln;
end;

Procedure Print_Spec;
begin
writeln;
textcolor(13);
writeln('                                          Specimen');
textcolor(11);
writeln('          ____________________________________');
textcolor(white);
writeln(surface[5,7]:15:0,surface[5,6]:7:0,surface[5,5]:7:0,
```

```
        surface[5,4]:7:0,surface[5,3]:7:0,surface[5,2]:7:0,
        surface[5,1]:7:0);
for n:= w downto 1 do begin
writeln(spec[n,7]:15:0,spec[n,6]:7:0,spec[n,5]:7:0,spec[n,4]:7:0,spec[n,3]:7:0,
        spec[n,2]:7:0,spec[n,1]:7:0);
end;
textcolor(11);
writeln('                ___________________________________________');
writeln;
(*writeln(thefile,add:10:3,spec[1,7]:10:1,spec[2,7]:10:1,spec[3,7]:10:1,
         spec[4,7]:10:1,spec[5,7]:10:1);*)
writeln;
writeln('   Air Cooling before pass ',i:4,'    Time: ',add:4:2);

writeln(thefile,add:10:3,spec[1,7]:10:1,spec[5,7]:10:1);
end;

{----------------------}
{-     AIR COOLING     -}
{----------------------}

Procedure Air_bottomrowspec;
begin
for m:=2 to V-1 do begin
Q1      :=  0;
Q2      :=  0;
Q4      :=  0;
deltaT  :=  0;
Q1      :=  Q1 + (spec[1,m]-spec[2,m])*k*dx*dx*dtair[i]/dy[i-1];
Q2      :=  Q2 + (spec[1,m]-spec[1,m-1])*k*dy[i-1]*dtair[i];
Q4      :=  Q4 + (spec[1,m+1]-spec[1,m])*k*dy[i-1]*dtair[i];
Q[1,m]  :=  Q4 - Q2 - Q1;
deltaT  :=  deltat + Q[1,m]/(rho*s*dx*dx*dy[i-1]);
spec[1,m]:= spec[1,m] + deltaT;
end;
end;

Procedure Air_bottomrowtool;
begin
for m:=4 to 6 do begin
J3      :=   0;
J2      :=   0;
J4      :=   0;
deltaT  :=   0;
J3      :=   J3 + (tool[1,m]-tool[2,m])*k1*dx*dx*dtair[i]/dyy;
J2      :=   J2 + (tool[1,m]-tool[1,m-1])*k1*dyy*dtair[i];
J4      :=   J4 + (tool[1,m+1]-tool[1,m])*k1*dyy*dtair[i];
J[1,m]  :=   - J3 - J2 + J4 + factor*J3;
deltaT  :=   deltat + J[1,m]/(rhol*s1*dx*dx*dyy);
tool[1,m]:=  tool[1,m] + deltaT;
end;
end;

Procedure Air_bottomrightspec;
```

```
begin
Q1      :=  0;
Q2      :=  0;
deltat  :=  0;
Q1      :=  Q1 + (spec[1,V]-spec[2,V])*k*dx*dx*dtair[i]/dy[i-1];
Q2      :=  Q2 + (spec[1,V]-spec[1,V-1])*k*dy[i-1]*dtair[i];
Q[1,V]      - Q1 - Q2;
deltaT  :=  deltat + Q[1,V]/(rho*s*dx*dx*dy[i-1]);
spec[1,V]:= spec[1,V] + deltaT;
end;

Procedure Air_bottomrighttool;
begin
J3      :=  0;
J2      :=  0;
deltat  :=  0;
J3      :=  J3 + (tool[1,7]-tool[2,7])*k1*dx*dx*dtair[i]/dyy;
J2      :=  J2 + (tool[1,7]-tool[1,6])*k1*dyy*dtair[i];
J[1,7]  :=  - J3 - J2 + factor*J3;
deltaT  :=  deltat + J[1.7]/(rho1*s1*dx*dx*dww);
tool[1,7]:= tool[1,7] + deltaT;
end;

Procedure Air_righthandspec;
begin
For n:=2 to w-1 do begin
Q1      :=  0;
Q2      :=  0;
Q3      :=  0;
deltat  :=  0;
Q1      :=  Q1 + (spec[n,v]-spec[n+1,v])*k*dx*dx*dtair[i]/dy[i-1];
Q2      :=  Q2 + (spec[n,v]-spec[n,v-1])*k*dy[i-1]*dtair[i];
Q3      :=  Q3 + (spec[n-1,v]-spec[n,v])*k*dx*dx*dtair[i]/dy[i-1];
Q[n,V]  :=  Q3 - Q1 - Q2;
deltat  :=  deltat + Q[n,V]/(rho*s*dx*dx*dy[i-1]);
spec[n,v]:= spec[n,v] + deltat;
end;
end;

Procedure Air_righthandtool;
begin
for n:=2 to w-1 do begin
J1      :=  0;
J2      :=  0;
J3      :=  0;
deltat  :=  0;
J1      :=  J1 + (tool[n,7]-tool[n+1,7])*k1*dx*dx*dtair[i]/dyy;
J2      :=  J2 + (tool[n,7]-tool[n,6])*k1*dyy*dtair[i];
J3      :=  J3 + (tool[n-1,7]-tool[n,7])*k1*dx*dx*dtair[i]/dyy;
J[n,7]  :=  J3 - J1 - J2;
deltat  :=  deltat + J[n,7]/(rho1*si*dx*dx*dyy);
tool[n,7]:= tool[n,7] + deltat;
end;
end;
```

```
Procedure Air_bottomleftspec;
begin
Q1        :=   0;
Q4        :=   0;
deltat    :=   0;
Q1        :=   Q1 + (spec[1,1]-spec[2,1])*k*dx*dx*dtair[i]/dy[i-1];
Q4        :=   Q4 + (spec[1,2]-spec[1,1])*k*dy[i-1]*dtair[i];
Q[1,1]    :=   Q4 - Q1 - factor*Q4;
deltat    :=   deltat + Q[1,1]/(rho*s*dx*dx*dy[i-1]);
spec[1,1]:=    spec[1,1] + deltat;
end;

Procedure Air_bottomlefttool;
begin
J3        :=   0;
J4        :=   0;
J5        :=   0;
deltat    :=   0;
H         :=   0;
H         :=   H  + 0.03227*(tool[1,3]-Tamb)+3.2319E-11*(sqr(sqr
               (tool[1,3]+273)) - sqr(sqr(tamb+273)));
J5        :=   J5 + H*dx*dyy*dtair[i]*1000;
J3        :=   J3 + (tool[1,3]-tool[2,3])*k1*dx*dx*dtair[i]/dyy;
J4        :=   J4 + (tool[1,4]-tool[1,3])*k1*dyy*dtair[i];
J[1,3]    :=   J4 - J3 - J5 - factor*J4;
deltat    :=   deltat + J[1,3]/(rho1*s1*dx*dx*dyy);
tool[1,3]:=    tool[1,3] + deltat;
end;

Procedure Air_firstspec;
begin
for n:= 2 to w-1 do begin
Q1        :=  0;
Q2        :=  0;
Q3        :=  0;
Q4        :=  0;
deltat    :=  0;
Q1        :=  Q1 + (spec[n,1]-spec[n+1,1])*k*dx*dx*dtair[i]/dy[i-1];
Q3        :=  Q3 + (spec[n-1,1]-spec[n,1])*k*dx*dx*dtair[i]/dy[i-1];
Q4        :=  Q4 + (spec[n,2]-spec[n,1])*k*dy[i-1]*dtair[i];
Q2        :=  Q2 + factor*Q4;
Q[n,1]    :=  Q3 + Q4 - Q2 - Q1;
deltaT    :=  deltaT + Q[n,1]/(rho*s*dx*dx*dy[i-1]);
spec[n,1]:=   spec[n,1] + deltaT;
end;
end;

Procedure Air_firsttool;
begin
for n:= 2 to w-1 do begin
J1        := 0;
J5        := 0;
J3        := 0;
J4        := 0;
```

```
H         := 0;
deltat    := 0;
H         := H  + 0.03227*(tool[n,3]- Tamb)+3.2319E-11*(sqr
             (sqr(tool[n,3]+273)) -  sqr(sqr(tamb+273)));
J5        := J5 + H*dx*dyy*dtair[i]*1000;
J1        := J1 + (tool[n,3]-tool[n+1,3])*k1*dx*dx*dtair[i]/dyy;
J3        := J3 + (tool[n-1,3]-tool[n,3])*k1*dx*dx*dtair[i]/dyy;
J4        := J4 + (tool[n,4]-tool[n,3])*k1*dyy*dtair[i];
J[n,3]    := J3 + J4 - J5 - J1;
deltaT    := deltaT + J[n,3]/(rho1*s1*dx*dx*dyy);
tool[n,3] := tool[n,3] + deltaT;
end;
end;

Procedure Air_internalspec;
begin
for m:= 2 to v-1 do begin
for n:= 2 to w-1 do begin
Q1      :=  0;
Q2      :=  0;
Q3      :=  0;
Q4      :=  0;
deltat  :=  0;
Q1      :=  Q1 + (spec[n,m]-spec[n+1,m])*k*dx*dx*dtair[i]/dy[i-1];
Q2      :=  Q2 + (spec[n,m]-spec[n,m-1])*k*dy[i-1]*dtair[i];
Q3      :=  Q3 + (spec[n-1,m]-spec[n,m])*k*dx*dx*dtair[i]/dy[i-1];
Q4      :=  Q4 + (spec[n,m+1]-spec[n,m])*k*dy[i-1]*dtair[i];
Q[n,m]  :=  Q3 + Q4 - Q2 - Q1;
deltaT  :=  deltaT + Q[n,m]/(rho*s*dx*dx*dy[i-1]);
spec[n,m]:= spec[n,m] + deltaT;
end;
end;
end;

Procedure Air_internaltool;
begin
for m:= 4 to 6 do begin
for n:= 2 to w-1 do begin
J1      :=  0;
J2      :=  0;
J3      :=  0;
J4      :=  0;
deltat  :=  0;
J1      :=  J1 + (tool[n,m]-tool[n+1,m])*k1*dx*dx*dtair[i]/dyy;
J2      :=  J2 + (tool[n,m]-tool[n,m-1])*k1*dyy*dtair[i];
J3      :=  J3 + (tool[n-1,m]-tool[n,m])*k1*dx*dx*dtair[i]/dyy;
J4      :=  J4 + (tool[n,m+1]-tool[n,m])*k1*dyy*dtair[i];
J[n,m]  :=  J3 + J4 - J2 - J1;
deltaT  :=  deltaT + J[n,m]/(rho1*s1*dx*dx*dyy);
tool[n,m]:= tool[n,m] + deltaT;
end;
end;
end;
```

```
Procedure Air_surfacespec;
begin
for m:=2 to V - 1 do begin
Q2       :=   0;
Q3       :=   0;
Q4       :=   0;
Q5       :=   0;
H        :=   0;
deltaT   :=   0;
Q2       :=   Q2 + (spec[W,m]-spec[W,m-1])*k*dy[i-1]*dtair[i];
Q3       :=   Q3 + (spec[W-1,m]-spec[W,m])*k*dx*dx*dtair[i]/dy[i-1];
Q4       :=   Q4 + (spec[W,m+1]-spec[W,m])*k*dy[i-1]*dtair[i];
H        :=   H  + 0.03227*(spec[W,m]-Tamb)+3.2319E-11*(sqr(sqr
                   (spec[W,m]+273)) -  sqr(sqr(tamb+273)));
Q5       :=   Q5 + H*dx*dx*dtair[i]*1000;
Q[W,m]   :=   - Q5 - Q2 + Q3 + Q4;
deltaT   :=   deltaT + Q[W,m]/(rho*s*dx*dx*dy[i-1]);
spec[W,m]:=   spec[W,m] + deltaT;
surface[W,m]:=spec[W,m] + H*1000*dy[i-1]*((w*w*w-exp(3*ln
              (w-1)))/3-w*w)/(2*w*k);
end;
end;


Procedure Air_surfacetool;
begin
for m:= 4 to 6 do begin
J2       :=   0;
J3       :=   0;
J4       :=   0;
J5       :=   0;
H        :=   0;
deltaT   :=   0;
J2       :=   J2 + (tool[W,m]-tool[W,m-1])*k1*dyy*dtair[i];
J3       :=   J3 + (tool[W-1,m]-tool[W,m])*k1*dx*dx*dtair[i]/dyy;
J4       :=   J4 + (tool[W,m+1]-tool[W,m])*k1*dyy*dtair[i];
H        :=   H+0.03227*(tool[W,m]-Tamb)+3.2319E-11*(sqr(sqr
              (tool[W,m]+273)) - sqr(sqr(tamb+273)));
J5       :=   J5 + H*dx*dx*dtair[i]*1000;
J[W,m]   :=   - J5 - J2 + J3 + J4;
deltaT   :=   deltaT + J[W,m]/(rho1*s1*dx*dx*dyy);
tool[W,m]:=   tool[W,m] + deltaT;
toolsurface[W,m]:= tool[W,m] + H*1000*dyy*
                   ((w*w*w-exp(3*ln(w-1)))/3-w*w)/(2*w*k1);
end;
end;

Procedure Air_surfaceleftspec;
begin
Q3          :=   0;
Q4          :=   0;
Q5          :=   0;
H           :=   0;
deltaT      :=   0;
```

```
Q3          :=   Q3 + (spec[W-1,1]-spec[W,1])*k*dx*dx*dtair[i]/dy[i-1];
Q4          :=   Q4 + (spec[W,2]-spec[W,1])*k*dy[i-1]*dtair[i];
H           :=   H+0.03227*(spec[W,1]-Tamb)+3.2319E-11*(sqr(sqr
                 (spec[W,1]+273)) - sqr(sqr(tamb+273)));
Q5          :=   Q6 + H*dx*dx*dtair[i]*1000;
Q[W,1]      :=   - Q5 - factor*Q4+Q3+Q4;
deltaT      :=   deltaT + Q[W,1]/(rho*s*dx*dx*dy[i-1]);
spec[W,1]   :=   spec[W,1] + deltaT;
surface[W,1]:=   spec[W,1] + H*1000*dy[i-1]*
                 ((w*w*w-exp(3*ln(w-1)))/3-w*w)/(2*w*k);
end;

Procedure Air_surfaceleftTool;
begin
J3          :=   0;
J4          :=   0;
J5          :=   0;
H           :=   0;
deltaT      :=   0;
J3          :=   J3 + (tool[W-1,3]-tool[W,3])*k1*dx*dx*dtair[i]/dyy;
J4          :=   J4 + (tool[W,4]-tool[W,3])*k1*dyy*dtair[i];
H           :=   H+0.03227*(tool[W,3]-Tamb)+3.2319E-11*(sqr(sqr
                 (tool[W,3]+273)) - sqr(sqr(tamb+273)));
J5          :=   J5 + H*dx*dx*dtair[i]*1000;
J[W,3]      :=   - J5 - factor*J4 + J3 + J4;
deltaT      :=   deltaT + J[W,3]/(rho1*s1*dx*dx*dyy);
tool[W,3]   :=   tool[W,3] + deltaT;
toolsurface[W,3]:= tool[W,3] + H*1000*dyy*
                   ((w*w*w-exp(3*ln(w-1)))/3-w*w)/(2*w*k1);
end;


Procedure Air_surfacerightspec;
begin
Q2          :=   0;
Q3          :=   0;
Q5          :=   0;
H           :=   0;
deltat      :=   0;
Q2          :=   Q2 + (spec[W,V]-spec[W,V-1])*k*dy[i-1]*dtair[i];
Q3          :=   Q3 + (spec[W-1,V]-spec[W,V])*k*dx*dx*dtair[i]/dy[i-1];
H           :=   H+0.03227*(spec[W,V]-Tamb)+3.2319E-11*
                 (sqr(sqr(spec[W,V]+273)) - sqr(sqr(tamb+273)));
Q5          :=   Q5 + H*dx*dx*dtair[i]*1000;
Q[w,v]      :=   -  Q5 + Q3 - Q2;
deltaT      :=   deltaT + Q[W,v]/(rho*s*dx*dx*dy[i-1]);
spec[W,v]   :=   spec[W,v] + deltaT;
surface[W,v]:=   spec[W,v] + H*1000*dy[i-1]*((w*w*w-exp
                 (3*ln(w-1)))/3-w*w)/(2*w*k);
end;


Procedure Air_surfacerighttool;
begin
```

```
J2          := 0;
J3          := 0;
J5          := 0;
H           := 0;
deltat      := 0;
J2          := J2 + (tool[W,7]-tool[W,6])*k1*dyy*dtair[i];
J3          := J3 + (tool[W-1,7]-tool[W,7])*k1*dx*dx*dtair[i]/dyy;
H           := H+0.03227*(tool[W,7]-Tamb)+3.2319E-11*(sqr
               (sqr(tool[W,7]+273)) - sqr(sqr(tamb+273)));
J5          := J5 + H*dx*dx*dtair[i]*1000;
J[W,7]      := -J5 + J3 - J2;
deltaT      := deltaT + J[W,7]/(rhol*sl*dx*dx*dyy);
tool[W,7]   := tool[W,7] + deltaT;
Toolsurface[W,7]:=tool[W,7] + H*1000*dyy*
                  ((w*w*w-exp(3*ln(w-1)))/3-w*w)/(2*w*k1);
end;


Procedure Print_Dtool;
begin
clrscr;
writeln;
textcolor(14);
writeln('                                    Platen');
textcolor(11);
writeln('          ____________________________');
textcolor(white);
for n:= 1 to w do begin
writeln(dtool[n,7]:15:0,dtool[n,6]:7:0,dtool[n,5]:7:0,
       dtool[n,4]:7:0, dtool[n,3]:7:0);
end;
textcolor(11);
writeln('          ____________________________');
writeln;
end;

Procedure Print_D   ;
begin
writeln;
textcolor(14);
writeln('                                              Specimen');
textcolor(11);
writeln('          ____________________________________________');
textcolor(white);
for n:= w downto 1 do begin
writeln(dspec[n,7]:15:0,dspec[n,6]:7:0,dspec[n,5]:7:0,dspec[n,4]:7:0,
                     dspec[n,3]:7:0,dspec[n,2]:7:0,dspec[n,1]:7:0);
end;
textcolor(11);
writeln('          ____________________________  _______');
(*writeln(thefile,add1:10:3,dspec[1,7]:10:1,dspec[2,7]:10:1,dspec[3,7]:10:1,
                      dspec[4,7]:10:1,dspec[5,7]:10:1);*)
writeln;
textcolor(14);
```

```
writeln('   Deformation:   Pass ',i:4,'    Time: ',add1:6:2);

writeln(thefile,add1:10:3,dspec[1,7]:10:1,dspec[5,7]:10:1);
end;


{--------------------}
{ -   Deformation   -}
{--------------------}


Procedure Toprow;
begin
for m:= 4 to 6 do begin
Q2      :=   0;
Q3      :=   0;
Q4      :=   0;
J2      :=   0;
J3      :=   0;
J4      :=   0;
F1      :=   0;
F2      :=   0;
F3      :=   0;
F4      :=   0;
HT      :=   0;
H       :=   0;
Hold    :=   0;
Hnew    :=   0;
Hmean   :=   0;
drop    :=   0;
rise    :=   0;
HT      :=   HT+0.03227*(dtool[W,m]-Tamb)+3.2319E-11*
             (sqr(sqr(dtool[W,m]+273)) - sqr(sqr(tamb+273)));
H       :=   H+0.03227*(dspec[W,m]-Tamb)+3.2319E-11*(sqr
             (sqr(dspec[W,m]+273)) - sqr(sqr(tamb+273)));
Q2      :=   Q2 + (dspec[W,m]-dspec[W,m-1])*k*dy[i]*dtdef[i];
Q3      :=   Q3 + (dspec[W-1,m]-dspec[W,m])*k*dx*dx*dtdef[i]/dy[i];
Q4      :=   Q4 + (dspec[W,m+1]-dspec[W,m])*k*dy[i]*dtdef[i];
J2      :=   J2 + (dtool[W,m]-dtool[W,m-1])*k1*dyy*dtdef[i];
J3      :=   J3 + (dtool[W-1,m]-dtool[W,m])*k1*dx*dx*dtdef[i]/dyy;
J4      :=   J4 + (dtool[W,m+1]-dtool[W,m])*k1*dyy*dtdef[i];
Q[W,m]  :=   (- Q2 + Q3 + Q4)/(rho*s*dx*dx*dy[i]/2); ;
J[W,m]  :=   (- J2 + J3 + J4)/(rho1*s1*dx*dx*dyy);
F1      :=   Q[w,m] - J[w,m];
dspec[W,m]      := dspec[W,m] + Q[w,m];
surface[W,m]    := dspec[W,m] + H*1000*dy[i]/2*((w*w*w-exp
                   (3*ln(w-1)))/3-w*w)/(2*w*k);
dtool[W,m]      := dtool[W,m] + J[w,m];
toolsurface[W,m]:= dtool[W,m] + HT*1000*dyy*((w*w*w-
                   exp(3*ln(w-1)))/3-w*w)/(2*w*k);
F2              := F2 + 0.1*C*dtdef[i]*(surface[w,m] - toolsurface
                   [w,m])*(1/(dyy*s1*rho1)+1/(dy[i]*s1*rho1));
F3              := F3 + 0.9*C*dtdef[i]*(1/(dyy*s1*rho1)+1/(dy[i]*
                   s1*rho1));
```

```
D_x             := sqrt(6*k*dtdef[i]/(rho*s));
Dxx             := Dx/(2*dy[i]/2);
F10             := 5.666;
F4              := F4 + C*((dy[i]/(2*w*k))*(2*W-Dxx)*Dxx  +
                   F10*dyy/(2*6*k1));
Hnew            := Hnew + C*((dspec[w,m] - dtool[w,m] + F1 - F2)/
                   (1 +F3 +F4));
Hold            := Hold + C*(surface[w,m] - toolsurface[w,m]);
Hmean           := Hmean + (Hold + 9*Hnew)/10;
dspec[w,m]      := dspec[w,m] + Q[w,m] - 1000*Hmean*dtdef[i]/
                   (dy[i]*s*rho/2);
dtool[w,m]      := dtool[w,m] + J[w,m] + 1000*Hmean*dtdef[i]/
                   (dyy*s1*rho1);
drop            := drop +     Hmean*dtdef[i]/(dy[i]*s*rho/2);
rise            := rise +     Hmean*dtdef[i]/(dyy*s1*rho1);
end;
end;

Procedure TopRight;
begin
Q2      :=0;
Q3      :=0;
J2      :=0;
J3      :=0;
F1      :=0;
F2      :=0;
F3      :=0;
F4      :=0;
HT      :=0;
H       :=0;
Hold    :=0;
Hnew    :=0;
Hmean   :=0;
drop    :=0;
rise    :=0;
HT      := HT+0.03227*(dtool[W,7]-Tamb)+3.2319E-11*(sqr
           (sqr(dtool[W,7]+273)) - sqr(sqr(tamb+273)));
H       := H+0.03227*(dspec[W,7]-Tamb)+3.2319E-11*(sqr(sqr
           (dspec[W,7]+273)) - sqr(sqr(tamb+273)));
Q2      := Q2 + (dspec[W,7]-dspec[W,6])*k*dy[i]*dtdef[i];
Q3      := Q3 + (dspec[W-1,7]-dspec[W,7])*k*dx*dx*dtdef[i]/dy[i];
J2      := J2 + (dtool[W,7]-dtool[W,6])*k1*dyy*dtdef[i];
J3      := J3 + (dtool[W-1,7]-dtool[W,7])*k1*dx*dx*dtdef[i]/dyy;
Q[W,7]  :=  (- Q2 + Q3 )/(rho*s*dx*dx*dy[i]/2); ;
J[W,7]  :=  (- J2 + J3 )/(rho1*s1*dx*dx*dyy);
F1      :=Q[W,7] - J[W,7];
dspec[W,7]      :=  dspec[W,7] + Q[W,7];
surface[W,7]    :=  dspec[W,7] + H*1000*dy[i]/2*((w*w*w-exp
                    (3*ln(w-1)))/3-w*w)/(2*w*k);
dtool[W,7]      :=  dtool[W,7] + J[W,7];
toolsurface[W,7] :=  dtool[W,7] + HT*1000*dyy*((w*w*w-exp(3*
                    ln(w-1)))/3-w*w)/(2*w*k);
F2              :=  F2 + 0.1*C*dtdef[i]*(surface[w,7]-toolsurface
                    [w,7])*(1/(dyy*s1*rho))+1/(dy[i]*s1*rho1));
```

```
F3              := F3 + 0.9*C*dtdef[i]*(1/(dyy*s1*rho1)+1/
                   (dy[i]*s1*rho1));
D_x             := sqrt(6*k*dtdef[i]/(rho*s));
Dxx             := Dx/(2*dy[i]/2);
F10             := 5.666;
F4              := F4 + C*((dy[i]/(2*w*k))*(2*W-Dxx)*Dxx +
                   F10*dyy/(2*6*k1));
Hnew            := Hnew + C*((dspec[w,7] - dtool[w,7] + F1 -
                   F2)/(1 +F3 +F4));
Hold            := Hold + C*(surface[w,7] - toolsurface[w,7]);
Hmean           := Hmean + (Hold + 9*Hnew)/10;
dspec[w,7]      := dspec[w,7] + Q[w,7] - 1000*Hmean*dtdef[i]/
                   (dy[i]*s*rho/2);
dtool[w,7]      := dtool[w,7] + J[w,7] + 1000*Hmean*dtdef[i]/
                   (dyy*s1*rho1);
drop            := drop + Hmean*dtdef[i]/(dy[i]*s*rho/2);
rise            := rise + Hmean*dtdef[i]/(dyy*s1*rho1);
end;

Procedure TopLeft;
begin
Q2   :=0,
Q3   :=0;
Q4   :=0;
J3   :=0;
J4   :=0;
J5   :=0;
F1   :=0;
F2   :=0;
F3   :=0;
F4   :=0;
HT   :=0;
H    :=0;
Hold :=0;
Hnew :=0;
Hmean:=0;
drop :=0;
rise :=0;
HT      := HT+0.03227*(dtool[W,3]-Tamb)+3.2319E-11*(sqr(sqr
           (dtool[W,3]+273)) - sqr(sqr(tamb+273)));
H       := H+0.03227*(dspec[W,3]-Tamb)+3.2319E-11*(sqr(sqr
           (dspec[W,3]+273)) - sqr(sqr(tamb+273)));
Q2      := Q2 + (dspec[W,3] - dspec[W,2])*k*dy[i]*dx*dtdef[i]/extension[i];
Q3      := Q3 + (dspec[W-1,3]-dspec[W,3])*k*dx*dx*dtdef[i]/dy[i];
Q4      := Q4 + (dspec[W,4]-dspec[W,3])*k*dy[i]*dtdef[i];
J3      := J3 + (dtool[W-1,3]-dtool[W,3])*k1*dx*dx*dtdef[i]/dyy;
J4      := J4 + (dtool[W,4]-dtool[W,3])*k1*dyy*dtdef[i];
J5      := J5 + H*dx*dyy*dtdef[i]*1000;
Q[W,3]  :=  (- Q2 + Q3 + Q4)/(rho*s*dx*dx*dy[i]/2); ;
J[W,3]  :=  (- J5 + J3 + J4)/(rho1*s1*dx*dx*dyy);
F1      :=Q[w,3] - J[w,3];
dspec[W,3]      :=dspec[W,3] + Q[w,3];
surface[W,3]    :=dspec[W,3] + H*1000*dy[i]/2*((w*w*w-exp(3*ln
                  (w-1)))/3-w*w)/(2*w*k);
```

```
dtool[W,3]       :=dtool[W,3] + J[W,3];
toolsurface[W,3]:=dtool[W,3] + HT*1000*dyy*((w*w*w-exp(3*ln
                  (w-1)))/3-w*w)/(2*w*k);
F2              := F2 + 0.1*C*dtdef[i]*(surface[w,3] - toolsurface
                   [w,3])*(1/(dyy*s1*rho1)+1/(dy[i]*s1*rho1));
F3              := F3 + 0.9*C*dtdef[i]*(1/(dyy*s1*rho1)+1/(dy[i]
                   *s1*rho1));
D_x             := sqrt(6*k*dtdef[i]/(rho*s));
Dxx             := Dx/(2*dy[i]/2);
F10             := 5.666;
F4              := F4 + C*((dy[i]/(2*w*k))*(2*W-Dxx)*Dxx  +
                   F10*dyy/(2*6*k1));
Hnew            := Hnew + C*((dspec[w,3] - dtool[w,3] + F1 - F2)/
                   (1 +F3 +F4));
Hold            := Hold + C*(surface[w,3] - toolsurface[w,3]);
Hmean           := Hmean + (Hold + 9*Hnew)/10;
dspec[w,3]      := dspec[w,3] + Q[w,3] - 1000*Hmean*dtdef[i]/
                   (dy[i]*s*rho/2);
dtool[w,3]      := dtool[w,3] + J[w,3] + 1000*Hmean*dtdef[i]/
                   (dyy*s1*rho1);
drop            := drop +  Hmean*dtdef[i]/(dy[i]*s*rho/2);
rise            := rise +  Hmean*dtdef[i]/(dyy*s1*rho1);
end;

Procedure  TopleftSpec ;
begin
Q3        :=0;
Q4        :=0;
Q5        :=0;
H         :=0;
deltaT    :=0;
Q3        := Q3 + (dspec[W-1,1]-dspec[W,1])*k*dx*dx*dtdef[i]/dyy;
Q4        := Q4 + (dspec[W,2]-dspec[W,1])*k*dyy*dtdef[i];
H         := H+0.03227*(dspec[W,1]-Tamb)+3.2319E-11*(sqr(sqr
             (spec[W,1]+273)) - sqr(sqr(tamb+273)));
Q5        := Q5 + H*dx*dx*dtdef[i]*1000;
Q[W,1]    := - Q5 - factor*Q4+Q3+Q4;
deltaT    := deltaT + Q[W,1]/(rho*s*dx*dx*dyy);
dspec[W,1]:= dspec[W,1] + deltaT;
surface[W,1]:= dspec[W,1] + H*1000*dyy*((w*w*w-exp(3*ln(w-1)))/
               3-w*w)/(2*w*k);
end;

Procedure Toprhomboid;
begin
Q2       :=0;
Q3       :=0;
Q4       :=0;
Q5       :=0;
H        :=0;
deltaT   :=0;
Q2       := Q2 + (dspec[W,2] - dspec[W,1])*k*dyy*dx*dtdef[i]/
            extension[i];
Q3       := Q3 + (dspec[W-1,2]-dspec[W,2])*k*dx*extension[i]*
```

```
            dtdef[i]/((dyy+dy[i])/2);
Q4        := Q4 + (dspec[W,3]-dspec[W,2])*k*dy[i]*dx*dtdef[i]/
            extension[i];
H         := H+0.03227*(dspec[W,2]-Tamb)+3.2319E-11*(sqr(sqr
            (spec[W,2]+273)) - sqr(sqr(tamb+273)));
Q5        := Q5 + H*dx*extension[i]*dtdef[i]*1000;
Q[W,2]    := - Q5 - Q2 + Q3 + Q4;
deltaT    := deltaT + Q[W,2]/(rho*s*dx*dx*dyy);
dspec[W,2]:= dspec[W,2]+ deltaT;
surface[W,2]:= dspec[W,2] + H*1000*dyy*((w*w*w-exp(3*ln(w-1)))/
              3-w*w)/(2*w*k);
end;

Procedure InternalSpec;
begin
for m:= 4 to 6 do begin
for n:= 2 to w-1 do begin
Q1        :=   0;
Q2        :=   0;
Q3        :=   0;
Q4        :=   0;
deltat    :=   0;
Q1        :=   Q1+(dspec[n,m]-dspec[n+1,m])*k*dx*dx*dtdef[i]/dy[i];
Q2        :=   Q2+(dspec[n,m]-dspec[n,m-1])*k*dy[i]*dtdef[i];
Q3        :=   Q3 + (dspec[n-1,m]-dspec[n,m])*k*dx*dx*dtdef[i]/dy[i];
Q4        :=   Q4+(dspec[n,m+1]-dspec[n,m])*k*dy[i]*dtdef[i];
Q[n,m]    :=   Q3 + Q4 - Q2 - Q1;
deltaT    :=   deltaT + Q[n,m]/(rho*s*dx*dx*dy[i]/2);
dspec[n,m]:= dspec[n,m] + deltaT;
end;
end;
end;

Procedure InternalTool;
begin
for m:= 4 to 6 do begin
for n:= 2 to w-1 do begin
J1        :=  0;
J2        :=  0;
J3        :=  0;
J4        :=  0;
deltat    :=  0;
J1        :=  J1+(dtool[n,m]-dtool[n+1,m])*k1*dx*dx*dtdef[i]/dyy;
J2        :=  J2+(dtool[n,m]-dtool[n,m-1])*k1*dyy*dtdef[i];
J3        :=  J3 + (dtool[n-1,m]-dtool[n,m])*k1*dx*dx*dtdef[i]/dyy;
J4        :=  J4+(dtool[n,m+1]-dtool[n,m])*k1*dyy*dtdef[i];
J[n,m]    :=  J3 + J4 - J2 - J1;
deltaT    :=  deltaT + J[n,m]/(rho1*s1*dx*dx*dyy);
dtool[n,m]:=dtool[n,m] + deltaT;
end;
end;
end;

Procedure firstcolspec;
```

```
begin
for n:= 2 to w-1 do begin
Q1      :=  0;
Q2      :=  0;
Q3      :=  0;
Q4      :=  0;
deltat  :=  0;
Q1      :=  Q1+(dspec[n,1]-dspec[n+1,1])*k*dx*dx*dtdef[i]/dyy;
Q3      :=  Q3 + (dspec[n-1,1]-dspec[n,1])*k*dx*dx*dtdef[i]/dyy;
Q4      :=  Q4+(dspec[n,2]-dspec[n,1])*k*dyy*dx*dtdef[i]/dyy;
Q2      :=  Q2 + factor*Q4;
Q[n,1]  :=  Q3 + Q4 - Q2 - Q1;
deltaT  :=  deltaT + Q[n,1]/(rho*s*dx*dx*dyy);
dspec[n,1]:= dspec[n,1] + deltaT;
end;
end;

Procedure  secondcolspec;
begin
for n:= 2 to w-1 do begin
Q1      :=  0;
Q2      :=  0;
Q3      :=  0;
Q4      :=  0;
deltat  :=  0;
Q1      :=  Q1+(dspec[n,2]-dspec[n+1,2])*k*dx*extension[i]*
            dtdef[i]/((dyy+dy[i])/2);
Q3      :=  Q3 + (dspec[n-1,2]-dspec[n,2])*k*dx*extension[i]*
            dtdef[i]/((dyy+dy[i])/2);
Q4      :=  Q4+(dspec[n,3]-dspec[n,2])*k*dyy*dx*dtdef[i]/
            extension[i];
Q2      :=  Q2 + (dspec[n,2] - dspec[n,1])*k*dy[i]*dx*dtdef[i]/
            extension[i];
Q[n,2]  :=  Q3 + Q4 - Q2 - Q1;
deltaT  :=  deltaT + Q[n,2]/(rho*s*dx*dx*(dyy+dy[i])/2);
dspec[n,2]:=dspec[n,2] + deltaT;
end;
end;

Procedure  thirdcolspec;
begin
for n:= 2 to w-1 do begin
Q1      :=  0;
Q2      :=  0;
Q3      :=  0;
Q4      :=  0;
deltat  :=  0;
Q1      :=  Q1+(dspec[n,3]-dspec[n+1,3])*k*dx*dx*dtdef[i]/dy[i];
Q3      :=  Q3 + (dspec[n-1,3]-dspec[n,3])*k*dx*dx*dtdef[i]/dy[i];
Q4      :=  Q4+(dspec[n,4]-dspec[n,3])*k*dy[i]*dtdef[i];
Q2      :=  Q2 + (dspec[n,3]-dspec[n,2])*k*dy[i]*dx*dtdef[i]/
            extension[i];
Q[n,3]  :=  Q3 + Q4 - Q2 - Q1;
deltaT  :=  deltaT + Q[n,3]/(rho*s*dx*dx*dy[i]);
```

```
dspec[n,3]:= dspec[n,3] + deltaT;
end;
end;

Procedure Firstcoltool;
begin
for n:= 2 to w-1 do begin
J1      :=  0;
J2      :=  0;
J3      :=  0;
J4      :=  0;
HT      :=  0;
deltat  :=  0;
HT      :=  HT+0.03227*(dtool[n,3]-Tamb)+3.2319E-11*(sqr
            (sqr(dtool[n,3]+273)) - sqr(sqr(tamb+273)));
J1      :=  J1+(dtool[n,3]-dtool[n+1,3])*k1*dx*dx*dtdef[i]/dyy;
J3      :=  J3 + (dtool[n-1,3]-dtool[n,3])*k1*dx*dx*dtdef[i]/dyy;
J4      :=  J4+(dtool[n,4]-dtool[n,3])*k1*dyy*dtdef[i];
J2      :=  J2 + Ht*dx*dyy*dtdef[i]*1000;
J[n,3]  :=  J3 + J4 - J2 - J1;
deltaT  :=  deltaT + J[n,3]/(rhol*s1*dx*dx*dyy);
dtool[n,3]:= dtool[n,3] + deltaT;
end;
end;

Procedure  Bottomrowspec;
begin
for m:=2 to V-1 do begin
Q1      :=    0;
Q2      :=    0;
Q4      :=    0;
deltaT  :=    0;
Q1      :=    Q1+(dspec[1,m]- dspec[2,m])*k*dx*dx*dtdef[i]/dy[i];
Q2      :=    Q2+(dspec[1,m]- dspec[1,m-1])*k*dy[i]*dtdef[i];
Q4      :=    Q4+(dspec[1,m+1]- dspec[1,m])*k*dy[i]*dtdef[i];
Q[1,m]  :=    - Q1 - Q2 + Q4;
deltaT  :=    deltat + Q[1,m]/(rho*s*dx*dx*dy[i]);
dspec[1,m]:=  dspec[1,m] + deltaT;
end;
end;

Procedure Bottomrowtool;
begin
for m:=4 to 6 do begin
J1      :=  0;
J2      :=  0;
J4      :=  0;
deltaT  :=  0;
J1      :=  J1+(dtool[1,m]-dtool[2,m])*k1*dx*dx*dtdef[i]/dyy;
J2      :=  J2+(dtool[1,m]-dtool[1,m-1])*k1*dyy*dtdef[i];
J4      :=  J4+(dtool[1,m+1]-dtool[1,m])*k1*dyy*dtdef[i];
J[1,m]  :=  - J1 - J2 + J4 + factor*J1;
deltaT  :=  deltat + J[1,m]/(rhol*s1*dx*dx*dyy);
dtool[1,m]:= dtool[1,m] + deltaT;
```

```
end;
end;

Procedure Bottomrightspec;
begin
Q1        :=    0;
Q2        :=    0;
deltat    :=    0;
Q1        :=    Q1+(dspec[1,V]-dspec[2,V])*k*dx*dx*dtdef[i]/dy[i];
Q2        :=    Q2+(dspec[1,V]-dspec[1,V-1])*k*dy[i]*dtdef[i];
Q[1,V]    :=    - Q1 - Q2;
deltaT    :=    deltat + Q[1,V]/(rho*s*dx*dx*dy[i]);
dspec[1,V]:=    dspec[1,V] + deltaT;
end;

Procedure Bottomrighttool;
begin
J1        :=    0;
J2        :=    0;
deltat    :=    0;
J1        :=    J1+(dtool[1,7]-dtool[2,7])*k1*dx*dx*dtdef[i]/dyy;
J2        :=    J2+(dtool[1,7]-dtool[1,6])*k1*dyy*dtdef[i];
J[1,7]    :=    - J1 - J2 + factor*J1;
deltaT    :=    deltat + J[1,7]/(rho1*s1*dx*dx*dyy);
dtool[1,7]:=    dtool[1,7] + deltaT;
end;

Procedure  Rightcolspec;
begin
for n:=2 to w-1 do begin
Q1        :=    0;
Q2        :=    0;
Q3        :=    0;
deltat    :=    0;
Q1        :=    Q1+(dspec[n,v]-dspec[n+1,v])*k*dx*dx*dtdef[i]/dy[i];
Q2        :=    Q2+(dspec[n,v]-dspec[n,v-1])*k*dy[i]*dtdef[i];
Q3        :=    Q3 + (dspec[n-1,v]-dspec[n,v])*k*dx*dx*dtdef[i]/dy[i];
Q[n,V]    :=    Q3 - Q1 - Q2;
deltat    :=    deltat + Q[n,V]/(rho*s*dx*dx*dy[i]);
dspec[n,v]:=    dspec[n,v] + deltat;
end;
end;

Procedure Rightcoltool;
begin
for n:=2 to w-1 do begin
J1        :=    0;
J2        :=    0;
J3        :=    0;
deltat    :=    0;
J1        :=    J1+(dtool[n,7]-dtool[n+1,7])*k1*dx*dx*dtdef[i]/dyy;
J2        :=    J2+(dtool[n,7]-dtool[n,6])*k1*dyy*dtdef[i];
J3        :=    J3 + (dtool[n-1,7]-dtool[n,7])*k1*dx*dx*dtdef[i]/dyy;
J[n,7]    :=    J3 - J1 - J2;
```

```
deltat    :=     deltat + J[n,7]/(rhol*s  dx*dx*dyy);
dtool[n,7]:=     dtool[n,7] + deltat;
end;
end;

Procedure Bottomleftspec;
begin
Q1     :=   0;
Q4     :=   0;
deltat:=    0;
Q1     :=   Q1+(dspec[1,1]-dspec[2,1])*k*dx*dx*dtdef[i]/dy[i];
Q4     :=   Q4+(dspec[1,2]-dspec[1,1])*k*dy[i]*dtdef[i];
Q[1,1]:=    Q4 - Q1 - factor*Q4;
deltat:=    deltat + Q[1,1]/(rho*s*dx*dx*dy[i]);
dspec[1,1]:=dspec[1,1] + deltat;
end;

Procedure  Bottomlefttool;
begin
J1        :=   0;
J4        :=   0;
J2        :=   0;
deltat    :=   0;
HT        :=   HT+0.03227*(dtool[1,3]-Tamb)+3.2319E-11*(sqr(sqr
               (dtool[1,3]+273)) - sqr(sqr(tamb+273)));
J2        :=   J2 + Ht*dx*dyy*dtdef[i]*1000;
J1        :=   J1+(dtool[1,3]-dtool[2,3])*k1*dx*dx*dtdef[i]/dyy;
J4        :=   J4+(dtool[1,4]-dtool[1,3])*k1*dyy*dtdef[i];
J[1,3]    :=   J4 - J1 + factor*J1 - J2;
deltat    :=   deltat + J[1,3]/(rhol*s1*dx*dx*dyy);
dtool[1,3]:= dtool[1,3] + deltat;
end;


BEGIN
clrscr;
textcolor(white);
writeln;
writeln;
writeln;
writeln;
writeln;
writeln('                    [redacted]                      ');
writeln('                 TEMPERATURE DISTRIBUTION DURING    ');
writeln('                    PLANE STRAIN COMPRESSION        ');
writeln;
writeln;
writeln('                           Written by               ');
writeln;
writeln('                            K.Banks                 ');
writeln;
writeln('                    [redacted]                      ');
writeln;
```

```
textcolor(11);
writeln;
writeln('Insert Data Storage Disc in Drive A:');
writeln;
writeln('Press ENTER to continue');
readln;
       Initial;
       Air_Stable_Time;
       Deform_Stable_Time;
plus1:= 0;
for i:= 1 to passes do
  begin
  repeat
       begin
       plus1:=plus1 + 1;
writeln(plus1:7);
       Air_bottomrowspec;
       Air_bottomrowtool;
       Air_bottomrightspec;
       Air_bottomrighttool;
       Air_righthandspec;
       Air_righthandtool;
       Air_bottomleftspec;
       Air_bottomleftspec;
       Air_firstspec;
       Air_firsttool;
       Air_internalspec;
       Air_internaltool;
       Air_surfacespec;
       Air_surfacetool;
       Air_surfaceleftspec;
       Air_surfacelefttool;
       Air_surfacerightspec;
       Air_surfacerighttool;
       Print_tool;
       Print_spec;
add:=  add + dtair[i];
end;
until add > add1 + timeair[i];

add1:= add;
plus2:= plus1;

for n:=1 to w do
begin
    for m:=3 to v do
        begin
        dspec[n,m]:=spec[n,m] + 1000*strain[i]*stress[i]/(rho*s);
        end;
end;
for n:=1 to w do
begin
    for m:=1 to 2 do
        begin
```

```
        dspec[n,m]:=spec[n,m];
        end;
end;
for n:=1 to w do
begin
    for m:=3 to 7 do
    begin
    dtool[n,m]:=tool[n,m];
    end;
end;
  repeat
        begin
        toprow;
        topright;
        topleft;
        topleftspec;
        toprhomboid;
        internalspec;
        internaltool;
        firstcolspec;
        secondcolspec;
        thirdcolspec;
        firstcoltool;
        bottomrowspec;
        bottomrowtool;
        bottomrightspec;
        bottomrighttool;
        rightcolspec;
        rightcoltool;
        bottomleftspec;
        bottomlefttool;
add1:=     add1 + dtdef[i];
plus2:=    plus2 + 1;
writeln(plus2:20);
        print_dtool;
        print_dspec;
        end;
until   add1 > add + deftime[i];
plus1:= plus2;
add:=   add1;

for n:=1 to w do
    begin
    for m:=1 to v do
        begin
        spec[n,m]:=dspec[n,m];
        end;
    end;
for n:=1 to w do
    begin
    for m:=3 to 7 do
        begin
        tool[n,m]:=dtool[n,m];
        end;
```

```
    end;
End;
nett:= plus1;
Close(thefile);
clrscr;
writeln;
writeln;
writeln;
writeln('Total number of pairs ',nett:4,'  Note this Value!');
readln;
END.
```

APPENDIX 2

Listing Of Computer Programmes To Convert Load, Displacement and Time Binary Data To Digital Format.

```
PRINT "Insert Disk Containing Force Data"
INPUT ; was
PRINT "Specify path of LOAD BINARY file"
INPUT ; file1$
PRINT "Filename for LOAD data"
INPUT ; filename$
DEF SEG = &HB800
BLOAD file1$, feedoff
range1 = 1500
OPEN filename$ FOR OUTPUT AS £1
FOR i = 1 TO 1166
a = (i - 1) * 2
demand = PEEK(feedoff + a) / 16 + (16 * PEEK(feedoff + a + 1))
demand = (demand - 2047) * (range1 / 2048)
PRINT £1, USING "£££££.£££"; demand
NEXT i
CLOSE £1
DEF SEG
END
```

```
PRINT "Insert Disk Containing Position Data"
INPUT ; was
PRINT " Specify path of BINARY POSITION file"
INPUT ; file3$
PRINT " Filename for Position Text File "
INPUT ; filename$
DEF SEG = &HB800
BLOAD file3$, pos off
range = 50
OPEN filename$ FOR OUTPUT AS £2
FOR i = 1 TO 1166
a = (i - 1) * 2
amo = PEEK(pos.off + a) / 16 + (16 * PEEK(pos.off + a + 1))
amo = (amo - 2047) * (range / 2048)
PRINT £2, USING "££££.££"; amo
NEXT i
CLOSE £2
DEF SEG
END
```

```
PRINT "Insert Disk in Drive A:"
INPUT ; was
PRINT " Binary time file"
INPUT ; file$
PRINT "Converted time file"
INPUT ; filename$
DEF SEG = &HB800
BLOAD file$, tim.off
OPEN filename$ FOR OUTPUT AS £1
FOR i = 1 TO 1326
b = (i - 1) * 4
amo = (PEEK(tim.off + b) + (256 * PEEK(tim.off + b + 1)) + (65536! * PEEK(
PRINT £1, USING "£££££.£££"; amo
NEXT i
CLOSE £1
DEF SEG
END
```

APPENDIX 3

1. Computer Programme For Communications Between IF85 Data Acquisition Unit And Computer.

2. Programme For Temperature Analog To Digital Conversion

```
90 CLS
190 DIM A$(20,20)
290 OPEN "COM1:1200,N,7,2,BIN" AS #1
390 INPUT "Number of readings  : ",M
490 INPUT "Channels to be read : ",CH1,CH2,CH3,CH4,CH5,CH6
590 PRINT CH1,CH2,CH3,CH4,CH5,CH6
690 FOR N=0 TO M
790 IF CH1 > 0 THEN GOTO 890 ELSE GOTO 1190
890 PRINT #1,"OD",1,N
990 LINE INPUT #1,A$(1,N)
1090 PRINT A$(1,N)
1190 IF CH2 > 0 THEN GOTO
1290 PRINT #1,"OD",5,N
1390 LINE INPUT #1,A$(5,N+1)
1490 PRINT A$(5,N+1)
1590 NEXT N
1690 CLOSE #1
1790 OPEN "OUTPUT" ,1,"DATA1"
1890 LINE INPUT "WUMSI";A$
1990 FOR I=1 TO M
2090 PRINT #1,A$(1,I)
2190 PRINT #1,A$(5,I+1)
2290 NEXT
2390 CLOSE 1
2490 PRINT "READING FROM FILE DATA1"
2590 OPEN "INPUT",1,"DATA1"
2690 FOR I = 1 TO M
2790 LINE INPUT #1,A$
2890 PRINT I,A$
2990 NEXT
3090 CLOSE 1
3190 END
```

```
uses
crt,dos;


type
     DataRec  = Record
                  Valid   : boolean;
                  Range   : string[1];
                  Channel : integer;
                  Value   : real;
                  Expon   : integer;
                  Pol     : string[1];
                End;

     DataArray = array[1..1200] of string[24];

var

Pasvalue          : array[1..1200] of DataRec;
datfile,tempfile  : text;
filename,filetemp : string[12];
i,points,j,result : integer;
k,nth             : integer;
MemArray          : DataArray;
Memvalue          : string[40];
Memvalid          : string[1];
Memrange          : string[1];
Memchannel        : string[1];
Mempol            : string[1];
Memexp            : string[3];
t,temp_time       : real;
key,s,kk           : string[3];
choice            : integer;


procedure Readdata;

begin
textcolor(15);
     writeln('IF85 Path \ File Name :');
     gotoxy(25,1);
     readln(filename);
     assign(datfile,filename);
     reset(datfile);
     i:=0;
while not EOF(datfile) do
      begin
           readln(datfile,memarray[i+1]);
           i:=succ(i);
      end;
      close(datfile);
      points:=i;
      writeln('Data Points / Channel : ',points div 3:2);
end;
```

```
procedure interval;
begin
writeln('Sampling Rate: Choose from 1;2;5;10;20;50;100;200 ms :');
gotoxy(56,4);
readln(choice);

case choice of

1  :   t:= 16.384/16384;
2  :   t:= 32.768/16384;
5  :   t:= 81.92/16384;
10 :   t:= 163.84/16384;
20 :   t:= 327.68/16384;
50 :   t:= 819.2/16384;
100:   t:= 1638.2/16384;
200:   t:= 3276.8/16384;
else
writeln('Incorrect choice - Try again');
end;
writeln('Data Interval (n) ');
readln(nth);
t := t * nth;
end;

procedure ConvertDat;

begin
for j:=1 to points do
begin
Memvalue   := copy(memarray[j],13,5);
Memvalid   := copy(memarray[j],2,1);
Memrange   := copy(memarray[j],6,1);
Memchannel := copy(memarray[j],10,1);
Mempol     := copy(memarray[j],12,1);
Memexp     := copy(memarray[j],18,3);

(*  if  Memvalid = 'S' then
      begin
           Pasvalue[j].valid := TRUE;
           writeln('O.K.');
       end
  else
            pasvalue[j].vali . := FALSE;
            writeln('No');*)

  with Pasvalue[j] do
       begin
          val(memvalue,Pasvalue[j].value,Result);
          val(memexp,Pasvalue[j].expon,Result);
          val(memchannel,Pasvalue[j].channel,Result);
       end;

if j = k - 3 then
       begin
```

```
        writeln( k / 3:5:0,temp_time:10:3,Pasvalue[j-2].Value/10.0:10:1);
        k := k + 3;
        temp_time := temp_time + t;
        end;

end;
writeln;
textcolor(11);
writeln('  Pt.    Time(sec)   Ch 1      Ch 3       Ch 5         millivolts');
readln;
end;

procedure temperature;
begin
clrscr;
writeln('Converted Temperature Path \ File Name :');
gotoxy(43,1);
readln(filetemp);
assign(tempfile,filetemp);
rewrite(tempfile);
for j:=1 to points do
begin
textcolor(14);
pasvalue[j].value := pasvalue[j].value/10.0;

if key = 'kk' then
pasvalue[j].value           :=           pasvalue[j].value*24.499           +
0.000496*sqr(pasvalue[j].value)
                    - 0.00132*sqr(pasvalue[j].value)*pasvalue[j].value +
                    2.75E-5*sqr(sqr(pasvalue[j].value));

if key = 's' then
pasvalue[j].value :=  pasvalue[j].value*145.46 - 7.8*
                      sqr(pasvalue[j].value)
                      + 0.375*sqr(pasvalue[j].value)*
                      pasvalue[j].value;

if j = k - 3 then
        begin
        writeln(TempFile,temp_time:10:3,Pasvalue[j-2].Value:10:0);
        writeln(k / 3:5:0,temp_time:10:3,Pasvalue[j-2].Value:10:0);
        k          := k + 3;
        temp_time := temp_time+t;
        end;

end;
close(tempfile);
textcolor(11);
writeln;
writeln('  Pt.    Time(sec)   Ch 1      Ch 3       Ch 5         °Celsius' );
end;

BEGIN
ClrScr;
```

```
writeln('Insert Disk In Drive A:');
readln;
clrscr;
writeln('thermocouple type s or kk');
readln(key);
clrscr;
    Readdata;
writeln;
    Interval;
temp_time := 0.0;
k := 6;
ClrScr;
    ConvertDat;
ClrScr;
temp_time := 0.0;
k := 6;
    Temperature;
END.
```

APPENDIX 4

LISTING OF COMPUTER PROGRAMME, PLATESIM, TO SIMULATE THE MECHANICAL AND METALLURGICAL CHANGES OCCURRING IN HOT ROLLING

```
USES

crt,dos,graph;

CONST

rad    = 1;
Xmin   = 0.0;
Xmax   = 500.0;
Ymin   = 0.0;
Ymax   = 250.0;
Tmin   = 1000.0;
Tmax   = 1300.0;
Ttick  = 60;
Ytick  = 50.0;
Xtick  = 50.0;
Y_min  = 750;
Y_max  = 1250;
Y_tick = 100.0;
Xlmin  = -1;
Xlmax  = 3;
SansSerifFont = 3;
HorizDir      = 0;
VertDir       = 1;


VAR

Flow,Tfinish,M_in,M_fi,Totalstrain,Cool_rate,Ferrite    :Real;
prev_D,prev_A,prev_B,prev_C,reheat,h0,rpm,pear,UTS      :Real;
Radius,inc,T_1,T_2,T_3,E_1,E_2,E_3,Yield,FATT           :Real;
R,i,j,Passes,Switch                                     :Integer;
Grdriver,Grmode,Errcode                                 :Integer;
Time99,Time,d,drex,h,T,Strain,dgg                       :Array[0..20]of real;
P,meanflow,roll_force,Z,F,B,M,PS,PF                     :Array[0..20]of real;
E,Totaltime,Temp,carbon,mn                              :Real;
tons,d_T_con,d_T_def,Heat_1,Q,S_rate                    :Array[0..20]of real;
key,k,l                                                 :Char;
File_input,File_mech,File_evol,File_output,Filetemp     :String[15];
Output_file,Input_file,Mech_file,Evol_file,Tempfile     :Text;

{- FUNCTIONS -}

function ptx(total:real):integer;
begin
ptx:=round((500-50)/(Xmax-Xmin)*(total-Xmin)+5);
end;

function ptxlog(total:real):integer;
begin
ptxlog:=round((500-50)/(Xlmax-Xlmin)*(total-Xlmin)+50);
end;

function pty(total:real):integer;
```

```
begin
pty:=round((-110)/(Ymax-Ymin)*total+60-((-110)/(Ymax-Ymin)*Ymax));
end;

function Ty(total:real):integer;
begin
Ty:=round((-215)/(Tmax-Tmin)*total+60-((-215)/(Tmax-Tmin)*Tmax));
end;

{$I grid.psl}
{$I grid_big.psl}
{$I inset_1.psl}
{$I inset_2.psl}
{$I inset_3.psl}

Procedure Input;
begin
clrscr;
textcolor(15);
writeln('  REHEAT              entry          ROLLING       exit             COOLING   ');
textcolor(9);
writeln('                                                                  ');
textcolor(7);
writeln('                                                                    ');
writeln('                                                                    ');
writeln('                                                                    ');
textcolor(3);
writeln('                                                                    ');
textcolor(11);
writeln('Inputs from (k)eyboard or fi(l)e :   ');
writeln('Reheat:       °C      Pass     h(mm)    °C      t(s)    Force     Finish Temp');
writeln('Thick :       mm');
writeln('W (i) :       mm');
writeln('W (f) :       mm');
writeln('Radius:       mm');
writeln('r.p.m :');
writeln('Passes:');
writeln('ro    :       µm');
writeln('t(ruf):       s');
writeln('Rotation :      ');
textcolor(12);
gotoxy(36,7);readln(key);
if key='k' then
begin
    (* gotoxy(1,23);writeln('File:');
     gotoxy(7,23);readln(file_output);*)
     file_output:='492.dat';
     Assign(output_file,file_output);
     Rewrite(output_file);
     {- START READ FROM KEYBOARD -}
     gotoxy(3,4);writeln('      ');
     textcolor(12);
     gotoxy(9,8);readln(T[0]);
     gotoxy(9,9);readln(h[0]);
```

```
gotoxy(9,10);readln(W_in);
gotoxy(9,11);readln(W_fi);
gotoxy(9,12);readln(Radius);
gotoxy(9,13);readln(RPM);
gotoxy(9,14);readln(passes);
d[0]:=exp(9.847-6601/(T[0]+273));
gotoxy(9,15);writeln(d[0]:2:0);
gotoxy(9,16);readln(time[0]);
gotoxy(12,17);readln(switch);
gotoxy(3,4);writeln('  .   ');

{- WRITE INPUTS TO FILE -}
writeln(output_file,T[0]:0:0);
writeln(output_file,h[0]:0:0);
writeln(output_file,W_in:0:0);
writeln(output_file,W_fi:0:0);
writeln(output_file,Radius:0:0);
writeln(output_file,RPM:0:0);
writeln(output_file,passes:0);
writeln(output_file,d[0]:0:0);
writeln(output_file,time[0]:0:0);
writeln(output_file,switch:0);


for i:= 1 to passes do
    begin
    textcolor(12);
    gotoxy(24,3);writeln('▒▒▒▒▒▒');
    gotoxy(20,8+i);writeln('‖  ',i);
    gotoxy(32,8+i);writeln('      ');
    gotoxy(32,8+i);readln(h[i]);
    writeln(output_file,h[i]:0:0);
    if h[i] > h[i-1] then
      begin
         repeat
         begin
              gotoxy(32,8+i);
              textcolor(15+blink);
              writeln('Press Enter');
              textcolor(12);
              readln;
              gotoxy(32,8+i);writeln('          ');
              gotoxy(32,8+i);readln(h[i]);
              writeln(output_file,h[i]:0:0);
          end;
         until h[i] < h[i-1];
      end;
      gotoxy(42,8+i);readln(T[i]);
      gotoxy(50,8+i);readln(time[i]);
      gotoxy(58,8+i);readln(tons[i]);
      writeln(output_file,T[i]:0:0);
      writeln(output_file,time[i]:0:0);
      writeln(output_file,tons[i]:0:0);
      textcolor(12);
```

```
          gotoxy(24,3);writeln('  .   ');
          gotoxy(46,3);writeln('[redacted]');
          readln;
          textcolor(15);
          gotoxy(46,3);writeln('   .         ');
        end;
        textcolor(12);
        gotoxy(68,3);writeln('[redacted]');
        gotoxy(68,9);writeln('              ');
        gotoxy(72,9);readln(Tfinish);
        writeln(output_file,Tfinish:0:0);
        gotoxy(72,10);
Close(Output_file);
end;
{- END WRITE TO FILE -}
{- END READ FROM KEYBOARD -}


If key = '1' then

{- START READ FROM FILE -}
begin
(*gotoxy(1,23);writeln('File:');
gotoxy(7,23);readln(file_input);*)
{-_____-}
{- Enter File Name Here     -}
{-_____-}

file_input:='490.dat';
Assign(Input_file,file_input);
Reset(Input_file);

        gotoxy(3,4);writeln('[redacted]');
        textcolor(12);
        read(Input_file,T[0]);
        gotoxy(9,8);writeln(T[0]:1:0);
        read(Input_file,h[0]);
        gotoxy(9,9);writeln(h[0]:1:0);
        read(Input_file,W_in);
        gotoxy(9,10);writeln(W_in:1:0);
        readln(Input_file,W_fi);
        gotoxy(9,11);writeln(W_fi:1:0);
        readln(Input_file,Radius);
        gotoxy(9,12);writeln(radius:1:0);
        readln(Input_file,RPM);
        gotoxy(9,13);writeln(rpm:1:0);
        readln(Input_file,passes);
        gotoxy(9,14);writeln(passes:1);
        d[0]:=exp(9.847-6601/(T[0]+273));
        gotoxy(9,15);writeln(d[0]:1:0);
        readln(Input_file,time[0]);
        gotoxy(9,16);writeln(time[0]:1:0);
        readln(Input_file,switch);
        gotoxy(12,17);writeln(switch:1);
```

```
        gotoxy(3,4);writeln('  .   ');

        for i:= 1 to passes do
            begin
            textcolor(12);
            gotoxy(24,3);writeln('[redacted]');
            gotoxy(20,8+i);writeln('|  ',i);
            readln(Input_file,h[i]);
            gotoxy(32,8+i);writeln(h[i]:1:0);
            if h[i] > h[i-1] then
                begin
                repeat
                    begin
                    gotoxy(32,8+i);
                    textcolor(15+blink);
                    writeln('Press Enter');
                    textcolor(12);
                    readln;
                    readln(Input_file,h[i]);
                    gotoxy(32,8+i);writeln(h[i]:1:0);
                    writeln(Input_file,h[i]:10:0);
                    end;
                until h[i] < h[i-1];
                end;
                readln(Input_file,T[i]);
            gotoxy(42,8+i);writeln(T[i]:1:0);
            readln(Input_file,time[i]);
            gotoxy(50,8+i);writeln(time[i]:1:0);
            readln(Input_file,tons[i]);
            gotoxy(58,8+i);writeln(tons[i]:1:0);
            textcolor(12);
            gotoxy(52,3);writeln('[redacted]');
(*            readln;       *)
            textcolor(15);
            gotoxy(52,3);writeln('   .  ');
            end;
      textcolor(12);
      gotoxy(72,3);writeln('[redacted]');
      gotoxy(72,9);writeln('       ');
      readln(Input_file,Tfinish);
      gotoxy(72,9);writeln(Tfinish:1:0);
      Close(Input_file);
      end;

{- END READ FROM FILE -}

gotoxy(72,10);readln;
end;


Procedure Deformation;
begin
clrscr;
totalstrain := 0;
```

```
for i:= 1 to passes do
  begin
  strain[i]:= ln(h[0]/h[i]) - totalstrain;
  totalstrain := totalstrain + strain[i];
  S_rate[1]     := 2*3.142*radius*rpm/60;
  S_rate[i]     := S_rate[i]*strain[i]/(sqrt(radius*(h[i-1]-h[i])));
  end;
end;


Procedure Temperature;
begin
Inset_2;
Grid_Big;
Temp      := T[0];
totaltime := 0;
E         := 0;
Setcolor(2);

{-____________________-}
{- Insert file name here-}
{-____________________-}

        filetemp:='490.tem';
        assign(tempfile,filetemp);
        rewrite(tempfile);
                  for i := 1 to passes do
                  begin
                  inc := 0;
                        Repeat
                        begin
                        inc       :=  inc + 1;
                        totaltime :=  totaltime + 1;
                        E         :=  (Temp)*(0.09[illegible]mp)/1000 -
                                      0.48)/1000 + [illegible];
                        Temp      :=  (Temp+273)/exp(0.33*ln(1 + 6 *
                                      5.67E-8 * E * (Temp+273)*
                                      (Temp+273)*(Temp+273) * inc /
                                      (7750*650*h[i]/1000)))-273;
                                      setcolor(3);
                        writeln(tempfile,totaltime:10:1,temp:10:1);
                        Circle(ptx(round(totaltime*5)+60),
                              Ty(round(temp)+20),1);
                        end;
                        Until inc = time[i];

                   Heat_1[i]  := Temp;
                   d_T_con[i] := 22E3*sqrt(strain[i]/(h[i]/
                                 1000*radius/1000)) * (heat_1[i] - 400)/
                                 ((1-strain[i])*3.142*7800*650*rpm/60);
(* meanflow *)     d_T_def[i] := 1E6*100*strain[i]/(7800*650)*2;
                   Temp       := heat_1[i] + d_T_def[i];
                   writeln(tempfile,totaltime:10:1,temp:10:1);
                   Temp       := temp - d_T_con[i];
```

```
                    writeln(tempfile,totaltime:10:1,temp:10:1);
                    writeln(temp:10:1,E:10:1,inc:10:1,heat_1[i]:10:1);
                    setcolor(15);
                    Circle(ptx(round(totaltime*5)+50),
                          Ty(round(T[i])+20),2);
                    end;
Close(Tempfile);
readln;
end;


Procedure Mechanics;
begin
     Clrscr;
     Setgraphmode(getgraphmode);
     setbkcolor(0);
     Inset_1;
     Grid;
{-_____________________-}
{- Insert file name here  -}
{-_____________________-}

     File_mech := '490.pro';
     Assign(Mech_file,File_mech);
     Rewrite(Mech_file);
     Writeln(Mech_file,'        E          σm (MPa)    F(meas)     F(sim)    T(s)°C      T(m)°C        d(um)
hold(s)');
     Writeln(Mech_file,'        ');
totalstrain  := 0;
roll_force[0]:= 0;
p[0]         := 0;
for i := 1 to passes do
    begin
    inc        := 0;
    flow       := 0;
    repeat
       begin
       prev_A      := totalstrain;
       prev_B      := flow;
       inc         := inc  + 0.001;
       totalstrain := totalstrain + 0.001;

if heat_1[i] > 1150 then
       begin
       flow        := exp(0.3*ln(S_rate[i])) *(0.8*(153*exp(0.4*ln(inc)) -
                          49*exp(0.8*ln(inc)) -
                          70*exp(1.2*ln(inc))));
       end;

if (heat_1[i] <= 1150) and (heat_1[i] > 1115) then
       begin
       flow        := exp(0.3*ln(S_rate[i])) *(153*exp(0.4*ln(inc)) -
                      49*exp(0.8*ln(inc))  -
                      70*exp(1.2*ln(inc)));
```

```
      end;

if (heat_1[i] <= 1115) and (heat_1[i] >= 1040) then
      begin
      flow        := exp(0.3*ln(S_rate[i])) *(179*exp(0.4*ln(inc)) -
                     79*exp(0.8*ln(inc))  -
                     44*exp(1.2*ln(inc)));
      end;

if (heat_1[i] < 1040) and (heat_1[i] >= 950) then
      begin
      flow        := exp(0.3*ln(S_rate[i])) *(204*exp(0.4*ln(inc)) -
                    109*exp(0.8*ln(inc))  -
                     18*exp(1.2*ln(inc)));
      end;

if (heat_1[i] < 950) then
      begin
      flow        := 200;
      end;

if (inc > 0.015) and (inc < 0.017) then
      begin
      setcolor(12);
      Circle(ptx(round(totalstrain*167)+50),pty(round(flow)+70),2):
      end;

      setcolor(12);
        Line(ptx(round(prev_A*167)+50),pty(round(prev_B)+70),
            ptx(round(totalstrain*167)+50),pty(round(flow)+70));
      end;
   until inc > strain[i];
      setcolor(12);
      Circle(ptx(round(totalstrain*167)+50),pty(round(flow)+70),2);

if heat_1[i] >= 1150 then
      begin
      meanflow[i] :=  exp(0.3*ln(S_rate[i])) *0.8 * ((153 / 1.4*exp(1.4*ln(strain[i]))
                        - 49  /  1.8*exp(1.8*ln(strain[i]))
                        - 70  /  2.2*exp(2.2*ln(strain[i]))
                        + 153 /  1.4
                        - 49  /  1.8
                        - 70  /  2.2));
     end;

if (heat_1[i] <= 1150) and (heat_1[i] >= 1040) then
      begin
      meanflow[i] :=  exp(0.3*ln(S_rate[i])) * (153 / 1.4*exp(1.4*ln(strain[i]))
                    - 49  / 1.8*exp(1.8*ln(strain[i]))
                    - 70  / 2.2*exp(2.2*ln(strain[i]))
                    + 153 / 1.4
                    - 49  / 1.8
                    - 70  / 2.2);
     end;
```

```
if (heat_1[i] < 1040) and (heat_1[i] >= 950) then
       begin
       meanflow[i] :=  exp(0.3*ln(S_rate[i])) * (204 / 1.4*exp(1.4*ln(strain[i]))
                     - 109 / 1.8*exp(1.8*ln(strain[i]))
                     - 18  / 2.2*exp(2.2*ln(strain[i]))
                     + 204 / 1.4
                     - 109 / 1.8
                     - 18  / 2.2);
      end;
if (heat_1[i] < 950) then
       begin
       meanflow[i] :=  200;
       end;
      writeln(' Mean flow stress ',i:4, meanflow[i]:6:1);
      Roll_force[i] := 0.25*(3.142 + sqrt((h[i-1]-h[i])*radius)/
                           ((h[i-1]+2*h[i])/3));
      Q[i]          := Roll_force[i];

      If i <= switch then
      Roll_force[i] := W_in*meanflow[i]*
                       roll_force[i]*sqrt(radius*(h[i-1]-h[i]))/100000
      Else
      Roll_force[i] := W_fi*meanflow[i]*
                       roll_force[i]*sqrt(radius*(h[i-1]-h[i]))/100000;
      p[i] := totalstrain;
      setcolor(3);
      Line(ptx(round(p[i-1]*167)+50),
           pty(round(roll_force[i-1]/2)+70),
           ptx(round(p[i]*167)+50),
           pty(round(roll_force[i]/2)+70));
      Circle(ptx(round(p[i]*167)+50),
           pty(round(roll_force[i]/2)+70),2);
    end;
end;


Procedure Metallurgy;
bugin
dgg[0]:=d[0];
totaltime := 0;
inc := 0;
for i := 1 to passes do
    begin
    totaltime := totaltime + time[i];
    inc := totaltime - time[i];
    setcolor(15);
    Circle(ptx(round(totaltime*2.5)+50),pty(round((T[i]-0)/10*2)-296),2);
    setcolor(3);
    Circle(ptx(round(totaltime*2.5)+50),pty(round((heat_1[i]-0)/10*2)-296),2);
    end;

totaltime := 0;
inc := 0;
heat_1[0]:=T[0];
```

```
for i := 1 to passes do
    begin
    totaltime := totaltime + time[i];
    inc := totaltime - time[i];
    drex[i]    := 0.5*exp(0.67*ln(d[i-1]))/strain[i];
    if drex[i] > d[i-1] then
    drex[i] := d[i-1];
    time99[i]  := 2*2.5E-19*sqr(drex[i])*exp(3E5/(8.31*
                  (heat_1[i]+273)))/sqr(sqr(strain[i]));
    dgg[i]     :=drex[i]*(1+0.195*ln(time[i]/time99[i])-
                  8E4*(1/(heat_1[i]+273) - 1/(heat_1[i-1]+273))/8.314);
    d[i]       := dgg[i];
    setcolor(13);
    Circle(ptx(round(totaltime*2.5)+50),
           pty(round(drex[i])-296),2);
    Circle(ptx(round(totaltime*2.5)+50),
           pty(round(dgg[i])-296),2);
    Line(ptx(round(inc*2.5)+50),
         pty(round(dgg[i-1])-296),
         ptx(round(tot[illegible]),
         pty(round(d[illegible]
    Line(ptx(round([illegible]2.[illegible]
         pty(round([illegible]-296),
         ptx(round(tot[illegible].ime*2.5)+50),
         pty(round(dgg[i])-296));
    Writeln(Mech_file,i:1,P[i]*100:10:2,Meanflow[i]:10:0,Tons[i]:10:0,
            Roll_force[i]*10:10:0,Heat_1[i]:10:0,
            T[i]:10:0,drex[i]:10:0,time[i]:10:0);
    writeln(Mech_file,i:1,P[i]*100:10:2,Meanflow[i]:10:0,Tons[i]:10:0,
            Roll_force[i]*10:10:0,Heat_1[i]:10:0,
            T[i]:10:0,dgg[i]:10:0,time[i]:10:0);
    end;
    setcolor(15+blink);
    outtextxy(ptx(round(totaltime*2.5)+50),
              pty(round(dgg[passes])-290),' <-- T final');
close(mech_file);
end;


Procedure Cooling;
begin
clrscr;
     Setgraphmode(getgraphmode);
     setbkcolor(0);
     Inset_3;
inc := 0;
Tfinish := Tfinish + 273;
T_3 := Tfinish;

Repeat
begin
prev_A := inc;
prev_D := T_3;
inc := inc + 2;
```

```
E_3 := (T_3-273)/1000*(0.125*(T_3-273)/1000 - 0.38) + 1.1;
T_3 := (Tfinish)/exp(0.333*ln(1 + 6 * 5.67E-8 * 0.8 *
       (Tfinish)*(Tfinish)*(Tfinish) * inc /
       (7750*650*h[passes]/1000)));
setcolor(14);
if prev_A <> 0 than
Line(ptx(log(0.4347*ln(prev_A)),pty(round(prev_D-273)/10*2 + 70),
     ptx(log(0.4347*ln(inc)),pty(round(T_3-273)/10*2 + 70));

end;
Until inc > 900;

setcolor(12);
Line(ptx(0+50),pty(820/10*2)-30,ptx(500+50),pty(820/10*2)-30);
Line(ptx(0+50),pty(720/10*2)-30,ptx(500+50),pty(720/10*2)-30);

setcolor(15);
Outtextxy(505,60,'Ac3');
Outtextxy(505,75,'Ac1');
setcolor(14);
Outtextxy(300,75,'F');
Outtextxy(350,84,'P');
Outtextxy(300,95,'B');
Outtextxy(100,95,'Ms');
Outtextxy(100,120,'M');

{- CCT 0.19C - 0.42Si - 1.20Mn -}
setcolor(15);
Z[1]  := 0.1; Z[2]  := 0.2; Z[3]  := 0.4;   Z[4]  := 0.6; Z[5]  := 0.8;
Z[6]  := 0.9; Z[7]  := 1.0; Z[8]  := 2.0;   Z[9]  := 4.0; Z[10] := 6.0;
Z[11] := 8  ; Z[12] := 10 ; Z[13] := 20 ;   Z[14] := 40 ; Z[15] := 60 ;
Z[16] := 80 ; Z[17] := 100; Z[18] := 200;   Z[19] := 400; Z[20] := 600;

M[1]  := 435; M[2]  := 435; M[3]  := 435;   M[4]  := 435; M[5]  := 435;
M[6]  := 435; M[7]  := 435; M[8]  := 435;   M[9]  := 420; M[10] := 405;
M[11] := 400; M[12] := 397; M[13] := 390;

B[6]  := 450; B[7]  := 470; B[8]  := 515;   B[9]  := 550; B[10] := 560;
B[11] := 570; B[12] := 580; B[13] := 585;   B[14] := 587;

F[7]  := 590; F[8]  := 670; F[9]  := 700; F[10] := 710; F[11] := 720;
F[12] := 723; F[13] := 730; F[14] := 750; F[15] := 755; F[16] := 760;
F[17] := 770; F[18] := 780; F[19] := 790; F[20] := 795;

PS[11] := 580; PS[12] := 600; PS[13] := 620;   PS[14] := 630; PS[15] := 635;
PS[16] := 640; PS[17] := 645; PS[18] := 650;   PS[19] := 653; PS[20] := 655;

PF[14] := 630; PF[15] := 635; PF[16] := 640;
PF[17] := 645; PF[18] := 650; PF[19] := 653; PF[20] := 655;

setcolor(13);
setlinestyle(1,0,1);

for i := 8 to 20 do
```

```
begin
line(ptxlog(0.4347*ln(Z[i-1]/2))+35,pty(F[i-1]/10*2+70),
     ptxlog(0.4347*ln(Z[i]/2))+35,pty(F[i]/10*2+70));
end;

for i := 12 to 20 do
begin
line(ptxlog(0.4347*ln(Z[i-1]/2))+35,pty(PS[i-1]/10*2+70),
     ptxlog(0.4347*ln(Z[i]/2))+35,pty(PS[i]/10*2+70));
end;

for i := 15 to 20 do
begin
line(ptxlog(0.4347*ln(Z[i-1]/2))+35,pty(PF[i-1]/10*2+70),
     ptxlog(0.4347*ln(Z[i]/2))+35,pty(PF[i]/10*2+70));
end;

for i := 2 to 13 do
begin
line(ptxlog(0.4347*ln(Z[i-1]/2))+35,pty(M[i-1]/10*2+70),
     ptxlog(0.4347*ln(Z[i]/2))+35,pty(M[i]/10*2+70));
end;

for i := 7 to 14 do
begin
line(ptxlog(0.4347*ln(Z[i-1]/2))+35,pty(B[i-1]/10*2+70),
     ptxlog(0.4347*ln(Z[i]/2))+35,pty(B[i]/10*2+70));
end;
readln;
end;



Procedure Properties;
begin
textcolor(12);
clrscr;
writeln;
writeln('     C:        Mn:          Cool Rate:       ');
textcolor(15);
gotoxy(12,2);readln(carbon);
gotoxy(22,2);readln(mn);
gotoxy(41,2);readln(cool_rate);
writeln;
writeln;
writeln;
writeln;
textcolor(12);
writeln('     Cool rate (°C/s)   τ(μm)   α(μm)   σy(MPa) σUTS(MPa) CVN 0°C');
textcolor(15);
writeln('     ┌──────────────────────────────────────────────────────────────┐');
(*Cool_rate := 1.1 - 0.35*(h[passes]-25)/15;*)
Pear:=24;
Ferrite   := 5.7*exp(-0.17*ln(cool_rate))*exp(0.333*ln(dgg[passes]));
```

```
Yield     := 321 + 255.3*Carbon + 32.4*Mn + 76.3*strain[passes] - 0.119*T[passes];
UTS       := 246 + 4.2*pear + 15/sqrt(ferrite/1000);
FATT      := 227 - 514.7*Carbon +37.8*strain[passes] - 0.095*T[passes];
writeln('     ',cool_rate:7:2,dgg[passes]:14:0,ferrite:10:1,yield:9:0,UTS:7:0,FATT:12:0,' ');
writeln('     ');
writeln;
writeln;
writeln;
writeln;
readln;
    clrscr;
    writeln;
    textcolor(12);
    writeln(' Pass   E    om   P(meas)   T(s)   T(m)   drex    dgg   Hold   P(s) Erate');
    textcolor(7);
    writeln('                                                                          ');
    textcolor(15);
    for i := 1 to passes do
    begin
    writeln(i:2,P[i]:8:2,Meanflow[i]:5:0,Roll_force[i]*10:8:0,
           Heat_1[i]:8:0,T[i]:8:0,drex[i]:7:0,dgg[i]:7:0,
           time[i]:5:0,Tons[i]:8:0,S_rate[i]:6:1);
    end;
    textcolor(7);
    writeln('                                                                          ');
readln;
end;


Procedure Introduction;
begin
clrscr;
textcolor(2);
writeln;
writeln;
writeln;
writeln;
writeln;
writeln;
writeln;
writeln;
writeln('                    ');
writeln('                    ');
writeln('                    ');
writeln('                    ');
writeln('                    ');
writeln('                    ');
writeln('                    ');
readln;
end;


BEGIN
Introduction;
```

```
Input;
Deformation;


Grdriver  := detect;
Initgraph(Grdriver, Grmode,'');
Errcode   := Graphresult;
if Errcode =  grOk then
     begin
     Temperature;
     Mechanics;
     Metallurgy;
     readln;
(*     Cooling;*)
     end
  else
    writeln('Graphics Error:',graphErrorMsg(Errcode));
    Closegraph;
    Properties;
    textcolor(15);
    clrscr;
END.
```